School of Earth and Planetary Science

On the Genesis and Significance of the Archean-hosted Carlow Castle Cu-Co-Au Deposit, Pilbara Craton, Western Australia

David Charles Mathieson Fox
0000-0001-7984-3657

This thesis is presented for the Degree of
Doctor of Philosophy
at
Curtin University
January 2022

Declaration

To the best of my knowledge and belief this thesis contains no material previously published by any other person except where due acknowledgment has been made. This thesis contains no material which has been accepted for the award of any other degree or diploma in any university.

Signature:

Date: 26/01/2022

Works published during the course of this thesis

Peer-reviewed journal articles:

Fox, D.C.M., Spinks, S., Barham, M., Kirkland, C. L., Pearce, M. A., Aspandiar, M., Mead, E., 2021, Working up an apatite: Enigmatic Mesoarchean hydrothermal Cu-Co-Au mineralization in the Pilbara Craton: Economic Geology, v. 116, p. 1561-1573. doi:https://doi.org/10.5382/econgeo.4842

Fox, D. C. M., Spinks, S., Pearce, M. A., Barham, M., Le Vaillant, M., Thorne, R., Aspandiar, M., Verrall, M., 2019, Plundering Carlow Castle: First Look at a Unique Mesoarchean-Hosted Cu-Co-Au Deposit: Economic Geology, v. 114, p. 1021-1031. doi:https://doi.org/10.5382/econgeo.4672

Conference presentations:

Fox D.C.M., Spinks, S., Pearce, M., Barham, M., Kirkland, C., Martin, L., Aspandiar, M., Hydrothermal Cu-Co-Au Ore Formation during the Mesoarchean: Implications for Archean Cu-Co Metallogenesis*, Goldschmidt 2020.*

Fox, D.C.M., Spinks, S., Pearce, M., Le Vaillant, M., Thorne, R., Barham, M., Kirkland, C., Aspandiar, M., The genesis of Carlow Castle: A unique Australian Cu-Co-Au deposit in the Archean Pilbara Craton, *Australasian Exploration and Geoscience Conference 2019*.

Fox, D.C.M., Spinks, S., Pearce, M., Le Vaillant, M., Thorne, R., Barham, M., Kirkland, C., Aspandiar, M., Cu-Co-Au mineralisation in the Pilbara Craton during the Mesoarchean, *Goldschmidt 2019*.

Fox, D.C.M., Spinks, S., Pearce, M., Le Vaillant, M., Thorne, R., Barham, M., Kirkland, C., Aspandiar, M., The genesis of Carlow Castle: A unique Australian Cu-Co-Au deposit in the Archean Pilbara Craton, *15th Biennial Meeting of the Society for Geology Applied to Mineral Deposits 2019*.

Fox, D.C.M., Spinks, S., Thorne, R., Aspandiar, M., Barham, M., Reduction Spheroids from the Tumblagooda Sandstone as Potential Biomarkers for the Terrestrialisation of Arthropods, *Australian Geoscience Council Convention 2018.*

Other publications:

Spinks, S. C., Pearce, M. A., Le Vaillant, M., **Fox, D.**, Tyler, I. M., Godel, B., Stromberg, J., Mead, E., White, A. J. R., 2021, The Neoarchean Conglomerate-Hosted Gold of the West Pilbara Craton, Western Australia: *Economic Geology*, v. 116, p. 629-650.

Fox, D. C. M., Spinks, S., Thorne, R., Aspandiar, M., Barham, M., Armstrong, J., Tonguc, U., Timms, N., Pearce, M. A., Verrall, M., Godel, B., Whisson, B., 2020, Mineralogy and geochemistry of atypical reduction spheroids from the Tumblagooda Sandstone, Western Australia: Sedimentology, v. 67, p. 677-698.

Noble, R., González-Álvarez, I., Reid, N., Krapf, C., Pinchand, T., **Fox, D.**, Ibrahimi, T., Cole, D., Lau, I., 2019, Coompana geochemistry – results from rapid Surface characterisation and a Deep vertical profile, *MESA*, v. 89, p. 4-14.

Spinks, S., Soerensen, C.; Thorne, R., Ryan, C., Moorhead, G., Noble, R, Pearce, M., **Fox, D.**, Hill, J., White, A., Brant, F., 2018, Geochemical and sedimentological characterization of the Proterozoic Blue Billy Formation shale-hosted Zn-Pb mineralization; Edmund Basin, Western Australia, CSIRO technical report #EP189868, 79 p.

Noble, R., Gonzalez-Alvarez, I., Reid, N., Krapf, C., Pinchard., T., Cole, D., Lau, I., **Fox, D.**, Brant, D., White, A., Klump, J., Petts, A., 2018, Regional Geochemistry of the Coompana Area, CSIRO technical report #EP187470, 105 p.

Curtin University

Authorship Agreement Form

The Curtin University Authorship, Peer Review and Publication of Research Findings Policy and Procedures[1] which references the Australian Code for the Responsible Conduct of Research[2], provides clear guidelines regarding attribution of authorship. This form is to assist researchers incapturing discussions around intended publications arising from joint work. It does not replace copyright or certification forms required by publishers.

Research

Project Title:	On the Genesis and Significance of the Archean-hosted Carlow Castle Cu-Co-Au Deposit, Pilbara Craton, Western Australia		
Project identifier (if applicable)			
Principal Investigator	Mehrooz Aspandiar		
Other named Investigator /s#	David Fox	**Role**	PhD Student
Other researcher/s#	Milo Barham	**Role**	Supervisor
	Sam Spinks	**Role**	Supervisor

Publications/Outputs – the intended outputs from the above research are identified below

Pub.#	Description (e.g., method paper)	Publication Type (Conference, journal article, etc.)
1	**Fox, D.**, Spinks, S., Pearce, M.A., Barham, M., Le Vaillant, M., Thorne, R., Aspandiar, M. and Verrall, M. (2019) Plundering Carlow Castle: First Look at a Unique Mesoarchean-Hosted Cu-Co-Au Deposit. Economic Geology 114, 1021-1031. **Published.**	Journal article
2	**Fox, D.**, Spinks, S., Barham, M., Kirkland, C.L., Pearce, M.A., Aspandiar, M., Birchall, R., and Mead, E. (2021) Working up an apatite: Enigmatic Mesoarchean hydrothermal Cu-Co-Au mineralization in the Pilbara Craton. Economic Geology 116, 1561-1573. **Published.**	Journal article
3	**Fox, D.**, Spinks, S., Barham, M., Martin, L., Liu, W., Pearce, M., Kirkland, C., Aspandiar, M. Mesoarchean oxygenation accompanied massive copper-cobalt mineralisation. **In review**.	Journal article (In review)
4	**Fox, D.**, McGee, L., Farkas, J., Payne, J., Spinks, S., Barham, M., Aspandiar, M., Copper isotopes in Archean hydrothermal systems: A	Journal article (In review)

	case study from the Mesoarchean Carlow Castle Cu-Co-Au deposit. **In review.**	

[1] https://policies.curtin.edu.au/findapolicy/#A

[2] https://www.nhmrc.gov.au/guidelines-publications/r39

Proposed order of authors

Pub .*	Author**	Corresponding? Y/N
1	1. David Fox	Y
	2. Samuel Spinks	N
	3. Mark Pearce	N
	4. Milo Barham	N
	5. Margaux Le Vaillant	N
	6. Robert Thorne	N
	7. Mehrooz Aspandiar	N
	8. Mike Verrall	N
2	1. David Fox	Y
	2. Samuel Spinks	N
	3. Milo Barham	N
	4. Chris Kirkland	N
	5. Mark Pearce	N
	6. Mehrooz Aspandiar	N
	7. Renee Birchall	N
	8. Edward Mead	N
3	1. David Fox	Y
	2. Samuel Spinks	N
	3. Milo Barham	N
	4. Laure Martin	N
	5. Weihua Liu	N
	6. Mark Pearce	N
	7. Chris Kirkland	N
	8. Mehrooz Aspandiar	N
4	1. David Fox	Y
	2. Lucy McGee	N
	3. Juraj Farkas	N
	4. Justin Payne	N
	5. Samuel Spinks	N
	6. Milo Barham	N
	7. Mehrooz Aspandiar	N

Confirmation of agreement

Author Name and Affiliation (if other than Curtin)	Author Signature	Date
1. David Fox		01/12/2021
2. Samuel Spinks (CSIRO/Teck)		06/12/2021
3. Milo Barham		02/12/2021
4. Mehrooz Aspandiar		02/12/2021
5. Chris Kirkland		02/12/2021
6. Robert Thorne (CSIRO)		10/01/2022
7. Margaux Le Vaillant (CSIRO)		01/12/2021
8. Mark Pearce (CSIRO)		10/01/2022
9. Mike Verrall (CSIRO)		07/01/2022
10. Renee Birchall (CSIRO)		10/01/2022
11. Edward Mead (Artemis Resources Ltd.)		01/12/2021

12. Laure Martin (University of Western Australia - CMCA)		13/01/2022
13. Weihua Liu (CSIRO)		02/12/2021
14. Lucy McGee (University of Adelaide)		03/12/2021
15. Juraj Farkas (University of Adelaide)		01/12/2021
16. Justin Payne (University of South Australia)		01/12/2021

11

12 **Authorship attribution**

13

Pub.	Authors	Concept and design	Acquisition of Data and method	Data Conditioning and manipulation	Analysis and Statistical method	Interpretation and Discussion	Final Approval
1	David Fox	x	x	x	x	x	x
	Samuel Spinks	x	x		x	x	x
	Mark Pearce	x	x				x
	Milo Barham	x				x	x
	Margaux Le Vaillant		x				x
	Robert Thorne					x	x
	Mehrooz Aspandiar	x				x	x
	Mike Verrall		x	x	x		x

14

Pub.	Authors	Concept and design	Acquisition of Data and method	Data Conditioning and manipulation	Analysis and Statistical method	Interpretation and Discussion	Final Approval
2	David Fox	x	x		x	x	x
	Samuel Spinks	X	x			x	x
	Milo Barham	X	x			x	x
	Chris Kirkland		x	x	x		x
	Mark Pearce	X					x
	Mehrooz Aspandiar	X					x
	Renee Birchall		X	X	X		X
	Edward Mead	x					x

15

Pub.	Authors	Concept and design	Acquisition of Data and Method	Data Conditioning and Manipulation	Analysis and Statistical method	Interpretation and Discussion	Final Approval
3	David Fox	x	x		x	x	x

	Samuel Spinks	x				x	x
	Milo Barham	x	x				x
	Laure Martin		x	x	x		x
	Weihua Liu		x		x	x	x
	Mark Pearce	x					x
	Chris Kirkland	x				x	x
	Mehrooz Aspandiar	x					x

16

Pub.	Authors	Concept and design	Acquisition of Data and Method	Data Conditioning and Manipulation	Analysis and Statistical method	Interpretation and Discussion	Final Approval
4	David Fox	x	x			x	x
	Lucy McGee		x	x	x	x	x
	Juraj Farkas		x			x	x
	Justin Payne		x	x	x		x
	Samuel Spinks	x				x	x
	Milo Barham	x				x	x
	Mehrooz Aspandiar	x				x	x

17

Abstract

Significant hydrothermal Cu-Co-Au deposits are generally restricted to Proterozoic or younger terranes, occurring overwhelmingly in sediment-hosted Cu-Co deposits. As such, the 2018 discovery of significant Cu-Co-Au mineralisation at *Carlow Castle* within a Paleo-Mesoarchean greenstone belt in the Pilbara Craton of northwest Western Australia was notable. However, little study had been conducted on the deposit previously. This thesis provides the first mineralogical, geochronological, and isotopic constraints on the formation of the Carlow Castle Cu-Co-Au deposit.

Petrographic analysis demonstrates that Cu-Co-Au mineralisation from Carlow Castle occurs within quartz-carbonate veins through heavily hydrothermally altered wall-rocks within the Regal Thrust; a regionally extensive crustal-scale thrust fault that likely acted as a critical conduit for mineralising fluids. Mineralisation is defined by two distinct ore mineral assemblages. Ore mineral Assemblage One is defined primarily by pyrite and chalcopyrite, whilst Assemblage Two is defined by the presence of cobaltite, chalcocite, and electrum. Additional minor and trace phases include pyrrhotite, uraninite, and several telluride and selenide minerals. Mineral paragenetic relationships appear to reflect an increasing sulphur fugacity defined by a transition from selenides and tellurides through to sulphosalts and subsequently base-metal sulphides. Additionally, electrum appears to be paragenetically associated with cobaltite, suggesting Au was transported simultaneously with Co and Cu; most likely via chloride complexation.

In-situ U-Pb dating of syn-mineralisation hydrothermal apatite via laser ablation ICP-MS dates ore formation to 2957 ± 67 Ma. This age makes Carlow Castle the oldest known hydrothermal Cu-Co deposit on Earth, coincident with the late stages of the formation of the proximal De Grey Superbasin (3066-2919 Ma) during post-orogenic extension and back-arc rifting related to subduction at the northwest margin of the Pilbara Craton. The hydrothermal alteration mineral assemblage of Carlow Castle is dominated by calc-silicate minerals which collectively define a classic propylitic alteration assemblage. This propylitic alteration assemblage is characteristic of ore-formation at peak temperatures of ~300°C and alkaline fluid conditions. These constraints demonstrate continuity of Cu-Co mineralisation at moderate hydrothermal conditions well into the Archean and may suggest that Archean greenstone belts globally may be prospective for analogous deposits.

Multiple sulphur isotope analysis of sulphide mineralisation from Carlow Castle reveals a conspicuous lack of 'Archean sulphur' within the mineral system, with $\Delta^{33}S$ values within a very narrow range between -0.17‰ and 0.12‰. Additionally, $\delta^{34}S$ values range between -3.4‰ and 6.1‰; with the majority of these data ranging between 2‰ and 4‰. This is consistent with an isotopically heavy seawater sulphate contribution to the ore system. The unique absence of mass-independent sulphur isotope fractionation within the system is explained through a connection to contemporaneous oxidative conditions during deposition of glacial diamictites within the Pongola Basin of South Africa around 2950 Ma with similarly attenuated $\Delta^{33}S$ signatures. Thermodynamic modelling of hydrothermal Cu and Co solubility, indicates significant metal mobilisation necessitates sulphate-stable oxidised conditions. These findings support emerging models of the evolution of the Archean atmosphere, which suggest that it was subject to periods of transient oxygenation following the evolution of oxygenic photosynthesis.

This thesis presents the first application of Cu isotope analysis to an Archean Cu ore deposit. Analysis of 19 Archean primary Cu sulphide ore samples and 11 secondary supergene Cu ore samples reveal that primary ore samples display light isotopic fractionation ($\delta^{65}Cu$ = -0.80 to 0.00‰) and supergene Cu ore samples are comparably isotopically heavy ($\delta^{65}Cu$ = -0.50 to 0.62‰). Across primary Cu ore samples a Rayleigh fractionation process is recorded and modelled, defined by evolution of the hydrothermal system toward isotopically heavy and Cu-poor compositions. This is coeval with a decline in alteration temperature. This modelling also supports a mafic igneous source of ore metals, consistent with other significant hydrothermal Co-rich deposits globally. Relatively limited heavy isotopic fractionation within supergene Cu ore samples is explained through in-situ oxidative weathering of vein-hosted Cu sulphides, with minimal Cu transport. These findings demonstrate that Cu isotope analysis may be a valuable tool to understand ore genesis in Archean hydrothermal Cu deposits.

Acknowledgements

I owe a great deal of gratitude to so many people whose help and support has been invaluable throughout my PhD. It goes without saying that I could not have completed this project without them.

I am indebted to my supervisors Sam Spinks, Milo Barham, and Mehrooz Aspandiar for their guidance, encouragement, dedication, and patience through these last few years. You have been there every step of the way throughout my scientific journey and for that I am immensely grateful, on a professional and personal level.

This project has offered me an incredible opportunity to meet and learn from a lot of exceptional people, not all of whom I am able to acknowledge here appropriately for the sake of keeping this list of acknowledgements to a reasonable length. I am so grateful to Lucy McGee, Juraj Farkas, and Justin Payne for hosting me in Adelaide and facilitating the copper isotope analysis, despite what at times seemed like endless analytical and COVID-related issues. I would like to thank Mike Verrall for his analytical assistance on many occasions, his patient tutelage, and for humouring my many questions. I am also deeply thankful to everyone at CSIRO who has helped to facilitate my research, including Rob Hough; Sandi Occhipinti; Mark Pearce; Renee Birchall; Rob Thorne; Margaux Le Vaillant; and many others. Additionally, Derek Winchester provided excellent assistance with sample preparation, which enabled all my analyses.

I am grateful to Chris Kirkland for his help with overcoming the challenges posed by apatite geochronology and for graciously inviting me to join the Timescales of Mineral Systems team. Laure Martin and Matvei Aleshin are thanked for their diligent help with sulphur isotope analysis, which included analytical complications and several late nights and early mornings. Julian Menuge, Steve Hollis, Sean Johnson, and the SGA were very generous in hosting me in Ireland on what was an educational and incredibly memorable pre-conference field trip.

I was supported through this project with a Curtin University Research Training Program scholarship and a CSIRO Mineral Resources postgraduate student scholarship. Additionally, generous support for field work, sample collection, and analysis was provided by Artemis Resources Pty Ltd.

I am very appreciative of all the close friends that I have made throughout my PhD. Your company has made this process so much richer than you may know.

Finally, I must thank my family for their endless love and support during my PhD and education more generally, even when it seemed to become all-consuming.

Table of Contents

List of Tables

List of Figures

Chapter 1

Introduction

The utilisation of Earth's mineral resources has been vital to the industrial development of civilisation. However, as technology has evolved, the diversity of mineral resources utilised by the global economy has grown substantially and the relative importance of individual mineral commodities has varied significantly Schulz, DeYoung Jr, Seal Ii, and Bradley (2017). As the global economy evolves and the transition from fossil fuel to renewable energy sources continues, many mineral commodities, of previously niche importance, are forecast to become critically important (Arrobas, Hund, McCormick, Ningthoujam, & Drexhage, 2017; Schulz et al., 2017). Because of the variable nature of many renewable energy sources, a necessity for battery storage has been identified in order to enable this renewable energy transition (Leonard, Michaelides, & Michaelides, 2020). As such, several 'battery metals'; such as Co, Li, Ni, and Cu have emerged as potentially critical to the future economy due to their primary importance in battery production (Mudd et al., 2018). A significant increase in global demand for these battery metals is widely projected, necessitating the discovery of new sources to supply these metals (Arrobas et al., 2017; Mudd et al., 2018). In the case of cobalt, the importance of discovering new deposits is compounded by widely publicised supply risks (Horn et al., 2021; Slack, Kimball, & Shedd, 2017a). Exploration efforts for these ore deposits can be optimised through understanding the full range of geological processes that produce them (McCuaig, Hronsky, Kelley, & Golden, 2014). The development of more informed exploration strategies and novel exploration techniques for these ore deposits is especially important given the declining discovery rates for new deposits of all varieties (Groves & Santosh, 2015). To understand these ore-forming processes, this thesis presents a multifaceted analysis of *Carlow Castle*; a distinctive Cu-Co-Au deposit in the Pilbara Craton in north-western Western Australia.

Carlow Castle Cu-Co-Au was chosen as the subject of this study as it represents a unique style of hydrothermal vein-hosted Cu-Co-Au mineralisation within a Paleo-Mesoarchean greenstone belt, which had not previously been subject to any detailed study. As the vast majority of significant Cu-Co deposits occur in terranes of Proterozoic age or younger (Petavratzi et al., 2019; Slack et al., 2017a), Carlow Castle presents an opportunity to understand the ore-forming

processes required to produce significant hydrothermal Cu-Co mineralisation in Archean greenstone belts. Understanding these ore-forming processes could be important in more fully developing the understanding of Cu-Co deposit genesis, particularly with regard to the geological setting and temporal distribution of hydrothermal Cu-Co deposits. This is particularly relevant to broad-scale prospectivity analysis for Cu-Co mineralisation, where future exploration for Cu-Co mineralisation may need to look toward unconventional settings to discover the next generation of deposits. This thesis provides the first analysis of Carlow Castle Cu-Co-Au deposit's mineralisation and the first insights into the key ore-forming processes responsible for its unique style of mineralisation.

1.1 Background

1.1.1 Carlow Castle Cu-Co-Au deposit

Carlow Castle copper-cobalt-gold (Cu-Co-Au) deposit is situated in the Pilbara Craton of Western Australia and has an inferred resource estimate of 14.3 million tonnes (Mt) at 0.4% Cu, 0.05% Co, and 0.7 g/t Au as of May 2021, updated from 8 Mt at 0.6% Cu, 0.08% Co, and 1.6 g/t Au as of 2019 (Artemis Resources Limited, 2021). Carlow Castle was first discovered in 1872 and sporadically mined on a small scale throughout the late 19th and early 20th centuries (Hickman, 1983). However, significant underlying Cu-Co-Au mineralization was discovered during drilling conducted in 2017 (Artemis Resources Limited, 2017). Given the recency of this discovery, no substantive research had been conducted on the nature and origin of Carlow Castle. The only existing references to Carlow Castle in the literature prior to this project were passing mentions in reviews and other literature focussed on the Geology of the Pilbara Craton more broadly (Hickman, 2016; Hickman, Huston, Van Kranendonk, & Smithies, 2006; Ruddock, 1999b). Carlow Castle occurs in a series of steeply dipping veins through the Ruth Well and Nickol River Formations (Figure 1.1), a sequence of Paleoarchean mafic volcanic and marine sedimentary rocks, proximal to the Regal Thrust; a crustal-scale orogenic thrust fault (Hickman, 1983; Ruddock, 1999b). As such, it had been suggested that Carlow Castle may have been an orogenic Cu-Co-enriched Au deposit (Hickman, 2016). However, whilst Carlow Castle does occur through an orogenic structure (Regal Thrust); providing a maximum mineralisation age, its temporal relationship to orogenesis was largely unknown due to the lack of absolute age constraints. As such, the ore-forming tectonic event that produced Carlow Castle was largely unconstrained.

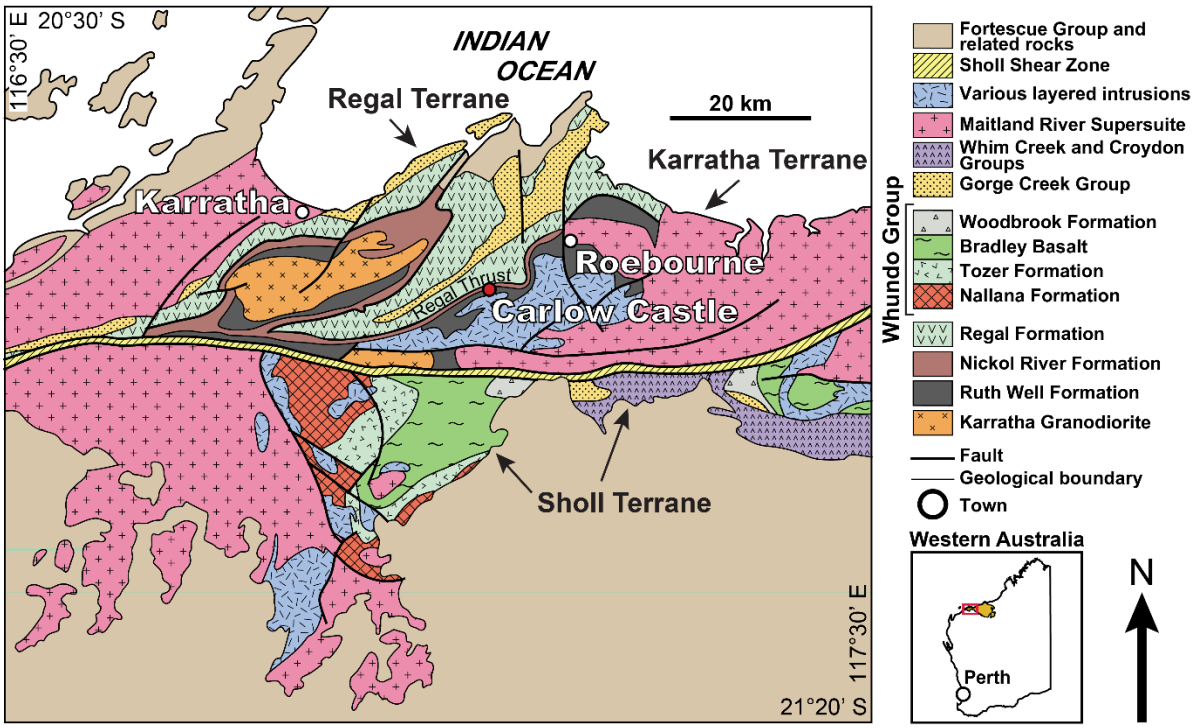

Figure 1.1 - Geologic map of the northwest Pilbara Craton. The Pilbara Craton is highlighted in orange within the inset map. Modified after Van Kranendonk, Hickman, Smithies, Nelson, and Pike (2002).

1.1.2 Formation of the West Pilbara Superterrane

Carlow Castle occurs within the West Pilbara Superterrane, an accreted tectonic unit composed of several Paleo-Mesoarchean terranes. The West Pilbara Superterrane is sub-divided into the Karratha Terrane (3280-3236 Ma), Nickol River Basin (3220-3160 Ma), Regal Terrane (3200-3160 Ma), Sholl Terrane (3130-3093 Ma), and portions of the Elizabeth Hill Supersuite (3068-3066 Ma) (Hickman, 2016). Within this framework, Carlow Castle Cu-Co-Au deposit is located primarily through the Karratha Terrane and Nickol River Basin. However, its structurally-hosted nature within the Regal Thrust, which defines the boundary between the Regal and Karratha Terranes, complicates this slightly. The oldest of these terranes; the Karratha Terrane most likely represents a rifted portion of the early Paleoarchean Pilbara Craton, which separated from the East Pilbara Terrane around 3280 Ma during a transition from vertical tectonics to more modern-style horizontal tectonics (Hickman, 2021; Hickman et al., 2006; Hickman & Van Kranendonk, 2012). During this period of rifting, the Nickol River Basin formed on a passive margin at the edge of the rifted Karratha Terrane, hosting a sedimentary succession composed predominantly of shale, marine carbonates, and banded iron formations (Hickman, 2012; Kiyokawa, Taira, Byrne, Bowring, & Sano, 2002). As a result of

this period of extension, the Central Pilbara Basin developed as a rift basin between the Karratha Terrane and the East Pilbara Terrane; composed predominantly of basaltic oceanic crust now represented as the Regal Terrane within the West Pilbara Superterrane (Hickman, 2004b; Hickman, 2016). A renewed period of convergence between the Karratha and East Pilbara Terranes, potentially caused by collision of the Karratha Terrane with an unidentified tectonic plate to the northwest of the Pilbara Craton, initiated from 3160 Ma causing the closure of the Central Pilbara Basin (Hickman, 2016). This renewed convergence also produced the Sholl Terrane as a volcanic oceanic island arc, during ocean-ocean convergence and development of a subduction zone within the Central Pilbara Basin from 3130-3093 Ma (Hickman & Van Kranendonk, 2012). Convergence continued until ~3070 Ma, when it culminated in the Prinsep Orogeny with the accretion of the Nickol River Basin and Karratha, Regal, and Sholl terranes into the West Pilbara Superterrane due to collision with the East Pilbara Terrane (Hickman, 2016; Hickman et al., 2006). During the Prinsep Orogeny, the Regal Terrane was thrust over the Karratha Terrane and Nickol River Basin along the Regal Thrust; the host structure of Carlow Castle (Van Kranendonk, Smithies, Hickman, Wingate, & Bodorkos, 2010). This orogenic event was also associated with the intrusion of the Elizabeth Hill granitic Supersuite. Hickman (2016) interpreted there to be a probable genetic relationship to the Prinsep Orogeny between Carlow Castle and other deposits hosted within the Regal Thrust. However, Hickman et al. (2006) previously noted that an absolute temporal relationship between this mineralisation and the Prinsep Orogeny had not been established.

The Prinsep Orogeny and accretion of the West Pilbara Superterrane was followed by a significant period of crustal extension and the formation of the De Grey Superbasin (3066-2919 Ma) (Hickman, 2016). The formation of the De Grey Superbasin initiated with a protracted period of post-orogenic relaxation and subsidence, allowing for the formation of the Gorge Creek Basin (3066-3015 Ma) within the De Grey Superbasin as a shallow water epicontinental basin over most of the Pilbara Craton (Hickman, 2016, 2021). Sedimentation within the Gorge Creek Basin was dominated by deposition of sandstones, conglomeratic units, and carbonaceous shales in addition to banded iron formation and cherts (Van Kranendonk et al., 2006). This was followed by the formation of the Whim Creek (3009-2991 Ma) and Mallina (3015-2931 Ma) basins as later constituents of the De Grey Superbasin. Interpretations about the tectonic setting responsible for the development of the Whim Creek and Mallina basins have varied, with the key difference relating to whether basin formation was contemporaneous

with proximal subduction at the northwest margin of the Pilbara Craton. The first model proposed that basin formation was contemporaneous with subduction and that the Whim Creek Basin represents a continental volcanic arc, composed of volcanic, volcaniclastic, and intrusive rocks, whilst the Mallina Basin to the southeast represents a back-arc basin dominated by a thick clastic sedimentary succession (Hickman, 2012, 2016, 2021; Hickman, Smithies, & Tyler, 2010). The progressive south-eastward younging of granite ages throughout the Pilbara Craton has been invoked as evidence of subduction at the northwest margin of the Pilbara Craton (Hickman, 2016; Hickman et al., 2010). Conversely, it has been proposed that these basins formed due to continental rifting (Van Kranendonk et al., 2006; Van Kranendonk, Smithies, Hickman, & Champion, 2007; Van Kranendonk et al., 2010). It is suggested that granitic magmatism was a product of an influx of mantle material beneath the craton due to the break-off of the slab that was previously subducted from 3130 Ma (Van Kranendonk et al., 2007). Nonetheless, it is generally agreed that this long-lived period of extension ended with the beginning of the North Pilbara Orogeny from 2955-2919 Ma (Hickman, 2016, 2021; Hickman & Van Kranendonk, 2012; Van Kranendonk et al., 2006; Van Kranendonk et al., 2007; Van Kranendonk et al., 2010). This was most likely caused by continued northwest-southeast convergence and ongoing subduction (Hickman, 2016, 2021). Convergence was associated with significant compressional deformation across the West Pilbara Superterrane, Mallina Basin, and portions of the East Pilbara Terrane, along with intrusive magmatism of the Sisters Supersuite through the Whim Creek and Mallina Basins and the East Pilbara Terrane (2954-2919 Ma) (Hickman, 2016, 2021; Van Kranendonk et al., 2007). The North Pilbara Orogeny represents the last period in the development of the northwest Pilbara Craton of probable relevance to Carlow Castle Cu-Co-Au deposit's formation.

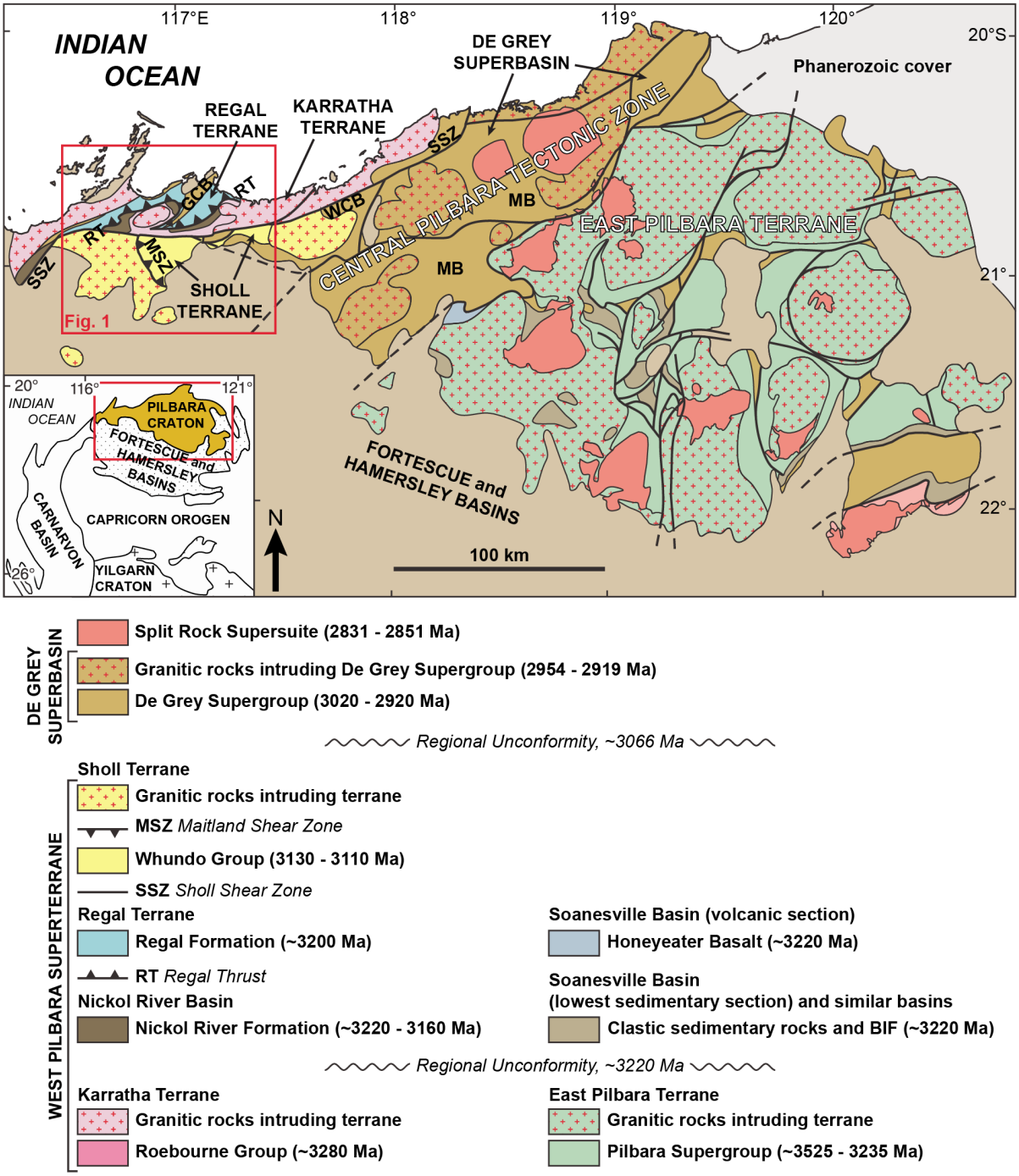

Figure 1.2 - Geological map of the Pilbara Craton, modified after Hickman (2016). MB = Mallina Basin, WCB = Whim Creek Basin, GCB = Gorge Creek Basin. Note that the extent of the area of the northwest Pilbara Craton within Figure 1.1 is indicated.

1.1.3 Hydrothermal copper-cobalt deposits

Generally, the occurrence of Co mineralisation with grades sufficient to be considered economically viable for primary Co extraction are relatively rare (Hitzman, Bookstrom, Slack, & Zientek, 2017). The only ore deposit on Earth where Co is currently mined as a primary

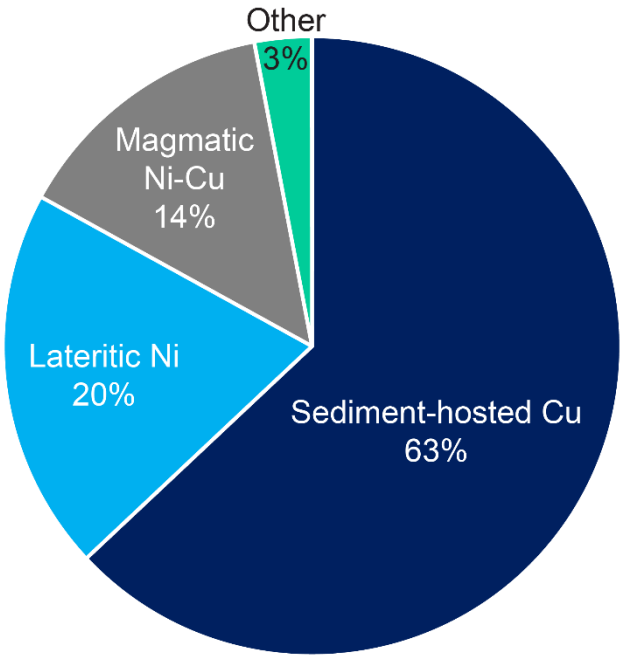

Figure 1.3 - Cobalt production by ore deposit mineralisation style (Petavratzi, Gunn, & Kresse, 2019).

product is Bou Azzer in Morocco; a Neoproterozoic polymetallic vein-hosted deposit with a Co grade of ~1% in 100,000 tonnes of ore (Bouabdellah, Maacha, Levresse, & Saddiqi, 2016; Horn et al., 2021). Instead, Co is typically extracted as a by-product of Cu or Ni mining (Petavratzi et al., 2019; Slack et al., 2017a). Stratiform sediment-hosted deposits are by far the most significant global source of Co; accounting for 63% of global Co production, followed by Ni-Co laterite deposits (20%), magmatic polymetallic sulphide deposits (14%), and other minor deposits (3%) (Figure 1.3; Petavratzi et al., 2019). However, in terms of total assessed recoverable resources, laterites are the most significant deposits, accounting for 41.7% of global Co resources, followed by sediment-hosted (39%), iron oxide copper gold (IOCG) (10.9%), magmatic sulphide (7%), volcanogenic massive sulphide (VMS) (0.8%), and various other deposits (0.8%) (Mudd, Weng, Jowitt, Turnbull, & Graedel, 2013). The occurrence of Carlow Castle as structurally controlled vein-hosted mineralisation suggests a probable hydrothermal origin (Ruddock, 1999b). As such, Carlow Castle bears little similarity to a lateritic or magmatic sulphide deposit and is more analogous to the sediment-hosted, IOCG, VMS, or other minor Co-bearing styles of hydrothermal mineralisation.

Sediment-hosted Cu deposits commonly occur at the boundary between underlying oxidised terrestrial siliciclastic rocks and overlying reduced organic-rich marine sedimentary rocks within a basin sedimentary sequence (Hitzman, Selley, & Bull, 2010). Among sediment-hosted Cu deposits, the Kupferschiefer of Central Europe and Central African Copperbelt are by far the two largest mining districts, with each containing >200 Mt of total Cu (Hitzman, Kirkham, Broughton, Thorson, & Selley, 2005). These mining districts represent classic type-localities of sediment-hosted Cu mineralisation (Taylor et al., 2013). Several schemes to sub-divide types of sediment-hosted Cu deposits have been proposed based on various deposit characteristics.

However, these ore systems are generally defined by several common characteristics; including (i) Cu-rich mafic volcanic or immature mafic-rich siliciclastic sediments to act as a metal source, (ii) oxidised, near neutral pH basinal brines to transport dissolved ore metals, (iii) preferential migration of basinal brines due to sediment dewatering, (iv) physical traps for ore-bearing fluids, e.g., impermeable beds or structures, and (v) reduced organic-rich or pyritic sedimentary rocks to induce in-situ reductive ore precipitation from an oxidised ore-bearing brine (Figure 1.3; Taylor et al., 2013).

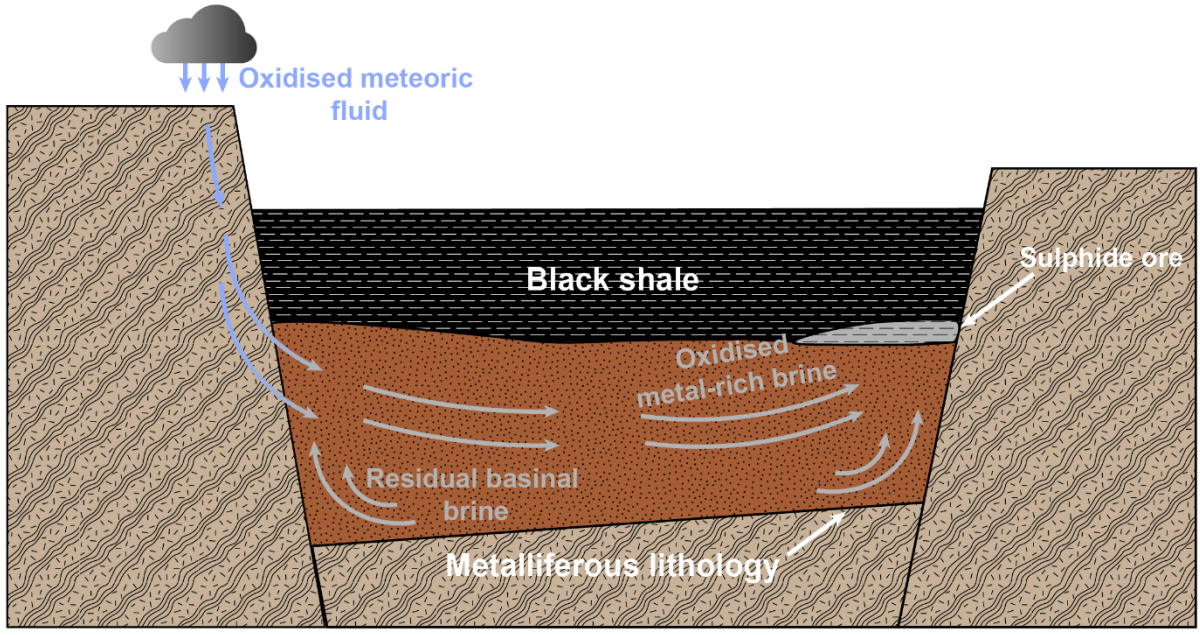

Figure 1.4 - Generalised basin-scale model for a sediment-hosted Cu deposit, modified after Brown (2014); Hitzman et al. (2010).

Cox, Lindsey, Singer, and Diggles (2003) initially proposed to sub-divide these sediment-hosted Cu deposits based on characteristics of their host lithologies and this scheme was adopted with slight modifications by Taylor et al. (2013) and Hayes, Cox, Bliss, Piatak, and Seal Ii (2015). This scheme divides deposits into (i) reduced-facies Cu deposits (shale-hosted), (ii) sandstone Cu deposits, and (iii) red bed Cu deposits. However, Kirkham (1989) and Hitzman et al. (2005) preferred to divide these deposits based on their basinal setting into Kupferschiefer-type and red bed-type deposits. Under this scheme, most significant deposits are classified as Kupferschiefer-type, with red bed-type deposits being comparably minor in tonnage (Hitzman et al., 2005). Unlike Carlow Castle, the occurrence of sediment-hosted Cu-Co deposits in Archean terranes is extremely rare (Brown, 2014). This is generally accepted to reflect the importance of oxidised basinal fluids to mobilise metals in sediment-hosted Cu

deposits, and the lack of available oxidised fluids within crustal systems during the widespread anoxia that characterised most of the Archean (Figure 1.4; Brown, 2014; Hitzman et al., 2010).

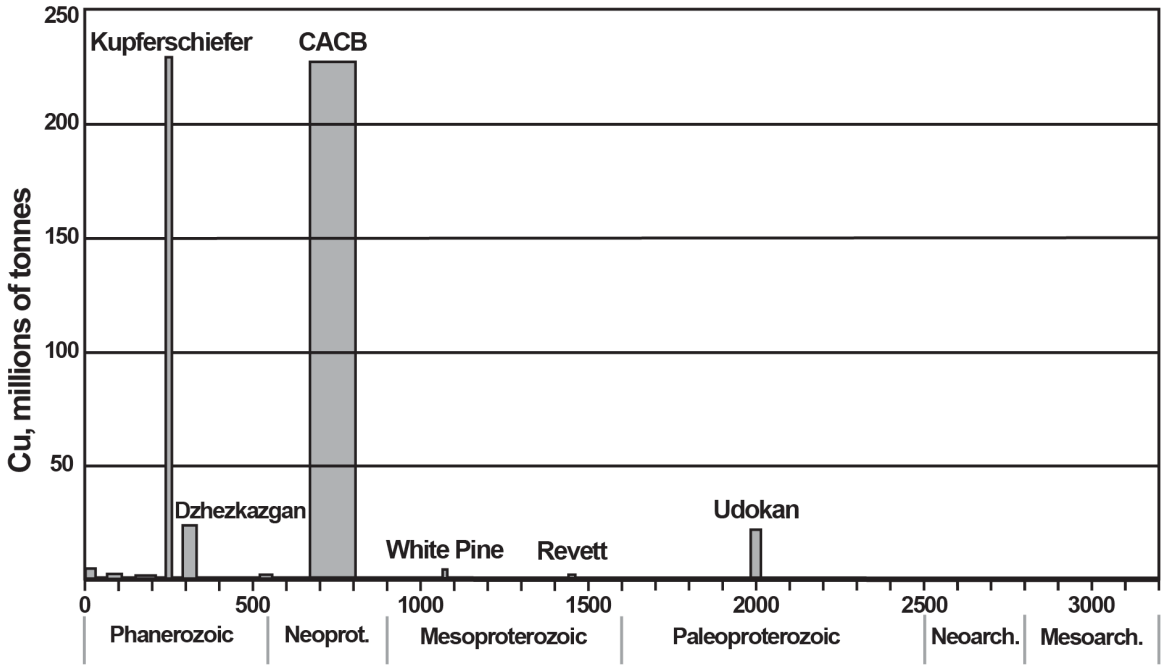

Figure 1.5 - Occurrence of sediment-hosted Cu deposits through geological time. Note the lack of Archean examples, reflecting the lack of available oxidised basinal fluids to mobilise base metals. CACB = Central African Copper Belt. Modified after Hitzman et al. (2010).

Aside from sediment-hosted Cu deposits, Co-bearing examples of many hydrothermal mineralisation styles are relatively rare. Amongst IOCG deposits, Olympic Dam (0.02% Co) and Ernest Henry (0.05% Co) deposits in Australia contain appreciable Co concentrations. However, Co is not currently produced from either of these deposits and Co-rich IOCG deposits are generally uncommon (Petavratzi et al., 2019; Slack et al., 2017a). Cobalt-bearing volcanogenic massive sulphide (VMS) deposits are similarly rare, though some pelitic-mafic-type (Besshi-type) are relatively Co-rich; most notably Windy Craggy, Canada (0.66% Co) and Outokumpu, Finland (0.25% Co) (Franklin, Gibson, Jonasson, & Galley, 2005; Hitzman et al., 2017). These mineralisation styles differ significantly from the previously discussed sediment-hosted deposits as they represent magmatic-hydrothermal systems in quite distinct geodynamic settings, with variably significant magmatic fluid input and ore formation at significantly higher temperatures (Franklin et al., 2005; Williams et al., 2005). Other, more obscure and relatively minor, Co-rich styles of mineralisation include metasedimentary rock-hosted Co-Cu-

Au, polymetallic Co-rich vein deposits (also known as five-element vein deposits), and black shale-hosted Ni-Cu-Zn-Co deposits (Petavratzi et al., 2019; Slack et al., 2017a). Amongst metasedimentary rock-hosted Co-Cu-Au deposits, the Blackbird deposit in the Idaho Cobalt Belt represents the most significant example (Bookstrom, 2013). These deposits are poorly understood with a range of different genetic models proposed. Metasedimentary rock-hosted Co-Cu-Au deposits are typically Proterozoic, with an epigenetic origin, and a connection to proximal magmatism in many deposits has been suggested along with a possible relationship between this deposit class and Co-rich IOCG deposits (Slack et al., 2013). Polymetallic Co-rich vein deposits are a diverse group of deposits that occur as structurally-hosted Co (± Ag, Ni, As, Bi) bearing veins through igneous and sedimentary rocks of maximum Proterozoic age (Kissin, 1992; Lefebure, 1996). These deposits are generally mineralogically complex and are believed to reflect multiple distinct stages of mineralisation, notable examples include deposits of the Bou Azzer district of Morocco and the Cobalt district of Ontario, Canada (Ahmed, Arai, & Ikenne, 2009; Kissin, 1992; Slack et al., 2017a). Finally, black shale-hosted Ni-Cu-Zn-Co deposits are relatively rare and occur as accumulations of significant base-metal mineralisation in, typically, Proterozoic organic-rich shales (Petavratzi et al., 2019; Slack et al., 2017a). Talvivaara in Finland is the most significant Co-bearing example (Figure 1.5) and is believed to have formed due to a multistage mineralisation process during diagenesis and regional metamorphism (Loukola-Ruskeeniemi & Lahtinen, 2013; Slack et al., 2017a).

Carlow Castle appears to bear some broad similarities to the deposits of the polymetallic Co-rich vein and metasedimentary rock-hosted Co-Cu-Au deposits. However, the rarity of comparable Archean-hosted examples of these deposits classes is striking (Kissin, 1992; Slack et al., 2013; Slack et al., 2017a); especially given the significant endowment of Archean terranes with hydrothermal and magmatic ore deposits of other varieties (Goldfarb, Bradley, & Leach, 2010). Much like in the case of the sediment-hosted Cu-Co deposits, the temporal distribution of these Co-rich hydrothermal ore deposits is most likely a reflection of the strongly redox-controlled nature of Cu and Co solubility in hydrothermal systems at low to moderate temperatures (Rose, 1989). Similar temporal patterns are also observable for other base-metal deposits with strong redox controls (Goldfarb et al., 2010). As such, the scarcity of these deposits in the Archean most likely reflects the relative immobility of Cu and Co in reduced hydrothermal fluids and the relative rarity of oxidised near-surface environments during the Archean to supply oxidised ore fluids to hydrothermal systems. In this regard, the

availability of oxygen to near surface environments imparts a fundamental control on hydrothermal Cu-Co mineralisation through geological time. Whilst acidic (pH <5 at 150°C) dissolution of metals provides an alternative mechanism for Cu-Co dissolution within reduced fluids, the rarity of significant Archean magmatic-hydrothermal Cu-Co deposits implies that this pathway is of comparably limited geological significance. This pathway is also explored in subsequent chapters within this thesis. Therefore, the occurrence of Carlow Castle in a Paleo-Mesoarchean greenstone belt makes it a notable outlier.

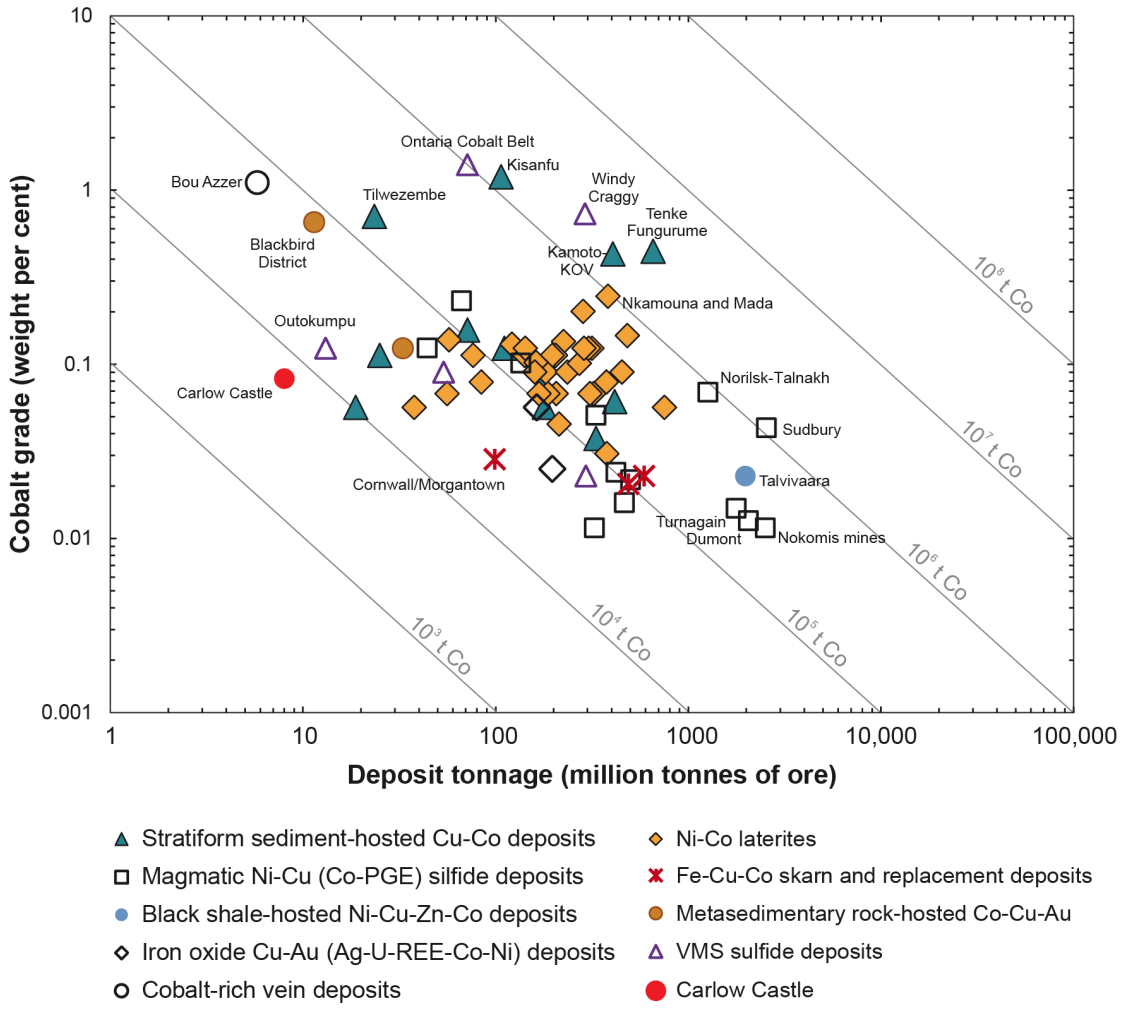

Figure 1.6 - Grade-tonnage graph for terrestrial Co-bearing deposits. Modified after Petavratzi et al. (2019) and Slack et al. (2017a).

1.2 Research Objectives

The principal objective of this project was to provide a foundational understanding of the Carlow Castle ore system and its key genetic processes. A secondary aim of the project was to establish a methodology for Cu isotope analysis of Cu sulphide minerals in collaboration with

the Metal Isotopes Group at the University of Adelaide and use the Carlow Castle deposit as a case study area for this Cu isotope analytical methodology. This serves the dual purpose of improving the currently limited understanding of Archean Cu isotope systematics whilst providing further insights into the genesis of the Carlow Castle ore deposit.

These objectives were to be achieved through the following research goals:

1. Characterise the nature and style of Carlow Castle Cu-Co-Au deposit's mineralisation.
2. Determine the age of Carlow Castle and its temporal relationship to major tectonic events during the formation of the Pilbara Craton.
3. Characterise the multiple sulphur isotope composition of Carlow Castle, to inform about potential ore-forming processes and the ore system's sulphur source.
4. Develop a robust method for Cu isotope analysis of Cu sulphides in collaboration with the Metal Isotopes Group, University of Adelaide.
5. Characterise the Cu isotope signature of Carlow Castle Cu-Co-Au deposit, as a test of the applicability of Cu isotope analysis to understanding Archean hydrothermal systems and to inform about potential metal source and ore-forming processes.

1.3 Thesis structure

This thesis presents a compilation of published papers and manuscripts prepared for publication in peer-review academic journals. As such, each of these papers represents a distinct aspect of this thesis, attempting to address the above-listed aims and objectives of the research project. However, because this thesis essentially represents a compilation of several smaller case studies there is some unavoidable repetition of content between different thesis chapters due to need for these chapters to be understood independently. Chapters Two and Three are published in peer-reviewed journals and are reproduced in this thesis with minor modifications. Chapters Four and Five have been submitted to academic journals and are currently under review.

Chapter Two – Plundering Carlow Castle: First Look at a Unique Mesoarchean-Hosted Cu-Co-Au Deposit

This chapter provides the first analysis of Carlow Castle Cu-Co-Au deposit and a foundation for subsequent studies of the deposit. This work characterises Carlow Castle as a hydrothermal Cu-Co-Au deposit, with ore mineralisation occurring through a series of quartz-carbonate veins, hosting Cu and Co sulphides. Two distinct ore minerals assemblages are identified, with the first being composed primarily of pyrite and chalcopyrite and the second being composed

primarily of chalcocite, cobaltite, and electrum. The mineralisation occurs through a heavily brecciated portion of the Roebourne Group adjacent to the Regal Thrust; a regionally significant crustal-scale orogenic thrust fault. The chapter also provides a comparison of Carlow Castle to other styles of Cu-Co mineralisation, noting the relative rarity of comparable hydrothermal Cu-Co deposits in Archean terranes. Finally, it is suggested that Carlow Castle is of probable Archean age, though the need for absolute age constraints is acknowledged.

Chapter Three – Working up an Apatite: Enigmatic Mesoarchean Hydrothermal Cu-Co-Au Mineralization in the Pilbara Craton

Chapter Three establishes the first absolute age constraints on Carlow Castle Cu-Co-Au deposit's formation using in-situ U-Pb dating of hydrothermal apatite that are interpreted to have formed coeval with mineralisation. Analyses of these apatite grains in-situ gave a discordia age of 2957 ± 67 Ma, making Carlow Castle among the oldest Cu-Co deposits on Earth. This age suggests that Carlow Castle significantly post-dates its orogenic host structure, the Regal Thrust, which formed around 3070 Ma during the Prinsep Orogeny. Instead, ore formation at Carlow Castle is contemporaneous with the rifting of the De Grey Superbasin following orogenesis. A potential connection is also drawn to base-metal ore formation within the proximal Whim Creek Basin around 2955 Ma. Additionally, characterisation of the alteration mineral assemblage of Carlow Castle indicates that it is characteristic of a classic propylitic alteration assemblage; dominated by chlorite, actinolite, epidote, calcite, quartz, and K-feldspar. This is suggestive of peak temperatures of hydrothermal ore formation of ~300°C and neutral-alkaline pH ore fluids.

Chapter Four - Mesoarchean oxygenation accompanied massive copper-cobalt mineralization

In chapter Four, analysis of the multiple sulphur isotope signature of mineralisation from Carlow Castle is provided through in-situ analysis of chalcopyrite, pyrite, and pyrrhotite via secondary-ion mass spectrometry. This sulphide mineralisation displays $\delta^{34}S$ values between -3.4‰ and 6.1‰ and $\Delta^{33}S$ values between -0.17‰ and 0.12‰. These $\Delta^{33}S$ data are consistent with processes of mass-dependent sulphur fractionation, with no contamination from supracrustal 'Archean sulphur' which displays large magnitude mass-independent sulphur fractionation evident in $\Delta^{33}S$ values greater than 0.2‰ and less than -0.2‰. However, paradoxically the $\delta^{34}S$ signature is not consistent with a mantle sulphur source ($\delta^{34}S = 0 \pm 2$‰).

In this regard, Carlow Castle is unique amongst Archean hydrothermal ore deposits. Carlow Castle is contemporaneous with well-established oxidative conditions at ~2950 Ma, which potentially drove Earth's first major glaciation and attenuated $\Delta^{33}S$ values in the Archean sedimentary sulphur isotope record. As such, it is suggested that the genesis of Carlow Castle may have been associated with this brief period of increased atmospheric oxygen concentration. This is also supported by thermodynamic modelling demonstrating the importance of oxidised fluids to mobilise Cu and Co at physicochemical conditions consistent with ore formation, as established in Chapter Three.

Chapter Five - Copper isotopes in Archean hydrothermal systems: A case study from the Mesoarchean Carlow Castle Cu-Co-Au deposit

Chapter Five provides an analysis of Carlow Castle Cu-Co-Au deposit utilising Cu isotope geochemistry of the deposit's primary Cu sulphide ore and overlying supergene Cu-bearing minerals. This study serves the dual purposes of constraining key genetic processes in the formation of Carlow Castle Cu-Co-Au deposit whilst also addressing a key gap in the current understanding of Cu isotopic analysis in ore deposits by providing the first Cu isotope analysis of an Archean Cu ore deposit. The primary sulphide ore from Carlow Castle displays lightly fractionated $\delta^{65}Cu$ values ranging between -0.80‰ to 0.00‰ whilst supergene Cu mineralization is slightly isotopically heavier, ranging between -0.50‰ to 0.62‰. The light isotopic fractionation in primary sulphide mineralization demonstrates fractionation beyond bulk silicate Earth compositions, controlled primarily by Rayleigh-type fractionation driven by preferential ^{63}Cu precipitation during ore formation. This process is modelled, and a Rayleigh fractionation model is derived from Cu grade (ppm) and isotopic data of analysed samples. From this model, a mafic igneous source is suggested as the most likely Cu source for ore metals in Carlow Castle. The limited positive isotopic fractionation of the supergene samples analysed in this study suggests limited redox cycling of Cu, this is interpreted to reflect in-situ oxidation of vein-hosted Cu sulphides to form this supergene Cu mineralisation rather than significant Cu transport and enrichment necessary to form significant supergene isotopic fractionation.

Chapter Six – Synthesis and conclusions

Chapter Six is the final chapter of this thesis and provides a synthesis of the findings of the preceding chapters. These findings are developed into a mineral systems model for Carlow

757 Castle Cu-Co-Au deposit. Additionally, the implications of this research are discussed, along
758 with discussion of the limitations of the current findings and outlook for further research.

1.4 References

Ahmed, H. A., Arai, S., & Ikenne, M. (2009). Mineralogy and Paragenesis of the Co-Ni Arsenide Ores of Bou Azzer, Anti-Atlas, Morocco. *Economic Geology, 104*(2), 249-266.

Arrobas, D. L. P., Hund, K. L., McCormick, M. S., Ningthoujam, J., & Drexhage, J. R. (2017). *The Growing Role of Minerals and Metals for a Low Carbon Future*. Retrieved from Washington, D.C.: http://documents.worldbank.org/curated/en/207371500386458722/The-Growing-Role-of-Minerals-and-Metals-for-a-Low-Carbon-Future

Artemis Resources Limited. (2017). Cobalt Update - Carlow Castle Project [Press release]. Retrieved from https://artemisresources.com.au/investors-relations/announcements

Artemis Resources Limited. (2021). June 2021 Quarterly Report [Press release]. Retrieved from https://wcsecure.weblink.com.au/pdf/ARV/02400741.pdf

Bookstrom, A. A. (2013). The Idaho cobalt belt. *Northwest Geology, 42*, 149-162.

Bouabdellah, M., Maacha, L., Levresse, G., & Saddiqi, O. (2016). The Bou Azzer Co–Ni–Fe–As(±Au ± Ag) District of Central Anti-Atlas (Morocco): A Long-Lived Late Hercynian to Triassic Magmatic-Hydrothermal to Low-Sulphidation Epithermal System. In M. Bouabdellah & J. F. Slack (Eds.), *Mineral Deposits of North Africa* (pp. 229-247). Cham: Springer International Publishing.

Brown, A. C. (2014). Low-Temperature Sediment-Hosted Copper Deposits. In K. Turekian & H. Holland (Eds.), *Treatise on Geochemistry* (2nd ed., Vol. 13, pp. 251-271). Oxford: Elsevier Science.

Cox, D. P., Lindsey, D. A., Singer, D. A., & Diggles, M. F. (2003). *Sediment-hosted copper deposits of the world: Deposit models and database* (2003-107). Retrieved from http://pubs.er.usgs.gov/publication/ofr2003107

Franklin, J. M., Gibson, H. L., Jonasson, I. R., & Galley, A. G. (2005). Volcanogenic Massive Sulfide Deposits. In J. W. Hedenquist, J. F. H. Thompson, R. J. Goldfarb, & J. P. Richards (Eds.), *Economic Geology One Hundredth Anniversary Volume* (pp. 523-560). Littleton, Colorado: Society of Economic Geologists.

Goldfarb, R. J., Bradley, D. W., & Leach, D. L. (2010). Secular Variation in Economic Geology. *Economic Geology, 105*(3), 459-465.

790 Groves, D. I., & Santosh, M. (2015). Province-scale commonalities of some world-class gold
791 deposits: Implications for mineral exploration. *Geoscience Frontiers, 6*(3), 389-399.
792 doi:https://doi.org/10.1016/j.gsf.2014.12.007
793 Hayes, T. S., Cox, D. P., Bliss, J. D., Piatak, N. M., & Seal Ii, R. R. (2015). *Sediment-hosted*
794 *stratabound copper deposit model* (2010-5070M). Retrieved from Reston, VA:
795 http://pubs.er.usgs.gov/publication/sir20105070M
796 Hickman, A. H. (1983). *Geology of the Pilbara Block and its environs / by Arthur H. Hickman*.
797 Perth [W.A.]: Geological Survey of Western Australia.
798 Hickman, A. H. (2004b). Two contrasting granite−greenstone terranes in the Pilbara Craton,
799 Australia: evidence for vertical and horizontal tectonic regimes prior to 2900Ma.
800 *Precambrian Research, 131*(3), 153-172.
801 doi:https://doi.org/10.1016/j.precamres.2003.12.009
802 Hickman, A. H. (2012). Review of the Pilbara Craton and Fortescue Basin, Western Austrlia:
803 Crustal evolution providing environments for early life. *Island Arc, 21*(1), 1-31.
804 Hickman, A. H. (2016). *Northwest Pilbara Craton: a record of 450 million years in the growth*
805 *of Archean continential crust*. Retrieved from Perth:
806 Hickman, A. H. (2021). *East Pilbara Craton: a record of one billion years in the growth of*
807 *Archean continental crust*. Retrieved from
808 Hickman, A. H., Huston, D., Van Kranendonk, M. J., & Smithies, R. H. (2006). *Geology and*
809 *mineralization of the west Pilbara - a field guide*. Retrieved from
810 Hickman, A. H., Smithies, R. H., & Tyler, I. M. (2010). *Evolution of active plate margins:*
811 *West Pilbara Superterrane, De Grey Superbasin, and the Fortescue and Hamersley*
812 *Basins — a field guide*. Retrieved from Perth:
813 Hickman, A. H., & Van Kranendonk, M. J. (2012). Early Earth evolution: Evidence from the
814 3.5-1.8 Ga geological history of the Pilbara region of Western Australia. *Episodes,*
815 *35*(1), 283-297. doi:https://doi.org/10.18814/epiiugs/2012/v35i1/028
816 Hitzman, M., Bookstrom, A. A., Slack, J. F., & Zientek, M. L. (2017). *Cobalt—Styles of*
817 *Deposits and the Search for Primary Deposits*. Retrieved from Virginia:
818 https://doi.org/10.3133/ofr20171155
819 Hitzman, M., Kirkham, R. V., Broughton, D., Thorson, J., & Selley, D. (2005). The Sediment-
820 Hosted Stratiform Copper Ore System. *Economic Geology, 100th Anniversary Volume*,
821 609-642. doi:https://doi.org/10.5382/AV100.19

822 Hitzman, M., Selley, D., & Bull, S. (2010). Formation of Sedimentary Rock-Hosted Stratiform
823 Copper Deposits through Earth History. *Economic Geology, 105*(3), 627-639.
824 doi:https://doi.org/10.2113/gsecongeo.105.3.627
825 Horn, S., Gunn, A. G., Petavratzi, E., Shaw, R. A., Eilu, P., Törmänen, T., . . . Wall, F. (2021).
826 Cobalt resources in Europe and the potential for new discoveries. *Ore Geology Reviews,*
827 *130*, 103915. doi:https://doi.org/10.1016/j.oregeorev.2020.103915
828 Kirkham, R. V. (1989). Distribution, Settings, and Genesis of Sediment-hosted Stratiform
829 Copper Deposits. *Geological Association of Canada Special Paper, 36*, 3-38.
830 Kissin, S. A. (1992). Five-element (Ni-Co-As-Ag-Bi) Veins. *Geoscience Canada, 19*(3), 113-
831 124.
832 Kiyokawa, S., Taira, A., Byrne, T., Bowring, S., & Sano, Y. (2002). Structural evolution of the
833 middle Archean coastal Pilbara terrane, Western Australia. *Tectonics, 21*(5), 1-24.
834 Lefebure, D. V. (1996). Five-element Veins Ag-Ni-Co-As+/-(Bi,U). In D. V. Lefebure & T.
835 Höy (Eds.), *Selected British Columbia Mineral Deposit Profiles* (Vol. 2, pp. 89-92).
836 Vancouver: British Columbia Ministry of Employment and Investment.
837 Leonard, M. D., Michaelides, E. E., & Michaelides, D. N. (2020). Energy storage needs for the
838 substitution of fossil fuel power plants with renewables. *Renewable Energy, 145*, 951-
839 962. doi:https://doi.org/10.1016/j.renene.2019.06.066
840 Loukola-Ruskeeniemi, K., & Lahtinen, H. (2013). Multiphase evolution in the black-shale-
841 hosted Ni–Cu–Zn–Co deposit at Talvivaara, Finland. *Ore Geology Reviews, 52*, 85-99.
842 doi:https://doi.org/10.1016/j.oregeorev.2012.10.006
843 McCuaig, T. C., Hronsky, J. M. A., Kelley, K. D., & Golden, H. C. (2014). The Mineral System
844 Concept: The Key to Exploration Targeting. In *Building Exploration Capability for the*
845 *21st Century* (Vol. 18, pp. 0): Society of Economic Geologists.
846 Mudd, G. M., Weng, Z. H., Jowitt, S. M., Turnbull, I. D., & Graedel, T. E. (2013). Quantifying
847 the recoverable resources of by-product metals: The case of cobalt. *Ore Geology*
848 *Reviews, 55*, 87-98.
849 Mudd, G. M., Werner, T. T., Weng, Z. H., Yellitshetty, M., Yuan, Y., McAlpine, S. R. B., . . .
850 Czarnota, K. (2018). *Critical Minerals in Australia: A Review of Opportunities and*
851 *Research Needs*. Retrieved from Canberra, Australia:
852 Petavratzi, E., Gunn, G., & Kresse, C. (2019). *Commodity Review: Cobalt*. Retrieved from
853 Rose, A. (1989). Mobility of Copper and Other Heavy Metals in Sedimentary Environments.
854 *Special Paper - Geological Association of Canada, 36*, 97-110.

Ruddock, I. (1999b). *Mineral occurrences and exploration potential of the West Pilbara / by I. Ruddock*. Perth, W.A: Geological Survey of Western Australia.

Schulz, K. J., DeYoung Jr, J. H., Seal Ii, R. R., & Bradley, D. C. (2017). *Critical mineral resources of the United States—An introduction* (1802A). Retrieved from Reston, VA: http://pubs.er.usgs.gov/publication/pp1802A

Slack, J. F., Johnson, C. A., Causey, J. D., Lund, K., Schulz, K. J., Gray, J. E., & Eppinger, R. G. (2013). *Descriptive and geoenvironmental model for Co-Cu-Au deposits in metasedimentary rocks: Chapter G in Mineral deposit models for resource assessment* (2010-5070G). Retrieved from Reston, VA: http://pubs.er.usgs.gov/publication/sir20105070G

Slack, J. F., Kimball, B. E., & Shedd, K. B. (2017a). Cobalt. In K. J. Schulz, J. H. DeYoung., R. R. Seal, & D. W. Bradley (Eds.), *Critical Mineral Resources of the United States—Economic and Environmental Geology and Prospects for Future Supply* (Vol. Chapter F, pp. 40 p.). Reston, Virginia: U.S. Geological Survey.

Taylor, C. D., Causey, J. D., Denning, P. D., Hammartstrom, J. M., Hayes, T. S., Horton, J. D., . . . Zientek, M. L. (2013). *Descriptive Models, Grade-Tonnage Relations, and Databases for the Assessment of Sediment-Hosted Copper Deposits—With Emphasis on Deposits in the Central African Copperbelt, Democratic Republic of the Congo and Zambia*. Retrieved from Reston, Virginia:

Van Kranendonk, M. J., Hickman, A. H., Smithies, R. H., Nelson, D. R., & Pike, G. (2002). Geology and Tectonic Evolution of the Archean North Pilbara Terrain, Pilbara Craton, Western Australia. *Economic Geology, 97*(4), 695-732. doi:https://doi.org/10.2113/gsecongeo.97.4.695

Van Kranendonk, M. J., Hickman, A. H., Smithies, R. H., Williams, I. R., Bagas, L., & Farrell, T. R. (2006). *Revised lithostratigraphy of Archean supracrustal and intrusive rocks in the northern Pilbara Craton, Western Australia*. Retrieved from

Van Kranendonk, M. J., Smithies, R. H., Hickman, A. H., & Champion, D. (2007). Review: secular tectonic evolution of Archean continental crust: interplay between horizontal and vertical processes in the formation of the Pilbara Craton, Australia. *Terra Nova, 19*(1), 1-38.

Van Kranendonk, M. J., Smithies, R. H., Hickman, A. H., Wingate, M. T. D., & Bodorkos, S. (2010). Evidence for Mesoarchean (~3.2Ga) rifting of the Pilbara Craton: The missing link in an early Precambrian Wilson cycle. *Precambrian Research, 177*, 145-161.

888 Williams, P. J., Barton, M. D., Johnson, D. A., Fontbote, L., De Haller, A., Mark, G., . . .
889 Marschik, R. (2005). Iron Oxide Copper-Gold Deposits: Geology, Space-Time
890 Distribution, and Possible Modes of Origin. In J. W. Hedenquist, J. F. H. Thompson,
891 R. J. Goldfarb, & J. P. Richards (Eds.), *Economic Geology One Hundredth Anniversary*
892 *Volume*: Society of Economic Geologists.

893

Chapter 2

Plundering Carlow Castle: first look at a unique Mesoarchean-hosted Cu-Co-Au deposit

This chapter is published as an *Express Letter* in *Economic Geology* as:

Fox, D. C. M., Spinks, S., Pearce, M. A., Barham, M., Le Vaillant, M., Thorne, R., Aspandiar, M. F., Verrall, M. (2019). Plundering Carlow Castle: First Look at a Unique Mesoarchean-Hosted Cu-Co-Au Deposit. Economic Geology, 114(6), 1021-1031. doi:https://doi.org/10.5382/econgeo.4672

2.1 Abstract

Economically significant and geologically complex veined Cu-Co-Au mineralization was recently discovered at Carlow Castle in the Pilbara region of north-western Western Australia. The inferred resource estimate for Carlow Castle as of May 2021 is 8 Mt at 0.7 g/t Au, 0.4% Cu, and 0.05% Co (Artemis Resources Limited, 2021), making it one of Australia's most significant known Cu-Co-Au deposits. Here we provide the first account and scientific analysis of Carlow Castle. This analysis suggests that it is a hydrothermal Cu-Co-Au deposit, with mineralization hosted in sulfide-rich quartz-carbonate veins. The ore is hosted in veins that occur within a pervasively chloritized shear zone through the regionally significant Regal Thrust. At Carlow Castle the shear zone associated with this thrust occurs within the Ruth Well and Nickol River Formations; an Archean mafic volcano-sedimentary sequence. Within the mineralized veins the dominant ore minerals are pyrite (FeS_2), chalcopyrite ($CuFeS_2$), chalcocite (Cu_2S), cobaltite (CoAsS), and electrum (Au,Ag). The genesis of the Carlow Castle deposit is still under investigation; however, the origin of the Cu-Co-Au mineralization is most likely related to the migration of metalliferous fluids along the Regal Thrust. Based on Carlow

Castle's stratigraphic position within the Pilbara Craton and the craton's relative stability since the Archean, an Archean age of mineralization is most likely. The distinct Cu-Co-Au enrichment at Carlow Castle makes it unique among Archean ore deposits generally, as the majority of Cu-Co deposits are of maximum Proterozoic age. Therefore, understanding the genesis of the Carlow Castle deposit has important implications for understanding the unique processes through which Cu-Co-Au mineralization outside of basin-hosted ore deposits may be formed, particularly in Archean terranes.

2.2 Introduction

The Carlow Castle copper-cobalt-gold (Cu-Co-Au) deposit is hosted in the Roebourne greenstone belt within the West Pilbara region, Western Australia (Figure 2.1). The current inferred resource for Carlow Castle amounts to 7.7 Mt at 0.51% Cu, 0.08% Co, and 1.06 g/t Au (Artemis Resources Limited, 2019a); making it one of Australia's most well-endowed Cu-Co-Au deposits (Britt et al., 2017). These resource estimates are based on extensive exploration and drilling campaigns through 2017 and 2018, which resulted in the discovery of mineralization proximal to the previously abandoned minor Carlow Castle Cu workings. This drilling effort comprised infill drilling of historic exploration drill holes that had noted minor Cu-Au mineralization. However, despite extensive drilling targeting mineralization, the geology of the Carlow Castle deposit and the origin of its peculiar Cu-Co-Au mineralization remain poorly documented and constrained. This work is particularly topical given the remarkable endowment of Carlow Castle's mineralization in Co. Indeed, Co has been designated as a critically important metal by governmental agencies in the UK; the European Union; Australia; and the USA (British Geological Survey, 2015; European Commission, 2017; Mudd et al., 2018; U.S. Department of the Interior, 2018), with increased demand from the battery sector due to the status of Co as a key metal in Li-ion batteries (US Geological Survey, 2018). Due to proliferation of electric vehicles and the challenge of stabilizing renewable energy generation, Co is a critical metal for the evolving global economy. Presently, >50% of the world's Co is supplied by the Democratic Republic of Congo, which is exposed to significant geopolitical risk (Olivetti, Ceder, Gaustad, & Fu, 2017). Beyond its economic significance, the distinctive Cu-Co enrichment of the Carlow Castle deposit makes it an oddity among Au deposits hosted in Archean greenstone belts (Groves, Goldfarb, Gebre-Mariam, Hagemann, & Robert, 1998; Kerrich, Goldfarb, Groves, Garwin, & Jia, 2000; Saunders, Hofstra, Goldfarb, & Reed, 2014). The present work provides a robust geological and

mineralogical background to the Cu-Co-Au mineralization at Carlow Castle to provide a basis for different analytical approaches in subsequent chapters, including geochronology and isotope geochemistry of the Cu-Co-Au mineralization. To this end, we provide interpretations regarding Carlow Castle's genesis based on this geological and mineralogical characterization.

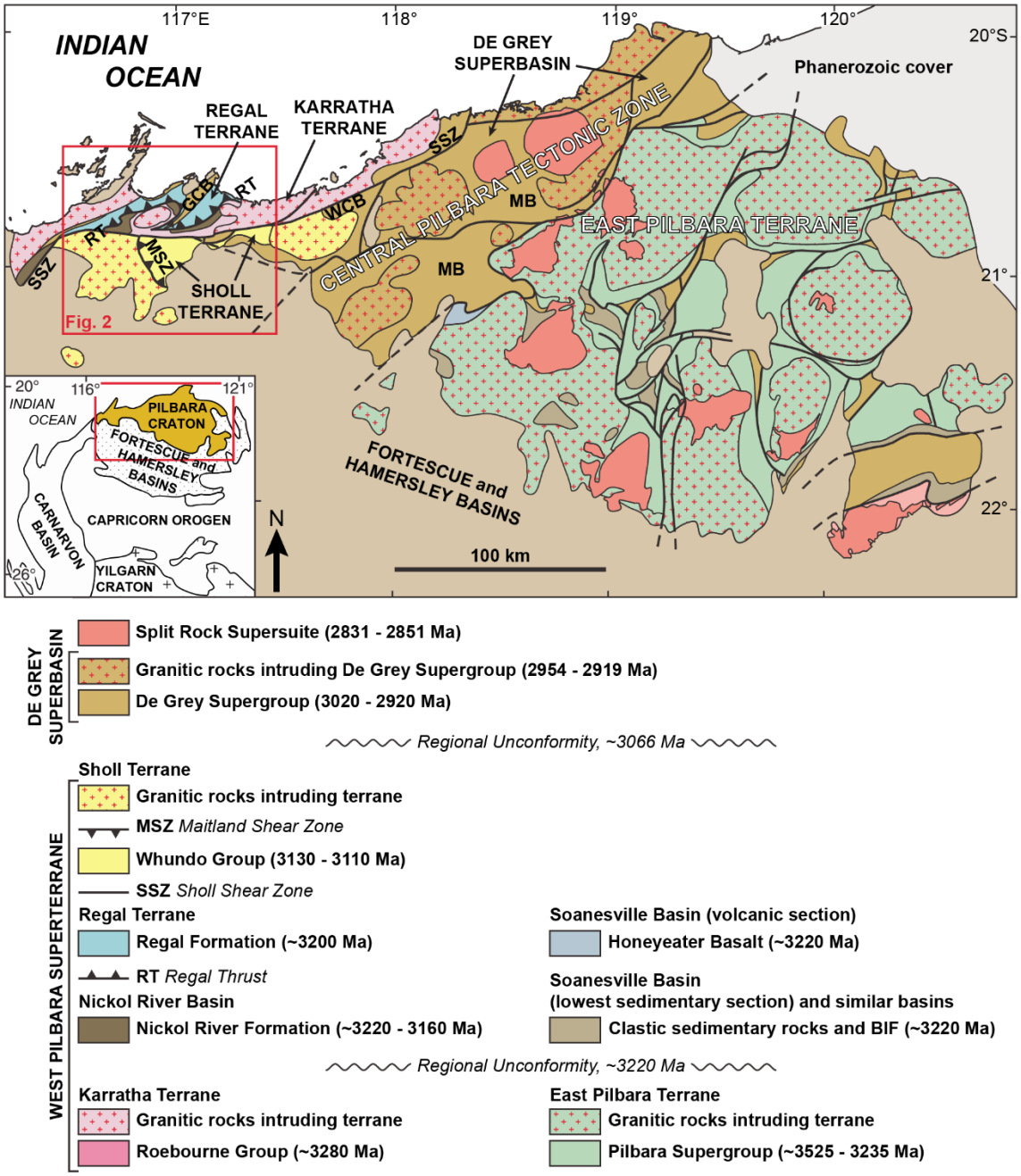

Figure 2.1 - Geological map of the Pilbara Craton, modified after Hickman (2016). MB = Mallina Basin, WCB = Whim Creek Basin, GCB = Gorge Creek Basin. Note that the extent of the area of the northwest Pilbara Craton within Figure 2.2 is indicated and the symbology of different terranes is noted in the figure legend.

2.3 Exploration history

The first discovery of Cu mineralization at Carlow Castle, formerly known as Glenroebourne, dates to 1872. Minor surficial Cu and Au mining occurred intermittently until 1957 (Openpit Mining Limited, 1987; Ruddock, 1999a). It has since been the subject of several minor exploration efforts, with limited success until major mineralized intersections were encountered during drilling in 2017 and 2018 (Artemis Resources Limited, 2017, 2018a). Artemis Resources released a resource estimate of 4.5 Mt at 0.4% Cu, 0.07% Co, and 0.9g/t Au for Carlow Castle in January 2018 (Artemis Resources Limited, 2018b). The current inferred resource estimate is 7.7 Mt at 0.51% Cu, 0.08% Co, and 1.06 g/t Au, as of March 2019 (Artemis Resources Limited, 2019b). A third phase of drilling was initiated in December 2018 aiming for extensions of mineralization east and west along strike; results are pending (Artemis Resources Limited, 2018b).

2.4 Geological Setting

The Carlow Castle Cu-Co-Au deposit is hosted within the Archean to Proterozoic northwest Pilbara Craton (Figure 2.1; Ruddock, 1999a; Smithies, Hickman, & Nelson, 1999). The northwest Pilbara Craton is broadly divided into two major tectonic units; the De Grey Superbasin (3066-2919 Ma) and the West Pilbara Superterrane (3280-3066 Ma) (Hickman, 2016). The West Pilbara Superterrane, which hosts the Carlow Castle deposit, is further divided into the Nickol River Basin and Sholl, Regal, and Karratha Terranes (Figure 2.1; Hickman, 2016; Kemp, Hickman, Kirkland, & Vervoort, 2015; Peterson et al., 2019). These Terranes form a chain of several granite-greenstone belts composed of a mix of Archean mafic volcanic rocks and intrusive granitic complexes (Hickman et al., 2006). This provides a unique geological setting for Cu-Co-Au mineralization, the majority of which is hosted in terranes of Proterozoic or younger age (US Geological Survey, 2018). The West Pilbara Superterrane is presently interpreted to have formed during the Prinsep Orogeny (3070 Ma) via the accretion of the Sholl, Regal, and Karratha Terranes. The Karratha Terrane (3280-3236 Ma) is interpreted to represent a separated portion of the early Paleoarchean Pilbara Craton that rifted from the East Pilbara Terrane (3530-3223 Ma), which presently crops out ~130 km east of Carlow Castle (Figure 2.1), during the initiation of horizontal plate tectonics around 3220 Ma (Hickman, 2021). Subsequently, a thin basaltic oceanic crust, that presently composes the Regal Terrane (3200-3160 Ma), developed within the Central Pilbara Basin between the rifted Karratha and East Pilbara Terrranes. The Nickol River Basin developed along a passive margin

of the rifted Karratha Terrane as a sequence of marine sediments (Hickman, 2021; Hickman et al., 2010). Renewed convergence of the Karratha and East Pilbara Terranes from 3160 Ma initiated subduction within the Central Pilbara Basin and ultimately resulted in basin closure (Hickman, 2016). Convergence and subduction within the Central Pilbara Basin between 3130-3093 Ma initiated the formation of the Sholl Terrane as a volcanic oceanic island arc (Van Kranendonk et al., 2007). This extended period of convergence ultimately culminated in the Prinsep Orogeny at 3070 Ma and the accretion of the Nickol River Basin and Sholl, Karratha, and Regal Terranes into the West Pilbara Superterrane (Hickman, 2016, 2021). The Prinsep Orogeny is also generally interpreted to have produced the Regal Thrust; a regionally significant thrust fault that separates the overlying Regal Terrane to the north from the underlying Karratha Terrane to the south (Figure 2.2) and has been associated with Cu-Au mineralization regionally (Hickman, 2004a, 2016; Hickman et al., 2006; 2010; Van Kranendonk et al., 2010). The Regal Thrust likely represents the plane along which the Regal Terrane was thrust over the Karratha Terrane and Nickol River Basin when the West Pilbara Superterrane collided with the East Pilbara Terrane (Hickman, 2016).

Following the accretion of the West Pilbara Superterrane, an extended period of post-orogenic crustal relaxation, extension, and basin formation initiated across the Pilbara Craton (Hickman et al., 2006). This extensional period led to the formation of the De Grey Superbasin (3066-2919 Ma); beginning with the formation of the Gorge Creek Basin (3066-3015 Ma) as a shallow-water basin covering much of the West Pilbara Superterrane and East Pilbara Terrane (Hickman, 2016). Within the Gorge Creek Basin, sedimentation was dominated by a succession of sandstones, conglomerate, and shales in addition to chert and banded iron formations (Hickman, 2016; Van Kranendonk et al., 2007). A new phase of regional convergence resulted in the development of a subduction zone along the northwest margin of the Pilbara Craton. Continued development of this subduction zone ultimately resulted in the formation of the Whim Creek Basin (3009-2991 Ma) as a volcanic arc over the Pilbara Craton to the southeast of Carlow Castle (Figure 2.1) and significant mafic and felsic magmatism resulting in the intrusion of the Orpheus (3023-3012 Ma) and Maitland River (3006-2982 Ma) Supersuites (Figure 2.2) through much of the West Pilbara Superterrane (Hickman, 2021). In particular, the layered mafic-ultramafic Andover Intrusion (3016 ± 4 Ma) is observed to crop out immediately south of Carlow Castle and the Ruth Well Formation, where it occurs as a series of layered ultramafic and gabbroic rocks (Hickman, 2016). During the emergence of the Whim

Creek Basin volcanic arc, the Mallina Basin (3015-2931 Ma) developed to the southeast (Figure 2.1) as a back-arc basin (Hickman, 2016, 2021; Hickman et al., 2010). The Mallina Basin preserves 2-4 km of sediment fill that is composed predominantly of conglomerate, sandstone, and shale (Eriksson, 1982; Hickman et al., 2010). Extension within the Mallina Basin was eventually halted following the initiation of convergence across most of the northwestern Pilbara Craton during the latter stages of the North Pilbara Orogeny from 2955-2919 Ma (Hickman et al., 2010; Hickman & Van Kranendonk, 2012). This period was associated with major granitic magmatism, with the intrusion of the Sisters Supersuite (2954-2919 Ma) throughout the Mallina Basin (Hickman et al., 2010). The North Pilbara Orogeny represents the final stage of the cratonization of the Pilbara Craton and the final reconvergence of the West Pilbara Superterrane and the East Pilbara Terrane (Hickman, 2016).

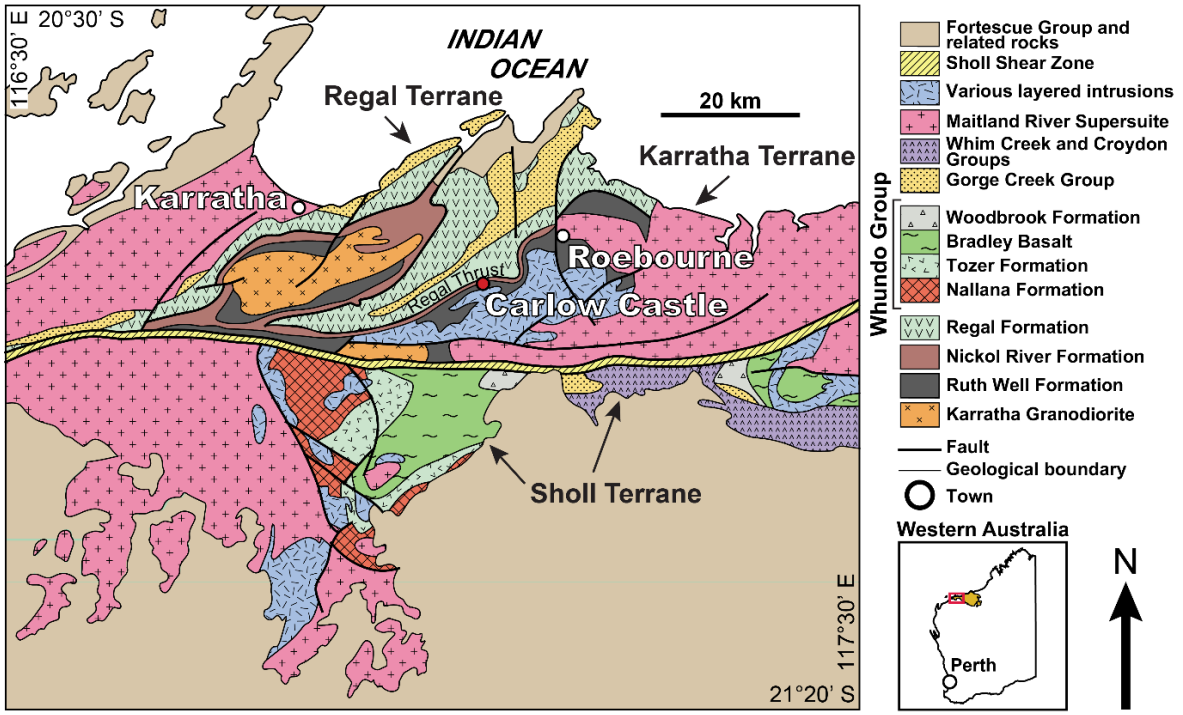

Figure 2.2 - Geological map of the northwest Pilbara Craton. The Pilbara Craton is highlighted in orange within the inset map. Modified after Van Kranendonk et al. (2002).

Carlow Castle is hosted in a tectonized zone through the Nickol River and Ruth Well formations, on the southern side of the Regal Thrust; separating the Nickel River and Ruth Well Formations from the Regal Terrane (Figure 2.3; Hickman, 2016; Ruddock, 1999a). The Ruth Well Formation (~3280 Ma) is a ~1500 m thick volcano-sedimentary succession dominated by variably altered metamorphosed peridotite and basalt, with minor chertified shale (Hickman, 2016; Van Kranendonk et al., 2002). Locally pillowed basalt within the Ruth Well

Formation provide evidence of submarine extrusion (Hickman, 2016). This is conformably overlain by the Weerianna Basalt; a metamorphosed basalt unit up to 1000 m in thickness, which lacks peridotite and chert units (Hickman, 2016). Together the Ruth Well Formation and Weerianna Basalt constitute the Roebourne Group within the Karratha Terrane (Figure 2.2), which was historically interpreted to have formed as an Archean mid-ocean ridge basalt (Kato et al., 1998; Kiyokawa et al., 2002; Shibuya, Kitajima, Komiya, Terabayashi, & Maruyama, 2007). However, recently Hickman (2016) has argued that the Roebourne Group was instead extruded onto continental crust of probable tonalite-trondhjemite-granodiorite (TTG) composition that formed part of the original Paleoarchean Pilbara Craton prior to rifting. The felsic rocks of the East Pilbara Terrane (3720-3165 Ma), which developed independently for much of the Archean, are considered to represent a record of this original TTG-dominated Paleoarchean Pilbara Craton crust (Hickman, 2016; Van Kranendonk et al., 2006). The rocks of the Roebourne Group are overlain by the intensely sheared metasediments of the Nickol River Formation (~3220 Ma); a succession of fine-grained marine siliciclastic rocks initially deposited during Paleoarchean rifting of the East Pilbara Terrane (Hickman, 2016).

On the deposit-scale, the lithologies in proximity to the Carlow Castle ore zone are covered with a cover sequence of quaternary colluvium and alluvium (Hickman, 2002). However, rocks of the Ruth Well Formation of probable basaltic composition are observed to crop out within the ore zone, whilst gabbroic intrusive outcrops of the Orpheus Supersuite Andover Intrusion are observed due south of the ore zone (Figure 2.3). The northern edge of the Carlow Castle ore zone is defined by a ridge of mylonitized and chertified shale and minor banded iron formations of the Nickol River Formation that strikes broadly from southwest to northeast along the interpreted extent of the Regal Thrust across the southeastern boundary of the Regal Terrane (Figure 2.1). The Carlow Castle ore zone occurs over a strike length of approximately 1.2 km, striking roughly east-west; parallel to the outcropping chert ridge that defines the preserved extent of the Nickol River Formation and Regal Thrust (Figure 2.3). Within the ore zone, mineralization is structurally-controlled and occurs through a series of Cu-, Co-, and Au-bearing lodes within mineralized faults that strike broadly northeast-southwest. These mineralized faults are marked on Figure 2.3 and are interpreted based on the results of a sub-audio magnetics survey conducted by Artemis Resources Limited (Eremenco, Mortimer, & Mead, 2019).

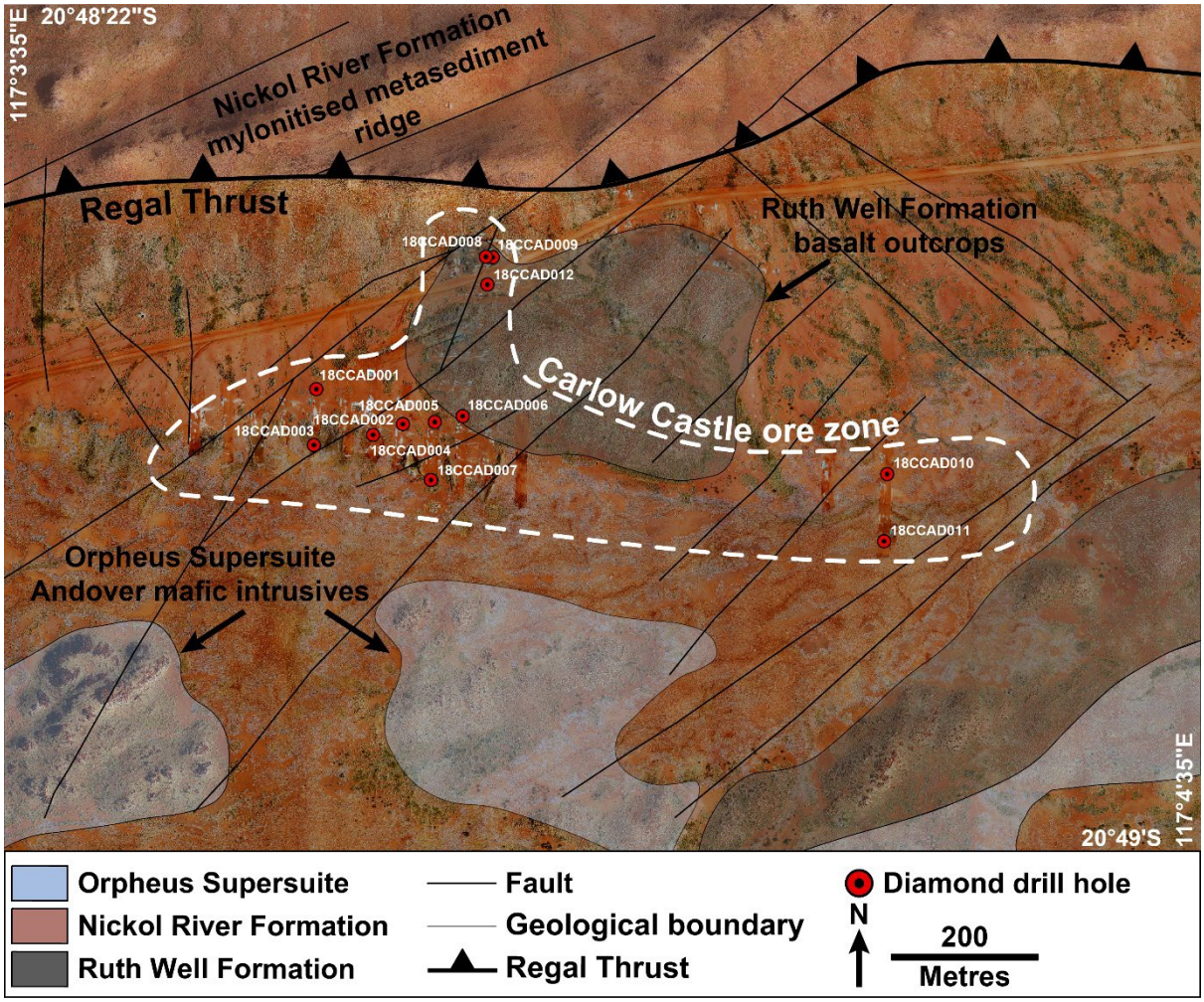

Figure 2.3 – Geological map of outcrop lithologies proximal to Carlow Castle Cu-Co-Au deposit, modified after (Hickman, 2002) and internally produced maps by Artemis Resources Limited.

2.5 Methods

For this study 44 samples were taken from core from 12 drill holes that penetrated the Carlow Castle ore body in 2018 (Figure 2.3; down hole geochemistry plots of drill hole data in Appendix 2.1; sample list in Appendix 2.2). Core from these drill holes was logged in detail by Geologists from Artemis Resources Limited and the authors, representative samples of mineralisation of varying mineralogical and geochemical characteristics were then collected. Eleven halved core samples from these drill holes were then polished for X-ray fluorescence (XRF) mapping and polished blocks were prepared for petrographic analysis. The XRF elemental mapping of Cu and Co was conducted using a Bruker M4 TORNADO Micro-XRF mapper with a beam diameter of 25 µm, point spacing of 40 µm, and a dwell time of 10 ms.

Preliminary petrographic analysis was conducted through reflected light optical microscopy using a Nikon LV100N POL petrographic microscope to roughly establish mineralogy and mineral textures. This was followed by detailed petrographic analysis through SEM imaging and quantitative elemental mapping, conducted using a Philips XL 40 environmental SEM fitted with a Bruker X-Flash energy dispersive X-ray spectroscopy (EDS) detector. These analyses were conducted using the facilities at the CSIRO Advanced Characterisation Facility in the Australian Resources Research Centre in Perth, Western Australia.

2.6 Results

2.6.1 Style of mineralization

Mineralization at Carlow Castle is hosted in a heavily chlorite-silica altered mafic volcano-sedimentary sequence, within the Nickol River and Ruth Well Formations. It is often difficult to constrain the primary host lithology of Carlow Castle mineralization due to extensive post-depositional alteration during ore formation. However, based on unaltered equivalent sections of the host formations observed by Hickman (2016); Ruddock (1999a); Van Kranendonk et al. (2006), it is likely that the host lithology was dominated by a volcanic sequence of mafic to ultramafic rocks along with carbonaceous shale and minor chert beds. It has previously been observed outside of the Carlow Castle ore zone that these formations have been metamorphosed to amphibolite facies, most likely during the period of tectonic convergence preceding the Prinsep Orogeny between 3160-3070 Ma (Hickman, 2016). Within the Nickol River and Ruth Well Formations, the hypogene Co-Cu-Au mineralization typically occurs within 100 m of the contemporary surface (see drill hole geochemistry logs in Appendix 2.1). This mineralization occurs as a primary sulfide ore zone with an overlying supergene oxidized zone that varies from 25 m to 50 m thick. Within this oxidized supergene layer, there is partial to complete replacement of the original sulfide mineralization with secondary Cu-oxides, silicates, and carbonates (e.g., chrysocolla, malachite). The primary sulfide mineralization is the most significant and is structurally-hosted; where mineralization occurs in quartz-carbonate and sulfide veins through brecciated and sheared host rock.

2.6.2 Structure

The Nickol River and Ruth Well Formations at Carlow Castle bear evidence of several phases of deformation. Brittle deformation is intense in some areas, with brecciation forming a network of mineralized fractures within the ore zone (Figure 2.4a, b). In addition to these brittle structures, there is also extensive evidence of ductile deformation at Carlow Castle, where

quartz and sulfide veins within the Carlow Castle ore zone occur through intensely sheared and folded host rocks. Both brittle and ductile structures at Carlow Castle host mineralization, which occurs infilling these structures as a series of disseminated to discordant quartz-sulfide veins. The timing of these structures relative to the sulfide mineralization at Carlow Castle is presently unconstrained. Regardless, these structures appear to have been critical to the genesis of the mineralization as they provided permeable structures to focus migrating mineralizing fluids at Carlow Castle. This includes mineralizing fluids that may have flowed along the proximal Regal Thrust.

2.6.3 Mineralogy

The hypogene structurally-hosted mineralization at Carlow Castle comprises two sulfide-dominated mineral assemblages (Table 2.1): (i) a pyrite-chalcopyrite assemblage (Assemblage One hereafter; Figure 2.4a; Appendix 2.3a, b), and (ii) a cobaltite-gold-chalcocite assemblage (Assemblage Two hereafter; Figure 2.4b, Appendix 2.3c). However, it is unclear if the presence of these two mineral assemblages does not appear to reflect any systematic spatial zonation in the mineralogy and geochemistry of the ore body at Carlow Castle. Assemblage One occurs within the main shear zone at Carlow Castle and is the most volumetrically dominant structurally-hosted sulfide mineralization at Carlow Castle, whereas Assemblage Two occurs primarily in comparably minor vein networks.

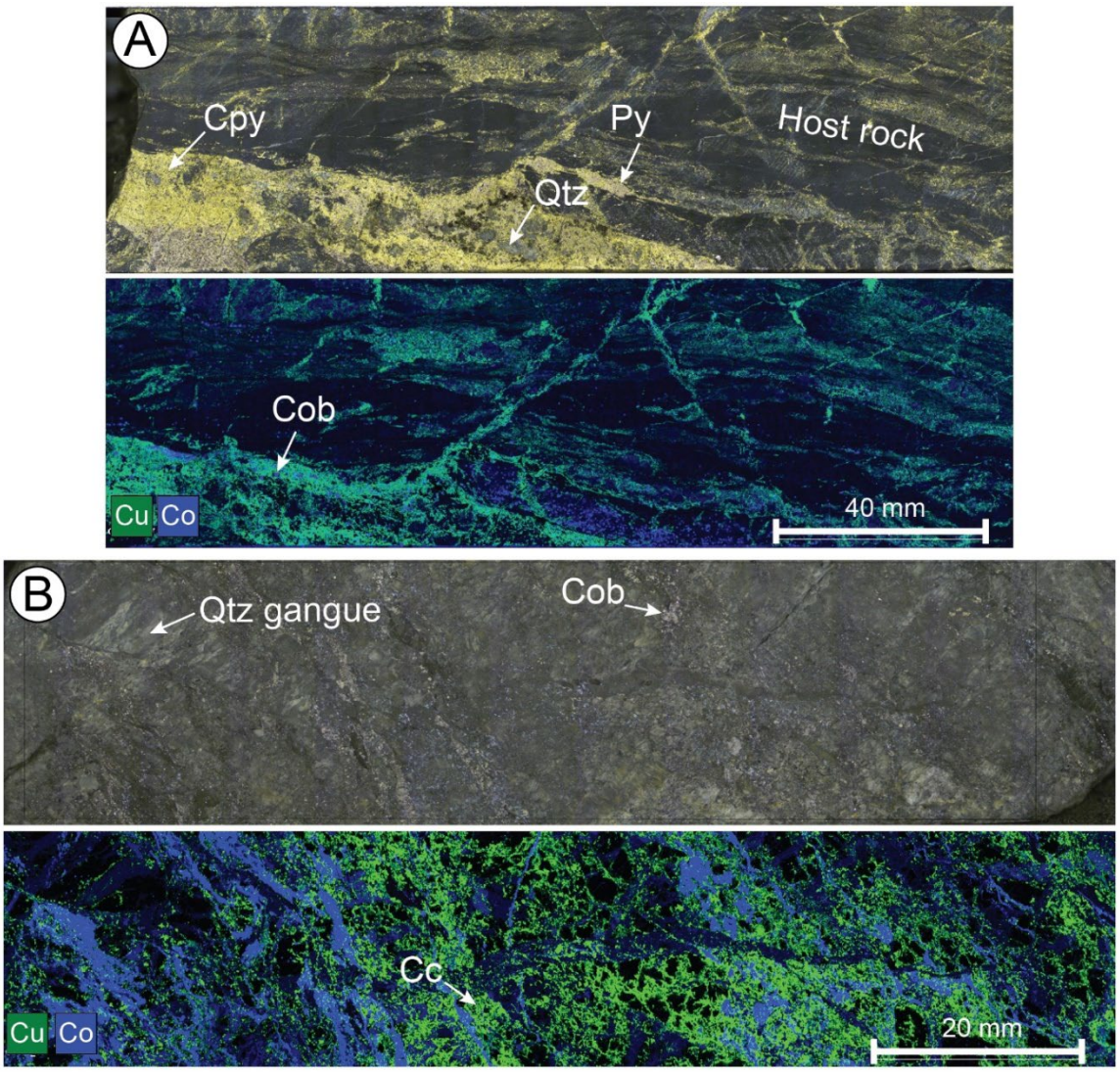

Figure 2.4 - A. Photograph mosaic and XRF map (Sample CC010_137) of chalcopyrite (green) and pyrite-rich mineralization with minor cobaltite (blue). Mineralization occurs as veins through pervasively chloritized and sheared host basalt (Assemblage One from Carlow Castle) B. Photograph mosaic and XRF map (Sample CC007_41) of chalcocite (green) and cobaltite-rich (blue) ore. Mineralization occurs as veinlets through a larger quartz-carbonate vein (Assemblage Two from Carlow Castle). Note Cu is highlighted in green and Co in blue.

Assemblage One is characterized by intergrown chalcopyrite, pyrite, and minor pyrrhotite at both microscopic and macroscopic scales. This assemblage commonly occurs as a series of sulfide-quartz-carbonate veins infilling a breccia network and through sheared bands of sulfides within the heavily chloritized host rock (Figure 2.4a). Cobaltite is observed as dispersed finer aggregates throughout some of the samples rather than distinct cobaltite-rich

veinlets as in Assemblage Two, though cobaltite does not always occur within Assemblage One. Where cobaltite is present in quartz-carbonate veins, pyrite and chalcopyrite tend to be anhedral and form stringy veinlet networks infilling space between quartz (Figure 2.5a). These veinlet networks of chalcopyrite and pyrite are occasionally associated with and crosscut paragenetically earlier euhedral to subhedral grains of cobaltite (Figure 2.5a). Assemblage One also occurs in texturally distinct thick (>20 cm) and particularly sulfide-rich veins where the volume of gangue quartz and carbonate is limited (<10 vol. %) and the host rock has been pervasively replaced by sulfides, forming a massive sulfide texture. These veins almost exclusively comprise massive sulfide in the form of coarse-grained, intergrown anhedral pyrite, pyrrhotite and chalcopyrite with accessory needles of chlorite and actinolite, along with epidote and subhedral quartz (Figure 2.5b). Within these coarse-grained massive sulfide samples (Figure 2.5b) cobaltite is less common in comparison to the more quartz-rich veinlet textured samples (Figure 2.5a). Occasionally, pyrrhotite and chalcopyrite are observed to be extensively and intimately intergrown with volumetrically abundant chlorite from the altered host rock (Figure 2.5c).

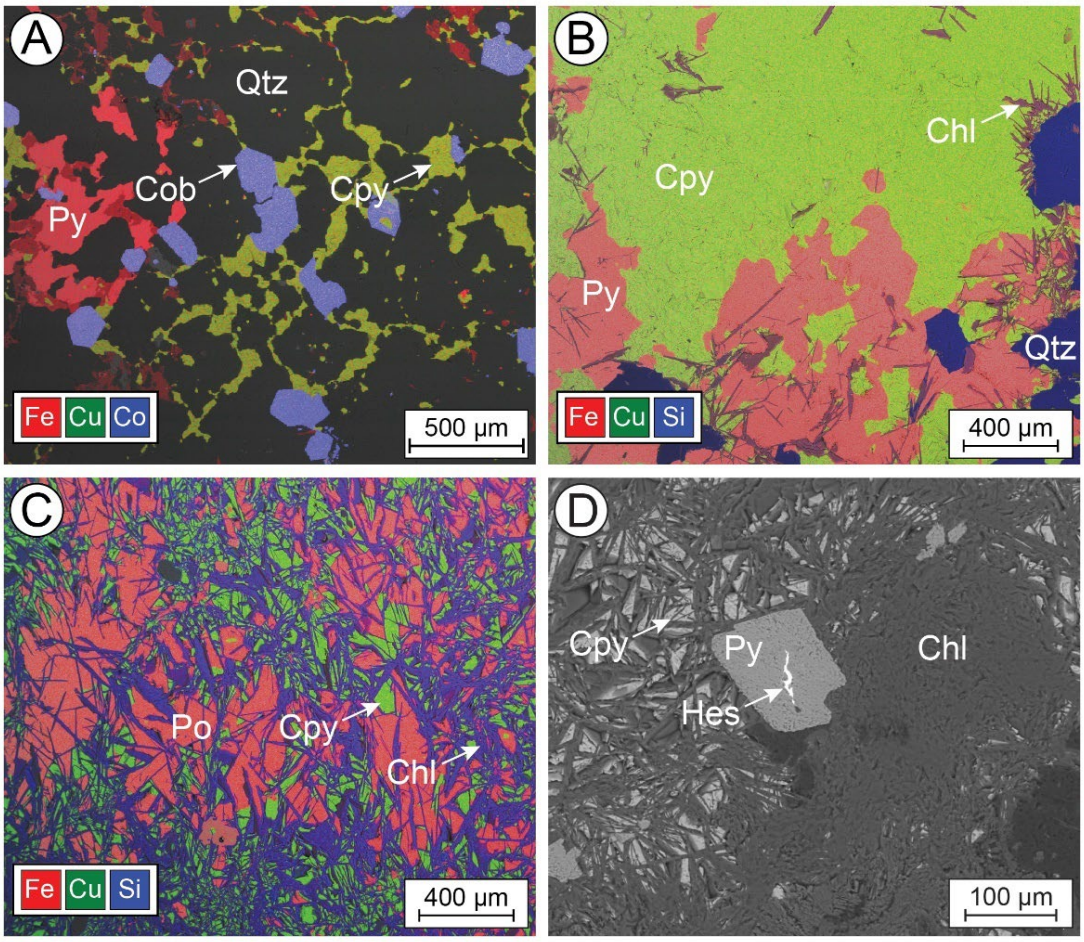

Figure 2.5 - SEM photomicrographs of mineralization from Assemblage One. A. Element map (Sample CC003_61) of Fe (red), Cu (green), and Co (blue) showing the occurrence of coarse subhedral to euhedral cobaltite (cob) with veinlets of anhedral chalcopyrite (cpy) and pyrite (py) within a larger quartz (qtz) cement. B. Element map (Sample CC007_102) of Fe (red), Cu (green), and Si (blue) showing the occurrence of coarse intergrown chalcopyrite and pyrite within massive samples, with minor quartz and coarse chlorite (chl). C. Element map (Sample CC007_102) of Fe (red), Cu (green), and Si (blue) showing syngenetic pyrrhotite (po) and chalcopyrite intergrown with coarse chlorite. D. Secondary electron image (Sample CC007_102) of a hessite (hes) inclusion within pyrite.

The dominant sulfide minerals within Assemblage Two are cobaltite and chalcocite. Within Assemblage Two cobaltite tends to occur as a series of discordant veinlets composed of aggregates of cobaltite grains (Figure 2.4b). However, chalcocite generally occurs as an interconnected network of thin veinlets infilling a quartz-carbonate breccia (Figure 2.4b). Within these veinlets cobaltite occurs as coarse aggregates of individual euhedral-subhedral grains cemented by quartz and siderite/calcite (Figure 2.6a) with comparably minor pyrite

(<10%), which is occasionally observed enveloping grains of cobaltite (Figure 2.6a, b, c). Primary chalcocite often crosscuts these cobaltite-rich veinlets; here chalcocite envelopes cobaltite grains and forms an interconnected network through the quartz-carbonate cement. Additionally, this chalcocite is commonly observed to partially replace pyrite; forming around the edges of pyrite grains (Figure 2.6b).

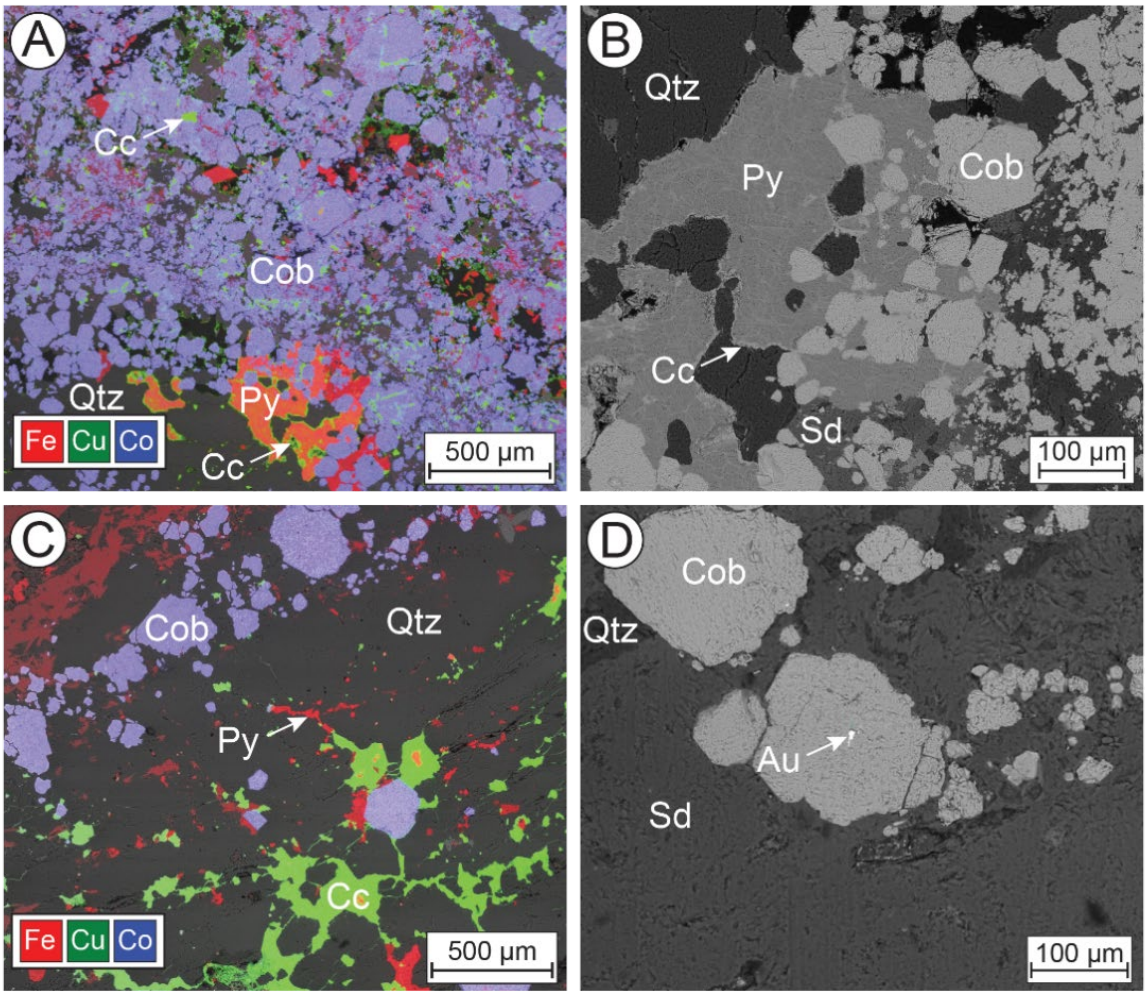

Figure 2.6 - SEM photomicrographs of mineralization from Assemblage Two. A. Element map (Sample CC007_41) of Fe (red), Cu (green), and Co (blue) within a quartz vein dominated by a cobaltite-rich aggregate with minor pyrite and paragenetically late chalcocite (cc). B. Secondary electron image (Sample CC007_41) of a cobaltite-rich quartz-siderite (sd) vein with late pyrite being partially replaced by chalcocite. C. Element map (CC009_48) of Fe (red), Cu (green), and Co (blue) from within a quartz vein hosting coarse blocky cobaltite and stringy veinlets of chalcocite and pyrite. D. Secondary electron image (Sample CC009_48) of cobaltite within a quartz-siderite vein showing the common occurrence of Au as inclusions within cobaltite.

Across both Assemblage One and Two, Au generally occurs as electrum (Au,Ag), typically >75% Au. Volumetrically, gold occurs in trace abundances as micron scale inclusions within the sulfide minerals of Assemblage One and Two (Figures 2.6d and 2.7a, b). However, in general, Au mineralization tends to be more abundant in samples from Assemblage Two and is comparably rare in Assemblage One. Across Carlow Castle there appears to be a clear genetic relationship between gold and cobaltite mineralization, as within these samples electrum most commonly occurs as micron-scale inclusions within cobaltite grains (Figures 2.6d and 2.7a). This may account for the comparably greater abundance of electrum within Assemblage Two, which hosts cobaltite in much greater abundances than Assemblage One. In addition to electrum, trace inclusions of various selenide and telluride minerals (BiTe, PbSe, AgTe) and uraninite (UO_2) are observed to occur as inclusions within cobaltite in Assemblage Two (Figure 2.7a). In Assemblage One, where cobaltite is less abundant, these tellurides and selenides occur more commonly as inclusions within pyrite (Figure 2.5d).

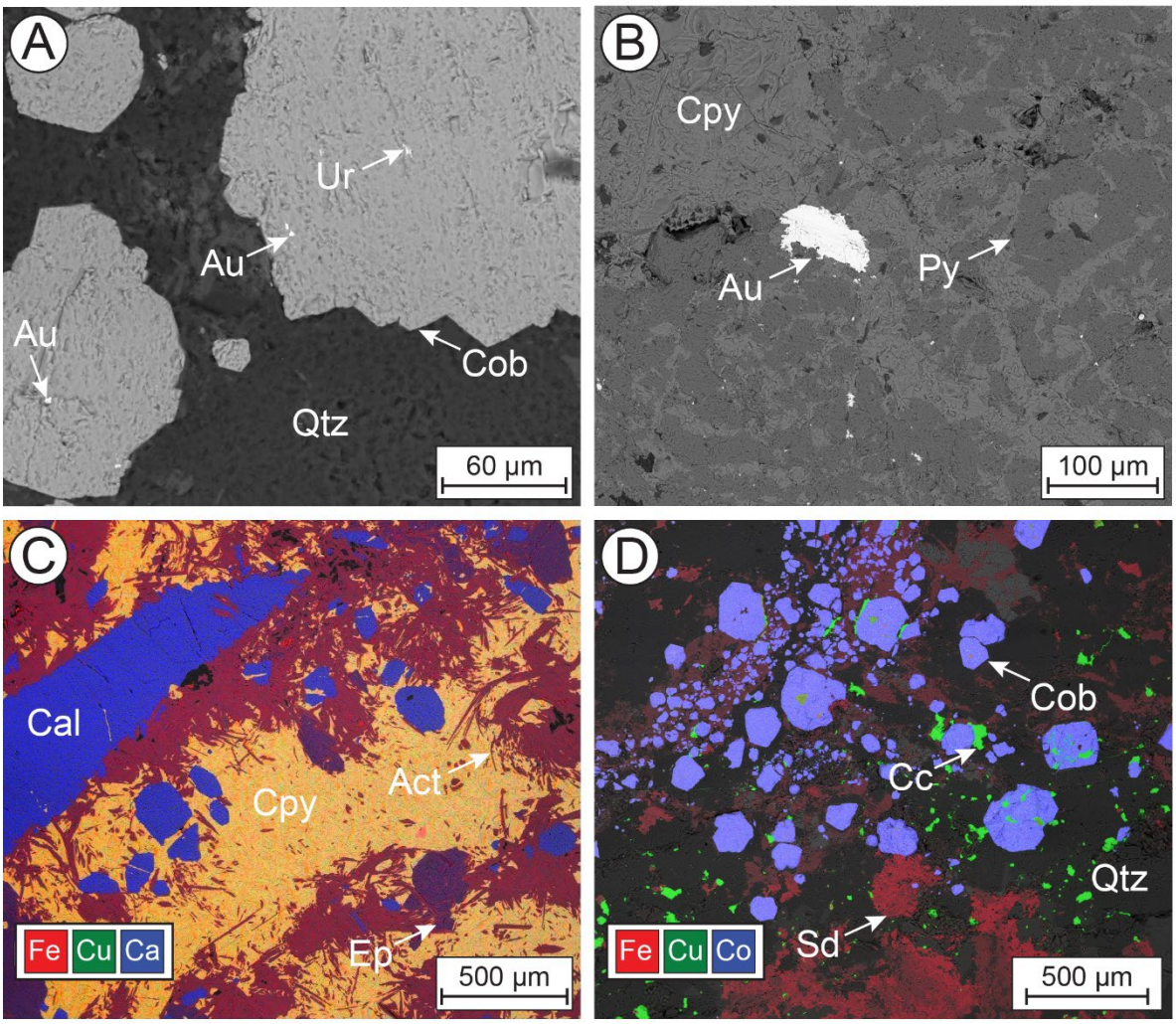

Figure 2.7 – SEM photomicrographs from Assemblages One and Two. A. Secondary electron image of cobaltite containing micron-scale inclusions of uraninite (Ur) and electrum from ore mineral Assemblage Two (Sample CC009_48). B. Secondary electron image showing scattered electrum mineralisation (bright phases) within a matrix of coarse grained pyrite and chalcopyrite from Assemblage One (Sample CC003_61). C. Element map (Sample CC012_67) of Fe (red), Cu (green), and Ca (blue) of paragenetically early calcite (cal), epidote (ep), and actinolite (act) alteration phases entrained in massive chalcopyrite mineralisation. D. Element map (Sample CC009_48) of Fe (red), Cu (green), and Co (blue) showing scattered euhedral cobaltite grains within a quartz-siderite vein with minor chalcocite mineralisation. Note that chalcocite appears to cross-cut or envelop some cobaltite grains.

Table 2.1 - Summary of ore mineralogy of Assemblages One and Two.

	Mineral Assemblage One	Mineral Assemblage Two
Cu phases	Chalcopyrite, ± chalcocite	Chalcocite, ± chalcopyrite
Co phases	± Cobaltite	Cobaltite
Au phases	± Electrum	Electrum
Other	Pyrrhotite, pyrite, ± tellurobismuthite(?) (BiTe), ± hessite(?) (AgTe)	± Pyrite, ± uraninite (UO_2), ± tellurobismuthite(?), ± clausthalite(?) (PbSe)

2.7 Discussion

2.7.1 Paragenetic relationships and relative geochronology

The paragenetic relationships and relative geochronology of ore minerals within Assemblage One and Assemblage Two are summarized in Figure 2.8. Quartz, epidote, chlorite, and siderite/calcite are common paragenetically early phases across both Assemblage One and Two (Figure 2.7c). Within these assemblages quartz and siderite/calcite represent the early cementing minerals that fill most of the system of mineralized veins (e.g., Figures 2.5a and 2.6c, d). Within both assemblages chlorite appears to be roughly synchronous with, or slightly predates these minerals and as such it is most likely a product of the extensive hydrothermal alteration of ferromagnesian minerals within the mafic-ultramafic volcanics and shales of the Nickol River and Ruth Well Formations, coinciding with the flow of the hydrothermal fluid that produced the Cu-Co-Au mineralization. Chlorite is an extremely common alteration mineral in hydrothermal gold systems, particularly in those hosted in mafic lithologies that are rich in ferromagnesian minerals (De Caritat, Hutcheon, & Walshe, 1993; Saunders et al., 2014). Extensive paragenetically early quartz-carbonate veining is similarly common in hydrothermal gold deposits (Kerrich et al., 2000; Zhu, Fang, & Tan, 2011).

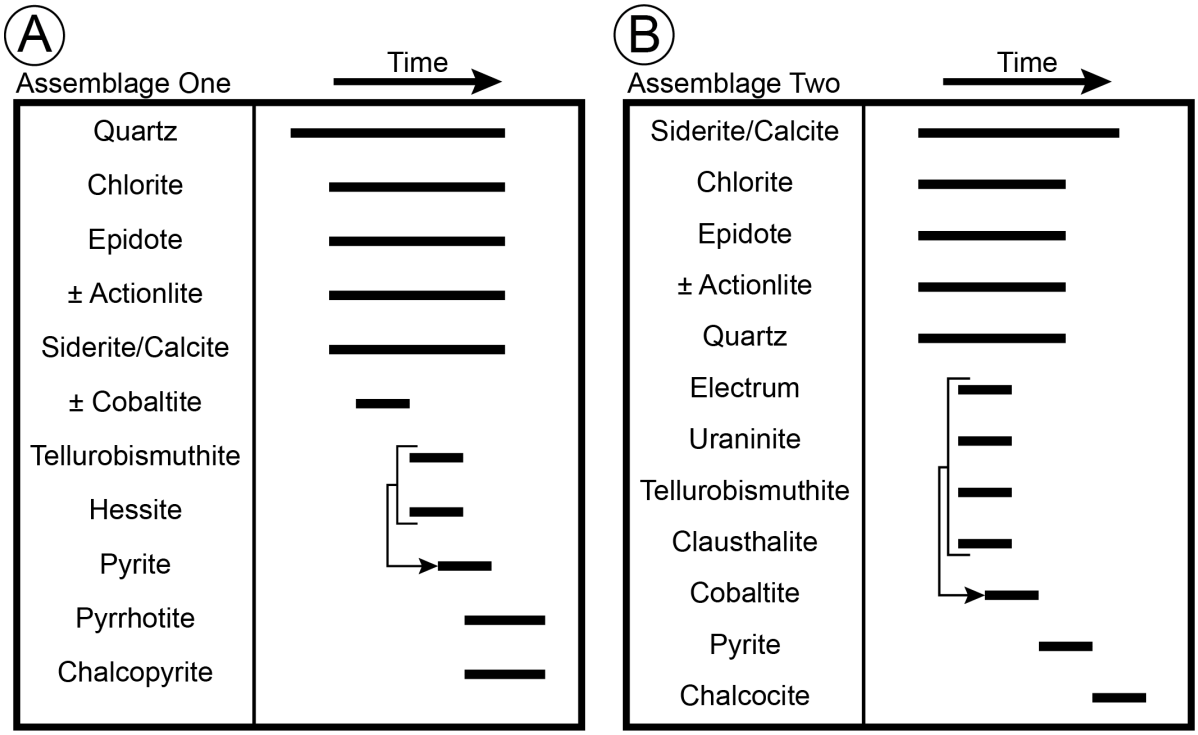

Figure 2.8 - A. Generalized paragenetic sequence of ore minerals for Assemblage One. B. Generalized paragenetic sequence of ore minerals for Assemblage Two. Note that arrows drawn between minerals denote the occurrence of one mineral exclusively as inclusions within another (e.g., gold occurs exclusively as inclusions within cobaltite); suggesting a genetic relationship.

In Assemblage One, the early phase of quartz-carbonate-chlorite mineralization was followed by a phase of limited cobaltite mineralization, with a subsequent phase of telluride mineralization hosted in pyrite grains (Figure 2.5d). However, in Assemblage Two telluride and selenide mineralization was synchronous with electrum and uraninite mineralization, all of which are associated with Co mineralisation (Figure 2.7a). This is interpreted from the occurrence of electrum, uraninite, and these telluride/selenides almost exclusively as inclusions within cobaltite in this assemblage (Figures 2.6c and 2.7a). The co-occurrence of these phases implies they are genetically related, associated with common transport and co-precipitation. A similar affinity between Au and cobaltite has previously been noted in hydrothermal Au-Cu systems (Le Vaillant et al., 2018; Soloviev, Kryazhev, & Dvurechenskaya, 2013). This was followed by the growth of pyrite around pre-existing cobaltite grains (Figure 2.6b). In Assemblage One this phase of pyrite precipitation was followed by the co-precipitation of chalcopyrite and pyrrhotite within an interlocking framework of chlorite (Figure 2.5c). This textural relationship indicates that either the synchronous precipitation of chalcopyrite and

pyrrhotite infilled this pre-existing chlorite lattice or that the chlorite, pyrrhotite, and chalcopyrite were approximately synchronous. In Assemblage Two the pyrite precipitation phase was instead followed by a final phase of chalcocite mineralization, which is observed to have partially replaced the preceding pyrite and forms a thin layer around or cross-cuts some cobaltite grains (Figures 2.6a, b, c and 2.7d).

Across both Assemblage One and Assemblage Two, the paragenetic sequence of ore minerals in Figure 2.8 appears to reflect a progressive sequence of Au, Co, and then Cu mineralization. Within Assemblage One this is reflected in the sequential mineralization of cobaltite (Co), then chalcopyrite (Cu). In Assemblage Two this sequence is represented by the mineralization of electrum (Au), then cobaltite, and finally chalcocite (Cu). However, as Assemblage One and Two are typically spatially distinct, it is difficult to ascertain the nature of their relative timing. As such, whether the existence of these two distinct assemblages represent the progressive geochemical evolution of a single ore fluid arising from a single mineralizing event or two distinct phases of mineralization with two genetically distinct ore fluids is as yet unconstrained. However, the significant difference in the prevalence of cobaltite and predominant stable copper sulfide phase between these two assemblages suggest potential physicochemical differences in the hydrothermal conditions under which these phases formed (Crerar & Barnes, 1976; Jansson & Liu, 2020; Liu et al., 2011; Zhao, Brugger, Ngothai, & Pring, 2014). Additionally, the rarity of samples containing both ore mineral assemblages may suggest that the existence of these distinct assemblages reflects a spatial geochemical and mineralogical zonation within the Carlow Castle ore zone.

2.7.2 Preliminary constraints on Carlow Castle ore fluid

The mineralogical analyses conducted in this study provide several key insights into the genesis of Carlow Castle's Cu-Co-Au mineralization; particularly pertaining to the nature of its ore fluid, metal mobilization processes, and metal concentration processes. Firstly, the pervasive carbonate veining throughout the ore zone and the surrounding tectonized zone precludes the possibility that Carlow Castle's ore fluid was strongly acidic, due to the well-established reactivity of carbonate minerals with acidic fluids (Golubev, Benezeth, Schott, Dandurand, & Castillo, 2009; Mikucki & Ridley, 1993). The prevalence of carbonate veining hosting Cu-Co-Au mineralisation at Carlow Castle suggests that dissolution of metals under acidic (pH <4) conditions was unlikely to be a critical metal transport process within the ore fluid, unlike in many porphyry Cu or high-sulfidation epithermal Au deposits for example (Keith, Smith,

Jenkin, Holwell, & Dye, 2018; Seedorff et al., 2005). The abundance of this carbonate veining also suggests that the ore fluid contained a significant amount of dissolved carbonate (Chi, Liu, & Dube, 2009; Kerrich & Fyfe, 1981). Additionally, the occurrence of Cu, Co, Au mineralization at Carlow Castle as, or in association with, base metal sulfides/sulfarsenides, tellurides/selenides, uraninite, and siderite is clear evidence of the precipitation of these metals under reducing conditions due to the well-documented influence of redox conditions on the stability of these phases (Grundler et al., 2013; Keith et al., 2018; Plasil, 2014; Postma, 1983). This may indicate that a shift in redox conditions within the ore fluid towards reducing conditions at the site of mineralization may have been key to inducing Cu, Co, Au precipitation, particularly if these metals were transported in Cl^- complexes within an oxidized ore fluid (Heinrich & Candela, 2014; Pokrovski, Akinfie, Borisova, Zotov, & Kouzmanov, 2014; Saunders et al., 2014). It is possible that the interaction of such an oxidized ore fluid with reduced mineral phases within the black shales and mafic volcanic rocks of the Nickol River and Ruth Well Formations at the site of mineralization may have driven the evolution of this ore fluid toward reducing conditions. Therefore, it is feasible that the Cu, Co, Au mineralization at Carlow Castle precipitated from a brine that was near-neutral in pH, carbonate-bearing, and reducing at the point of mineralization.

The co-occurrence of Cu, Co, and Au-bearing minerals within Carlow Castle, with no evidence of successive overprinting phases of mineralization, indicates that the ore fluid must have been capable of simultaneously transporting these metals. This is particularly the case for Co and Au, which have already been demonstrated to display a clear genetic relationship in their mineralogical occurrence. While generally Cl^--complexation is the dominant process for metal transport in most hydrothermal Cu-Co systems (Brown, 2014; Hitzman et al., 2010; Rose, 1989), it is generally the less common mechanism for Au transportation in hydrothermal solutions <500°C (Liu et al., 2014b; Zhu et al., 2011). Instead complexation with HS^- is typically the preferred process for Au mobilization in most hydrothermal Au systems, though Au may still be transported through Cl^-- or OH^--complexation (Saunders et al., 2014; Zhu et al., 2011). However, the presence of significant volumes of dissolved HS^- in an ore fluid would generally preclude the transport of Cu and Co in the volumes required to form Carlow Castle, unless under strongly acidic (pH <4) conditions (Gaboury, 2019; Saunders et al., 2014). Additionally, Au dissolution via complexation with Cl^- is most effectively facilitated under oxidizing conditions; which are similarly conducive to Cu and Co transport (Pokrovski et al.,

2014; Rose, 1989). As such, within this ore fluid Cl^-- or OH^--complexation of these metals is the most probable process for metal mobilization. While it is possible that the metal enrichments may have been carried in multiple stages, with Au initially transported in a HS^- rich fluid and a second distinct Cl^--rich fluid carrying Cu and Co, this interpretation is not supported by the petrographic evidence that indicates that Co and Au appear to have co-precipitated. This interpretation implies that the Carlow Castle ore fluid was saline and more characteristic of an ore fluid in a basin-hosted mineral system or a magmatically-derived fluid, rather than a low-salinity metamorphic fluid that is more typical of lode gold mineralization (Heinrich & Candela, 2014; Saunders et al., 2014).

The paragenetic sequences of ore mineralization (Figure 2.8) for Assemblage One and Two appear to record evidence of the geochemical evolution of the Carlow Castle ore fluid. Broadly within both sequences, but particularly Assemblage Two, there is a clear trend regarding sulfur fugacity within the hydrothermal system. This is reflected in the sequence of initial telluride, selenide, and alloy precipitation; followed by sulfarsenide precipitation; and finally base metal sulfide precipitation. This sequence appears to reflect an increase in sulfur fugacity within the system through time; this is suggested by the early occurrence of electrum in association with tellurides and/or selenides and a simultaneous lack of sulfides. This is characteristic of many sulfur undersaturated hydrothermal Au deposits (Hedenquist, Arribas, & Gonzalez-Urien, 2000; Saunders et al., 2014; White & Hedenquist, 1995). Following this, the gradual addition of sulfur to the system could account for the occurrence of cobaltite; a sulfarsenide. If this additional sulfur was supplied as HS^- or another reduced sulfur species, this could act as a reductant to induce Co precipitation into cobaltite from the ore fluid that carried these metals (Heinrich & Candela, 2014; Seward, Williams-Jones, & Migdisov, 2014). Following Co precipitation, the continued addition of sulfur may have induced a final phase of Cu mineralization hosted solely in base metal sulfides. This sequence also coincides with the sequential Au, Co, and Cu mineralization observed at Carlow Castle and most likely reflects the different solubility of Co, Cu, and particularly Au in the presence of HS^- (Hofmann, 1999; Saunders et al., 2014; Saunders & Schoenly, 1995). The progressive increase in sulfur fugacity through this sequence and the insolubility of Cu and Co in most HS^--rich fluids suggests that the HS^- necessary for sulfide mineralization may have been supplied to the Cu-Co-Au bearing ore fluid at a late stage, proximal to the site of mineralization. As such, it can be tentatively interpreted that this HS^- was supplied either by the mixing of Carlow Castle's ore fluid with a

distinct HS^- rich fluid that was also channeled into the Carlow Castle tectonized zone, or potentially from the interaction of the ore fluid with a HS^--rich wall rock. The gradual addition of HS^- to the ore fluid from either of these sources could have induced the reductive precipitation of Au, Co, and Cu and account for the progressive increase in sulfur fugacity within the system; recorded by the increase in sulfur through the paragenetic sequence of ore minerals (Figure 2.8). The black shales that occur through the Nickol River and Ruth Well Formations may have provided this HS^- if they formed a significant portion of the wall rock at Carlow Castle. However, this is difficult to determine due to the extensive hydrothermal alteration of the wall rock and sulfur isotope studies are required to fully understand the nature of Carlow Castle's sulfur source.

2.7.3 Probable age and fluid pathway

As there are presently no geochronological constraints on Carlow Castle's formation, fitting its genesis into the established model for the tectonic evolution of the northwest Pilbara Craton is challenging. However, the nature of its occurrence within the stratigraphy of the Pilbara Craton and the insights about the nature of its mineralization provided by this study may still provide some constraints on the mineral system. Presently, the best indication of Carlow Castle's age is provided by its occurrence within higher-order faults that are interpreted here to be a product of deformation along the Regal Thrust. The Regal Thrust formed during the convergent tectonic regime that preceded the Prinsep Orogeny (~3070 Ma); wherein the Regal Terrane was obducted onto the Karratha Terrane (Hickman, 2016). This provides a maximum possible age of 3070 Ma for Carlow Castle's mineralization. However, this provides little insight into its minimum possible age. It has previously been recognized that the Carlow Castle area has been affected by multiple stages of deformation, with at least one stage of major deformation post-dating the Prinsep Orogeny and potentially coinciding with the North Pilbara Orogeny (Hickman, 2016; Kiyokawa et al., 2002). As such, several different tectonic events during the formation of the Pilbara Craton could have been associated with the formation of the Carlow Castle deposit and its higher-order host structures within the Regal Thrust. Additionally, there is also significant potential for deformation of the deposit following ore formation. With this considered, the exceptional tectonic stability of the northwest Pilbara Craton subsequent to the initiation of the Fortescue Rift and the formation of the Fortescue Basin ~50 km to the south around 2775 Ma (Hickman, 2012, 2016) makes a major post-Archean ore-forming event unlikely. Nonetheless, these constraints leave a range of ~295 Ma over which Carlow Castle

may have formed during the evolution of the Pilbara Craton; with several distinct potential ore-forming tectonic events. While the timing of the ore-forming event that produced the distinctive Cu-Co-Au mineralization remains ambiguous, the Regal Thrust was unambiguously a key component of the mineral system. Regionally, the Regal Thrust would have likely acted as a major conduit to allow for the flow of Cu-Co-Au rich ore fluids. These Cu-Co-Au rich fluids could have then been focused into and trapped within complex higher-order structures through the brecciated and sheared zone at Carlow Castle, leading to metal precipitation.

2.7.4 Comparisons to other deposits

Due to its distinctive Cu-Co-Au endowment, the Carlow Castle deposit bears a similar ore element enrichment to Co-rich sediment-hosted stratiform Cu (SSC) deposits, such as those in the Central African Copper Belt (Saintilan, Selby, Creaser, & Dewaele, 2017), which are also typically Cu-Co sulphide-dominated (Hitzman et al., 2005). However, there are several critical characteristics that distinguish Carlow Castle from those deposits; most importantly Carlow Castle's geological setting, the age of its host terrane, key aspects of its genesis, and the nature of its mineralization. First, Carlow Castle's occurrence within an accretionary greenstone belt dominated by mafic volcanic rocks and minor shales distinguishes it from Co-rich SSC deposits, which are most commonly hosted in rift-basins associated with thick sequences of immature first-cycle clastic sediment (Brown, 2014). Additionally, the occurrence of Carlow Castle within a Mesoarchean host terrane, and the probable Archean age of mineralization, contrasts strongly with the occurrence of SSC deposits overwhelmingly in host sequences of maximum Proterozoic age (Hitzman et al., 2010). This speaks to significant differences in the genetic processes that produced these deposits. In SSC deposits the oxidized ore fluid is commonly interpreted to derive from oxidized saline basinal brines, while the most common metal source is from immature metalliferous clastic material within the thick red bed sequences that commonly underlie these deposits (Brown, 2014; Hitzman et al., 2005; Kirkham, 1989). These are almost certainly not the sources of ore fluids or metals within the Carlow Castle mineral system due to the critical control that the oxidation state of the Earth's atmosphere imparts on the formation of these, and the lack of significant oxygenation of the Earth's atmosphere during the Archean (Lyons, Reinhard, & Planavsky, 2014). Finally, the occurrence of this mineralization on a deposit scale further distinguishes it from an SSC deposit. At Carlow Castle the dominantly structurally-controlled nature of the mineralization through a heavily tectonized zone proximal to a regionally significant thrust fault, hosted in quartz-carbonate

veins, with extensive chloritic hydrothermal wall-rock alteration is distinct from mineralization in typical SSC deposit. In contrast, in SSC deposits mineralization typically occurs as a laterally extensive stratiform ore body along the redox boundary between an underlying oxidized red bed and an overlying organic-rich reduced bed (Lyons et al., 2014). Reflecting these differences, Carlow Castle appears to represent an unconventional and genetically distinct class of hydrothermal Cu-Co-Au.

Although Carlow Castle does not appear to resemble a Co-rich SSC deposit beyond its distinctive Cu-Co-Au metal endowment, it does bear some resemblance to some previously studied unconventional Co deposits. In the Bou Azzer district, Morocco Carboniferous Co-mineralization occurs as Co-Ni-Fe arsenide dominated orebodies hosted in quartz-carbonate veins through a series of tectonic structures within the Neoproterozoic Bou Azzer ophiolite complex (Le Blanc & Billaud, 1982; Oberthür et al., 2009). Additionally, Cu-Fe sulfides, sulfosalts, and Au-Ag alloys are also observed in variable amounts in association with this Co mineralization (Ahmed et al., 2009). This ophiolite complex is composed predominantly of a mix of serpentinized peridotites, submarine mafic volcanics, and mafic-ultramafic cumulates (Ahmed et al., 2009). The current genetic model for the Bou Azzer Co district posits that it was a product of the migration of a saline brine related to felsic magmatism during the Late Paleozoic Hercynian/Variscan orogeny (Ahmed et al., 2009; En-Naciri, Barbanson, & Touray, 1997). Within this model it is proposed that this magmatic fluid leached ore metals from the serpentinites of the Bou Azzer ophiolite complex and precipitated these metals under increasing pH, sulfur fugacity, and decreasing O_2 fugacity in response to mixing with a cool meteoric fluid (Ahmed et al., 2009; En-Naciri et al., 1997; Essaraj, Boiron, Cathelineau, Banks, & Benharref, 2005). In some respects, the preliminary interpretations made about the Carlow Castle ore fluid in this study resemble those of Bou Azzer. Additionally, the paragenetic sequence at Bou Azzer is comparable to Carlow Castle's; with a sequence reflecting increasing sulfur fugacity and sequential Au-Co/Ni/As-Cu mineralization (Ahmed et al., 2009). Finally, it is interesting to note that rocks of the Bou Azzer ophiolite complex are most probably of comparable bulk composition to the dominantly mafic-ultramafic volcanics of the Ruth Well Formation, within which Carlow Castle is hosted. If the ultramafic rocks of this ophiolite complex were a key source of ore metals for the formation of the Bou Azzer, then this may likewise apply to the genesis of Carlow Castle.

Additional deposits that share some geological characteristics with Carlow Castle and Bou Azzer include the five element (Ni-Co-As-Ag-Bi) deposits of Cobalt, Ontario, Canada and the Co-Cu-Au deposits of the Idaho Co belt, USA. Most notable among these shared characteristics are their distinctly Co-dominated ore mineralogies, vein-hosted sulfide and sulfarsenide mineralization, and occurrence within convergent metamorphosed terranes (Bookstrom et al., 2016; Kissin, 1992). Therefore, Carlow Castle may represent an addition to the distinct and relatively rare class of hydrothermal and volcanogenic polymetallic deposits that Ahmed et al. (2009) collectively grouped the above mentioned deposits into. As such, comparisons to the established genetic models for these deposits could be useful in constraining the genesis of Carlow Castle.

2.8 Implications and future study

The primary significance of Carlow Castle stems from its unique Cu-Co-Au metal association and distinctive ore mineralogy given its geological setting. The fact that Carlow Castle occurs within an Archean greenstone belt and is of probable Meso-Neoarchean age is particularly notable due to the scarcity of significant hydrothermal Co mineralization outside of basin-hosted systems and even greater scarcity of hydrothermal Co mineralization in Archean terranes. This is because the majority of the world's Cu-Co deposits are hosted in sedimentary basins of Proterozoic or younger age (US Geological Survey, 2018). Therefore, understanding the unique confluence of processes necessary to form this distinctive Cu-Co-Au mineralization is of particular importance. Understanding the genesis of Carlow Castle has important implications for potentially uncovering other Cu-Co deposits in Archean terranes. Following this initial study, further analysis will be undertaken to better constrain the genesis of the Carlow Castle mineral system. This will include S-isotope analysis, to assist in constraining the sulfur source for Carlow Castle's mineralization, and absolute geochronology to account for Carlow Castle's formation within the established tectonic evolution of the Pilbara Craton.

Acknowledgements

This research was supported by an Australian Government Research Training Program Scholarship and a CSIRO Mineral Resources postgraduate student scholarship. Artemis Resources Ltd. are acknowledged for their logistical, and material support.

References

Ahmed, H. A., Arai, S., & Ikenne, M. (2009). Mineralogy and Paragenesis of the Co-Ni Arsenide Ores of Bou Azzer, Anti-Atlas, Morocco. *Economic Geology, 104*(2), 249-266.

Artemis Resources Limited. (2017). Cobalt Update - Carlow Castle Project [Press release]. Retrieved from https://artemisresources.com.au/investors-relations/announcements

Artemis Resources Limited. (2018a). 2.32% Cobalt in Shallow Drilling at Carlow Castle [Press release]. Retrieved from https://artemisresources.com.au/investors-relations/announcements

Artemis Resources Limited. (2018b). 4.5 Mt of Cobalt/Copper/Gold JORC Resources at Carlow Castle - Karratha, Western Australia [Press release]. Retrieved from https://artemisresources.com.au/investors-relations/announcements

Artemis Resources Limited. (2018c). High Grade Cobalt Drilled over 1.2km at Carlow Castle [Press release]. Retrieved from https://www.asx.com.au/asxpdf/20181015/pdf/43z7lvpq8r2kvt.pdf

Artemis Resources Limited. (2019a). 5,000m Diamond Drilling Programme for Carlow Castle [Press release]. Retrieved from https://artemisresources.com.au/investors-relations/announcements

Artemis Resources Limited. (2019b). Carlow Castle Au-Cu-Co Resource Grows by 71% to 7.7Mt [Press release]. Retrieved from https://artemisresources.com.au/investors-relations/announcements

Artemis Resources Limited. (2021). June 2021 Quarterly Report [Press release]. Retrieved from https://wcsecure.weblink.com.au/pdf/ARV/02400741.pdf

Bookstrom, A. A., Box, S. E., Cossette, P. M., Frost, T. P., Gillerman, V. S., King, G. R., & Zirakparvar, N. A. (2016). Geologic history of the Blackbird Co-Cu district in the Lemhi subbasin of the Belt-Purcell Basin. In J. S. MacLean & J. W. Sears (Eds.), *Belt Basin: Window to Mesoproterozoic Earth: Geological Society of America Special Paper* (Vol. 522, pp. 185-219). United States: Geological Society of America.

British Geological Survey. (2015). *Risk List 2015*. Retrieved from Nottingham, United Kingdom:

Britt, A., Summerfield, D., Senior, A., Kay, P., Huston, D., Hitchman, A., . . . Schofield, A. (2017). *Australia's Identified Mineral Resources 2017*. Retrieved from Canberra:

1514 Brown, A. C. (2014). Low-Temperature Sediment-Hosted Copper Deposits. In K. Turekian &
1515 H. Holland (Eds.), *Treatise on Geochemistry* (2nd ed., Vol. 13, pp. 251-271). Oxford:
1516 Elsevier Science.
1517 Chi, G., Liu, Y., & Dube, B. (2009). Relationship between CO2-dominated fluids,
1518 hydrothermal alterations and gold mineralization in the Red Lake greenstone belt,
1519 Canada. *Applied Geochemistry, 24*, 504-516.
1520 Crerar, D., & Barnes, H. (1976). Ore solution chemistry; V, Solubilities of chalcopyrite and
1521 chalcocite assemblages in hydrothermal solution at 200 degrees to 350 degrees C.
1522 *Economic Geology, 71*(4), 772-794.
1523 De Caritat, P., Hutcheon, I., & Walshe, J. L. (1993). Chlorite Geothermometry: A Review.
1524 *Clays and Clay Minerals, 41*(2), 219-239.
1525 En-Naciri, A., Barbanson, L., & Touray, J. (1997). Brine inclusions from the Co-As(Au) Bou
1526 Azzer District, Anti-Atlas Mountains, Morocco. *Economic Geology, 92*(3), 360-367.
1527 Eremenco, D., Mortimer, R., & Mead, E. (2019). Delineating cobalt targets from a galvanic
1528 and inductive source Sub-Audio Magnetics (SAM) at the Carlow Castle project,
1529 Western Australia. *ASEG Extended Abstracts, 2019*(1), 1-4.
1530 doi:10.1080/22020586.2019.12072960
1531 Eriksson, K. A. (1982). Geometry and internal characteristics of Archaean submarine channel
1532 deposits, Pilbara Block, Western Australia. *Journal of Sedimentary Research, 52*(2),
1533 383-393. doi:10.1306/212F7F5E-2B24-11D7-8648000102C1865D
1534 Essaraj, S., Boiron, M., Cathelineau, M., Banks, D. A., & Benharref, M. (2005). Penetration of
1535 surface-evaporated brines into the Proterozoic basement and deposition of Co and Ag
1536 at Bou Azzer (Morocco): Evidence from fluid inclusions. *Journal of African Earth*
1537 *Sciences, 41*(1-2), 25-39.
1538 European Commission. (2017). *The 2017 List of Critical Raw Materials for the EU*. Retrieved
1539 from Brussels, Belgium:
1540 Gaboury, D. (2019). Parameters for the formation of orogenic gold deposits. *Applied Earth*
1541 *Science*, 1-10.
1542 Golubev, S. V., Benezeth, P., Schott, J., Dandurand, J. L., & Castillo, A. (2009). Siderite
1543 dissolution kinetics in acidic aqueous solutions from 25 to 100 °C and 0 to 50 atm
1544 pCO2. *Chemical Geology, 265*(1-2), 13-19.
1545 Groves, D. I., Goldfarb, R. J., Gebre-Mariam, M., Hagemann, S. G., & Robert, F. (1998).
1546 Orogenic gold deposits: A proposed classification in the context of their crustal

distribution and relationship to other gold deposit types. *Ore Geology Reviews, 13*, 7-27.

Grundler, P. V., Brugger, J., Etschmann, B., Helm, L., Liu, W., Spry, P. G., . . . Pring, A. (2013). Speciation of aqueous tellurium(IV) in hydrothermal solutions and vapors, and the role of oxidized tellurium species in Te transport and gold deposition. *Geochimica et Cosmochimica Acta, 120*.

Hedenquist, J. W., Arribas, A., & Gonzalez-Urien, E. (2000). Exploration for Epithermal Gold Deposits *SEG Reviews, 13*, 245-277.

Heinrich, C. A., & Candela, P. A. (2014). 13.1 - Fluids and Ore Formation in the Earth's Crust. In H. Holland & K. Turekian (Eds.), *Treatise on Geochemistry (Second Edition)* (Vol. 13, pp. 1-28). Amsterdam: Elsevier Science.

Hickman, A. H. (2002). *Geology of the Roebourne 1:100 000 sheet*. Retrieved from

Hickman, A. H. (2004a). Two contrasting granite–greenstone terranes in the Pilbara Craton, Australia: evidence for vertical and horizontal tectonic regimes prior to 2900 Ma. *Precambrian Research, 131*(3-4), 153-172.

Hickman, A. H. (2012). Review of the Pilbara Craton and Fortescue Basin, Western Austrlia: Crustal evolution providing environments for early life. *Island Arc, 21*(1), 1-31.

Hickman, A. H. (2016). *Northwest Pilbara Craton: a record of 450 million years in the growth of Archean continential crust*. Retrieved from Perth:

Hickman, A. H. (2021). *East Pilbara Craton: a record of one billion years in the growth of Archean continental crust*. Retrieved from

Hickman, A. H., Huston, D., Van Kranendonk, M. J., & Smithies, R. H. (2006). *Geology and mineralization of the west Pilbara - a field guide*. Retrieved from

Hickman, A. H., Smithies, R. H., & Tyler, I. M. (2010). *Evolution of active plate margins: West Pilbara Superterrane, De Grey Superbasin, and the Fortescue and Hamersley Basins — a field guide*. Retrieved from Perth:

Hickman, A. H., & Van Kranendonk, M. J. (2012). Early Earth evolution: Evidence from the 3.5-1.8 Ga geological history of the Pilbara region of Western Australia. *Episodes, 35*(1), 283-297. doi:https://doi.org/10.18814/epiiugs/2012/v35i1/028

Hitzman, M., Kirkham, R. V., Broughton, D., Thorson, J., & Selley, D. (2005). The Sediment-Hosted Stratiform Copper Ore System. *Economic Geology, 100th Anniversary Volume*, 609-642. doi:https://doi.org/10.5382/AV100.19

1579 Hitzman, M., Selley, D., & Bull, S. (2010). Formation of Sedimentary Rock-Hosted Stratiform
1580 Copper Deposits through Earth History. *Economic Geology, 105*(3), 627-639.
1581 doi:https://doi.org/10.2113/gsecongeo.105.3.627
1582 Hofmann, B. A. (1999). *Geochemistry of Natural Redox Fronts - A Review*. Retrieved from
1583 Wettingen, Switzerland:
1584 Jansson, N. F., & Liu, W. (2020). Controls on cobalt and nickel distribution in hydrothermal
1585 sulphide deposits in Bergslagen, Sweden - constraints from solubility modelling. *GFF,*
1586 *142*(2), 87-95. doi:https://doi.org/10.1080/11035897.2020.1751270
1587 JORC. (2012). *Australasian Code for Reporting of Exploration Results, Mineral Resources*
1588 *and Ore Reserves*. Retrieved from
1589 Kato, Y., Ohta, I., Tsunematsu, T., Watanabe, Y., Isozaki, Y., Maruyama, S., & Imai, N.
1590 (1998). Rare earth element variations in mid-Archean banded iron formations:
1591 implications for the chemistry of ocean and continent and plate tectonics. *Geochimica*
1592 *et Cosmochimica Acta, 62*(21-22), 3475-3497.
1593 Keith, M., Smith, D. J., Jenkin, G. R. T., Holwell, D. A., & Dye, M. T. (2018). A review of Te
1594 and Se systematics in hydrothermal pyrite from precious metal deposits: Insights into
1595 ore-forming processes. *Ore Geology Reviews, 96*, 269-282.
1596 Kemp, A. I. S., Hickman, A. H., Kirkland, C. L., & Vervoort, J. (2015). Hf isotopes in detrital
1597 and inherited zircons of the Pilbara Craton provide no evidence for Hadean continents.
1598 *Precambrian Research, 261*, 112-126.
1599 Kerrich, R., & Fyfe, W. S. (1981). The gold—carbonate association: Source of CO2, and CO2
1600 fixation reactions in Archaean lode deposits. *Chemical Geology, 33*(1-4), 265-294.
1601 Kerrich, R., Goldfarb, R. J., Groves, D. I., Garwin, S., & Jia, Y. (2000). The characteristics,
1602 origins, and geodynamic settings of supergiant gold metallogenic provinces. *Science in*
1603 *China D: Earth Sciences, 43*(1), 1-68.
1604 Kirkham, R. V. (1989). Distribution, Settings, and Genesis of Sediment-hosted Stratiform
1605 Copper Deposits. *Geological Association of Canada Special Paper, 36*, 3-38.
1606 Kissin, S. A. (1992). Five-element (Ni-Co-As-Ag-Bi) Veins. *Geoscience Canada, 19*(3), 113-
1607 124.
1608 Kiyokawa, S., Taira, A., Byrne, T., Bowring, S., & Sano, Y. (2002). Structural evolution of the
1609 middle Archean coastal Pilbara terrane, Western Australia. *Tectonics, 21*(5), 1-24.
1610 Le Blanc, M., & Billaud, P. (1982). Cobalt Arsenide Orebodies Related to an Upper
1611 Proterozoic Ophiolite: Bou Azzer (Morocco). *Economic Geology, 77*(1), 162-175.

Le Vaillant, M., Barnes, S. J., Fiorentini, M. L., Barnes, S., Bath, A., & Miller, J. (2018). Platinum-group element and gold contents of arsenide and sulfarsenide minerals associated with Ni and Au deposits in Archean greenstone belts. *Mineralogical Magazine, 82*(3), 325-347.

Liu, S., Borg, S., Testemale, D., Etschmann, B., Hazemann, J., & Brugger, J. (2011). Speciation and thermodynamic properties for cobalt chloride complexes in hydrothermal fluids at 35–440° C and 600 bar: an in-situ XAS study. *Geochimica et Cosmochimica Acta, 75*(5), 1227-1248. doi:https://doi.org/10.1016/j.gca.2010.12.002

Liu, W., Etschmann, B., Testemale, D., Hazemann, J., Rempel, K., Muller, H., & Brugger, J. (2014b). Gold transport in hydrothermal fluids: Competition among the Cl−, Br−, HS− and NH3(aq) ligands. *Chemical Geology, 376*, 11-19.

Lyons, T. W., Reinhard, C. T., & Planavsky, N. J. (2014). The rise of oxygen in Earth's early ocean and atmosphere. *Nature, 506*, 307-315. doi:https://doi.org/10.1038/nature13068

Mikucki, E. J., & Ridley, J. R. (1993). The hydrothermal fluid of Archa an lode-gold deposits at different metamorphic grades: compositional constraints from ore and wallrock alteration assemblages. *Mineralium Deposita, 28*, 469-481.

Mudd, G. M., Werner, T. T., Weng, Z. H., Yellitshetty, M., Yuan, Y., McAlpine, S. R. B., . . . Czarnota, K. (2018). *Critical Minerals in Australia: A Review of Opportunities and Research Needs*. Retrieved from Canberra, Australia:

Oberthür, T., Melcher, F., Henjes-Kunst, F., Gerdes, A., Stein, H., Zimmerman, A., & El Ghorfi, M. (2009). Hercynian age of the cobalt-nickel-arsenide-(Gold) Ores, Bou Azzer, Anti-Atlas, Morocco: Re-Os, Sm-Nd, and U-Pb age determinations. *Economic Geology, 104*(7), 1065-1079.

Olivetti, E. A., Ceder, G., Gaustad, G. G., & Fu, X. (2017). Lithium-Ion Battery Supply Chain Considerations: Analysis of Potential Bottlenecks in Critical Metals. *Joule, 1*(2), 229-243.

Openpit Mining Limited. (1987). *Roebourne Project Progress Report of Exploration for 1987*. Retrieved from Perth: https://geodocsget.dmirs.wa.gov.au/api/GeoDocsGet?filekey=d8f8222d-9c0f-4a7d-9cb1-3188991bf768-m7nok2ay4ykgnw2exiit357u15npjxp0wx8891s1

Peterson, A., Kemp, A. I. S., Hickman, A. H., Whitehouse, M. J., Martin, L., & Gray, C. M. (2019). A new 3.59 Ga magmatic suite and a chondritic source to the east Pilbara Craton. *Chemical Geology, 511*, 51-70.

Plasil, J. (2014). Oxidation–hydration weathering of uraninite: the current state-of-knowledge. *Journal of Geosciences, 59*(2), 99-114.

Pokrovski, G. S., Akinfie, V., Borisova, A. Y., Zotov, A. V., & Kouzmanov, K. (2014). Gold speciation and transport in geological fluids: insights from experiments and physical-chemical modelling. In P. S. Garofalo & J. R. Ridley (Eds.), *Gold-Transporting Hydrothermal Fluids in the Earth's Crust* (Vol. Special Publications 402). London: Geological Society.

Postma, D. (1983). Pyrite and siderite oxidation in swamp sediments. *Journal of Soil Science, 34*(1), 163-182.

Rose, A. (1989). Mobility of Copper and Other Heavy Metals in Sedimentary Environments. *Special Paper - Geological Association of Canada, 36*, 97-110.

Ruddock, I. (1999a). *Mineral occurences and exploration potential of the west Pilbara*. Retrieved from Perth, Western Australia:

Saintilan, N. J., Selby, D., Creaser, R. A., & Dewaele, S. (2017). Sulphide Re-Os geochronology links orogenesis, salt and Cu-Co ores in the Central African Copperbelt. *Scientific Reports, 8*(1).

Saunders, J. A., Hofstra, A. H., Goldfarb, R. J., & Reed, M. H. (2014). 13.15 - Geochemistry of Hydrothermal Gold Deposits. In H. Holland & K. Turekian (Eds.), *Treatise on Geochemistry* (2 ed., Vol. 13, pp. 383-424). Amsterdam: Elsevier.

Saunders, J. A., & Schoenly, P. A. (1995). Boiling, colloid nucleation and aggregation, and the genesis of bonanza Au-Ag ores of the sleeper deposit, Nevada. *Mineralium Deposita, 30*(3-4), 199-210.

Seedorff, E., Dilles, J. H., Proffett, J. M., Jr., Einaudi, M. T., Zurcher, L., Stavast, W. J. A., . . . Barton, M. D. (2005). Porphyry Deposits: Characteristics and Origin of Hypogene Features. In J. W. Hedenquist, J. F. H. Thompson, R. J. Goldfarb, & J. P. Richards (Eds.), One Hundredth Anniversary Volume (pp. 0): Society of Economic Geologists. Retrieved from https://doi.org/10.5382/AV100.10. doi:10.5382/AV100.10

Seward, T. M., Williams-Jones, A. E., & Migdisov, A. A. (2014). 13.2 - The Chemistry of Metal Transport and Deposition by Ore-Forming Hydrothermal Fluids. In H. Holland

& K. Turekian (Eds.), *Treatise on Geochemistry (Second Edition)* (Vol. 13, pp. 29-57). Amsterdam: Elsevier Science.

Shibuya, T., Kitajima, K., Komiya, T., Terabayashi, M., & Maruyama, S. (2007). Middle Archean ocean ridge hydrothermal metamorphism and alteration recorded in the Cleaverville area, Pilbara Craton, Western Australia. *Journal of Metamorphic Geology, 25*(7), 751-767.

Smithies, R. H., Hickman, A. H., & Nelson, D. R. (1999). New constraints on the evolution of the Mallina Basin, and their bearing on relationships between contrasting eastern and western granite–greenstone terranes of the Archaean Pilbara Craton,Western Australia. *Precambrian Research, 94*(1-2), 11-28.

Soloviev, S. G., Kryazhev, S. G., & Dvurechenskaya, S. S. (2013). Geology, mineralization, stable isotope geochemistry, and fluid inclusion characteristics of the Novogodnee–Monto oxidized Au–(Cu) skarn and porphyry deposit, Polar Ural, Russia. *Mineralium Deposita, 48*(5), 603-627.

U.S. Department of the Interior. (2018). *Final List of Critical Minerals 2018*. Retrieved from Washington D.C., United States of America:

US Geological Survey. (2018). *Mineral commodity summaries 2018*. Retrieved from

Van Kranendonk, M. J., Hickman, A. H., Smithies, R. H., Nelson, D. R., & Pike, G. (2002). Geology and Tectonic Evolution of the Archean North Pilbara Terrain, Pilbara Craton, Western Australia. *Economic Geology, 97*(4), 695-732. doi:https://doi.org/10.2113/gsecongeo.97.4.695

Van Kranendonk, M. J., Hickman, A. H., Smithies, R. H., Williams, I. R., Bagas, L., & Farrell, T. R. (2006). *Revised lithostratigraphy of Archean supracrustal and intrusive rocks in the northern Pilbara Craton, Western Australia*. Retrieved from

Van Kranendonk, M. J., Smithies, R. H., Hickman, A. H., & Champion, D. (2007). Review: secular tectonic evolution of Archean continental crust: interplay between horizontal and vertical processes in the formation of the Pilbara Craton, Australia. *Terra Nova, 19*(1), 1-38.

Van Kranendonk, M. J., Smithies, R. H., Hickman, A. H., Wingate, M. T. D., & Bodorkos, S. (2010). Evidence for Mesoarchean (~3.2Ga) rifting of the Pilbara Craton: The missing link in an early Precambrian Wilson cycle. *Precambrian Research, 177*, 145-161.

White, N. C., & Hedenquist, J. W. (1995). Epithermal gold deposits: styles, characteristics and exploration. *SEG Newsletter, 23*(1), 9-13.

Zhao, J., Brugger, J., Ngothai, Y., & Pring, A. (2014). The replacement of chalcopyrite by bornite under hydrothermal conditions. *American Mineralogist, 99*(11-12), 2389-2397. doi:10.2138/am-2014-4825

Zhu, Y., Fang, A., & Tan, J. (2011). Geochemistry of hydrothermal gold deposits: A review. *Geoscience Frontiers, 2*(3), 367-374.

Appendix 2.1 – Spatially grouped down hole geochemistry plots (Cu, Co, Au) of twelve sampled diamond drill holes from the Carlow Castle ore body

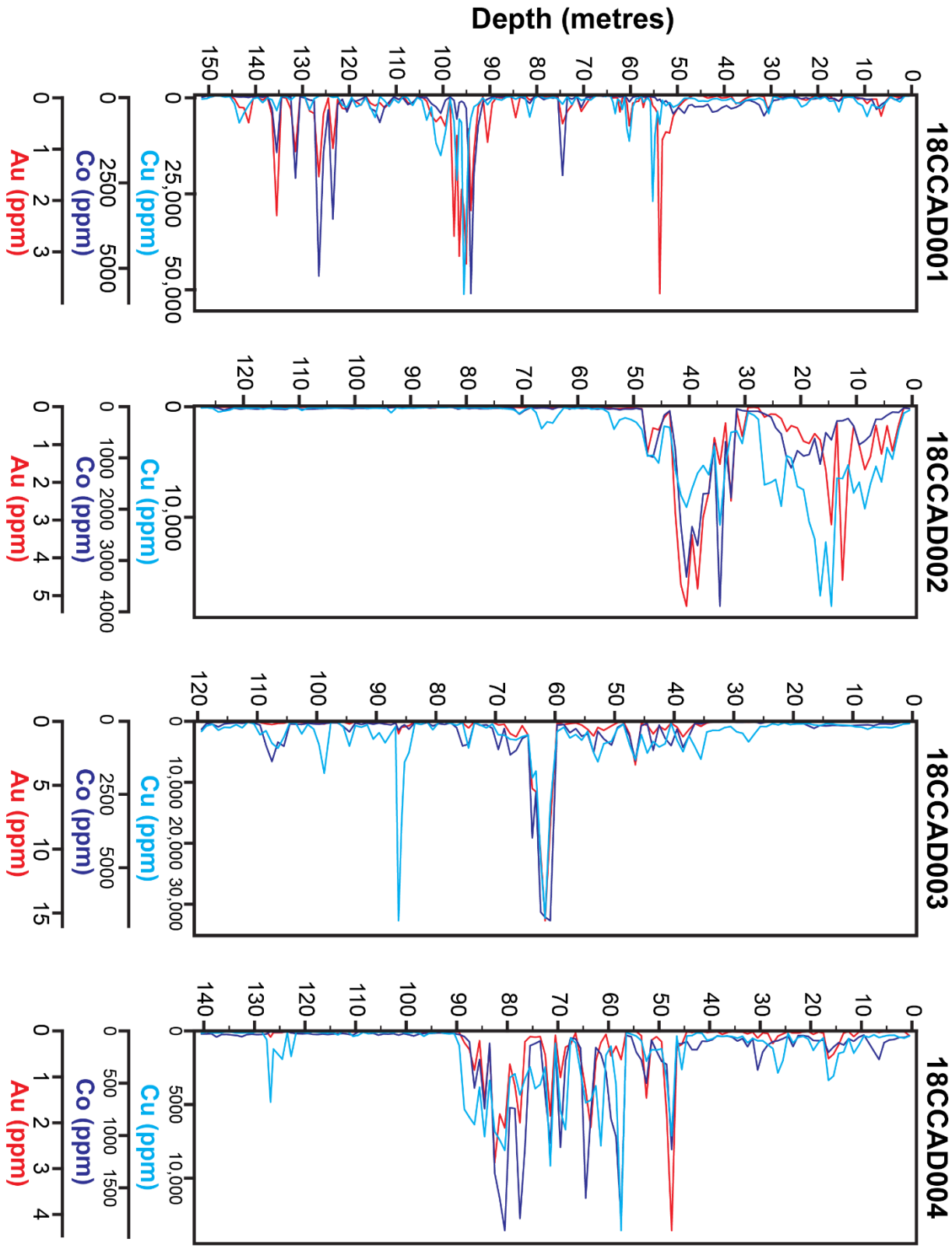

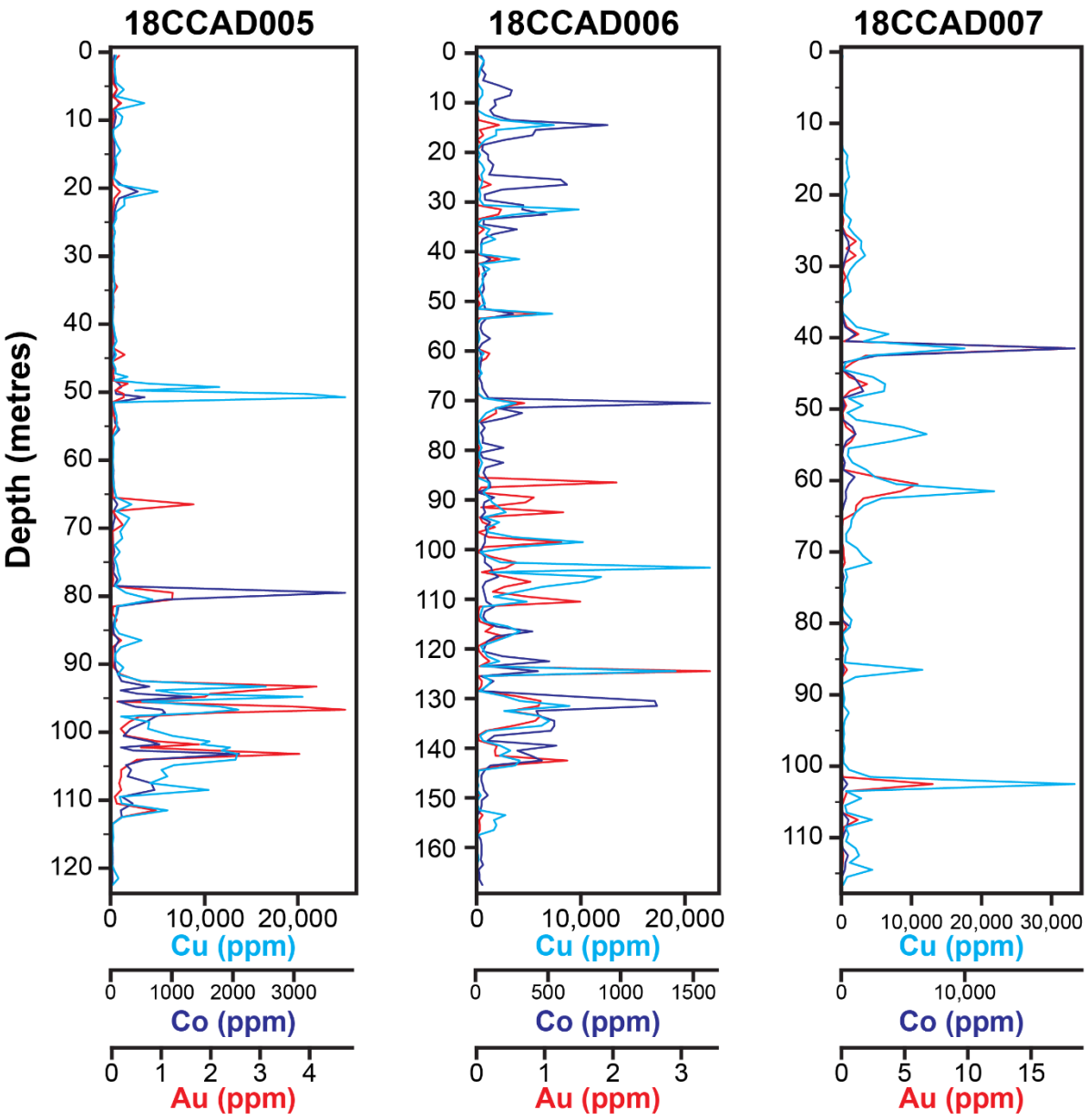
18CCAD005
18CCAD006
18CCAD007
Depth (metres)
Cu (ppm)
Co (ppm)
Au (ppm)

1717

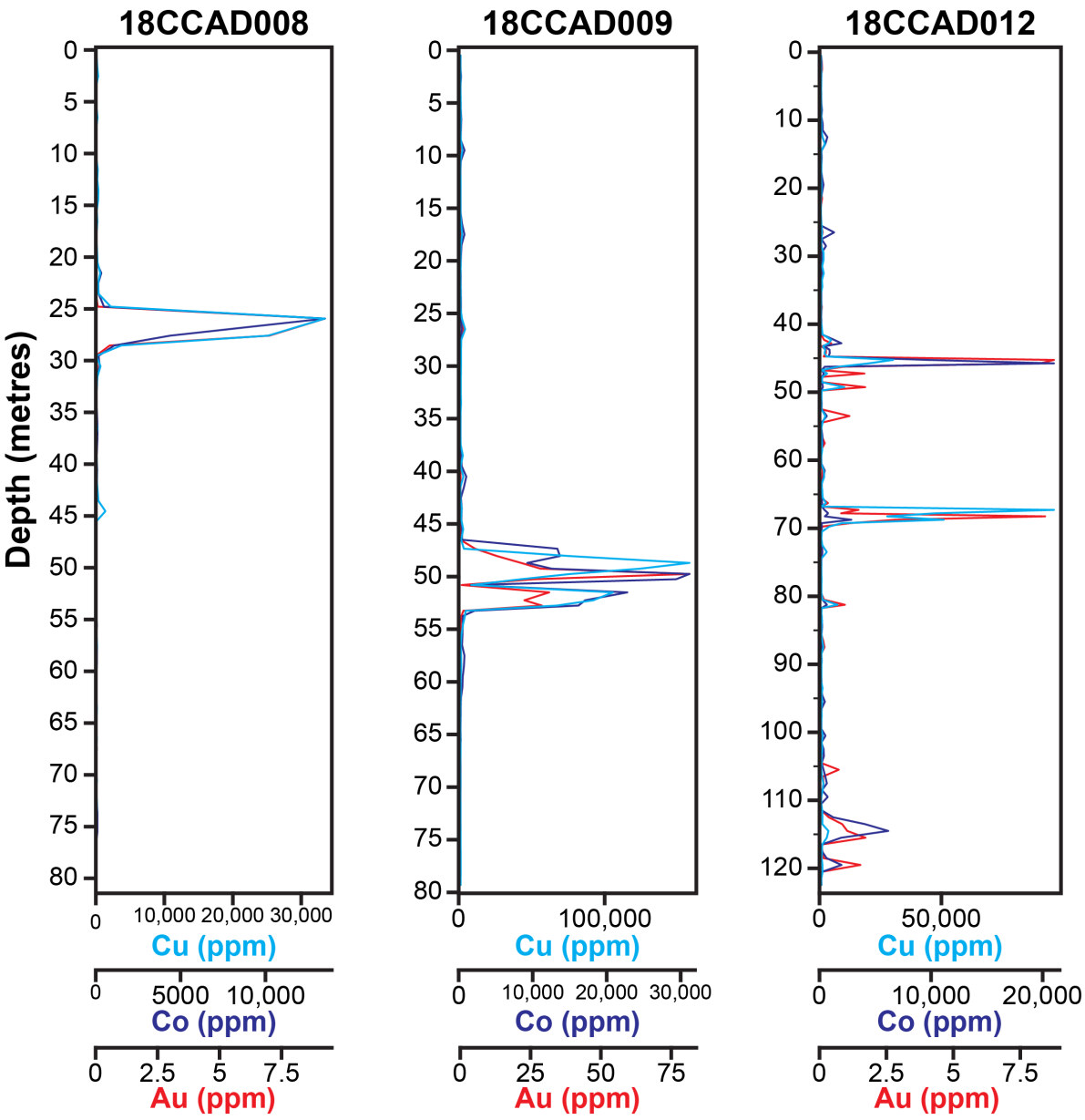
18CCAD008
18CCAD009
18CCAD012
Depth (metres)
Cu (ppm)
Co (ppm)
Au (ppm)

1718

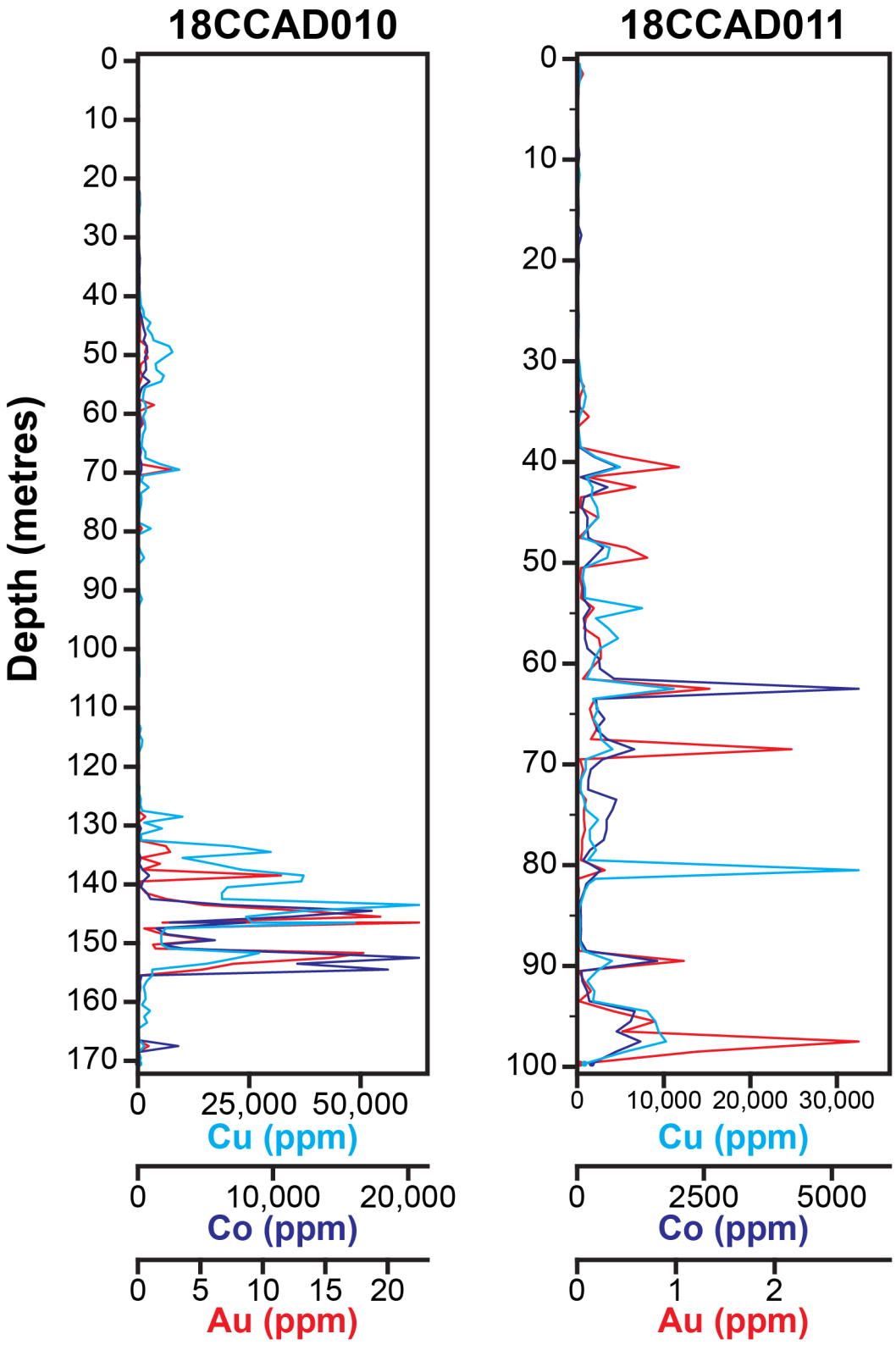

1719

1720 Note that these plots are produced from publicly available JORC (2012) compliant drilling data

1721 released to the Australian Securities Exchange (Artemis Resources Limited, 2018c).

Appendix 2.2 – List of drill core samples from Carlow Castle Cu-Co-Au deposit

Appendix 2.1 is accessible via this link and provides an .xlsx file containing a full list of drill core samples taken from the Carlow Castle Cu-Co-Au deposit ore body

Appendix 2.3 – High resolution optical microscope thin section scans of select analysed sample from ore mineral Assemblage One and Two

Appendix 2.3a is accessible via this link and provides a .pdf file containing a labelled optical thin section scan of sample CC003_61 from ore mineral Assemblage One.

Appendix 2.3b is accessible via this link and provides a .pdf file containing a labelled optical thin section scan of sample CC012_67 from ore mineral Assemblage One.

Appendix 2.3c is accessible via this link and provides a .pdf file containing a labelled optical thin section scan of sample CC007_41b from ore mineral Assemblage Two.

Chapter 3

Working up an apatite: Enigmatic Mesoarchean hydrothermal Cu-Co-Au mineralization in the Pilbara Craton

This chapter is published in *Economic Geology as*:

Fox, D., Spinks, S., Barham, M., Kirkland, C. L., Pearce, M. A., Aspandiar, M., Birchall, R., Mead, E. (2021). Working up an apatite: Enigmatic Mesoarchean hydrothermal Cu-Co-Au mineralization in the Pilbara Craton. Economic Geology, 116(7), 1561-1573. doi:https://doi.org/10.5382/econgeo.4842

3.1 Abstract

Globally, significant examples of hydrothermal Cu-Co mineralization are rare within Archean greenstone belts, especially relative to the endowment of these terranes with other world-class hydrothermal ore deposits, particularly Au deposits. Using U-Pb geochronology of hydrothermal apatite, this study provides the first absolute age constraints on the timing of mineralization for the Carlow Castle Cu-Co-Au deposit. Carlow Castle is a complex shear-zone hosted veined Cu-Co-Au mineral system situated within the Paleo-Mesoarchean Roebourne greenstone belt of the Pilbara Craton of northwestern Western Australia. Although U-Pb geochronology of this deposit is challenging due to low levels of radiogenic Pb in syn-mineralization apatite, mineralization is best estimated at 2957 ± 67 Ma (n = 61). Additionally, analysis of alteration phases associated with Carlow Castle's mineralization suggest that it is dominated by a propylitic assemblage that is characteristic of alkaline fluid chemistry and peak temperatures ~300°C. Within proximal portions of the northwest Pilbara Craton, the period of Carlow Castle's formation constrained here was associated with significant base-metal VMS mineralization and magmatic activity related to back-arc rifting. This period of extension and

rifting was the most likely source of Carlow Castle's unique Cu-Co-Au mineralization. Carlow Castle's Mesoarchean mineralization age makes it among the oldest discovered Cu-Co-Au deposits on Earth, and relatively unique in the broader context of hydrothermal Cu-Co-Au deposits. Globally, hydrothermal Cu-Co mineralization occurs almost exclusively as Proterozoic and Phanerozoic stratiform sediment-hosted Cu-Co deposits due to the necessity of oxidized basinal ore fluids in their formation. This research therefore has implications for exploration for atypical Cu-Co deposits and Cu-Co metallogenesis through recognition of comparably uncommon Archean hydrothermal Cu-Co-Au ore-forming processes and, consequently, the potential for analogous Cu-Co-Au mineralization in other Archean greenstone belts.

3.2 Introduction

The world's most significant sources of cobalt are sediment-hosted copper-cobalt (Cu-Co) deposits; these deposits account for ~60% of global Co production and are the only globally significant style of hydrothermal Cu-Co mineralization (Mudd et al., 2013; Slack et al., 2017a). Temporally, these deposits are constrained to basins of maximum Paleoproterozoic age (Figure 3.1; Hitzman et al., 2010). This is thought to reflect the critical role of atmospheric oxygen in the formation of these deposits, due to the redox sensitive nature of Cu and Co mobility (Brown, 2014). It is generally accepted that Earth's atmosphere was not significantly oxygenated until the Great Oxygenation Event (GOE) at ~2400 Ma (Lyons et al., 2014).

Carlow Castle is a Cu-Co-Au deposit hosted in a Paleo-Mesoarchean volcano-sedimentary sequence in the Pilbara Craton of northwestern Western Australia and has previously been hypothesized to be of Archean age (Fox et al., 2019; Hickman, 2016). It thus appears to sit outside the usual models of hydrothermal Cu-Co metallogenesis (Fox et al., 2019). As of November 2019, Carlow Castle's inferred resource estimate is 8 million tonnes (Mt) at 0.51% Cu, 0.08% Co, 1.6g/t Au (Artemis Resources Limited, 2019c), placing it among Australia's most significant Cu-Co-Au deposits. Carlow Castle's occurrence as a structurally-controlled hydrothermal Cu-Co-Au deposit within the Paleo-Mesoarchean Roebourne volcano-sedimentary greenstone belt makes it unique among Cu-Co-Au deposits, with no other known deposits of comparable style and setting (Hitzman et al., 2017). As such, Carlow Castle may have implications for understanding the controls on Cu-Co metallogenesis through Earth history, and particularly during the Archean. To better constrain the age of Carlow Castle, we studied the geochemistry and geochronology of what appears to be syn-mineralization

hydrothermal apatite. In addition to this, the alteration assemblage of the host rocks associated with Carlow Castle's sulfide mineralization were also analysed and interpreted to provide evidence of the prevailing physicochemical conditions during hydrothermal ore formation.

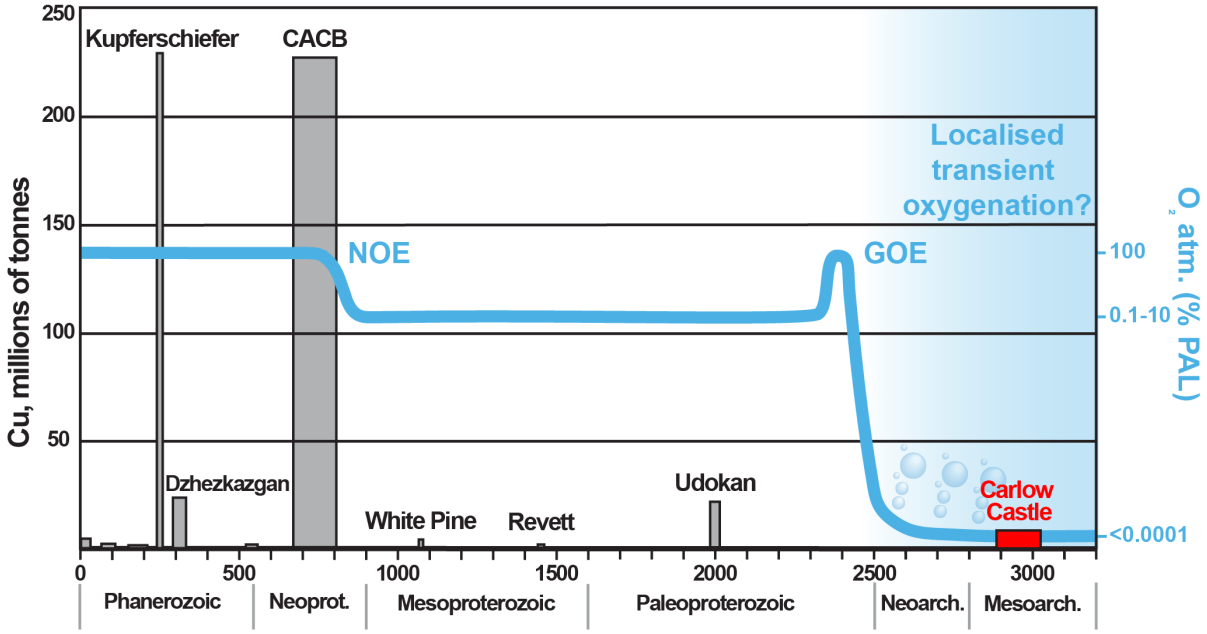

Figure 3.1 - Timing of major sediment-hosted Cu deposit formation relative to Carlow Castle's formation and compared with atmospheric O_2 evolution following the Great Oxygenation Event (GOE) and Neoproterozoic Oxygenation Event (NOE). Modified after Hitzman et al. (2010) and Lyons et al. (2014). CACB = Central African Copperbelt, PAL = present atmospheric level.

3.3 Geological Setting

The Carlow Castle deposit occurs in the West Pilbara Superterrane (3280-3066 Ma) in northwest Western Australia (Figures 3.2 and 3.3; Hickman, 2016; Van Kranendonk et al., 2002). The West Pilbara Superterrane comprises several Paleo-Mesoarchean volcano-sedimentary greenstone belts and associated intrusive granitic supersuites (Hickman et al., 2006). The Karratha (~3280 Ma), Regal (~3200 Ma), and Sholl (3130-3110 Ma) terranes were assembled into the West Pilbara Superterrane during a period of convergence from ~3160 Ma that culminated in the Prinsep Orogeny at ~3070 Ma (Van Kranendonk et al., 2007). This convergence ultimately led to the obduction of the Regal Terrane over the Karratha Terrane, forming the Regal Thrust (Figures 3.2 and 3.3); a regionally extensive (~2000 km^2) thrust fault defined by a laterally continuous belt of mylonitized stratigraphy (Hickman, 2016). The

Prinsep Orogeny was followed by the formation of the nearby De Grey Superbasin (3066-2919 Ma; Figure 3.2) during a period of significant post-orogenic rifting from 3066 Ma (Hickman, 2016). The formation of the De Grey Superbasin was initially driven by post-collisional crustal relaxation and extension following the Prinsep Orogeny and subsequently by the initiation of subduction at the northwest margin of the Pilbara Craton from 3023 Ma (Hickman, 2016; Hickman et al., 2010). Ultimately, the formation of the De Grey Superbasin was terminated during the North Pilbara Orogeny (NPO) from 2955-2919 Ma (Hickman, 2016).

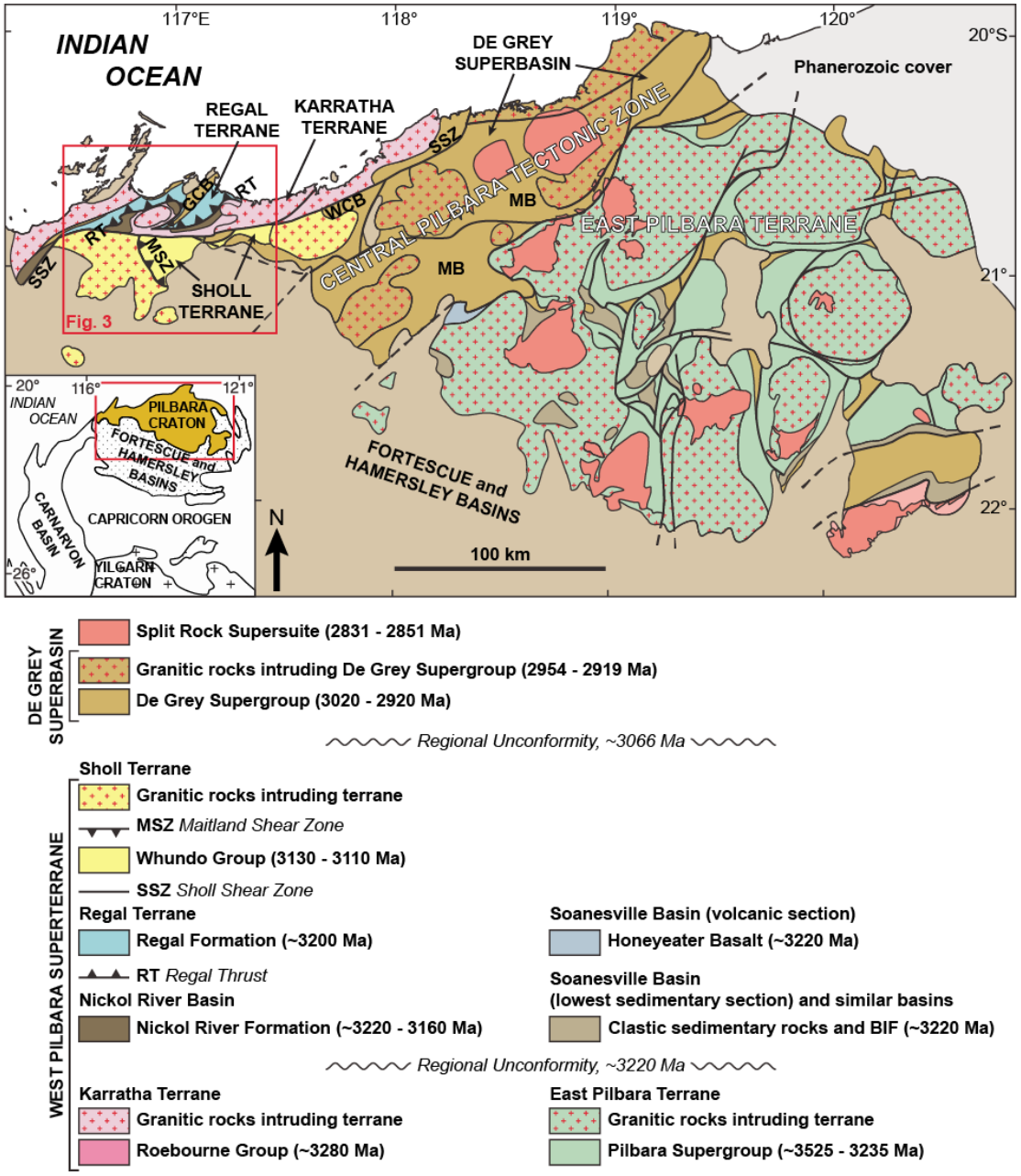

Figure 3.2 - Geological map of the Pilbara Craton, modified after Hickman (2016). MB = Mallina Basin, WCB = Whim Creek Basin, GCB = Gorge Creek Basin. Note that the

extent of the area of the northwest Pilbara Craton within Figure 3.3 is indicated and the extent of different terranes is noted in the figure legend.

Mineralization at Carlow Castle occurs within a heavily tectonized zone on the south-eastern footwall of the Regal Thrust (Figure 3.2) through the Nickol River (~3220 Ma) and Ruth Well (~3280 Ma) Formations; the latter of which is a constituent of the Roebourne Group in the Karratha Terrane (Hickman et al., 2006). The Ruth Well Formation is up to 2 km thick and is composed predominantly of extrusive basalt and peridotite with interstratified silicified carbonaceous shale units. These are overlain by fine-grained marine siliciclastic sedimentary rocks of the Nickol River Formation (Hickman, 2016; Hickman & Van Kranendonk, 2012). However, within the mineralized zone of Carlow Castle, the host formation is pervasively chloritized, effectively obscuring the primary lithology of the host rock (Fox et al., 2019).

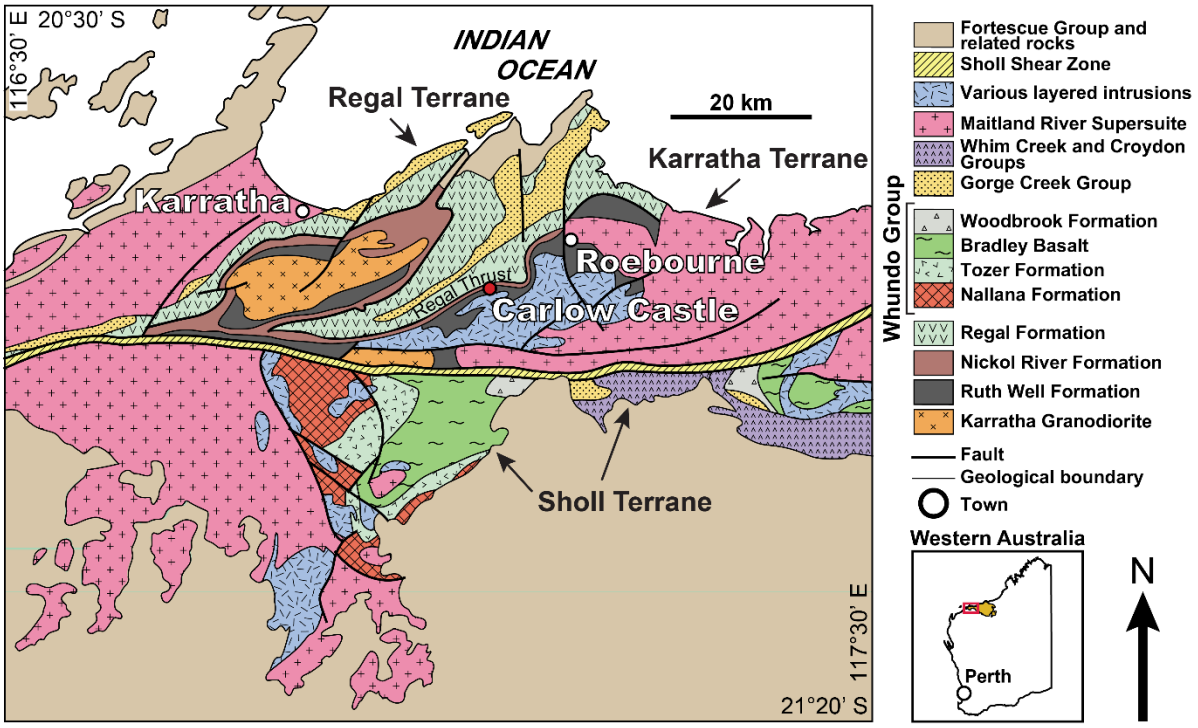

Figure 3.3 - Geologic map of the northwest Pilbara Craton. Modified after Van Kranendonk et al. (2002).

3.3.1 Ore deposit geology

The Cu-Co-Au ore at Carlow Castle occurs as base-metal sulfides through a network of pervasive quartz-carbonate veining and can be broadly separated into two distinct ore mineral assemblages (Fox et al., 2019). Assemblage One is more volumetrically significant and composed primarily of pyrite and chalcopyrite with minor cobaltite, pyrrhotite, and trace

electrum. Assemblage Two is significantly more Co- and Au-rich and is dominated by cobaltite and chalcocite with electrum typically occurring as micron-scale inclusions within cobaltite grains. Throughout the mineralized zone, the sulfide ore is intergrown with chlorite and actinolite from the extensively hydrothermally altered wall-rock. Syn-mineralization hydrothermal apatite occurs plentifully throughout both ore mineral assemblages, intergrown with the sulfide ore and hydrothermal alteration minerals (Figures 3.4 and 3.5; Appendix 3.1). Detailed characterization and discussion of Carlow Castle's style of mineralization is provided in Fox et al. (2019).

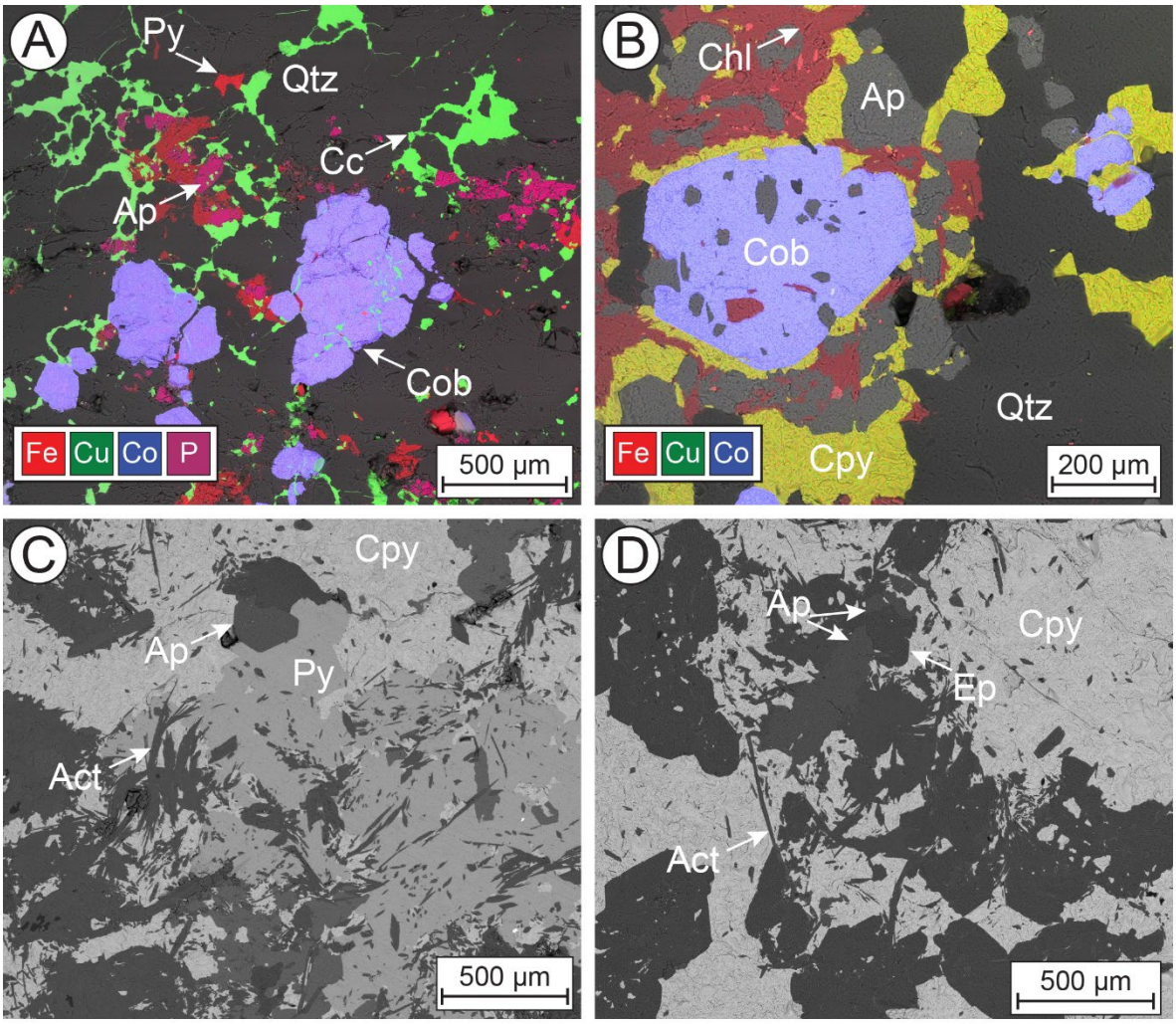

Figure 3.4 – Scanning electron microscope (SEM) photomicrographs showing syn-mineralization hydrothermal apatite associated with sulfide mineralization at Carlow Castle Cu-Co-Au deposit. A. Element map from Sample CC009_48 of Fe (red), Cu (green), Co (blue), and P (pink) within a mineralized quartz (qtz) vein containing cobaltite (cob), chalcocite (cc), pyrite (py), and apatite (ap). Note how apatite is intergrown with

chalcocite within this vein. B. Element map from Sample CC003_61 of Fe (red), Cu (green), Co (blue) showing a cobaltite grain rimmed by chalcopyrite and hydrothermal apatite, suggesting apatite post-dates cobaltite within the mineral paragenetic sequence. C. Euhedral apatite hosted within massive intergrown coarse-grained pyrite and chalcopyrite mineralization (Sample CC012_67). D. Apatite intergrown with epidote and actinolite alteration minerals, hosted within massive coarse-grained chalcopyrite (Sample CC012_67).

3.4 Methods and materials

3.4.1 Samples

Hydrothermal apatite within a representative mineralized polished block section of sample CC012_67 (Figure 3.5, Appendix 3.1) from ore mineral Assemblage One (Fox et al., 2019), from the Carlow Castle ore body was selected for U-Pb geochronology. Sample CC012_67 contains abundant coarse euhedral apatite grains contemporaneous with sulfide mineralization, ideal for in-situ laser ablation analysis. This sample comprises coarse-grained intergrown pyrite and chalcopyrite, with minor pyrrhotite and trace sphalerite and cobaltite. Gangue quartz, calcite, siderite, chlorite, actinolite, epidote, and apatite are also common throughout the sample. The hydrothermal apatite analyzed within this sample occur as clusters of syn-mineralization apatite grains intergrown with other hydrothermal gangue or sulfide minerals (Figures 3.4 and 3.5, Appendix 3.1).

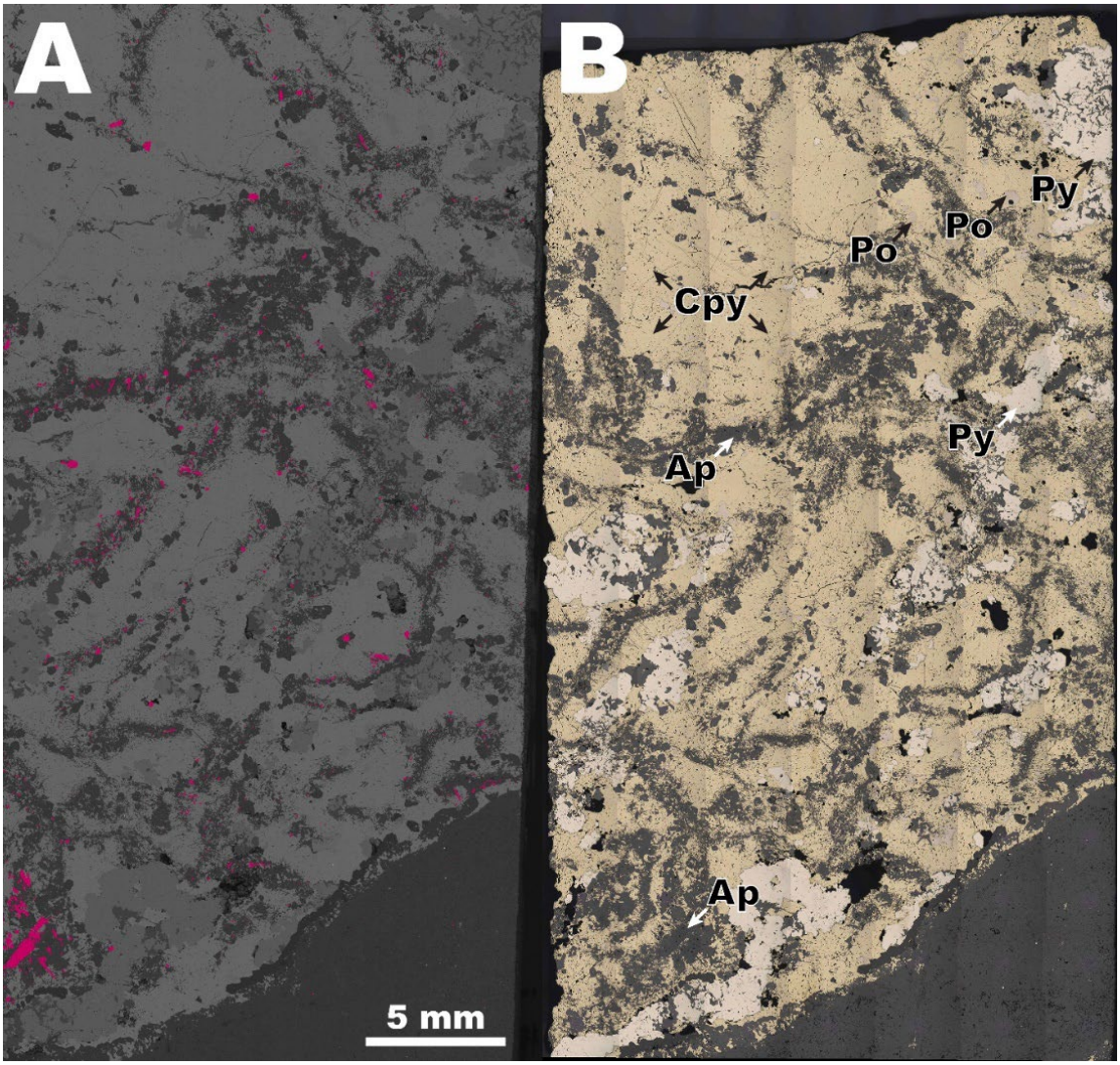

Figure 3.5 - A. SEM backscattered electron mineral map of apatite grains (pink) within laser ablation sample CC012_67. B. Reflected light photomosaic of sample CC012_67 with major mineral phases labelled. Note visible laser ablation pits within apatite grains.

In addition to sample CC012_67, polished block sections of samples CC003_61 and CC009_48 were also prepared as representative samples of veined mineralization for small-scale mineralogical analysis. Sample CC003_61 is composed predominantly of chalcopyrite and pyrite, typical of ore mineral Assemblage One, hosted within quartz-carbonate veins. Sample CC009_48 is representative of ore mineral Assemblage Two and contains cobaltite and chalcocite hosted within a quartz-carbonate vein.

3.4.2 Scanning electron microscopy

Polished sections of samples CC012_67, CC009_48, and CC003_61 were carbon coated for mineralogical analysis using a Tescan Integrated Mineral Analyzer (TIMA) at the

Commonwealth Scientific and Industrial Research Organisation (CSIRO) Advanced Resource Characterisation Facility at the Australian Resources Research Centre. These samples were analyzed through collection of energy dispersive X-ray spectra (EDS) dot maps (Appendix 3.1) of the samples with a backscattered electron (BSE) pixel size of 3 μm, spectra were collected every 10 μm and/or where a change in BSE contrast was detected. These analyses used an accelerating voltage of 25 kV, beam intensity of 18, beam current of 4.35 nA, spot size of 51 nm, and working distance of 15 mm. After the samples were imaged in BSE and EDS spectra collected, the mineralogical composition of these samples was determined via referencing these parameters to a customized TIMA mineral library.

3.4.3 Apatite spot analysis

Laser Ablation Inductively Coupled Plasma Mass Spectrometry (LA-ICP-MS) for U-Pb geochronology and trace element geochemistry was performed at the GeoHistory Facility in the John De Laeter Centre at Curtin University in Perth, Western Australia. Single spot ablations (76) were performed across 71 in-situ apatite grains within polished section CC012_67, with simultaneous collection of age and geochemical data from each ablation volume. Ablations were performed with a Resonetics RESOlution M-50A-LR, utilizing a COMPex 193 nm excimer laser in constant energy mode using a 50 μm spot size, 5 Hz laser repetition rate, and a laser energy of 1.80 J cm^{-2}. Isotope geochemistry was measured by an Agilent 7700s quadrupole ICP-MS, using high purity Ar as a plasma gas. Each spot analysis included a 30 s background acquisition and a 35 s ablation. A total of 28 isotopes were measured ^{29}Si, ^{31}P, ^{43}Ca, ^{44}Ca, ^{55}Mn, ^{88}Sr, ^{89}Y, ^{91}Zr, ^{139}La, ^{140}Ce, ^{141}Pr, ^{146}Nd, ^{147}Sm, ^{151}Eu, ^{157}Gd, ^{163}Dy, ^{165}Ho, ^{166}Er, ^{169}Tm, ^{172}Yb, ^{175}Lu, ^{201}Hg, ^{204}Pb, ^{206}Pb, ^{207}Pb, ^{208}Pb ^{232}Th, and ^{238}U. The measurement time was 0.02 s for isotopes of Pb, Th, U, and 0.01 s for all other isotopes. McClure Mountain syenite apatite was used as the primary reference material (Thomson, Gehrels, Ruiz, & Buchwaldt, 2012). Duluth Complex apatite (U-Pb zircon age of 1099.1 ± 0.2 Ma (Schmitz, Bowring, & Ireland, 2003)) was used as a secondary reference material, and treated as an unknown. The age obtained, by free regression, on the secondary reference Duluth Complex apatite (1123 ± 39; MSWD = 1.15; n = 13 of 14) is within analytical uncertainty of the expected value (Appendix 3.2; Kirkland et al., 2018).

Time-resolved mass spectra were reduced using Iolite (Paton, Hellstrom, Paul, Woodhead, & Hergt, 2011) and U-Pb and Pb-Pb ages were produced and interpreted using the Isoplot Visual Basic add-in for Microsoft Excel (Ludwig, 1991). Isoplot 4.15 was used to calculate common

(non-radiogenic) ^{207}Pb-corrected ^{238}U/^{206}Pb ages for each apatite spot analysis based upon an estimate of common Pb using the Stacey and Kramers (1975) model of the Earth's Pb isotope evolution (Figure 3.6). An iterative approach was applied to determine the appropriate common ^{207}Pb/^{206}Pb ratio to use in ^{207}Pb-correction, where an initial ^{207}Pb/^{206}Pb age was used as an estimate for a model common Pb composition. Following this, an initial estimated ^{207}Pb-corrected age was used to revise the common Pb model to calculate a ^{207}Pb-corrected ^{238}U/^{206}Pb age. This process was repeated until no change in ^{207}Pb-corrected age resulted from a change in common Pb value. Such ^{207}Pb-corrected individual ages are used to distinguish different age components. A regression (green in Figure 3.6) through the population anchored from a common Pb value was used for the final age estimate.

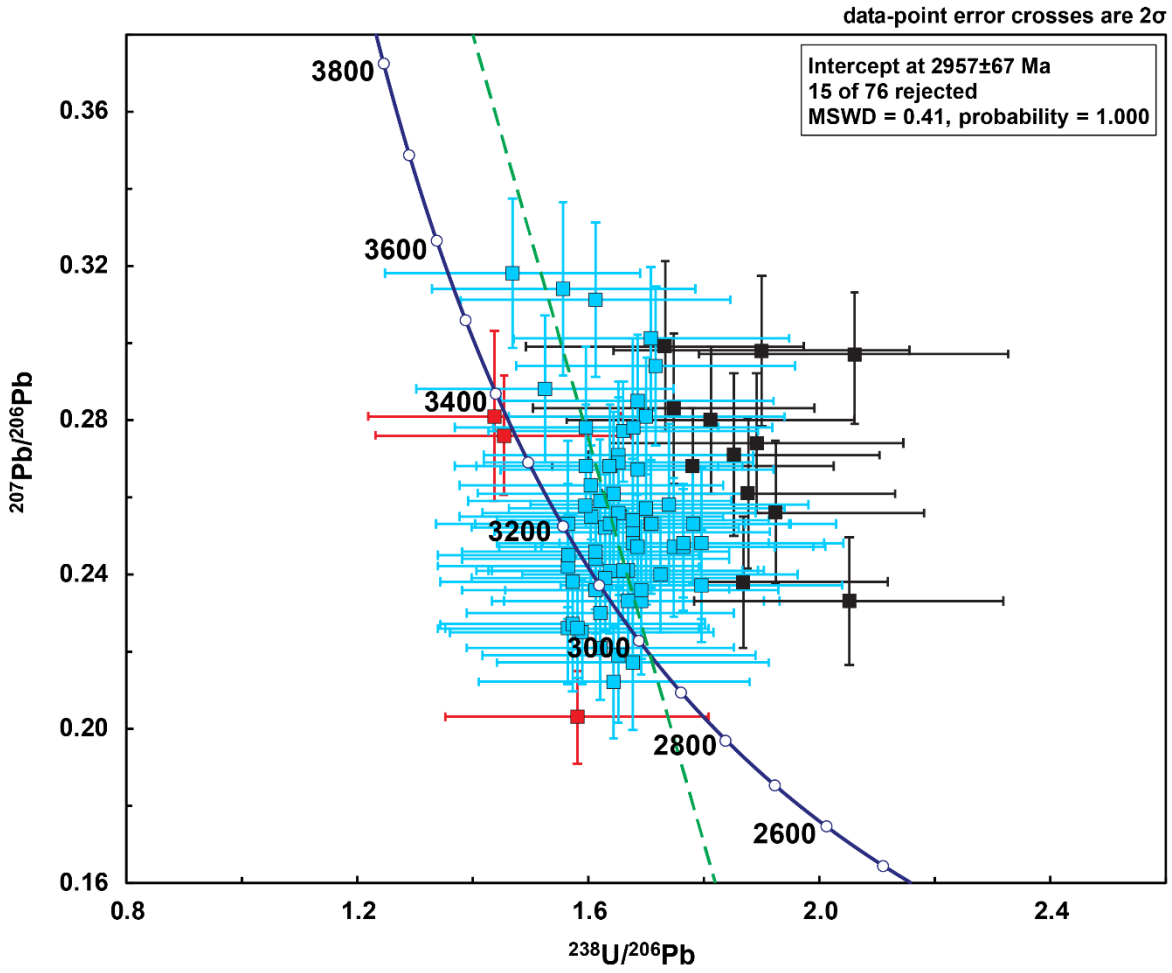

Figure 3.6 - U-Pb concordia plot of 76 apatite analyses from sample CC012_67. The regression line (green) through roughly concordant analyses (blue) intersects the concordia curve at 2957 Ma. Note rejected analyses are colored red for those left of

concordia with apparent ages older than the host terrane and black for those to the far right of concordia that have undergone radiogenic Pb loss.

3.5 Results

3.5.1 Sample mineralogy

Consistent with the previous mineralogical categorization based on visual observation; CC012_67 and CC003_61 belong to the chalcopyrite and pyrite dominated ore mineral Assemblage One, whilst CC009_48 belongs to the more cobaltite- and chalcocite-rich ore mineral Assemblage Two (Table 3.1). In addition to these ore minerals, an alteration assemblage composed of actinolite, chlorite (dominantly chamosite, based on EDS mapping results), epidote, K-feldspar, quartz, siderite, and calcite occurs within the samples; replacing the primary basaltic host-rock (Appendix 3.1). However, the abundance of individual alteration minerals within each sample varies significantly (Table 3.1). Whilst CC012_67 is particularly actinolite-rich in addition to siderite; epidote; and minor K-feldspar and chlorite, the alteration assemblages within CC009_48 and CC003_61 are composed strongly of greater amounts of chlorite with significantly less actinolite and epidote (Appendix 3.1). The alteration assemblage of CC009_48 is composed of quartz, chlorite, siderite, and minor K-feldspar and actinolite. Despite their different ore mineral assemblages, the alteration assemblage of CC003_61 is comparable but more chloritic; being composed of quartz, chlorite, K-feldspar, calcite, and minor to trace siderite and actinolite. CC009_48 and CC003_61 are also particularly quartz-rich due to their quartz vein hosted occurrence, in contrast to CC012_67, which is exceptionally chalcopyrite rich and more comparable to coarse-grained massive sulfide.

Table 3.1 - Quantitative mineralogy of samples analysed with TIMA from Carlow Castle.

Sample/Mineral	CC012_67	CC009_48	CC003_61
Chalcopyrite	52.29%	0.04%	15.34%
Actinolite	17.22%	0.21%	0.04%
[Unclassified]	10.53%	7.19%	8.06%
Pyrite	8.38%	0.0035%	3.41%
Siderite	3.06%	5.36%	0.14%
Epidote	3.00%	0.0004%	-
Pyrrhotite	1.71%	0.0009%	0.1%
K-feldspar	0.89%	0.34%	2.83%

Chlorite (chamosite)	0.83%	7.36%	19.34%
Apatite	0.67%	1.23%	1.03%
Quartz	0.60%	69.45%	46.17%
Holes	0.56%	3.07%	0.64%
Biotite (annite)	0.10%	0.02%	0.25%
Cobaltite	0.01%	4.81%	0.37%
Chalcocite	-	0.76%	0.0002%
Calcite	0.01%	0.02%	1.83%
Ilmenite/rutile	-	0.03%	0.44%
Other	0.14%	0.1052%	0.0098%

3.5.2 Geochronology

U-Pb ratios in 61 measurements of the hydrothermal apatite define a broadly concordant distribution (Figure 3.6) with some scatter towards common Pb, consistent with a common-radiogenic mixing line. While the low U content of these grains (mean: 1.6 ppm) makes geochronology challenging, only fifteen out of 61 data points do not conform to a single ^{207}Pb-corrected age population. Three data points (red) (*12_67 – 9, 19, 55*) have apparent ^{207}Pb-corrected ages significantly older than the host rock's formation age (~3300 Ma) and plot left of concordia. Additionally, these spots were sited on grain edges where they may reflect mixtures with other phases containing radiogenic Pb. A further 12 data points (black) (*12_67 – 1, 2, 3a, 25, 27, 33, 35, 45, 46, 49, 55, 57, 77)* may have undergone minor radiogenic Pb loss, are discordant, and plot to the right of a radiogenic to common Pb mixing array. No distinct chemical variation is noted between different components, and there is no apparent relationship between the ^{207}Pb-corrected age of a given apatite grain and its trace element geochemistry. Nonetheless, several statistical outliers that were rejected are geochemically anomalous and contain highly variable heavy rare earth element (REEs) concentrations, with many being depleted relative to the concordant analyses though, some are comparably enriched. In general, the 15 discordant outliers exhibit greater variability in HREE concentration than the concordant population. Excluding the 15 statistical outliers, 61 measurements yield a concordia intercept age of 2957 ± 67 Ma (MSWD = 0.41, p = 1), calculated from a common Pb composition corresponding to a terrestrial Pb model of 2960 Ma (^{207}Pb/^{206}Pb: 0.90) as per Stacey and Kramers (1975). The calculated apparent age is stable despite varying the common Pb value in

the model up to 3300 Ma ($^{207}Pb/^{206}Pb$: 0.83) (corresponding to the maximum age of the host formation). This is due to the near concordance of the data, making the final age insensitive to the choice of common Pb value. All U-Pb data are provided in Appendix 3.2.

3.5.3 Apatite geochemistry

Carlow Castle apatite crystals are typical in terms of major element geochemistry relative to apatite in magmatic-hydrothermal ore deposits (Mao, Rukhlov, Rowins, Spence, & Coogan, 2016), though values for P tend to vary more significantly than Ca. Si varies considerably, between 180-9100 ppm (mean: 1730 ppm). Mn, Sr, Zr, and Hg concentrations vary within a relatively narrow range (Table 3.2) and Zr and Hg values are commonly below detection limits. Total U, Th, and Pb concentrations within the apatite are particularly low in comparison to apatite associated with various ore deposits (Table 3.2) (Mao et al., 2016). There is no consistent relationship between total P, Ca, Mn, Sr, Si, Zr, Hg, U, Th, and Pb concentrations, and the ages of the apatite grains. The full geochemical data for all analyzed elements are provided in Appendix 3.3.

Table 3.2 - Summary of apatite LA-ICP-MS geochemical data. Note values are in ppm; DL = detection limit, SD = standard deviation.

	P	Ca	Mn	Sr	Si	Zr	Hg	U	Th	Pb
Minimum	154,600	384,000	216	109	180	<DL	<DL	1.015	<DL	0.019
Maximum	194,200	395,400	324	197	9100	0.19	74	2.473	0.0184	0.305
Mean	166,320	388,932	270	145	1730	0.17	18	1.64	0.0032	0.0736
Median	165,000	389,000	268	147	890	0.012	21	1.608	0.0028	0.065
Range	39,600	11,400	108	88	8920	-	-	1.46	-	0.29
SD	8980	2033	22.58	12.08	2182	0.036	27.69	0.302	0.0034	0.043

Broadly the REE profiles of the apatite define a single population, characterized by a negatively sloped REE profile with a notable negative Eu anomaly (Figure 3.7). Similarly to U, absolute concentrations of REEs within these apatite are low; with ∑REE+Y ranging between 487.94-1545.14 ppm (mean: 929.16 ppm). ∑LREE (La + Ce + Pr + Sm + Eu) range between 261.17 and 864.13 ppm (mean: 558.47 ppm), whilst ∑HREE (Gd + Dy + Yb) values range between 69.79 and 214.18 ppm with some outliers skewing toward higher HREE concentrations (mean: 112.64 ppm). Across the population there is a strong positive correlation ($r^2 = 0.733$) between LREE and U concentrations, whilst there is a moderate positive correlation ($r^2 = 0.222$) between HREE and U concentrations (Figure 3.8a, b).

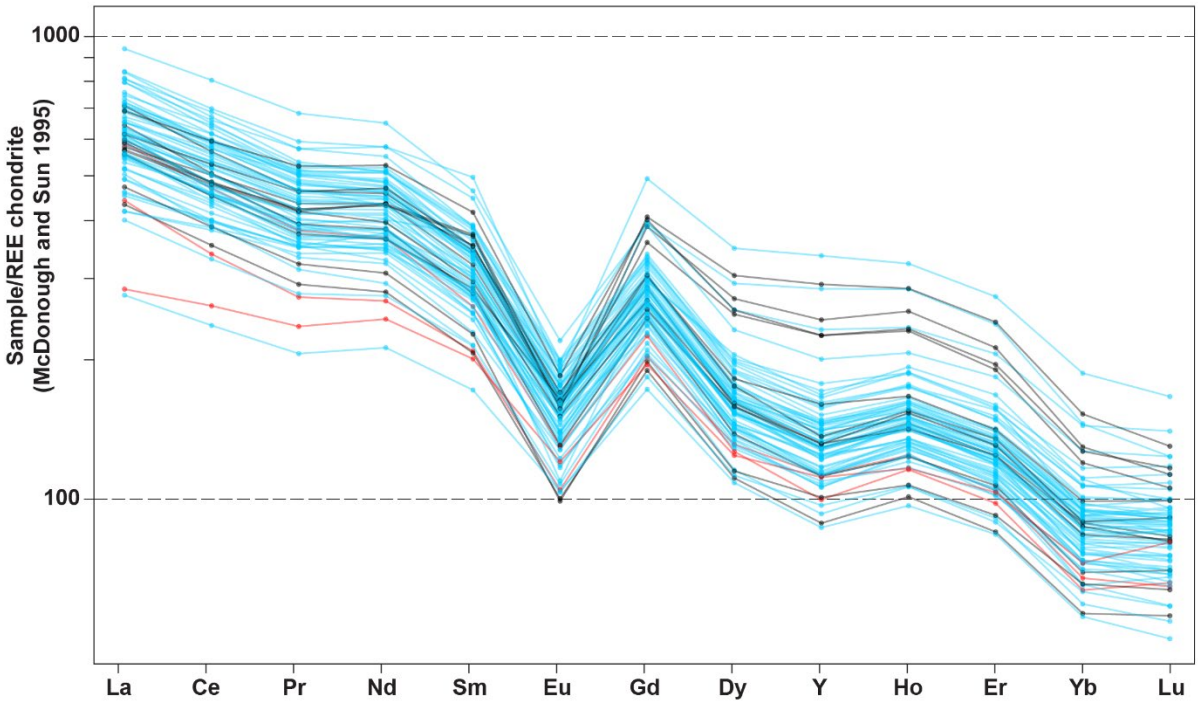

Figure 3.7 - Rare earth element plot for 76 apatite analyses from CC012_67, displaying a consistently negative slope and negative Eu anomaly characteristic of a single population. The coloring scheme (blue, red, black) reflects the assigned group of each analysis on the concordia plot in Figure 3.6. Note the disproportionately low REE values of red analyses.

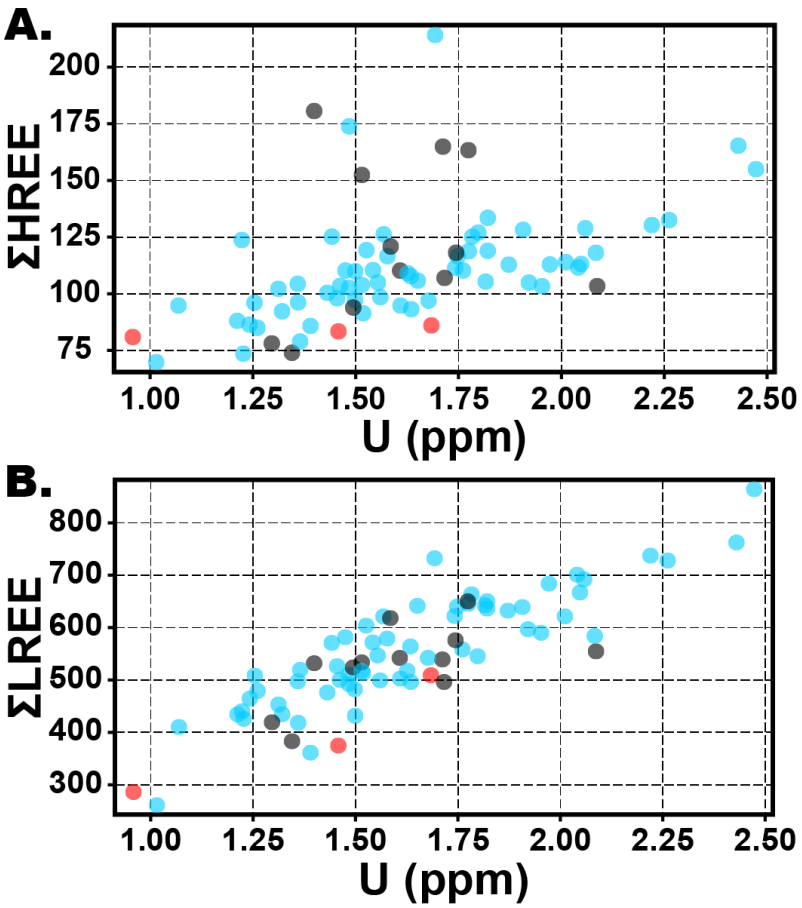

Figure 3.8 - A. ΣHREE plotted against U (ppm) content of 76 apatite analyses. B. ΣLREE plotted against U (ppm) of 76 apatite analyses. Note the strong positive linear relationship between ΣLREE and U. Colors for each data point are consistent with those in Figure 3.6 and Figure 3.7.

3.6 Discussion

3.6.1 Geochronological constraints on the timing of ore formation

The Mesoarchean (2957 ± 67 Ma) age of the hydrothermal apatite grains dated in this study is interpreted to represent the age of Carlow Castle's Cu-Co-Au mineralization, based on textural evidence of their syn-mineralization formation (intimate intergrowth with sulfides and ore-stage hydrothermal alteration phases; Figure 3.5). Although the age variation of the 61 near-concordant apatite analyses is higher than expected for a single population, they define a broadly Gaussian distribution and their trace element geochemistry defines a single population (Figure 3.7); supporting a single growth stage. Apatite in the population with particularly old ages can be accounted for through the incorporation of a radiogenic Pb component from mixtures with other uranium-bearing minerals on the margins of apatite inadvertently sampled

by the laser during analysis. Conversely, apatite that lie to the right of a regression from the common Pb anchor, i.e., apparently young ^{207}Pb-corrected ages within the population, are explained through Pb loss. Both of these features are frequently encountered in laser ablation of apatite and are a routine consideration when conducting apatite geochronology (Kirkland et al., 2018). Additionally, the anomalous REE variation within discordant outliers lying to the right of the best fit regression may reflect the alteration of the chemistry of these apatite grains post-crystallization via various processes that could have simultaneously altered the original REE and U-Pb contents of some grains (Cherniak, 2005; Cherniak, Lanford, & Ryerson, 1991; Hughes & Rakovan, 2015). Conversely, relatively REE-enriched discordant outlier grains to the right of the best fit regression may be explained by the presence of trace U, Pb, and REE-bearing phases as inclusions within these grains that were not noticed prior to analysis.

By comparison to whole rock REE data of basaltic portions of the Ruth Well Formation published by Smithies, Champion, Van Kranendonk, and Hickman (2007), the Carlow Castle apatite display notable REE fractionation with a clear depletion in HREEs relative to LREEs. Additionally, the Carlow Castle apatite also display a significantly more pronounced negative Eu anomaly than the host Ruth Well Formation. These fractionated REE patterns along with the notably low concentrations of U, Pb, Th, and ∑REE are not uncommon within apatite from hydrothermal ore deposits, especially when compared with igneous apatite (Mao et al., 2016). These trace element concentrations within the Carlow Castle apatite most likely reflect the preferential partitioning of U, Pb, Th, and REEs into other ore and alteration phases. The comparable rarity of such U-, Pb-, Th-, and REE-bearing ore and alteration phases in igneous rocks, accounts for the commonly observed fractionation and depletion of these elements in hydrothermal apatite relative to igneous apatite (Krneta, Ciobanu, Cook, Ehrig, & Kontonikas-Charos, 2017; Mao et al., 2016). For example, the occurrence of uraninite in Carlow Castle's Cu-Co-Au mineralization suggests that its hydrothermal fluid was uraniferous (Fox et al., 2019). Initially this is difficult to reconcile with the low U concentrations in the Carlow Castle apatite; however, the presence of uraninite is likely the reason that Carlow Castle's apatite are so U poor. This is because any dissolved U in this fluid was most likely preferentially incorporated into uraninite, this would leave relatively little dissolved U to be incorporated into the hydrothermal apatite. This is supported by evidence in Figure 3.4b, that apatite appears to post-date cobaltite paragenetically. Given that uraninite is known to be associated with cobaltite mineralisation within Carlow Castle (Fox et al., 2019), it is likely that apatite also

post-dates uraninite mineralisation. A similar process would also account for the REE concentrations observed within these apatite, as several hydrothermal minerals observed within Carlow Castle may incorporate REEs up to thousands of ppm; including uraninite, epidote, chlorite, calcite, K-feldspar, and amphibole (Fryer & Taylor, 1987; Pike, Cas, & Smithies, 2002; Tillberg et al., 2019). As such, the strongly fractionated REE pattern along with the low absolute U and REE concentrations within the Carlow Castle apatite may reflect the synchronous or subsequent growth of these apatite crystals with other REE- and U-bearing hydrothermal minerals and the consequent competition for these components during crystal growth. This geochemical evidence supports previously noted textural evidence of a hydrothermal origin for these apatite, that is contemporaneous with Carlow Castle's hydrothermal Cu-Co-Au mineralization; suggesting that the age of the apatite measured by this study can also be interpreted to be the age of Cu-Co-Au mineralization.

Prior to this study, a maximum age constraint of 3070 Ma on Carlow Castle was provided by the Regal Thrust host structure (Hickman, 2016). While a minimum possible age was uncertain, it was suggested that Carlow Castle was unlikely to be significantly younger than the initiation of rifting in the Fortescue Basin around 2775 Ma due to the paucity of obvious subsequent ore-forming tectonothermal events in the Pilbara Craton (Fox et al., 2019). The Carlow Castle deposit was originally hypothesized to be an orogenic Au system with atypical Cu-Co enrichment, with the Prinsep Orogeny (~3070 Ma) being the likely event responsible for mineralization (Fox et al., 2019; Hickman, 2016). This interpretation was based on Carlow Castle's occurrence within the Regal Thrust, an orogenic structure, and several similarities in style and setting to an orogenic mineral system (Fox et al., 2019). However, the age of mineralization constrained by this study (2957 ± 67 Ma) suggests instead that Carlow Castle's ore formation post-dates the Prinsep Orogeny. Therefore, whilst the critical structures (Regal Thrust) that host Carlow Castle's ore are almost certainly a product of orogenesis, Carlow Castle's mineralizing processes are most likely related to the later stages of the NW Pilbara Craton's evolution.

3.6.2 Tectonic process and regional metallogenesis

The age range over which the Carlow Castle deposit most likely formed (3024-2890 Ma) significantly postdates the age of the host Karratha Terrane (3280-3236 Ma) and instead corresponds to the formation of the nearby De Grey Superbasin (3066-2931 Ma) within the Central Pilbara Tectonic Zone (CPTZ) of the NW Pilbara Craton (Hickman, 2016; Figure 3.2).

Within the De Grey Superbasin, the inferred age of Carlow Castle's mineralization coincides with the formation of three distinct sub-basins: (i) the Gorge Creek Basin (3066-3015 Ma); a shallow water intracontinental basin of dominantly marine siliciclastic fill over the northern Pilbara Craton, (ii) the Whim Creek Basin (3009-2991 Ma); a small fault-bounded volcanic arc to the southeast, and (iii) the Mallina Basin (3015-2931 Ma); a back-arc basin further to the southeast of the Whim Creek Basin volcanic arc (Hickman, 2016; Hickman et al., 2010). The formation of the Gorge Creek and Whim Creek Basins was not associated with any economically significant mineralization, except iron ore (Hickman, 2016; Hickman et al., 2006).

The formation of the Mallina Basin was terminated by the North Pilbara Orogeny (NPO; 2955-2919 Ma), with peak metamorphism and deformation between 2940-2920 Ma (Hickman, 2016; Hickman et al., 2006; Van Kranendonk et al., 2007). During the NPO, regional mineralization is interpreted to have occurred in two discrete phases. Mineralization between 2955-2940 Ma was dominated by volcanogenic massive sulfide (VMS) mineralization of Pb, Zn, Ag, Cu, and V within the Whim Creek greenstone belt during continued extension and granitic magmatism within the Mallina Basin, along with PGE and Ni-Cu mineralization associated with the intrusion of mafic-ultramafic sills throughout the central Mallina Basin (Hickman, 2016; Huston, Smithies, & Sun, 2000; Huston et al., 2002b; Pike et al., 2002). This period produced the most diverse assemblage of mineralization of any terrane in the northern Pilbara Craton (Hickman, 2016). This was followed by a subsequent period of mineralization during the metamorphic peak of the NPO (2940-2920 Ma) dominated by shear zone hosted orogenic Au in addition to layered intrusive Ni-Cu and PGE mineralization (Hickman, 2016; Hoatson & Sun, 2002; Huston et al., 2002a).

The high intensity of tectonism during the period of Carlow Castle's potential mineralization makes it difficult to identify exactly which tectonic event is likely to have driven the formation of the ore system. However, our data suggests Carlow Castle's metal enrichment likely formed through the reactivation of pre-existing orogenic structures associated with the Regal Thrust (~3070 Ma) during a later extensional regime that prevailed for most of the development of the proximal CPTZ. This interpretation is supported by the observation of multiple generations of deformation fabrics within the Carlow Shear Zone by Kiyokawa et al. (2002), with evidence of late-stage post-orogenic deformation produced by extension and basin formation between 3020-2925 Ma. It is perhaps unsurprising that Carlow Castle formed during this period, given

that the CPTZ is the portion of the Pilbara Craton most endowed in hydrothermal and magmatic gold and base-metal ore deposits (Hickman, 2016; Hickman et al., 2006; Huston, Blewett, Mernagh, Sun, & Kamprad, 2001). This suggests that the formation of the CPTZ was associated with geological processes that were particularly conducive to ore formation more broadly. In consideration of the current understanding of the northeast Pilbara Craton's major ore-forming events, Carlow Castle was most likely produced by the major period of hydrothermal base-metal mineralization during the latter stages of the Mallina Basin's development between 2955-2940 Ma.

3.6.3 Conditions of ore genesis

Whilst there remains some ambiguity regarding the specific tectonic event associated with Carlow Castle's ore formation based on age constraints alone, the hydrothermal alteration mineral assemblages associated with Carlow Castle's Cu-Co-Au mineralization can provide insights into key aspects of its ore genesis. The alteration assemblages present within the samples analyzed in this study are consistent with the propylitic hydrothermal alteration of basaltic rocks (Corbett & Leach, 1997; Reed, 1997). However, there is clear variation in the abundance of the different characteristic propylitic alteration minerals across these samples; most notably chlorite, epidote, and actinolite (Table 3.1). The increase in actinolite and epidote in sample CC012_67 relative to samples CC009_48 and CC003_61 at the expense of chlorite most likely reflects a relative increase in the temperature of alteration; from the middle range toward the upper temperature bound (250 to 350°C) of propylitic alteration according to the scheme established by Corbett and Leach (1997) based on compiled data from various localities. The more chloritic assemblages of CC009_48 and CC003_61 are consistent with temperatures around 200-250°C, whilst the alteration assemblage of CC012_67 is within the realm of actinolite and epidote stability at temperatures around 280-340°C (Corbett & Leach, 1997; Henley & Ellis, 1983; Reyes, 1990). These alteration assemblages are comparable with those of the contemporaneous base-metal deposits in the Whim Creek greenstone belt produced through crustal extension and granitic magmatism within the Mallina Basin between 2955-2940 Ma (Hickman, 2016; Pike et al., 2002). Additionally, this temperature estimate for Carlow Castle is comparable with the temperature of ore formation (295 ± 35°C) estimated by Huston (2006) for the proximal and contemporaneous Mons Cupri VMS Cu-Zn-Pb deposit.

The consistent prevalence of calc-silicate and carbonate minerals across these samples suggest a more-or-less constant fluid chemistry; suggesting that differences in temperature were the

primary factor controlling the variation in alteration mineralogy between samples (Corbett & Leach, 1997). In this instance, this mineralogy is characteristic of alteration defined by neutral to slightly alkaline fluids (>6 pH), with minimal H^+ metasomatism (Corbett & Leach, 1997; Pirajno, 2009; Reed, 1997). The variation in alteration assemblage, and hence fluid temperature, appears to relate to the style of sulfide mineralization; with the highest temperature alteration assemblage being associated with the highest grade coarse-grained 'massive sulfide' mineralization and the lower temperature alteration being associated with the lower grade quartz-carbonate vein hosted mineralization, irrespective of ore mineralogy (Appendix 3.1a, b). It may be that the higher temperature coarse-grained high-grade massive sulfide ore formed closer to the center of the Carlow Castle ore body, with the lower temperature vein-hosted sulfide mineralization representing more peripheral mineralization at the outer edge of the ore body.

3.6.4 Copper-cobalt metallogenesis through geological time

Sediment-hosted Cu-Co deposits comprise the most significant Cu-Co deposits on Earth and are the only globally ubiquitous hydrothermal Cu-Co mineralization style (Hitzman et al., 2017). The established genetic model for sediment-hosted Cu-Co deposits proposes that they form via the migration of oxidizing low temperature (<200°C) meteoric fluids through metalliferous sedimentary red beds rich in detrital mafic minerals (Brown, 2014; Hitzman et al., 2010). These hydrothermal fluids mobilize and transport Cu and Co in chloride complexes and Cu/Co sulfides precipitate upon interaction with a reduced sulfide-rich sedimentary unit, such as an organic-rich shale (Brown, 2014). Due to the redox-sensitive nature of Cu and Co, sediment-hosted Cu-Co deposits are temporally limited to terranes of maximum Paleoproterozoic age; after which the atmosphere was sufficiently globally oxygenated to provide a source of oxidized meteoric fluids to mobilize Cu and Co (Figure 3.1; Hitzman et al., 2010; Lyons et al., 2014). Similarly, genetic models for other less significant Co deposit types, such as polymetallic (Ni-Co-As-Ag-Bi) vein deposits and primary Co-vein deposits (e.g., Bou Azzer, Morocco) (Slack et al., 2017a), also invoke oxygenated meteoric fluids as a critical component of the mineral system (Ahmed et al., 2009; Kissin, 1992). These deposit types are also perhaps more comparable to the Carlow Castle deposit in terms of mineralization style and host terrane lithology than sediment-hosted Cu-Co deposits (Fox et al., 2019). However, all of these deposits are similarly temporally limited to the Proterozoic onwards (Lefebure, 1996; Oberthür et al., 2009). Given the apparent paucity of Archean Cu-Co deposits, with the

exception of a few magmatically-associated deposits discussed later in the text, Carlow Castle's Mesoarchean age most likely makes it the oldest discovered Cu-Co deposit on Earth. Reflecting this it is important to understand the potential metallogenic processes for Cu-Co ore formation, and how these processes have evolved through time. Particularly as this could be critical for understanding the genesis of, and therefore exploring for, other Archean Cu-Co deposits.

The critical importance of atmospheric oxygen to mobilize metals in hydrothermal Cu-Co deposits makes the Mesoarchean age of Carlow Castle particularly notable. One way to account for Carlow Castle's genesis would be to suggest that it formed under the influence of atmospherically oxygenated fluids; mirroring the younger sediment-hosted Cu-Co and vein-hosted Co deposit types. Supporting this, there is growing evidence of temporally and spatially isolated oxygenated surface environments prior to the GOE (Eickmann et al., 2018; Lyons et al., 2014; Ohmoto, 2020; Planavsky et al., 2014). Additionally, several studies have postulated the possibility of pre-GOE oxygenated conditions specifically within the Pilbara Craton during the Archean, based on sulfur isotope and mineralogical evidence from several formations ranging in age between 3460-2500 Ma (Hickman & Van Kranendonk, 2012; Hoashi et al., 2009; Kato et al., 2009; Kaufman et al., 2007; Ohmoto, Watanabe, Ikemi, Poulson, & Taylor, 2006). If Carlow Castle's genesis was a product of ore-forming processes consistent with those younger Cu-Co deposits, this could contribute further evidence of transient locally oxygenated conditions during the Archean, which could have implications for global-scale base-metal metallogenesis in Archean cratons.

Whilst the most important pathway for Cu-Co mobilization in hydrothermal ore deposits relates to the availability of atmospherically-derived oxygenated (sulphate-stable) ore fluids, rare examples of hydrothermal Cu-Co mineralization in Archean terranes may provide insights into alternative Archean Cu-Co mineralizing processes; involving potential magmatic-hydrothermal interactions. These processes are important to consider given Carlow Castle's characteristic differences relative to a typical sediment-hosted Cu-Co deposit. Hannan South; a Neoarchean Au-Cu-(Co-Bi) oxidized endoskarn in the Eastern Goldfields Orogen of the Yilgarn Craton in Western Australia provides one example of such processes (Mueller, Lawrance, Muhling, & Pooley, 2012). In this instance, the critical processes for metal mobilization relate to the transportation of metals within a magmatically-derived hydrothermal fluid (Meinert, 1992). These fluids transport dissolved metals by virtue of their highly reactive physicochemical properties as they are commonly hot (>400°C), moderately to highly acidic,

moderately to highly saline, and/or oxidized (Meinert, Dipple, & Nicolescu, 2005; Misra, 2000). However, Carlow Castle lacks several of the defining characteristics of a skarn deposit (Misra, 2000).

Cobalt-bearing iron oxide Cu-Au (IOCG) systems of purported Archean age have also been identified; most notably the Neoarchean-Paleoproterozoic Guelb Moghrein Cu-Au deposit in Mauritania and the Neoarchean Salobo Cu-Au deposit of Carajas IOCG province in Brazil (de Melo, Monteiro, Xavier, Moreto, & Santiago, 2019; de Melo et al., 2017; Kirschbaum & Hitzman, 2016; Kolb & Petrov, 2016). Models for Salobo attribute its formation to high temperature (>500°C), corrosive (HF-bearing), oxidized, and highly saline magmatically-derived fluids produced by contemporaneous granitic magmatism (de Melo et al., 2019; de Melo et al., 2017). Conversely, models for Guelb Moghrein generally point to a metamorphic origin with limited contemporaneous granitic magmatism (Kirschbaum & Hitzman, 2016). Instead mineralization was produced by fluid mixing, redox change, and cooling of a hot (>400°C) oxidized saline metalliferous metamorphic fluid during retrograde metamorphism. However, the mechanism by which this metalliferous metamorphic fluid attained this chemistry has not been proposed and the possibility of derivation from an unexposed intrusive felsic magmatic source has been acknowledged (Kirschbaum & Hitzman, 2016; Kolb et al., 2008; Kolb et al., 2010; Kolb & Petrov, 2016; Sakellaris & Meyer, 2008). Nonetheless, Carlow Castle's mineralization similarly lacks several of the diagnostic features of an IOCG deposit (Williams et al., 2005).

Given Carlow Castle's probable formation during a period of major rifting with associated VMS mineralization, it is also worth considering the Cu-Co-Au mineralizing processes associated with VMS formation. Whilst Co-rich VMS deposits are not exceptionally common, Besshi-type (mafic-siliciclastic) VMS deposits are observed to be Co-bearing in some cases (Hitzman et al., 2017). However, Archean examples of these Co-bearing Besshi-type deposits are notably rare (Franklin et al., 2005; Huston, Pehrsson, Eglington, & Zaw, 2010; Schulz, 2012). The Neoarchean (~2.7 Ga) Noranda district, Canada is known to host Cu-Zn-Co-Au VMS mineralization of the bimodal-mafic VMS deposit sub-type (Boucher, 2011; Morgan & Schulz, 2012). Within the Noranda district, the Ansil deposit is known to contain Co mineralization in the form of Co-pentlandite and cobaltite associated with pyrrhotite and chalcopyrite, however these are relatively minor in comparison to Carlow Castle's Co mineralization (Boucher, 2011; Fox et al., 2019). Combining elements of deposit models

discussed previously, mineralization within the Noranda district has been proposed to have formed through a combination of hot (~350-450°C) reduced sulfur-bearing acidic magmatic fluids and cool oxidized sulfate-bearing seawater (Barrett, Maclean, & Cattalani, 1991; Boucher, 2011; Galley, Jonasson, & Watkinson, 2000; Galley, Watkinson, Jonasson, & Riverin, 1995; Sharman, Taylor, Minarik, Dube, & Wing, 2015). The magmatic fluid is believed to be derived from the underlying trondhjemitic Flavrian pluton that is coeval with mineralization (Sharman et al., 2015; Westendorp & Watkinson, 1991). Whilst a source of oxidized Archean seawater has not been accounted for, it has been suggested that seawater sulfate was supplied via photochemical oxidation of volcanically degassed SO_2 and that seawater sulfate levels through the Neoarchean may have been non-negligible (Sharman et al., 2015). Once again, magmatic fluids derived from proximal granitic melts appear to have been critical to the formation of Noranda's VMS mineralization.

3.6.5 Potential models for Carlow Castle Cu-Co-Au ore formation

Hydrothermal Cu-Co deposits through time can be grouped broadly into two categories based on their critical ore-forming processes; (i) deposits formed from the Proterozoic onward under the influence of oxidized meteoric hydrothermal fluids and (ii) deposits formed from the Archean onward as a product of magmatic-hydrothermal processes associated with significant crustal magmatism. In light of recent studies purporting to show evidence of potentially oxygenated environments on Earth during the Archean, it is tempting to suggest that Carlow Castle may have formed in a manner consistent with the Earth's major post-Proterozoic Cu-Co deposits; as a product of oxidized meteoric fluids. However, these models of the Earth's early atmospheric evolution are far from widely accepted and the relatively high alteration temperature provided by this study is not consistent with a relatively cool meteoric ore fluid. As such, Carlow Castle may have formed in relation to proximal magmatism in the northwest Pilbara; consistent with the other Archean hydrothermal Cu-Co deposits discussed. Supporting this, Carlow Castle's formation is contemporaneous with a period of major crustal rifting with the formation of a proximal volcanic arc and back-arc basin associated with significant crustal melting (Hickman, 2016); a classic environment for VMS ore formation (Franklin et al., 2005). Additionally, the formation of other significant base-metal VMS deposits within the proximal Whim Creek greenstone belt during this period could support a magmatically-related origin for Carlow Castle. The primary issue with this hypothesis is that there is limited evidence of contemporaneous granitic magmatism in close spatial association with Carlow Castle. Whilst

Carlow Castle is partially hosted through a tectonized portion of the dominantly mafic igneous Ruth Well Formation, these host rocks predate the deposit by ~330 Ma (Hickman, 2016). However, the geology underlying Carlow Castle at depth is not well known and the deep crustal scale of the pre-existing Regal Thrust host structure makes it a potentially effective conduit for regionally and deeply sourced fluids during rifting and magmatism on a broad scale; such as from the marine succession of the overlying Gorge Creek Basin and proximal Whim Creek greenstone belt and Mallina Basin during melting, extension, and associated VMS formation around 2950 Ma. As such, a magmatic association for Carlow Castle may be the most likely mechanism for its formation; in the context of its age, regional setting, and regional metallogenesis during its formation. This magmatic-hydrothermal connection to mineralization is consistent with the suggestion that Carlow Castle's formation was most likely associated with the period (2955-2940 Ma) of major base-metal VMS formation in the proximal Whim Creek greenstone belt during the late stages of the development of the De Grey Superbasin.

3.7 Conclusions

Newly presented apatite U-Pb geochronology indicate that the Carlow Castle deposit formed at 2957 ± 67 Ma, hundreds of millions of years before any comparable Cu-Co-Au deposit; most of which are of maximum Proterozoic age. Due to the critical role that atmospherically oxidized ore fluids play in mobilizing these ore metals to form these deposits, the formation of the Carlow Castle deposit in the Mesoarchean before widespread oxygenation of the atmosphere, provides evidence for alternative and comparably uncommon processes for hydrothermal Cu-Co metallogenesis. Additionally, new constraints on the physiochemical properties of Carlow Castle's hydrothermal ore fluid are provided; suggesting that it formed at peak temperatures ~300°C under near neutral fluid conditions. In this instance a magmatic origin is tentatively suggested given Carlow Castle's regional setting, Mesoarchean age, and broad similarities to proximal and contemporaneous magmatic-hydrothermal ore deposits. However, it is acknowledged that direct evidence of a magmatic source is not apparent. Carlow Castle's mineralization was most likely related to the significant contemporaneous magmatic activity and associated base-metal VMS mineralization within the proximal Whim Creek greenstone belt between 2955-2940 Ma. A magmatic-hydrothermal origin is consistent with other rare Archean hydrothermal Cu-Co deposits. Carlow Castle's occurrence suggests that similar hydrothermal Cu-Co-Au deposits in Archean greenstone belts could represent novel targets for future Cu-Co exploration, which has traditionally focused on Proterozoic and Phanerozoic

basins. Nonetheless, the uncertainties surrounding Carlow Castle's ore-forming processes suggest that further research is required to understand its genesis more fully.

Acknowledgements

This research was supported by an Australian Government Research Training Program Scholarship and a CSIRO Mineral Resources Research+ postgraduate student scholarship. Artemis Resources Ltd. are acknowledged for their support of this research. Mike Verrall's microscopy assistance is greatly appreciated. Bradley McDonald and Noreen Evans are thanked for their assistance with LA-ICP-MS. Thanks to Sean Makin for his assistance with Isoplot.

References

Ahmed, H. A., Arai, S., & Ikenne, M. (2009). Mineralogy and Paragenesis of the Co-Ni Arsenide Ores of Bou Azzer, Anti-Atlas, Morocco. *Economic Geology, 104*(2), 249-266.

Artemis Resources Limited. (2019c). Significant Resource Increase for Carlow Castle [Press release]. Retrieved from https://www.asx.com.au/asxpdf/20191120/pdf/44brd03vh31ncw.pdf

Barrett, T. J., Maclean, W. H., & Cattalani, S. (1991). Massive sulfide deposits of the Noranda area, Quebec. III. The Ansil mine *Canadian Journal of Earth Sciences, 28*(11), 1699-1730.

Boucher, S. M. (2011). *Ore Petrology and Alteration of the West Ansil Volcanic-hosted Massive Sulphide Deposit of the Noranda Mining Camp, Rouyn-Noranda, Québec.* (Master of Science Degree in Earth Sciences Master of Science), University of Ottawa, Ottawa.

Brown, A. C. (2014). Low-Temperature Sediment-Hosted Copper Deposits. In K. Turekian & H. Holland (Eds.), *Treatise on Geochemistry* (2nd ed., Vol. 13, pp. 251-271). Oxford: Elsevier Science.

Cherniak, D. J. (2005). Uranium and manganese diffusion in apatite. *Chemical Geology, 219*(1-4), 297-308.

Cherniak, D. J., Lanford, W. A., & Ryerson, F. J. (1991). Lead diffusion in apatite and zircon using ion implantation and Rutherford Backscattering techniques. *Geochimica et Cosmochimica Acta, 55*(6), 1663-1673.

Corbett, G. J., & Leach, T. M. (1997). Southwest Pacific Rim gold-copper systems: Structure, alteration and mineralization. *Society of Economic Geologists Special Publication, 6*, 240. doi:https://doi.org/10.5382/SP.06

de Melo, G. H. C., Monteiro, L. V. S., Xavier, R. P., Moreto, C. P. N., & Santiago, E. (2019). Tracing Fluid Sources for the Salobo and Igarapé Bahia Deposits: Implications for the Genesis of the Iron Oxide Copper-Gold Deposits in the Carajás Province, Brazil. *Economic Geology, 114*(4), 697-718.

de Melo, G. H. C., Monteiro, L. V. S., Xavier, R. P., Moreto, C. P. N., Santiago, E., Dufrane, S. A., . . . Santos, A. F. F. (2017). Temporal evolution of the giant Salobo IOCG deposit, Carajás Province (Brazil): constraints from paragenesis of hydrothermal alteration and U-Pb geochronology. *Mineralium Deposita, 52*, 709-732.

Eickmann, B., Hofmann, A., Wille, M., Bui, T., Wing, B. A., & Schoenberg, R. (2018). Isotopic evidence for oxygenated Mesoarchaean shallow oceans. *Nature Geoscience, 11*, 133-138. doi:https://doi.org/10.1038/s41561-017-0036-x

Fox, D., Spinks, S., Pearce, M. A., Barham, M., Le Vaillant, M., Thorne, R., . . . Verrall, M. (2019). Plundering Carlow Castle: First Look at a Unique Mesoarchean-Hosted Cu-Co-Au Deposit. *Economic Geology, 114*(6), 1021-1031. doi:https://doi.org/10.5382/econgeo.4672

Franklin, J. M., Gibson, H. L., Jonasson, I. R., & Galley, A. G. (2005). Volcanogenic Massive Sulfide Deposits. In J. W. Hedenquist, J. F. H. Thompson, R. J. Goldfarb, & J. P. Richards (Eds.), *Economic Geology One Hundredth Anniversary Volume* (pp. 523-560). Littleton, Colorado: Society of Economic Geologists.

Fryer, B. J., & Taylor, R. P. (1987). Rare-earth element distributions in uraninites: Implications for ore genesis. *Chemical Geology, 63*(1-2), 101-108.

Galley, A. G., Jonasson, I. R., & Watkinson, D. H. (2000). Magnetite-rich calc-silicate alteration in relation to synvolcanic intrusion at the Ansil volcanogenic massive sulfide deposit, Rouyn-Noranda, Quebec, Canada. *Mineralium Deposita, 35*, 619-637.

Galley, A. G., Watkinson, D. H., Jonasson, I. R., & Riverin, G. (1995). The Subsea-Floor Formation of Volcanic-Hosted Massive Sulfide: Evidence from the Ansil Deposit, Rouyn-Noranda, Canada. *Economic Geology, 90*(7), 2006–2017.

Henley, R. W., & Ellis, A. J. (1983). Geothermal Systems Ancient and Modern: A Geochemical Review. *Earth-Science Reviews, 19*(1), 1-50. doi:https://doi.org/10.1016/0012-8252(83)90075-2

Hickman, A. H. (2016). *Northwest Pilbara Craton: a record of 450 million years in the growth of Archean continential crust*. Retrieved from Perth:

Hickman, A. H., Huston, D., Van Kranendonk, M. J., & Smithies, R. H. (2006). *Geology and mineralization of the west Pilbara - a field guide*. Retrieved from

Hickman, A. H., Smithies, R. H., & Tyler, I. M. (2010). *Evolution of active plate margins: West Pilbara Superterrane, De Grey Superbasin, and the Fortescue and Hamersley Basins — a field guide*. Retrieved from Perth:

Hickman, A. H., & Van Kranendonk, M. J. (2012). Early Earth evolution: Evidence from the 3.5-1.8 Ga geological history of the Pilbara region of Western Australia. *Episodes, 35*(1), 283-297. doi:https://doi.org/10.18814/epiiugs/2012/v35i1/028

Hitzman, M., Bookstrom, A. A., Slack, J. F., & Zientek, M. L. (2017). *Cobalt—Styles of Deposits and the Search for Primary Deposits*. Retrieved from Virginia: https://doi.org/10.3133/ofr20171155

Hitzman, M., Selley, D., & Bull, S. (2010). Formation of Sedimentary Rock-Hosted Stratiform Copper Deposits through Earth History. *Economic Geology, 105*(3), 627-639. doi:https://doi.org/10.2113/gsecongeo.105.3.627

Hoashi, M., Bevacqua, D. C., Otake, T., Watanabe, Y., Hickman, A. H., Utsunomiya, S., & Ohmoto, H. (2009). Primary haematite formation in an oxygenated sea 3.46 billion years ago. *Nature Geoscience, 2*, 301-306. doi:https://doi.org/10.1038/ngeo465

Hoatson, D. M., & Sun, S. (2002). Archean Layered Mafic-Ultramafic Intrusions in the West Pilbara Craton, Western Australia: A Synthesis of Some of the Oldest Orthomagmatic Mineralizing Systems in the World. *Economic Geology, 97*(4), 847-872.

Hughes, J. M., & Rakovan, J. F. (2015). Structurally Robust, Chemically Diverse: Apatite and Apatite Supergroup Minerals. *Elements, 11*(3), 165-170.

Huston, D. (2006). Mineralization and regional alteration at the Mons Cupri stratiform Cu–Zn–Pb deposit, Pilbara Craton, Western Australia. *Mineralium Deposita, 41*, 17-32. doi:https://doi.org/10.1007/s00126-005-0036-4

Huston, D., Blewett, R., Keillor, B., Standing, J., Smithies, R. H., Marshall, A., . . . Kamprad, J. (2002a). Lode Gold and Epithermal Deposits of the Mallina Basin, North Pilbara Terrain, Western Australia. *Economic Geology, 97*(4), 801-818.

Huston, D., Blewett, R., Mernagh, T., Sun, S., & Kamprad, J. (2001). *Gold Deposits of the Pilbara Craton: Results of AGSO Research*. Retrieved from Canberra:

Huston, D., Pehrsson, S., Eglington, B. M., & Zaw, K. (2010). The Geology and Metallogeny of Volcanic-Hosted Massive Sulfide Deposits: Variations through Geologic Time and with Tectonic Setting. *Economic Geology, 105*(3), 571-591.

Huston, D., Smithies, R. H., & Sun, S. (2000). Correlation of the Archaean Mallina ‐ Whim Creek Basin: Implications for base ‐ metal potential of the central part of the Pilbara granite ‐ greenstone terrane. *Australian Journal of Earth Sciences, 47*(2), 217-230.

Huston, D., Sun, S., Blewett, R., Hickman, A. H., Van Kranendonk, M. J., Philips, D., . . . Brauhart, C. (2002b). The Timing of Mineralization in the Archean North Pilbara Terrain, Western Australia. *Economic Geology, 97*(4), 733-755.

Kato, Y., Suzuki, K., Nakamura, K., Hickman, A. H., Nedachi, M., Kusakabe, M., . . . Ohmoto, H. (2009). Hematite formation by oxygenated groundwater more than 2.76 billion years ago. *Earth and Planetary Science Letters, 278*(1-2), 40-49. doi:https://doi.org/10.1016/j.epsl.2008.11.021

Kaufman, A. J., Johnston, D. T., Farquhar, J., Masterson, A. L., Lyons, T. W., Bates, S., . . . Arnold, G. L. (2007). Late Archean Biospheric Oxygenation and Atmospheric Evolution. *Science, 317*(5846), 1900-1903. doi:https://doi.org/10.1126/science.1138700

Kirkland, C. L., Yakymchuk, C., Szilas, K., Evans, N. J., Hollis, J., McDonald, B., & Gardiner, N. J. (2018). Apatite: a U-Pb thermochronometer or geochronometer? *Lithos, 138-139*, 143-157.

Kirschbaum, M. J., & Hitzman, M. (2016). Guelb moghrein: An unusual carbonate-hosted iron oxide copper-gold deposit in Mauritania, Northwest Africa. *Economic Geology, 111*(3), 763-770.

Kissin, S. A. (1992). Five-element (Ni-Co-As-Ag-Bi) Veins. *Geoscience Canada, 19*(3), 113-124.

Kiyokawa, S., Taira, A., Byrne, T., Bowring, S., & Sano, Y. (2002). Structural evolution of the middle Archean coastal Pilbara terrane, Western Australia. *Tectonics, 21*(5), 1-24.

Kolb, J., Meyer, F. M., Vennemann, T., Hoffbauer, R., Gerdes, A., & Sakellaris, G. A. (2008). Geological setting of the Guelb Moghrein Fe oxide-Cu-Au-Co mineralization, Akjoujt area, Mauritania. *Geological Society, London, Special Publications, 297*, 53-75.

Kolb, J., Meyer, F. M., Vennemann, T., Sindern, S., Prantl, S., Bottcher, M. E., & Sakellaris, G. A. (2010). Characterisation of the Hydrothermal Fluids of the Guelb Moghrein Iron Oxide-Cu-Au-Co Deposit, Mauritania: Ore Mineral Chemistry, Fluid Inclusions and Isotope Geochemistry. In T. M. Porter (Ed.), *Hydrothermal Iron Oxide Copper-Gold and Related Deposits: A Global Perspective - Advances in the Understanding of IOCG Deposits* (Vol. 4, pp. 553-572). Adelaide: PGC Publishing.

Kolb, J., & Petrov, N. (2016). The Guelb Moghrein Cu–Au deposit: Neoarchaean hydrothermal sulfide mineralization in carbonate-facies iron formation. *Ore Geology Reviews, 78*, 573-577.

Krneta, S., Ciobanu, C. L., Cook, N. L., Ehrig, K., & Kontonikas-Charos, A. (2017). Rare Earth Element Behaviour in Apatite from the Olympic Dam Cu–U–Au–Ag Deposit, South Australia. *Minerals, 7*(8), 135.

Lefebure, D. V. (1996). Five-element Veins Ag-Ni-Co-As+/-(Bi,U). In D. V. Lefebure & T. Höy (Eds.), *Selected British Columbia Mineral Deposit Profiles* (Vol. 2, pp. 89-92). Vancouver: British Columbia Ministry of Employment and Investment.

Ludwig, K. R. (1991). *ISOPLOT: A Plotting and Regression Program for Radiogenic-Isotope Data*. Retrieved from Denver, Colorado:

Lyons, T. W., Reinhard, C. T., & Planavsky, N. J. (2014). The rise of oxygen in Earth's early ocean and atmosphere. *Nature, 506*, 307-315. doi:https://doi.org/10.1038/nature13068

Mao, M., Rukhlov, A. S., Rowins, S. M., Spence, J., & Coogan, L. A. (2016). Apatite Trace Element Compositions: A Robust New Tool for Mineral Exploration. *Economic Geology, 111*(5), 1187-1222.

Meinert, L. D. (1992). Skarns and Skarn Deposits. *Geoscience Canada, 19*(4), 145-162.

Meinert, L. D., Dipple, G. M., & Nicolescu, S. (2005). World Skarn Deposits. In J. W. Hedenquist, J. F. H. Thompson, R. J. Goldfarb, & J. P. Richards (Eds.), *Economic Geology* (Vol. One Hundredth Anniversary Volume): Society of Economic Geologists.

Misra, K. C. (2000). Skarn Deposits. In K. C. Misra (Ed.), *Understanding Mineral Deposits*. Dordrecht: Springer.

Morgan, L. A., & Schulz, K. J. (2012). Physical Volcanology of Volcanogenic Massive Sulfide Deposits. In W. C. P. Shanks, III & R. Thurston (Eds.), *Volcanogenic Massive Sulfide Occurrence Model* (Vol. 2010–5070–C, pp. 61-100). Reston, Virginia: U.S. Geological Survey.

Mudd, G. M., Weng, Z. H., Jowitt, S. M., Turnbull, I. D., & Graedel, T. E. (2013). Quantifying the recoverable resources of by-product metals: The case of cobalt. *Ore Geology Reviews, 55*, 87-98.

Mueller, A. G., Lawrance, L. M., Muhling, J., & Pooley, G. D. (2012). Mineralogy and PTX relationships of the Archean Hannan South Au-Cu (Co-Bi) deposit, Kalgoorlie, Western Australia: Thermodynamic constraints on the formation of a zoned intrusion-related skarn. *Economic Geology, 107*(1), 1-24.

Oberthür, T., Melcher, F., Henjes-Kunst, F., Gerdes, A., Stein, H., Zimmerman, A., & El Ghorfi, M. (2009). Hercynian age of the cobalt-nickel-arsenide-(Gold) Ores, Bou Azzer, Anti-Atlas, Morocco: Re-Os, Sm-Nd, and U-Pb age determinations. *Economic Geology, 104*(7), 1065-1079.

Ohmoto, H. (2020). A seawater-sulfate origin for early Earth's volcanic sulfur. *Nature Geoscience, 13*, 576-583. doi:https://doi.org/10.1038/s41561-020-0601-6

Ohmoto, H., Watanabe, Y., Ikemi, H., Poulson, S. R., & Taylor, B. E. (2006). Sulphur isotope evidence for an oxic Archaean atmosphere. *Nature, 442*, 908-911. doi:https://doi.org/10.1038/nature05044

Paton, C., Hellstrom, J., Paul, B., Woodhead, J., & Hergt, J. (2011). Iolite: Freeware for the visualisation and processing of mass spectrometric data. *Journal of Analytical Atomic Spectrometry, 26*(12), 2508-2518.

Pike, G., Cas, R., & Smithies, R. H. (2002). Geologic Constraints on Base Metal Mineralization of the Whim Creek Greenstone Belt, Pilbara Craton, Western Australia. *Economic Geology, 97*(4), 827-845. doi:https://doi.org/10.2113/gsecongeo.97.4.827

Pirajno, F. (2009). Hydrothermal Processes and Wall Rock Alteration. In F. Pirajno (Ed.), *Hydrothermal Processes and Mineral Systems* (Vol. 1, pp. 73-164). Dordrecht: Springer.

Planavsky, N. J., Asael, D., Hofmann, A., Reinhard, C. T., LaLonde, S. V., Knudsen, A. C., . . . Rouxel, O. (2014). Evidence for oxygenic photosynthesis half a billion years before the Great Oxidation Event. *Nature Geoscience, 7*, 283-286. doi:https://doi.org/10.1038/ngeo2122

Reed, M. H. (1997). Hydrothermal Alteration and Its Relationship to Ore Fluid Composition. In H. L. Barnes (Ed.), *Geochemistry of Hydrothermal Ore Deposits* (3 ed., pp. 303-365). New York: Wiley.

Reyes, A. G. (1990). Petrology of Philippine geothermal systems and the application of alteration mineralogy to their assessment. *Journal of Volcanology and Geothermal Research, 43*(1-2), 279-309. doi:https://doi.org/10.1016/0377-0273(90)90057-M

Sakellaris, G. A., & Meyer, F. M. (2008). *A metamorphic origin of the Guelb Moghrein Fe oxide-copper-gold-cobalt deposit, Mauritania.* Paper presented at the XIII International conference on thermobarogeochemistry and IVth APIFIS symposium, Moscow.

Schmitz, M. D., Bowring, S., & Ireland, T. R. (2003). Evaluation of Duluth complex anorthositic series (AS3) zircon as a U-Pb geochronological standard: new high-precision isotope dilution thermal ionization mass spectrometry results. *Geochimica et Cosmochimica Acta, 67*(19), 3665-3672.

Schulz, K. J. (2012). Regional Environment. In W. C. P. Shanks, III & R. Thurston (Eds.), *Volcanogenic Massive Sulfide Occurrence Model* (Vol. 2010–5070–C, pp. 37-60). Reston, Virginia: U.S. Geological Survey.

Sharman, E. R., Taylor, B. E., Minarik, W. G., Dube, B., & Wing, B. A. (2015). Sulfur isotope and trace element data from ore sulfides in the Noranda district (Abitibi, Canada): implications for volcanogenic massive sulfide deposit genesis. *Mineralium Deposita, 50*, 591-606.

Slack, J. F., Kimball, B. E., & Shedd, K. B. (2017a). Cobalt. In K. J. Schulz, J. H. DeYoung., R. R. Seal, & D. W. Bradley (Eds.), *Critical Mineral Resources of the United States—Economic and Environmental Geology and Prospects for Future Supply* (Vol. Chapter F, pp. 40 p.). Reston, Virginia: U.S. Geological Survey.

Smithies, R. H., Champion, D., Van Kranendonk, M. J., & Hickman, A. H. (2007). *Geochemistry of volcanic rocks of the northern Pilbara Craton, Western Australia*. Retrieved from Perth:

Stacey, J. S., & Kramers, J. D. (1975). Approximation of terrestrial lead isotope evolution by a two-stage model. *Earth and Planetary Science Letters, 26*(2), 207-221.

Thomson, S. N., Gehrels, G. E., Ruiz, J., & Buchwaldt, R. (2012). Routine low-damage apatite U-Pb dating using laser ablation–multicollector–ICPMS. *Geochemistry, Geophysics, Geosystems, 13*(2).

Tillberg, M., Maskenskaya, O. M., Drake, H., Hogmalm, J. K., Broman, C., Fallick, A. E., & Åström, M. E. (2019). Fractionation of Rare Earth Elements in Greisen and Hydrothermal Veins Related to A-Type Magmatism. *Geofluids*, 20. doi:https://doi.org/10.1155/2019/4523214

Van Kranendonk, M. J., Hickman, A. H., Smithies, R. H., Nelson, D. R., & Pike, G. (2002). Geology and Tectonic Evolution of the Archean North Pilbara Terrain, Pilbara Craton, Western Australia. *Economic Geology, 97*(4), 695-732. doi:https://doi.org/10.2113/gsecongeo.97.4.695

Van Kranendonk, M. J., Smithies, R. H., Hickman, A. H., & Champion, D. (2007). Review: secular tectonic evolution of Archean continental crust: interplay between horizontal and vertical processes in the formation of the Pilbara Craton, Australia. *Terra Nova, 19*(1), 1-38.

Westendorp, R. W., & Watkinson, D. H. (1991). Silicon-bearing zoned magnetite crystals and the evolution of hydrothermal fluids at the Ansil Cu-Zn mine, Rouyn-Noranda, Quebec. *Economic Geology, 86*(5), 1110-1114.

Williams, P. J., Barton, M. D., Johnson, D. A., Fontbote, L., De Haller, A., Mark, G., . . . Marschik, R. (2005). Iron Oxide Copper-Gold Deposits: Geology, Space-Time

Distribution, and Possible Modes of Origin. In J. W. Hedenquist, J. F. H. Thompson, R. J. Goldfarb, & J. P. Richards (Eds.), *Economic Geology One Hundredth Anniversary Volume*: Society of Economic Geologists.

2552 Appendix 3.1 – Quantitative mineralogy of representative samples from
2553 Carlow Castle Cu-Co-Au deposit

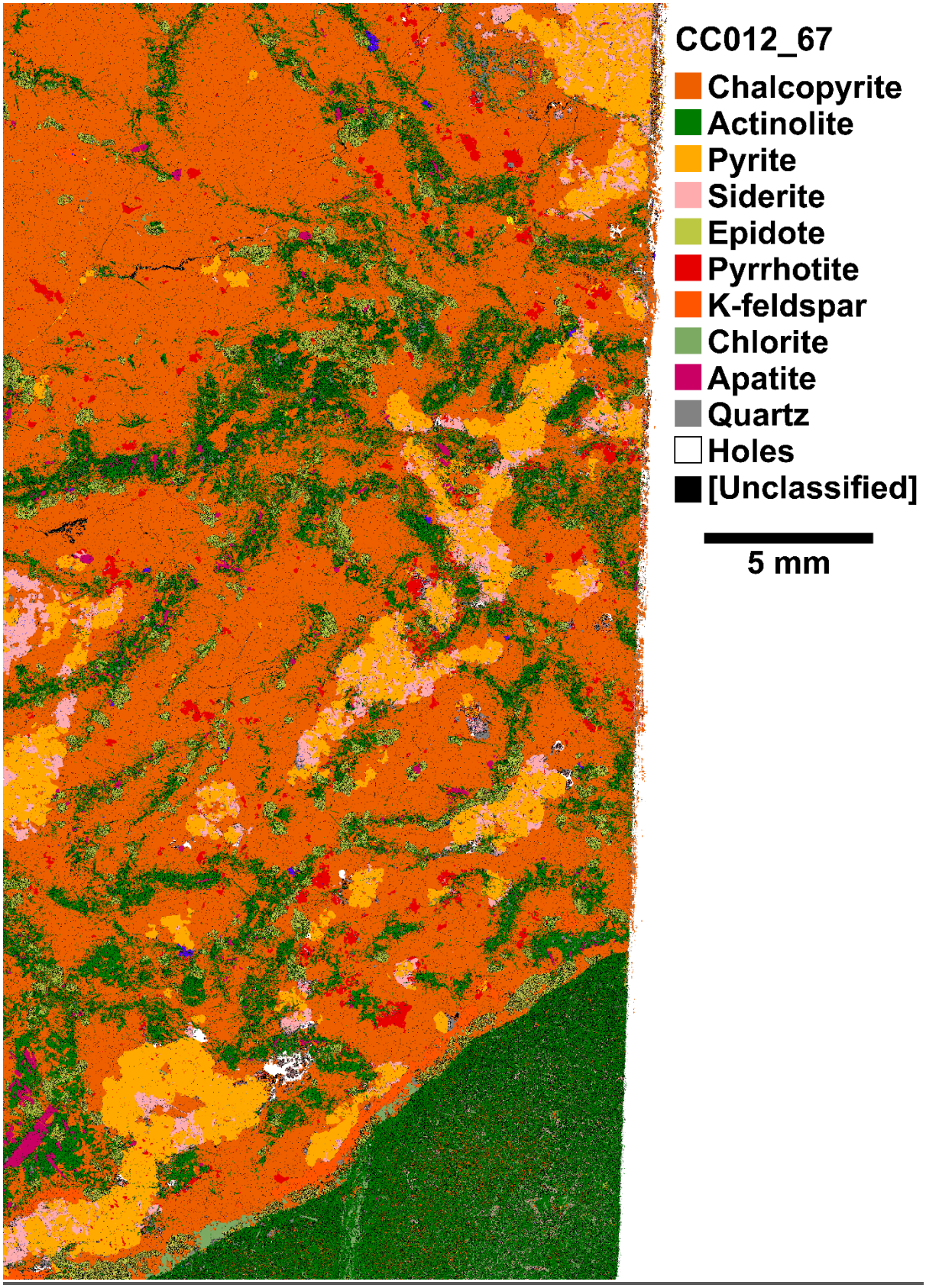

2554

Appendix 3.1a – Automated mineralogy map of sample CC012_67 from ore mineral Assemblage One of Carlow Castle. Chalcopyrite, pyrite, and pyrrhotite are the predominant ore minerals within this sample. Within this sample, these sulphide minerals are massive and relatively coarse-grained. Sulphide minerals are intergrown with actinolite, epidote, and minor chlorite throughout the sample, which occur as hydrothermal alteration minerals. Additionally, these alteration minerals are commonly intergrown with apatite, which tends to form either as isolated euhedral grains throughout the massive sulphide or as clusters of elongate grains that are commonly intergrown with actinolite and epidote.

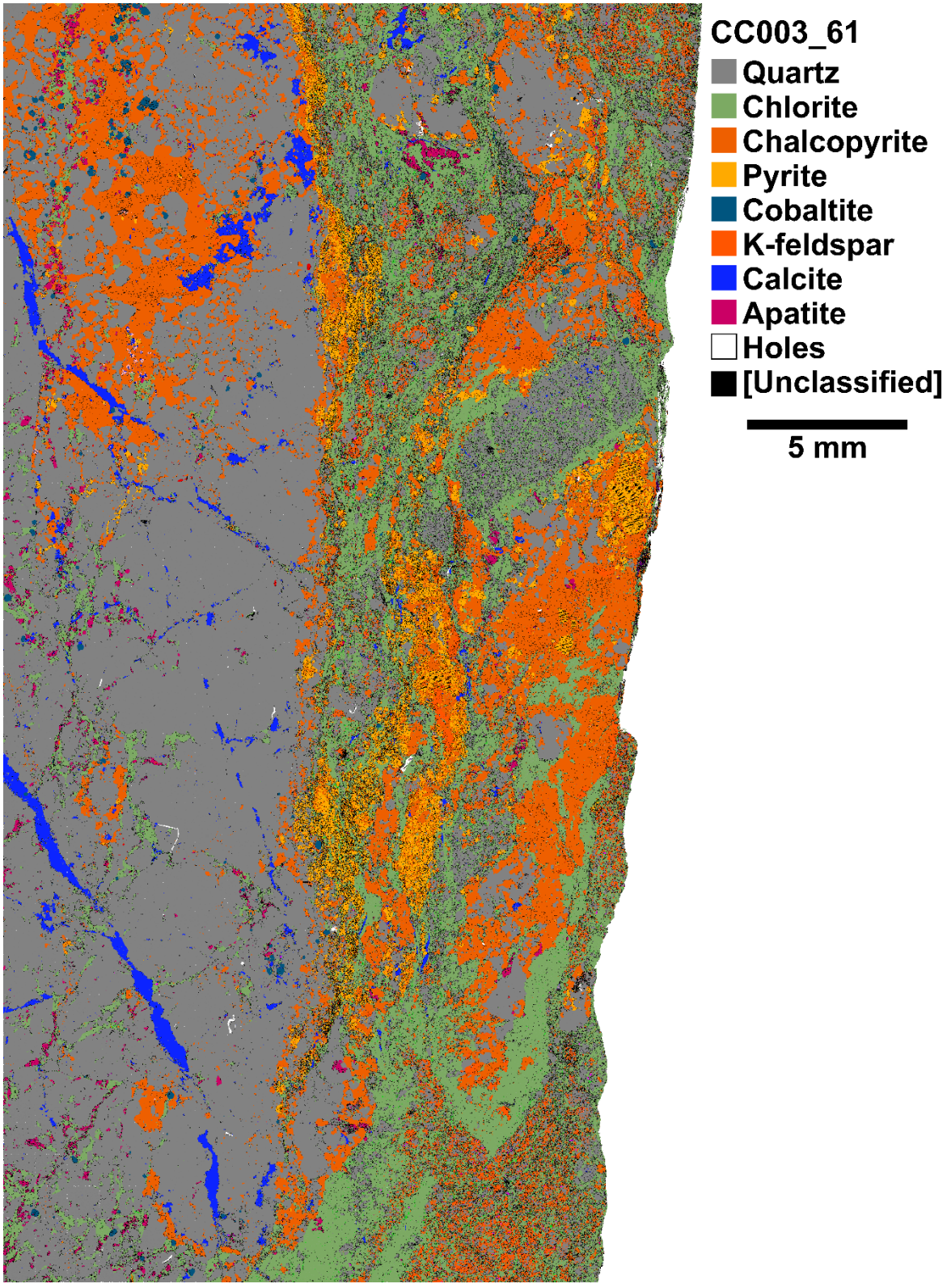

Appendix 3.1b – Automated mineralogy map of sample CC003_61 from ore mineral Assemblage One of Carlow Castle. Chalcopyrite and pyrite constitute the primary ore minerals within this sample, with cobaltite occurring as a minor constituent. Note the finer-grained nature of these sulphides and lower grade by comparison to CC012_67.

Additionally, CC003_61 is comparably richer in quartz, calcite, and chlorite and contains comparably little actinolite or epidote. Apatite appears to commonly occur in associated with chlorite.

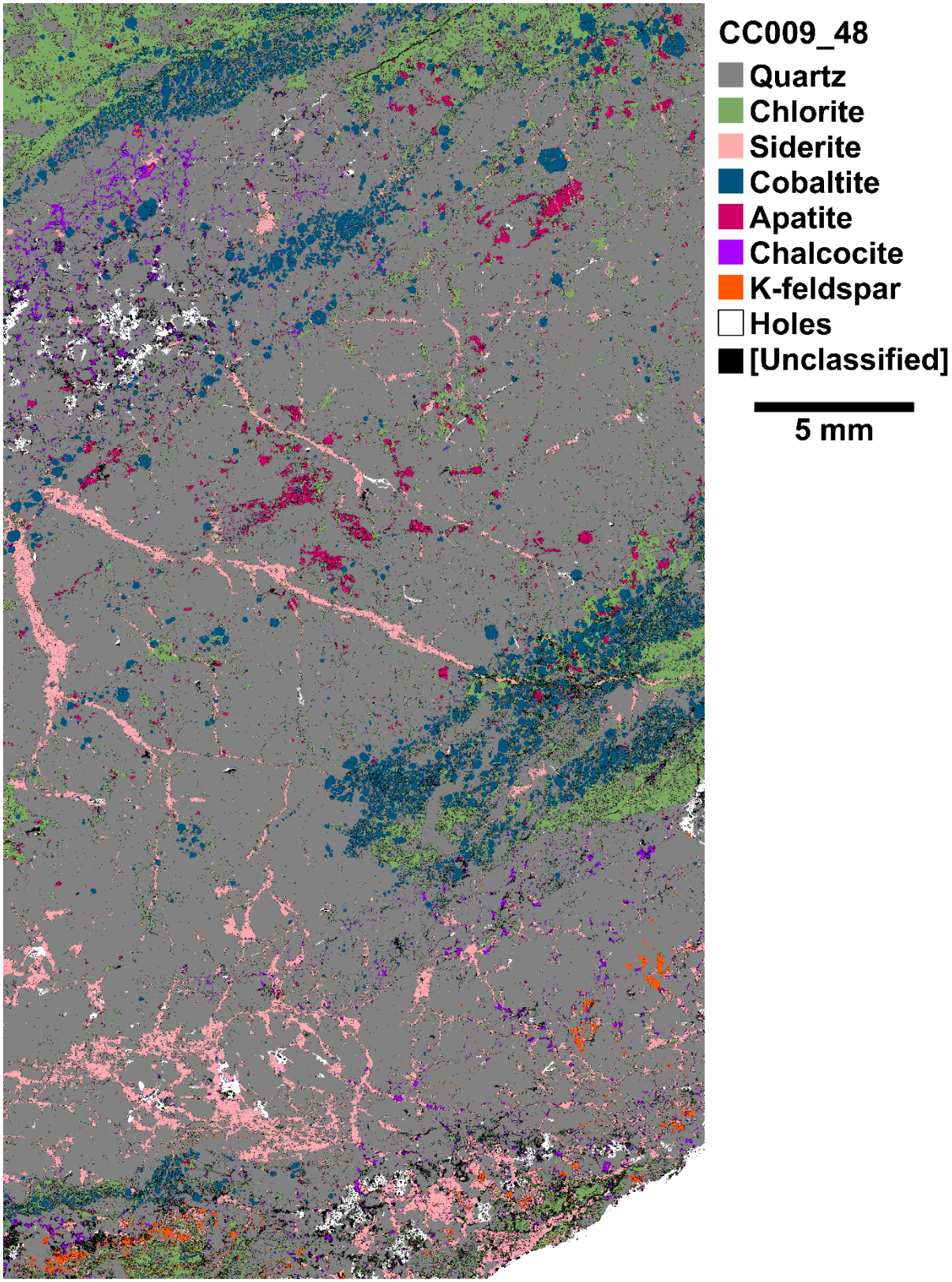

Appendix 3.1c – Automated mineralogy map of sample CC009_48 from ore mineral Assemblage Two of Carlow Castle. By contrast to samples CC012_67 and CC003_61, the sulphide mineralogy of sample CC009_48 is composed predominantly of cobaltite

and chalcocite with minimal pyrite or chalcopyrite. However, similarly to sample CC003_61, chlorite is the predominant alteration mineral along with minor K-feldspar and apatite. These ore and alteration minerals are hosted within a quartz-siderite vein.

Appendix 3.2 – Apatite U-Pb LA-ICP-MS data

Appendix 3.2 is accessible via this link and provides an .xlsx file containing U-Pb geochronology data for hydrothermal apatite analysed in this study.

Appendix 3.3 – Apatite major and trace element LA-ICP-MS data

Appendix 3.3 is accessible via this link and provides an .xlsx file containing major and trace element geochemical data for hydrothermal apatite analysed in this study.

Chapter 4

Mesoarchean oxygenation accompanied massive copper-cobalt mineralization

This chapter is currently under review for publication in *Science Advances*.

4.1 Abstract

Major hydrothermal Cu-Co mineralization in sedimentary rocks commenced following the Great Oxidation Event, 2.4 billion years ago. The emergence of Cu-Co deposits reflects the primary processes by which these metals are mobilized in Earth's crust, principally by oxidized fluids. However, a recently discovered significant Mesoarchean (~2.95 Ga) Cu-Co-Au deposit in the Pilbara Craton of Western Australia is difficult to reconcile within the traditional view of a pervasively and persistently anoxic Archean world. Here we show sulfur isotope signatures in the deposit lack mass-independent fractionation of anoxic Archean atmospheric sulfur. In-situ triple sulfur isotope (^{32}S, ^{33}S, ^{34}S) analysis of sulfide mineralization displays $\delta^{34}S$ values between -3.4 and 6.1‰, and critically, $\Delta^{33}S$ values between -0.17‰ and 0.12‰; within the defined bounds of mass-dependent sulfur fractionation. These sulfur isotopic data are atypical for Archean sulfides and, combined with thermodynamic modelling, suggest that Cu-Co mobilization occurred under oxidized fluid conditions. Cu-Co ore formation coincided with well-established ephemeral oxygenic conditions around 2.95 Ga, which directly preceded and potentially drove atmospheric changes that resulted in Earth's earliest major glaciation. Our findings are thus consistent with an emerging model that suggests the Mesoarchean atmosphere was subject to localized, transiently oxidized conditions following the emergence of oxygenic photosynthesis, sufficient to enable large-scale base-metal ore formation.

4.2 Introduction

There are very few examples of volumetrically large hydrothermal Cu-Co mineralization in the Archean, with the most significant examples of this mineralization style typically limited to basins no older than the Proterozoic (Hitzman et al., 2017; Hitzman et al., 2010). A reducing atmosphere meant that basinal fluids during the Archean were generally unable to mobilize strongly redox-sensitive metals like Cu and Co (Brown, 2014). However, the formation of the recently discovered Carlow Castle Cu-Co-Au deposit within the Pilbara Craton during the Mesoarchean necessitates large-scale Cu-Co mobility well into the Archean (Fox et al., 2021; Fox et al., 2019).

Carlow Castle Cu-Co-Au deposit is hosted in a Mesoarchean (3.07 Ga) orogenic thrust fault (Regal Thrust) through 3.28-3.16 Ga volcano-sedimentary rocks (peridotite, basalt, chert, carbonaceous shale) of the Roebourne greenstone belt of the West Pilbara Superterrane (3.28-3.066 Ga); an accretionary superterrane in northwest Western Australia (Figure 4.1; Hickman, 2016). Recent U-Pb apatite dating demonstrated that the deposit formed around ~2.955 Ga during major post-orogenic rifting and the formation of the proximal De Grey Superbasin (3.066-2.919 Ga) (Fox et al., 2021). The Carlow Castle ore deposit's exceptionally old age of mineralization and distinctive ore deposit character make it unique in the global context of Cu-Co mineralization (Fox et al., 2021). Detailed characterization of the Carlow Castle ore mineralization is given in Fox et al. (2019).

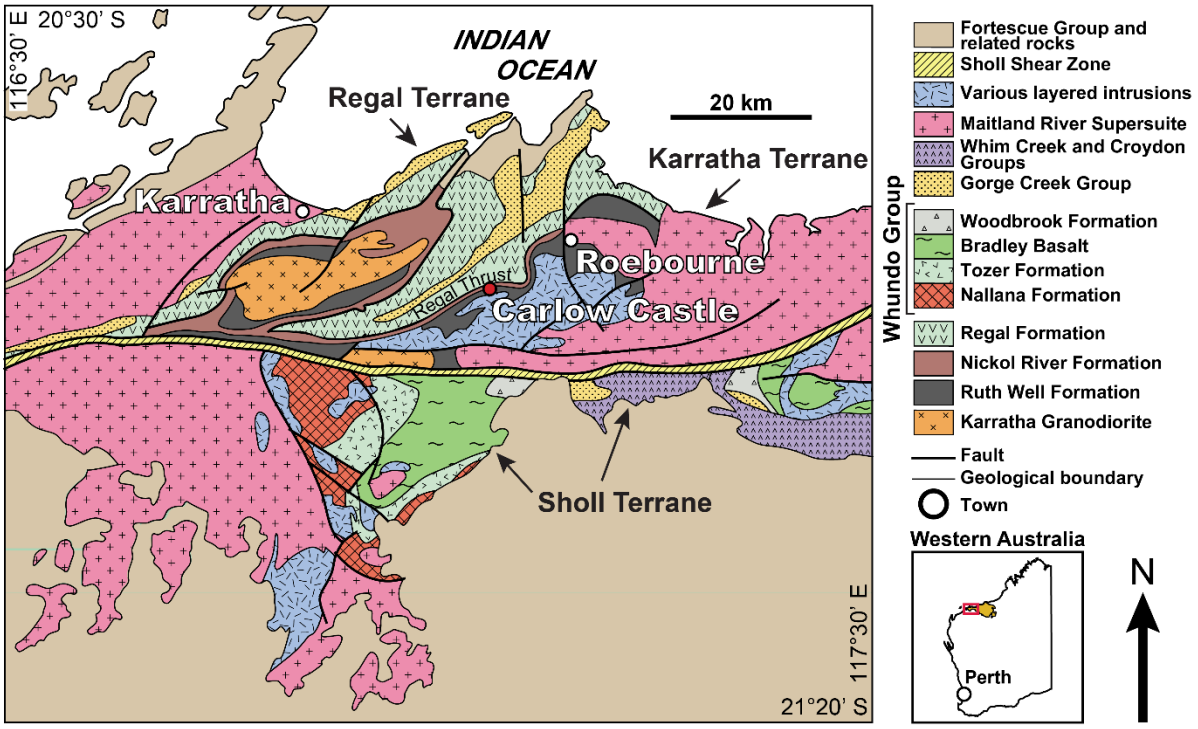

Figure 4.1 - Geologic map of the northwest Pilbara Craton. The Carlow Castle ore deposit site is indicated by the red circle. The Pilbara Craton is highlighted in orange within the inset map. Modified after Van Kranendonk et al. (2002).

Given difficulties explaining Cu-Co ore formation within the context of an anoxic Archean atmosphere, the concentration of Cu and Co at ~2.95 Ga (Fox et al., 2021) within the Carlow Castle deposit may support a model of spatially and temporally limited periods of oxygenation during the Mesoarchean. Localized transient oxygenated conditions during the Archean have been demonstrated recently in several studies from the Pilbara Craton and other Archean terranes (Figure 4.2; Appendix 4.1; Anbar et al., 2007; Catling & Zahnle, 2020; Eickmann et al., 2018; Frei, Gaucher, Poulton, & Canfield, 2009; Hickman & Van Kranendonk, 2012; Hoashi et al., 2009; Kato et al., 2009; Kaufman et al., 2007; Lyons & Gill, 2010; Lyons et al., 2014; Ono, Beukes, Rumble, & Fogel, 2006; Ossa Ossa et al., 2016; Ostrander, Johnson, & Anbar, 2021; Planavsky et al., 2014; Reinhard, Raiswell, Scott, Anbar, & Lyons, 2009; Wille et al., 2007), with some studies even suggesting the possibility of extended periods of pervasive Archean oxygenation (Ohmoto, 2020; Ohmoto et al., 2006). Whilst it is possible for Cu-Co transport to occur under reduced hydrothermal conditions, this would typically require high fluid temperatures or acidic fluid pH as an alternative mechanism for metal solubility (Brown, 2014; Rose, 1989), however such conditions are not supported by evidence from alteration patterns at Carlow Castle (Fox et al., 2021).

Multiple sulfur isotope analysis has been a key tool in many studies of the evolution of Earth's atmosphere and sulfur cycle, especially during the transition between the Archean and Proterozoic (Farquhar, Bao, & Thiemens, 2000). This is due to mass-independent fractionation (MIF-S) signatures imparted on atmospheric sulfur before the development of an atmospheric ozone shield, evidenced by the large $\Delta^{33}S$ fractionation within Archean sulfides (Farquhar & Wing, 2003). However, the attenuation of this $\Delta^{33}S$ MIF-S signal during the Mesoarchean, coinciding with the early emergence of oxygenic photosynthesis and the Pongola Glaciation (Catling & Zahnle, 2020; Kasting & Ono, 2006) has been interpreted to reflect a volatile, evolving early atmosphere that may have accumulated sufficient oxygen, whether ephemerally or persistently, to dampen MIF-S signals and displace the methane-rich Archean atmospheric greenhouse (Ono et al., 2006).

Given the importance of atmospheric oxygen for tracking the evolution of life, the biosphere, climate, element cycling, and ore deposit genesis, we utilized multiple sulfur isotopic analysis to resolve atmospheric conditions during the formation of Cu-Co-Au mineralization at Carlow Castle. This isotopic investigation was supported by thermodynamic modelling to constrain the conditions of the Carlow Castle hydrothermal ore-forming system.

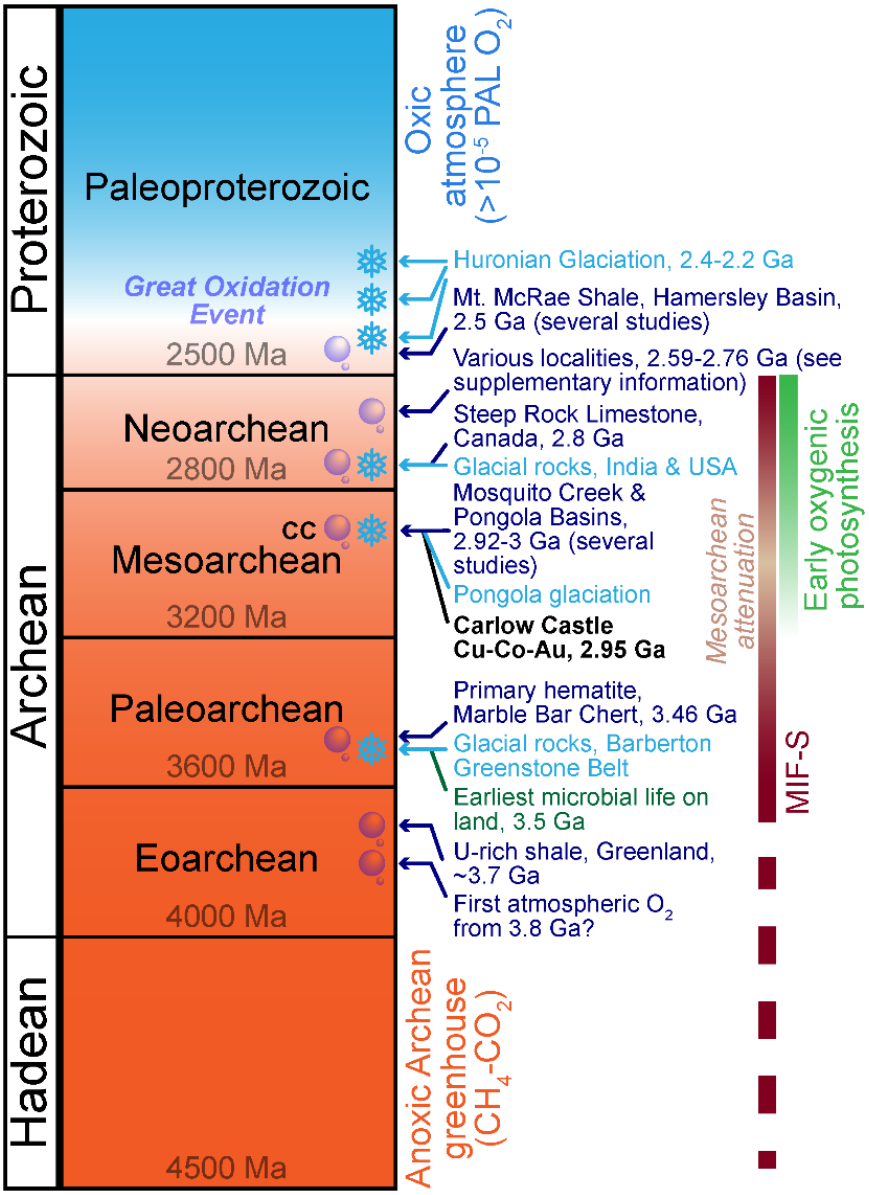

Figure 4.2 - Compilation of studies purporting to show evidence of 'whiffs' of oxygen before the Great Oxidation Event and Carlow Castle's relative temporal position. See full list of studies compiled in Appendix 4.1. PAL = present atmospheric level, MIF-S = mass-independent sulfur fractionation.

4.3 Results

4.3.1 Sulfur Isotope characteristics of Carlow Castle Cu-Co-Au deposit

The $\delta^{34}S$ values of all measured mineral phases across four samples define a relatively wide range, between -3.4‰ and 6.1‰ (Figure 4.3a). The mean and median values are 2.3‰, and standard deviation is 0.86‰. Fractionation between samples is limited, with CC012_67 showing the highest mean $\delta^{34}S$ of 2.9‰ and CC003_61 showing the lowest mean $\delta^{34}S$ of

2.06‰. Fractionation between phases within a given sample is also limited; the largest variation in mean $\delta^{34}S$ values between phases in a given sample is 0.8‰ between chalcopyrite (2.2‰) and pyrite (1.4‰) in CC003_61. The $\Delta^{33}S$ values show minimal variance; between -0.17‰ and 0.12‰, with a mean of -0.05‰, median of -0.06, and standard deviation of 0.05‰. All 183 measurements fall within the traditional bounds of mass-dependent sulfur fractionation (MDF-S) of 0 ± 0.2‰ and plot along the MDF-S line (Figure 4.3b). Full results are provided in Appendix 4.2.

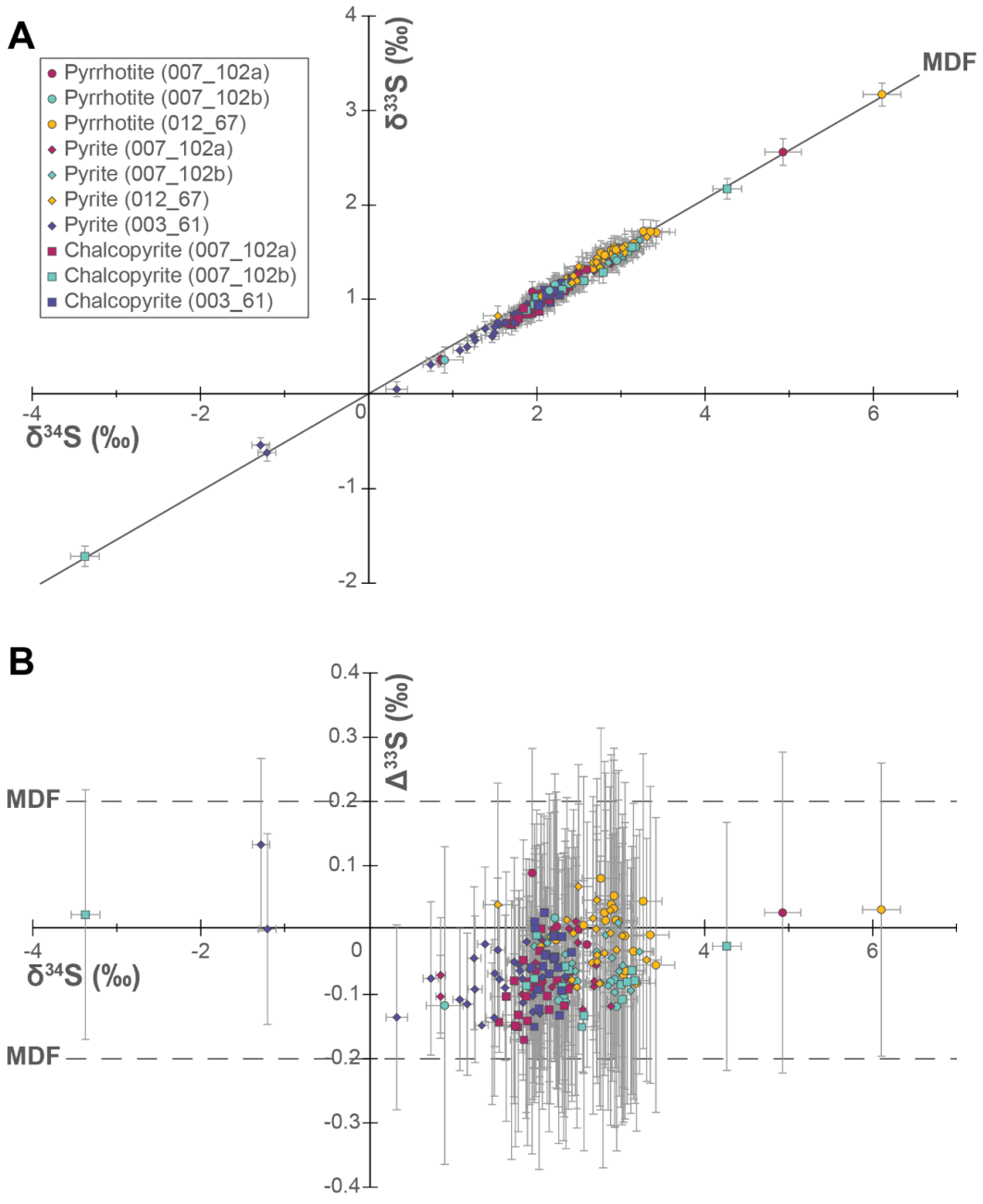

Figure 4.3 - (a, b) Multiple sulfur isotopes composition of Carlow Castle ore minerals (pyrrhotite, pyrite, and chalcopyrite). Note the clear mass-dependent fractionation pattern of $\Delta^{33}S$. Error bars are 2σ, as calculated according to method documented in LaFlamme et al. (2016).

4.3.2 Hydrothermal Cu-Co mobility

At a peak fluid temperature of 300°C and neutral pH (6.0 at 300°C), consistent with estimated conditions of Carlow Castle deposit's ore formation based on its propylitic hydrothermal alteration assemblage (Fox et al., 2021), the solubility of Co and Cu are controlled by $\log f(O_2)$

(Figure 4.4). Under oxidising conditions, at equilibrium with HSO_4^-/SO_4^{2-}, Co is mobile as $CoCl_4^{2-}$ and Cu is mobile as $CuCl_2^-$ complexes. Under increasingly reducing conditions Cu and Co become progressively less soluble and immobile at equilibrium with H_2S or S^{2-}, where they are stable as sulfides/sulfosalts. As such, rapid precipitation of Cu and Co from a 300°C, neutral, oxidized fluid could be induced through a sudden change in redox conditions and reduction of SO_4^{2-} to H_2S.

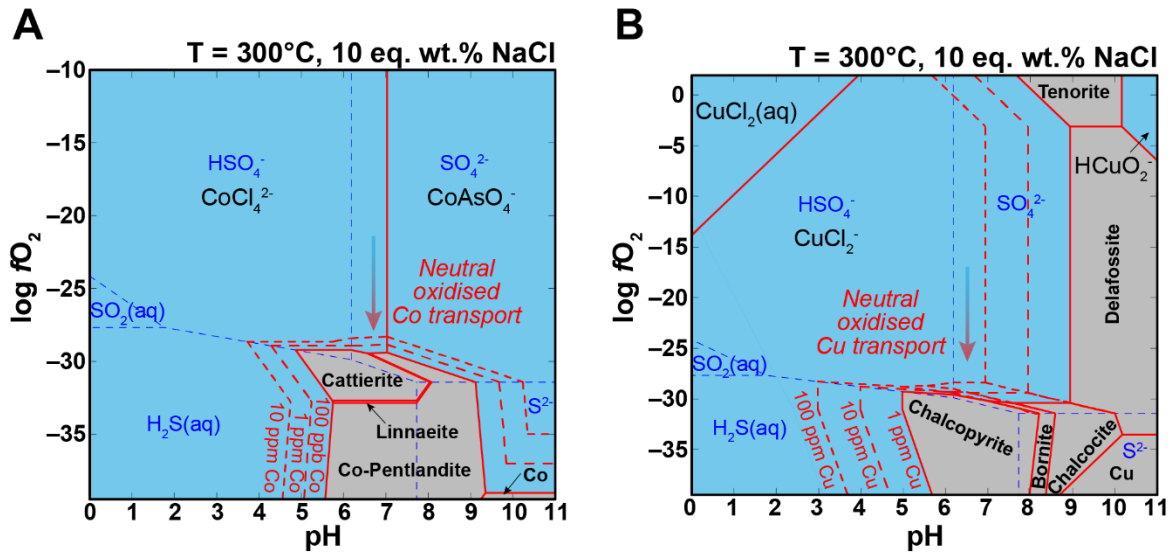

Figure 4.4 - Stability fields for selected minerals and dissolved species along with solubility contours for Co (a) and Cu (b) as a function of pH and oxygen fugacity at 300°C and water-saturated pressure. Both Co and Cu are mobile (as Cl^- complexes) under oxidized conditions with metal concentration increasing with acidity. Note that the dominance of propylitic hydrothermal alteration acts as a limit on minimum ore fluid pH. Neutral pH at 300°C is 6.0. Metals precipitate as sulfides/sulfosalts upon reduction. Fluid compositions: S_{total} = 0.01 molal, Cl_{total} = 2.0 molal, As_{total} = 0.001 molal, Fe_{total} = 0.01 molal.

4.4 Discussion

4.4.1 Sulfur source and absence of 'Archean sulfur'

The sulfur source most commonly implicated in the formation of typical post-Archean sediment-hosted Cu-Co deposits is a combination of evaporite-derived seawater sulfate and sedimentary sulfide produced by microbial sulfate reduction. Both sources tend to produce highly fractionated $\delta^{34}S$ signatures in derived sulfide ores (Hitzman et al., 2005). Conversely, the $\delta^{34}S$ signature of Archean sulfides generally exhibit extremely limited fractionation as

Mesoarchean seawater sulfate and sedimentary sulfides had yet to diverge significantly from bulk mantle compositions (Canfield, 2004). Reflecting this, the spread of most $\delta^{34}S$ signatures around 2‰ in the Carlow Castle deposit's sulfide mineralization is typical of Archean sulfides from various environments, including in sulfide ore deposits, sedimentary sulfides, and magmatic sulfides (Farquhar, Wu, Canfield, & Oduro, 2010; Johnston, 2011). This could be interpreted to reflect a homogenous mantle origin for sulfur in the ore deposit ($\delta^{34}S = 0 \pm 2$‰ (Seal, 2006)). Alternatively, the spread of the majority of data points beyond the typical bounds of mantle sulfur (130 of 183 data points), combined with the otherwise attenuated $\delta^{34}S$ signatures of Archean sulfur reservoirs, could be indicative of sulfur input from a slightly heavy Archean seawater sulfate source ($\delta^{34}S = 3$ to 8‰) (Muller, Philippot, Bard-Rollion, & Cartigny, 2016) into the Carlow Castle ore body. This latter interpretation of the $\delta^{34}S$ signature would support a model more akin to conventional post-Archean Cu-Co mineralization; necessitating an oxidized seawater sulfate-bearing ore fluid to enable Cu-Co mobility.

The $\Delta^{33}S$ signatures in our data are characteristic of mass-dependent fractionation processes and there is no evidence of any MIF-S signature indicative of typical Archean sulfur. By comparison, it is relatively rare to observe Archean hydrothermal ore deposits with no incorporation of MIF-S (Figure 4.5; Appendix 4.3). It is unlikely that the Carlow Castle deposit's lack of MIF-S can be explained purely through a magmatic sulfur source. Particularly as there are no mantle-derived rocks that are contemporaneous with, and proximal to the orebody mineralization, to allow for direct input of mantle sulfur without contamination from other Archean sulfur sources during ore fluid migration (Fox et al., 2021). However, sulfur derived from Archean sedimentary sulfide or seawater sulfate sources would be expected to exhibit significant MIF-S signatures, unless such oxidized ore fluids were also associated with a weakly oxygenated atmosphere that temporarily inhibited production or preservation of large magnitude MIF-S. This adapts the model presented by Kasting and Ono (2006); Ono et al. (2006) to account for attenuated MIF-S signatures evident within the Mesoarchean sedimentary record. As noted by Wang et al. (2018), the otherwise very small atmospheric O_2 reservoir of the Archean would have likely been highly dynamic and subject to significant variability following the evolution of oxygenic photosynthesis. As such, even subtle oxygen fluxes may have been sufficient to significantly alter Mesoarchean atmospheric chemistry and temporarily attenuate MIF-S signatures. With this considered, the small but consistently negative $\Delta^{33}S$ values (156 of 183 data points) displayed by the Carlow Castle deposit's ore sulfides are

consistent with the slightly heavy $\delta^{34}S$ and negative $\Delta^{33}S$ signals that are characteristic of Archean sulfate (Figure 4.5), but with heavily attenuated $\Delta^{33}S$ values (Johnston, 2011).

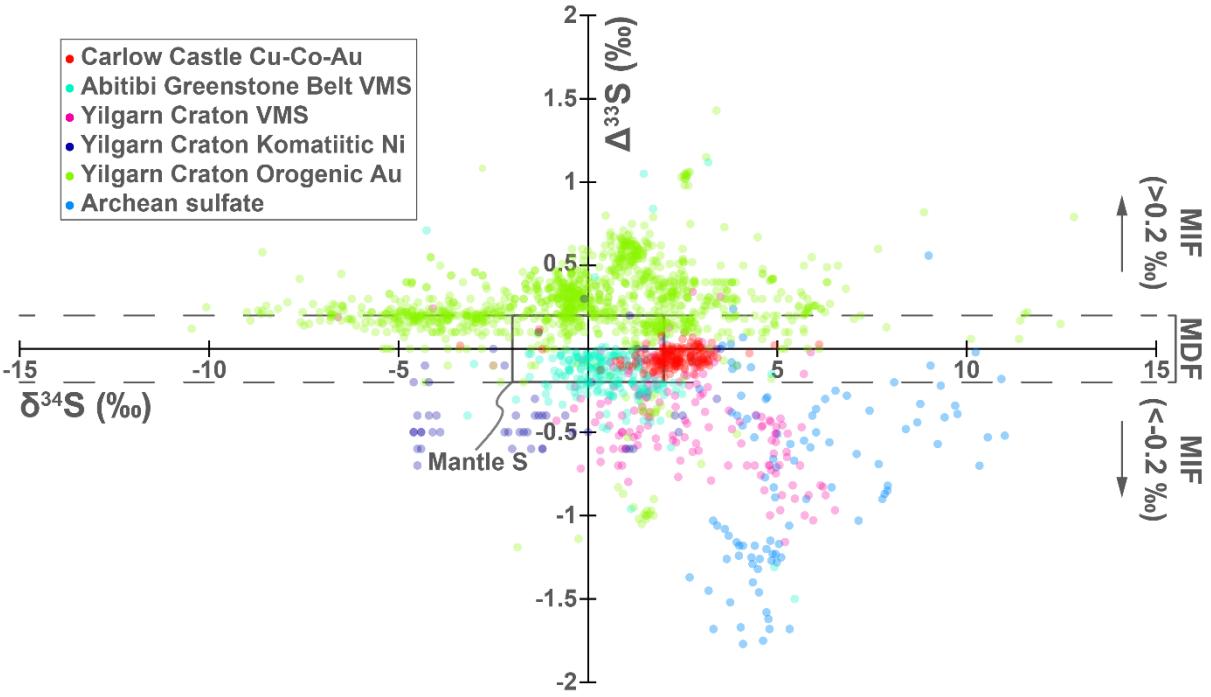

Figure 4.5 - Comparison of Archean greenstone-hosted hydrothermal and magmatic ore deposits with Carlow Castle deposit (red). Note that Carlow Castle is the only deposit with no clear MIF-S. Mantle sulfur range is marked by the grey box. Range of Archean SO_4^{2-} sulfur isotope compositions from Muller et al. (2016). Ore deposit sulfur isotope data compiled from various sources in Appendix 4.3.

4.4.2 Cu-Co mobility during Mesoarchean rifting

Given the established physicochemical constraints on Carlow Castle's hydrothermal system, our modelling shows that oxidized sulfate-bearing ore fluids were the fundamental chemical pathway to enable Cu-Co mobility prior to reductive precipitation of metal sulfide ore minerals upon interaction with a suitable redox buffer, i.e., mafic volcanics or carbonaceous shales (Figure 4.4). Therefore, if the Mesoarchean Pilbara Craton's atmosphere was sufficiently oxidized to inhibit the generation of MIF-S, we argue an oxidized seawater origin for the Carlow Castle deposit is possible. The shallow water margins of the overlying marine Gorge Creek Basin and Whim Creek volcanic arc within the De Grey Superbasin would be a potential source of seawater sulfate-bearing oxygenated fluids during a period of major crustal extension and increased crustal heat flow (Fox et al., 2021; Hickman, 2016). In support of this paleogeographic setting, there is a preponderance of evidence that supports the existence of

isolated photosynthetically oxygenated shallow marine environments from at least ~2.95 Ga (Eickmann et al., 2018; Planavsky et al., 2014; Wang et al., 2020). Following this, an atmosphere briefly oxygenated sufficiently to inhibit or attenuate MIF-S signatures could account for the atypical lack of MIF-S in the Carlow Castle deposit's ore sulfides in a manner that is also consistent with conventional post-Archean models of Cu-Co metallogenesis and the results of thermodynamic modelling in this study; relying on redox processes as a mechanism to mobilize Cu and Co. This model is summarised schematically in Figure 4.6.

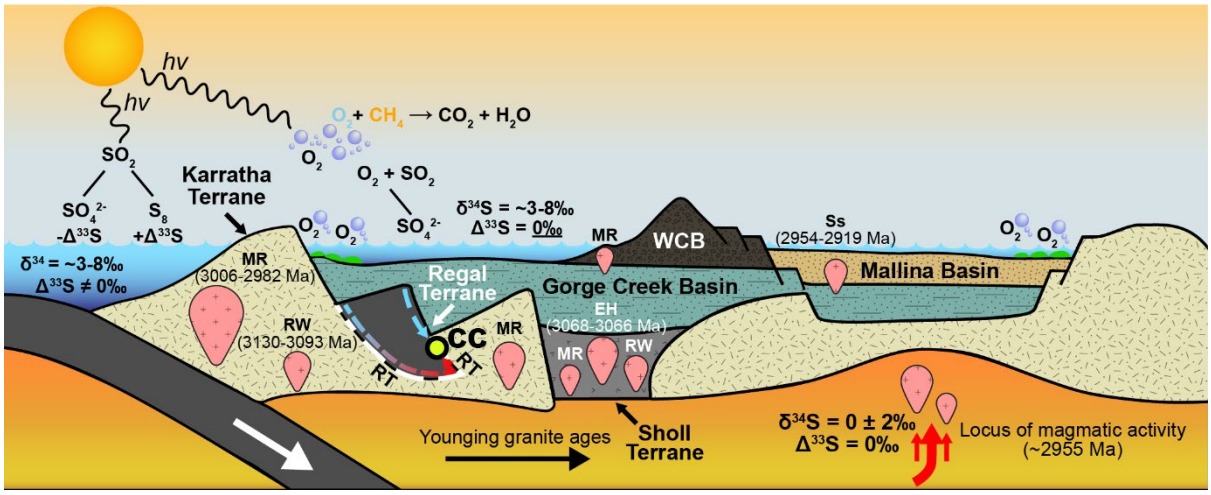

Figure 4.6 - Conceptual schematic model of the northwest Pilbara Craton during the formation of Carlow Castle (CC) and the De Grey Superbasin around 2.955 Ga. Note: MR = Maitland River Supersuite, RW = Railway Supersuite, EH = Elizabeth Hill Supersuite, Ss = Sisters Supersuite, WCB = Whim Creek Basin.

4.4.3 The Mesoarchean MIF-S record

The broad attenuation of MIF-S signatures throughout the Mesoarchean (Figure 4.7) is a widely discussed aspect of the Archean sedimentary sulfur isotopic record (Johnston, 2011). This phenomenon has been attributed to a variety of processes including variability in volcanic SO_2 output (Ohmoto et al., 2006), the oxidation state of volcanic sulfur volatiles (Halevy, Johnston, & Schrag, 2010), changes in anoxic atmospheric chemistry (Domagal-Goldman, Kasting, Johnston, & Farquhar, 2008; Farquhar et al., 2007; Thomazo, Ader, Farquhar, & Philippot, 2009), dilution by crustal MDF-S sources (Guy et al., 2012), and the potential for transient or prolonged oxygenation of the Mesoarchean atmosphere associated with the early emergence of oxygenic photosynthesis (Ohmoto et al., 2006; Ono et al., 2006; Wang et al., 2018). The latter argument has been disputed as some studies have demonstrated the preservation of MIF-S signatures through this period (Farquhar et al., 2007; Guy et al., 2012). Nonetheless, a notable

reduction in the magnitude of MIF-S is evident through the Mesoarchean, with significant MIF-S values generally being outliers during this period (Figure 4.7). This also coincided with a shift in uranium isotope systematics observed by Wang et al. (2018), which is similarly attributed to the evolution of oxygenic photosynthesis. It should be noted that once a large reservoir of MIF-S had been established in the Archean crust it is likely to have been recycled and therefore evident within the sulfur isotope record long after the generation of new large MIF-S anomalies had been attenuated due to a rise in atmospheric O_2 levels toward the critical 10^{-5} PAL (Philippot et al., 2018; Reinhard, Planavsky, & Lyons, 2013). This 'crustal memory effect' of MIF-S is also evident immediately following the GOE and implies that any attenuation of MIF-S evident in the sulfur isotope record, such as the one displayed through the Mesoarchean and especially around 2.95 Ga, is likely to understate the relative decrease in the magnitude of new attenuated MIF-S signatures generated due to contamination with the existing crustal reservoir of large MIF-S signatures. As such, the occurrence of some larger magnitude outlier MIF-S signatures within the Mesoarchean rock record doesn't necessarily discount the possibility of changes in atmospheric chemistry that are suggested by the general attenuation of these MIF-S values. Further, in those studies purporting to show evidence of the persistence of MIF-S through the Mesoarchean (Farquhar et al., 2007; Guy et al., 2012), it is notable that data from rocks coeval with glacial tillite and diamictites from ~2.95 Ga also generally show significantly attenuated MIF-S values broadly consistent with those presented by Ono et al. (2006). This would effectively support a connection between attenuated MIF-S signatures, changing atmospheric chemistry, and the Pongola Glaciation around 2.95 Ga.

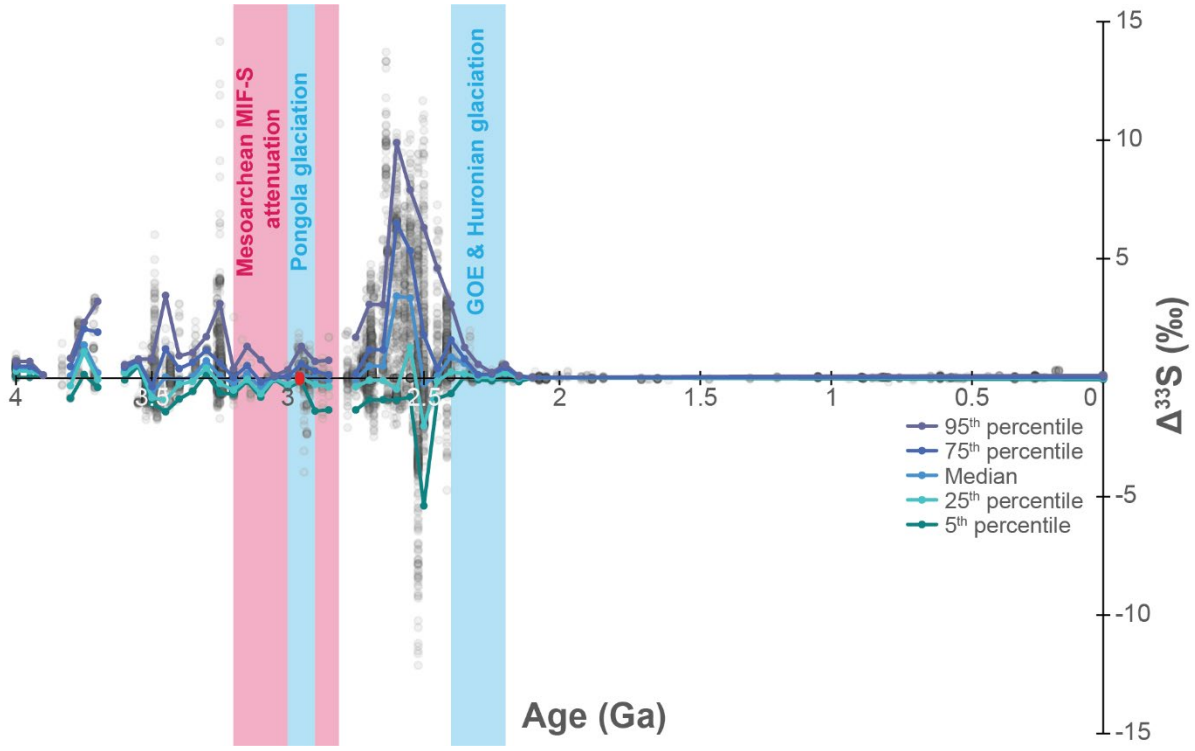

Figure 4.7 - Compilation of sedimentary sulfur isotope data through geological time (gray dots) compared to Carlow Castle sulfur isotope data (red dots). The colored lines here indicate the percentile values of these data, binned in periods of 50 My from 4 Ga through to 2.1 Ga. A clear minimum in the magnitude of MIF-S values is observable through the Mesoarchean, most likely coinciding with the first evolution of oxygenic photosynthesis. Note gaps here are a result of no data being available for a given 50 My period. Additionally, some time periods are biased by relatively small data sets. Modified from data compiled by Killingsworth et al. (2019) and Selvaraja, Caruso, Fiorentini, and LaFlamme (2017).

4.4.4 A whiff of oxygen at ~2.95 Ga

Here we suggest that the Carlow Castle deposit's mineralization and MDF-S signature is consistent with a 'whiff' of oxygen sufficient to destabilise Mesoarchean atmospheric anoxia. This is asserted based on (i) the absence of proximal and contemporaneous mantle-derived rocks to provide a mantle MDF-S source; (ii) the spread of $\delta^{34}S$ values beyond the generally accepted bounds of mantle sulfur (0 ± 2‰), and predominantly small negative $\Delta^{33}S$ values consistent with an attenuated Mesoarchean seawater SO_4^{2-} source (Figure 4.3); (iii) the rarity of pure MDF-S signatures in other Archean hydrothermal ore deposits (Figure 4.5), especially those without a proximal magmatic source; (iv) the thermodynamic necessity for oxidized

hydrothermal fluids, at equilibrium with HSO_4^-/SO_4^{2-}, to mobilize Cu/Co under neutral fluid conditions at 300°C (Figure 4.4); and (v) the close temporal correlation of Carlow Castle mineralization with glacial rocks of the Pongola and Witwatersrand basins that display similarly muted MIF-S signatures interpreted to relate to an ephemeral oxidation event preceding the Pongola Glaciation.

Ephemeral oxygenation within the northwest Pilbara Craton during the formation of the Carlow Castle deposit at ~2.955 Ga would have been contemporaneous with widely postulated photosynthetically oxygenated conditions during the deposition of the Pongola Supergroup in South Africa at ~2.95 Ga (Figure 4.2; Crowe et al., 2013; Eickmann et al., 2018; Kasting & Ono, 2006; Luskin, Wilson, Gold, & Hofmann, 2019; Ono et al., 2006; Ossa Ossa et al., 2019; Ossa Ossa et al., 2016; Planavsky et al., 2014). In addition to evidence from a variety of isotopic systems (Appendix 4.1), sedimentary pyrite in the Mozaan Group of the Pongola Supergroup also display muted MIF-S signatures. This has been interpreted as evidence of deposition under a weakly oxidized atmosphere (Ono et al., 2006). It has been suggested that during this time the Pilbara and Kaapvaal Cratons may have been connected as part of the supercontinent Vaalbara; however, this hypothesis remains contentious (de Kock, Evans, & Beukes, 2009; Evans & Muxworthy, 2018). Regardless of geographic connections between the northwest Pilbara Craton and Pongola Basin, the two regions demonstrate widespread development of oxidative conditions at that time based on these data. The independent coevolution of two oxygenated environments around 2.95 Ga could suggest that oxygenic metabolic processes were more globally widespread and productive than previously understood (Catling & Zahnle, 2020). This interpretation is consistent with previous hypotheses of an abrupt but ephemeral increase in atmospheric O_2 that destabilized a reduced methane-rich Mesoarchean atmosphere leading to the Pongola Glaciation around 2.95 Ga, evidenced by glacial diamictites of the Mozaan Group (Pongola Supergroup) in South Africa (Catling & Zahnle, 2020; Kasting & Ono, 2006; Lyons et al., 2014; Ono et al., 2006). As such, we argue that the significant oxygen required to form the Carlow Castle deposit's Cu-Co mineralization, may be a symptom of a global phenomenon associated with a broad increase in O_2 production around 2.95 Ga coinciding with, or immediately following, the early evolution of oxygenic photosynthesis (Crowe et al., 2013; Ono et al., 2006; Planavsky et al., 2014; Wang et al., 2018). This was sufficient to destabilize a methane-rich greenhouse Mesoarchean atmosphere, significantly reduce atmospheric temperatures, suppress MIF-S signatures, and modify large-scale metal

mobilization processes in the crust, leading to the formation of large base-metal deposits. These findings may also support previous studies, which suggest that fluctuations in the magnitude of $\Delta^{33}S$ signatures in the Archean rock record reflect the evolving chemistry of the atmosphere throughout the Archean (Ohmoto et al., 2006; Ono et al., 2006; Wang et al., 2018). These findings contradict the traditional model of pervasive and persistent Archean atmospheric anoxia and are consistent with more nuanced emerging models of ephemerally oxidized conditions in Archean surface environments following the evolution of oxygenic photosynthesis and the potential for associated fluctuations in atmospheric chemistry following this critical evolutionary milestone.

4.5 Materials and methods

4.5.1 Samples

The sulfur isotope compositions of four mineralized samples (CC012_67, CC007_102a, CC007_102b, CC003_61) from the Carlow Castle Cu-Co-Au deposit were characterized in this study (Appendix 4.4). These samples are composed predominantly of chalcopyrite, pyrite, pyrrhotite and minor cobaltite; hosted in quartz-calcite veins and intergrown with hydrothermal chlorite, actinolite, and epidote alteration minerals. Discs (~8 mm in diameter) of these samples were mounted into epoxy pucks and trimmed into a semi-circular shape to be accompanied by another semi-circular puck of standard reference materials in the sample holder. These samples were gold coated to a thickness of ~30 nm to prevent charging.

4.5.2 Secondary-ion mass spectrometry

In-situ triple sulfur isotope (^{32}S, ^{33}S, ^{34}S) analyses were conducted using a CAMECA 1280 large geometry secondary-ion mass spectrometer (SIMS) at the Centre for Microscopy and Microanalysis, University of Western Australia. After thorough cleaning in ethanol and distilled water, samples were coated with 20 nm of Au. A total of 183 analyses of pyrite, pyrrhotite, and chalcopyrite were conducted across the four mineralized samples.

The sample surfaces were sputtered over a 10x10 μm area using a 10 kV, Gaussian Cs^+ beam with an intensity of 3.5 nA and impact energy of 20 keV. Secondary ions were admitted to the mass spectrometer via a 90 μm entrance slit within a 3000 μm field aperture at ×133 field magnification. The NMR magnetic field controller locked the axial mass at the beginning of each session, and the mass spectrometer operated at a mass resolution (M/ΔM) of ~2500. The isobaric interference between ^{33}S and ^{32}S 1H peaks is not fully resolved in these conditions. The magnetic field was thus offset slightly on the low mass side to avoid the interference on

the ^{33}S peak. Three sulfur isotopes were detected simultaneously in multi-collection mode by three Faraday cups with 10^{11} Ω (L2, ^{32}S) and 10^{10} Ω (L1 and H1, ^{33}S and ^{34}S) resistors. Each analysis included 30 s of pre-sputtering followed by 20 cycles of 4 s counting time. Analytical drift and calibration were monitored through bracketing of analyses with matrix matched standards for pyrite (Sierra), chalcopyrite (Nifty-b), and pyrrhotite (Alexo). Reference values for these standards and data reduction procedures utilized in this study are documented in LaFlamme et al. (2016).

4.5.3 Thermodynamic modelling

Thermodynamic modelling of the hydrothermal solubility of Cu and Co was conducted using The Geochemist's Workbench (Bethke, 1996) and methodologies utilized by Jansson and Liu (2020). Metal solubility, speciation, and phase stability were modelled and log fO_2-pH diagrams were constructed for a peak ore fluid temperature of 300°C, consistent with temperature estimates of the Carlow Castle deposit's ore formation (Fox et al., 2021), and salinity of 10% NaCl. Thermodynamic properties for Cu- and Co-bearing minerals and aqueous species were taken from various published sources (Brugger et al., 2007; Helgeson, Delany, Nesbitt, & Bird, 1978; Liu et al., 2011; Liu & McPhail, 2005; Midgisov, Zezin, & Williams-Jones, 2011; Mills, 1974; Shock, Sassani, Willis, & Sverjensky, 1997; Vaughan, 1978; Wolery, 1992). However, the lack of thermodynamic data for cobaltite necessitates estimating stability based on chemically comparable solid Co-bearing phases.

Acknowledgements

This research was supported by an Australian Government Research Training Program Scholarship and a CSIRO Mineral Resources postgraduate student scholarship. Matvei Aleshin is acknowledged for technical assistance with SIMS analysis.

References

Albut, G., Kamber, B. S., Brüske, A., Beukes, N. J., Smith, A. J. B., & Schoenberg, R. (2019). Modern weathering in outcrop samples versus ancient paleoredox information in drill core samples from a Mesoarchaean marine oxygen oasis in Pongola Supergroup, South Africa. *Geochimica et Cosmochimica Acta, 265*, 330-353. doi:https://doi.org/10.1016/j.gca.2019.09.001

Anbar, A. D., Duan, Y., Lyons, T. W., Arnold, G. L., Kendall, B., Creaser, R. A., . . . Buick, R. (2007). A Whiff of Oxygen Before the Great Oxidation Event? *Science, 317*(5846), 1903-1906. doi:https://doi.org/10.1126/science.1140325

Bethke, C. M. (1996). *Geochemical Reaction Modeling: concepts and applications*. Oxford, UK: Oxford University Press.

Brocks, J. J., Logan, G. A., Buick, R., & Summons, R. E. (1999). Archean Molecular Fossils and the Early Rise of Eukaryotes. *Science, 285*(5430), 1033-1036. doi:10.1126/science.285.5430.1033

Brown, A. C. (2014). Low-Temperature Sediment-Hosted Copper Deposits. In K. Turekian & H. Holland (Eds.), *Treatise on Geochemistry* (2nd ed., Vol. 13, pp. 251-271). Oxford: Elsevier Science.

Brugger, J., Etschmann, B., Liu, W., Testemale, D., Hazemann, J., Emerich, H., & Beek, W. (2007). An XAFS study of the structure and thermodynamics of Cu(I) chloride complexes in brines up to supercritical conditions (400°C, 600 bars). *Geochimica et Cosmochimica Acta, 71*(20), 4920-4941. doi:https://doi.org/10.1016/j.gca.2007.08.003

Cabral, A. R., Creaser, R. A., Nägler, T., Lehmann, B., Voegelin, A. R., Belyatsky, B., . . . Escher, P. (2013). Trace-element and multi-isotope geochemistry of Late-Archean black shales in the Carajás iron-ore district, Brazil. *Chemical Geology, 362*, 91-104. doi:https://doi.org/10.1016/j.chemgeo.2013.08.041

Canfield, D. E. (2004). The evolution of the Earth surface sulfur reservoir. *American Journal of Science, 304*(10), 839-861. doi:https://doi.org/10.2475/ajs.304.10.839

Catling, D. C., & Zahnle, K. J. (2020). The Archean Atmosphere. *Science Advances, 6*(9), 1-16. doi:https://doi.org/10.1126/sciadv.aax1420

Crowe, S. A., Døssing, L. N., Beukes, N. J., Bau, M., Kruger, S. J., Frei, R., & Canfield, D. E. (2013). Atmospheric oxygenation three billion years ago. *Nature, 501*, 535-538. doi:https://doi.org/10.1038/nature12426

Czaja, A. D., Johnson, C. M., Roden, E. E., Beard, B. L., Voegelin, A. R., Nägler, T. F., . . . Wille, M. (2012). Evidence for free oxygen in the Neoarchean ocean based on coupled iron–molybdenum isotope fractionation. *Geochimica et Cosmochimica Acta, 86*, 118-137. doi:https://doi.org/10.1016/j.gca.2012.03.007

de Kock, M. O., Evans, D. A. D., & Beukes, N. J. (2009). Validating the existence of Vaalbara in the Neoarchean. *Precambrian Research, 174*(1-2), 145-154. doi:https://doi.org/10.1016/j.precamres.2009.07.002

Domagal-Goldman, S. D., Kasting, J. F., Johnston, D. T., & Farquhar, J. (2008). Organic haze, glaciations and multiple sulfur isotopes in the Mid-Archean Era. *Earth and Planetary Science Letters, 265*(1-2), 29-40. doi:https://doi.org/10.1016/j.epsl.2008.01.040

Duan, Y., Anbar, A. D., Arnold, G. L., Lyons, T. W., Gordon, G. W., & Kendall, B. (2010). Molybdenum isotope evidence for mild environmental oxygenation before the Great Oxidation Event. *Geochimica et Cosmochimica Acta, 74*(23), 6655-6668. doi:https://doi.org/10.1016/j.gca.2010.08.035

Eickmann, B., Hofmann, A., Wille, M., Bui, T., Wing, B. A., & Schoenberg, R. (2018). Isotopic evidence for oxygenated Mesoarchaean shallow oceans. *Nature Geoscience, 11*, 133-138. doi:https://doi.org/10.1038/s41561-017-0036-x

Eigenbrode, J. L., Freeman, K. H., & Summons, R. E. (2008). Methylhopane biomarker hydrocarbons in Hamersley Province sediments provide evidence for Neoarchean aerobiosis. *Earth and Planetary Science Letters, 273*(3), 323-331. doi:https://doi.org/10.1016/j.epsl.2008.06.037

Evans, M. E., & Muxworthy, A. R. (2018). Vaalbara Palaeomagnetism. *Canadian Journal of Earth Sciences, 56*(9), 912-916. doi:https://doi.org/10.1139/cjes-2018-0081

Farquhar, J., Bao, H., & Thiemens, M. (2000). Atmospheric Influence of Earth's Earliest Sulfur Cycle. *Science, 289*(5480), 756-758. doi:https://doi.org/10.1126/science.289.5480.756

Farquhar, J., Peters, M., Johnston, D. T., Strauss, H., Masterson, A. L., Wiechert, U., & Kaufman, A. J. (2007). Isotopic evidence for Mesoarchaean anoxia and changing atmospheric sulphur chemistry. *Nature, 449*, 706-709. doi:https://doi.org/10.1038/nature06202

Farquhar, J., & Wing, B. A. (2003). Multiple sulfur isotopes and the evolution of the atmosphere. *Earth and Planetary Science Letters, 213*(1-2), 1-13. doi:https://doi.org/10.1016/S0012-821X(03)00296-6

Farquhar, J., Wu, N., Canfield, D. E., & Oduro, H. (2010). Connections between Sulfur Cycle Evolution, Sulfur Isotopes, Sediments, and Base Metal Sulfide Deposits. *Economic Geology, 105*(3), 509-533. doi:10.2113/gsecongeo.105.3.509

Fox, D., Spinks, S., Barham, M., Kirkland, C. L., Pearce, M. A., Aspandiar, M., . . . Mead, E. (2021). Working up an apatite: Enigmatic Mesoarchean hydrothermal Cu-Co-Au mineralization in the Pilbara Craton. *Economic Geology, 116*(7), 1561-1573. doi:https://doi.org/10.5382/econgeo.4842

Fox, D., Spinks, S., Pearce, M. A., Barham, M., Le Vaillant, M., Thorne, R., . . . Verrall, M. (2019). Plundering Carlow Castle: First Look at a Unique Mesoarchean-Hosted Cu-Co-Au Deposit. *Economic Geology, 114*(6), 1021-1031. doi:https://doi.org/10.5382/econgeo.4672

Frei, R., Gaucher, C., Poulton, S. W., & Canfield, D. E. (2009). Fluctuations in Precambrian atmospheric oxygenation recorded by chromium isotopes. *Nature, 461*, 250–253. doi:https://doi.org/10.1038/nature08266

Garvin, J., Buick, R., Anbar, A. D., Arnold, G. L., & Kaufman, A. J. (2009). Isotopic Evidence for an Aerobic Nitrogen Cycle in the Latest Archean. *Science, 323*(5917), 1045-1048. doi:https://doi.org/10.1126/science.1165675

Guy, B. M., Ono, S., Gutzmer, J., Kaufman, A. J., Lin, Y., Fogel, M. L., & Beukes, N. J. (2012). A multiple sulfur and organic carbon isotope record from non-conglomeratic sedimentary rocks of the Mesoarchean Witwatersrand Supergroup, South Africa. *Precambrian Research, 216-219*, 208-231. doi:https://doi.org/10.1016/j.precamres.2012.06.018

Halevy, I., Johnston, D. T., & Schrag, D. P. (2010). Explaining the Structure of the Archean Mass-Independent Sulfur Isotope Record. *Science, 329*(5988), 204-207. doi:https://doi.org/10.1126/science.1190298

Helgeson, H. C., Delany, J. M., Nesbitt, H. W., & Bird, D. K. (1978). Summary and critique of the thermodynamic properties of rock-forming minerals. *American Journal of Science, 278A*, 229.

Hickman, A. H. (2016). *Northwest Pilbara Craton: a record of 450 million years in the growth of Archean continential crust*. Retrieved from Perth:

Hickman, A. H., & Van Kranendonk, M. J. (2012). Early Earth evolution: Evidence from the 3.5-1.8 Ga geological history of the Pilbara region of Western Australia. *Episodes, 35*(1), 283-297. doi:https://doi.org/10.18814/epiiugs/2012/v35i1/028

Hiebert, R. S., Bekker, A., Houlé, M. G., & Rouxel, O. J. (2018). Depositional setting of the Late Archean Fe oxide- and sulfide-bearing chert and graphitic argillite in the Shaw Dome, Abitibi greenstone belt, Canada. *Precambrian Research, 311*, 98-116. doi:https://doi.org/10.1016/j.precamres.2018.04.004

Hitzman, M., Bookstrom, A. A., Slack, J. F., & Zientek, M. L. (2017). *Cobalt—Styles of Deposits and the Search for Primary Deposits*. Retrieved from Virginia: https://doi.org/10.3133/ofr20171155

Hitzman, M., Kirkham, R. V., Broughton, D., Thorson, J., & Selley, D. (2005). The Sediment-Hosted Stratiform Copper Ore System. *Economic Geology, 100th Anniversary Volume*, 609-642. doi:https://doi.org/10.5382/AV100.19

Hitzman, M., Selley, D., & Bull, S. (2010). Formation of Sedimentary Rock-Hosted Stratiform Copper Deposits through Earth History. *Economic Geology, 105*(3), 627-639. doi:https://doi.org/10.2113/gsecongeo.105.3.627

Hoashi, M., Bevacqua, D. C., Otake, T., Watanabe, Y., Hickman, A. H., Utsunomiya, S., & Ohmoto, H. (2009). Primary haematite formation in an oxygenated sea 3.46 billion years ago. *Nature Geoscience, 2*, 301-306. doi:https://doi.org/10.1038/ngeo465

Jansson, N. F., & Liu, W. (2020). Controls on cobalt and nickel distribution in hydrothermal sulphide deposits in Bergslagen, Sweden - constraints from solubility modelling. *GFF, 142*(2), 87-95. doi:https://doi.org/10.1080/11035897.2020.1751270

Johnston, D. T. (2011). Multiple sulfur isotopes and the evolution of Earth's surface sulfur cycle. *Earth-Science Reviews, 106*(1-2), 161-183. doi:https://doi.org/10.1016/j.earscirev.2011.02.003

Kasting, J. F., & Ono, S. (2006). Palaeoclimates: the first two billion years. *Philosophical transactions of the Royal Society of London, 361*(1470), 917-929. doi:https://doi.org/10.1098/rstb.2006.1839

Kato, Y., Suzuki, K., Nakamura, K., Hickman, A. H., Nedachi, M., Kusakabe, M., . . . Ohmoto, H. (2009). Hematite formation by oxygenated groundwater more than 2.76 billion years ago. *Earth and Planetary Science Letters, 278*(1-2), 40-49. doi:https://doi.org/10.1016/j.epsl.2008.11.021

Kaufman, A. J., Johnston, D. T., Farquhar, J., Masterson, A. L., Lyons, T. W., Bates, S., . . . Arnold, G. L. (2007). Late Archean Biospheric Oxygenation and Atmospheric Evolution. *Science, 317*(5846), 1900-1903. doi:https://doi.org/10.1126/science.1138700

Kendall, B., Brennecka, G. A., Weyer, S., & Anbar, A. D. (2013). Uranium isotope fractionation suggests oxidative uranium mobilization at 2.50Ga. *Chemical Geology, 362*, 105-114. doi:https://doi.org/10.1016/j.chemgeo.2013.08.010

Kendall, B., Creaser, R. A., Reinhard, C. T., Lyons, T. W., & Anbar, A. D. (2015). Transient episodes of mild environmental oxygenation and oxidative continental weathering during the late Archean. *Science Advances, 1*(10), 6. doi:https://doi.org/10.1126/sciadv.1500777

Kendall, B., Reinhard, C. T., Lyons, T. W., Kaufman, A. J., Poulton, S. W., & Anbar, A. D. (2010). Pervasive oxygenation along late Archaean ocean margins. *Nature Geoscience, 3*(9), 647-652. doi:10.1038/ngeo942

Kerrich, R., & Said, N. (2011). Extreme positive Ce-anomalies in a 3.0Ga submarine volcanic sequence, Murchison Province: Oxygenated marine bottom waters. *Chemical Geology, 280*(1), 232-241. doi:https://doi.org/10.1016/j.chemgeo.2010.11.012

Killingsworth, B. A., Sansjofre, P., Philippot, P., Cartigny, P., Thomazo, C., & Lalonde, S. V. (2019). Constraining the rise of oxygen with oxygen isotopes. *Nature Communications, 10*(1), 4924. doi:10.1038/s41467-019-12883-2

LaFlamme, C., Martin, L., Jeon, H., Reddy, S. M., Selvaraja, V., Caruso, S., . . . Kilburn, M. R. (2016). In situ multiple sulfur isotope analysis by SIMS of pyrite, chalcopyrite, pyrrhotite, and pentlandite to refine magmatic ore genetic models. *Chemical Geology, 444*(1), 1-15. doi:https://doi.org/10.1016/j.chemgeo.2016.09.032.

Liu, S., Borg, S., Testemale, D., Etschmann, B., Hazemann, J., & Brugger, J. (2011). Speciation and thermodynamic properties for cobalt chloride complexes in hydrothermal fluids at 35–440° C and 600 bar: an in-situ XAS study. *Geochimica et Cosmochimica Acta, 75*(5), 1227-1248. doi:https://doi.org/10.1016/j.gca.2010.12.002

Liu, W., & McPhail, D. C. (2005). Thermodynamic properties of copper chloride complexes and copper transport in magmatic-hydrothermal solutions. *Chemical Geology, 221*(1-2), 21-39. doi:https://doi.org/10.1016/j.chemgeo.2005.04.009

Luskin, C., Wilson, A., Gold, D., & Hofmann, A. (2019). The Pongola Supergroup: Mesoarchaean Deposition Following Kaapvaal Craton Stabilization. In A. Kröner & A. Hofmann (Eds.), *The Archaean Geology of the Kaapvaal Craton, Southern Africa* (pp. 225-254). Cham: Springer International Publishing.

Lyons, T. W., & Gill, B. C. (2010). Ancient Sulfur Cycling and Oxygenation of the Early Biosphere. *Elements, 6*(2), 93-99. doi:https://doi.org/10.2113/gselements.6.2.93

Lyons, T. W., Reinhard, C. T., & Planavsky, N. J. (2014). The rise of oxygen in Earth's early ocean and atmosphere. *Nature, 506*, 307-315. doi:https://doi.org/10.1038/nature13068

Midgisov, A. A., Zezin, D., & Williams-Jones, A. E. (2011). An experimental study of cobalt (II) complexation in Cl− and H2S-bearing hydrothermal solutions. *Geochimica et Cosmochimica Acta, 75*(14), 4065-4079. doi:https://doi.org/10.1016/j.gca.2011.05.003

Mills, K. C. (1974). *Thermodynamic data for inorganic sulphides, selenides and tellurides*. London: Butterworths.

Muller, E., Philippot, P., Bard-Rollion, C., & Cartigny, P. (2016). Multiple sulfur-isotope signatures in Archean sulfates and their implications for the chemistry and dynamics of the early atmosphere. *Proceedings of the National Academy of Sciences, 113*(27), 7432-7437. doi:https://doi.org/10.1073/pnas.1520522113

Ohmoto, H. (2020). A seawater-sulfate origin for early Earth's volcanic sulfur. *Nature Geoscience, 13*, 576-583. doi:https://doi.org/10.1038/s41561-020-0601-6

Ohmoto, H., Watanabe, Y., Ikemi, H., Poulson, S. R., & Taylor, B. E. (2006). Sulphur isotope evidence for an oxic Archaean atmosphere. *Nature, 442*, 908-911. doi:https://doi.org/10.1038/nature05044

Ono, S., Beukes, N. J., Rumble, D., & Fogel, M. L. (2006). Early evolution of atmospheric oxygen from multiple-sulfur and carbon isotope records of the 2.9 Ga Mozaan Group of the Pongola Supergroup, Southern Africa. *South African Journal of Geology, 109*(1-2), 97-108. doi:https://doi.org/10.2113/gssajg.109.1-2.97

Ossa Ossa, F., Hofmann, A., Spangenberg, J. E., Poulson, S. W., Stüeken, E. E., Schoenberg, R., . . . Bekker, A. (2019). Limited oxygen production in the Mesoarchean ocean. *Proceedings of the National Academy of Sciences, 116*(14), 6647-6652. doi:https://doi.org/10.1073/pnas.1818762116

Ossa Ossa, F., Hofmann, A., Vidal, O., Kramers, J. D., Belyanin, G., & Cavallazi, B. (2016). Unusual manganese enrichment in the Mesoarchean Mozaan Group, Pongola Supergroup, South Africa. *Precambrian Research, 281*, 414-433. doi:https://doi.org/10.1016/j.precamres.2016.06.009

Ossa Ossa, F., Hofmann, A., Wille, M., Spangenberg, J. E., Bekker, A., Poulton, S. W., . . . Schoenberg, R. (2018). Aerobic iron and manganese cycling in a redox-stratified Mesoarchean epicontinental sea. *Earth and Planetary Science Letters, 500*, 28-40. doi:https://doi.org/10.1016/j.epsl.2018.07.044

Ostrander, C. M., Johnson, A. C., & Anbar, A. D. (2021). Earth's First Redox Revolution. *Annual Review of Earth and Planetary Sciences, 49*(1), 337-366. doi:10.1146/annurev-earth-072020-055249

Philippot, P., Ávila, J. N., Killingsworth, B. A., Tessalina, S., Baton, F., Caquineau, T., . . . Busigny, V. (2018). Globally asynchronous sulphur isotope signals require re-definition of the Great Oxidation Event. *Nature Communications, 9*(1), 2245. doi:10.1038/s41467-018-04621-x

Planavsky, N. J., Asael, D., Hofmann, A., Reinhard, C. T., LaLonde, S. V., Knudsen, A. C., . . . Rouxel, O. (2014). Evidence for oxygenic photosynthesis half a billion years before the Great Oxidation Event. *Nature Geoscience, 7*, 283-286. doi:https://doi.org/10.1038/ngeo2122

Reinhard, C. T., Planavsky, N. J., & Lyons, T. W. (2013). Long-term sedimentary recycling of rare sulphur isotope anomalies. *Nature, 497*(7447), 100-103. doi:10.1038/nature12021

Reinhard, C. T., Raiswell, R., Scott, C., Anbar, A. D., & Lyons, T. W. (2009). A Late Archean Sulfidic Sea Stimulated by Early Oxidative Weathering of the Continents. *Science, 326*(5953), 713-716. doi:https://doi.org/10.1126/science.1176711

Riding, R., Fralick, P., & Liang, L. (2014). Identification of an Archean marine oxygen oasis. *Precambrian Research, 251*, 232-237. doi:https://doi.org/10.1016/j.precamres.2014.06.017

Rose, A. (1989). Mobility of Copper and Other Heavy Metals in Sedimentary Environments. *Special Paper - Geological Association of Canada, 36*, 97-110.

Rosing, M. T., & Frei, R. (2004). U-rich Archaean sea-floor sediments from Greenland – indications of >3700 Ma oxygenic photosynthesis. *Earth and Planetary Science Letters, 217*(3), 237-244. doi:https://doi.org/10.1016/S0012-821X(03)00609-5

Seal, R. R. (2006). Sulfur Isotope Geochemistry of Sulfide Minerals. *Reviews in Mineralogy and Geochemistry, 61*(1), 633-677. doi:https://doi.org/10.2138/rmg.2006.61.12

Selvaraja, V., Caruso, S., Fiorentini, M. L., & LaFlamme, C. (2017). The Global Sedimentary Sulfur Isotope Database. *The Centre for Exploration Targeting - Univeristy of Western Australia*.

Shock, E. I., Sassani, D. C., Willis, M., & Sverjensky, D. A. (1997). Inorganic species in geologic fluids: correlations among standard molal thermodynamic properties of aqueous ions and hydroxide complexes. *Geochimica et Cosmochimica Acta, 61*(5), 907-950. doi:https://doi.org/10.1016/S0016-7037(96)00339-0

Steadman, J. A., Large, R. R., Blamey, N. J., Mukherjee, I., Corkrey, R., Danyushevsky, L. V., . . . Lécuyer, C. (2020). Evidence for elevated and variable atmospheric oxygen in the Precambrian. *Precambrian Research, 343*, 105722. doi:https://doi.org/10.1016/j.precamres.2020.105722

Stüeken, E. E., Buick, R., & Anbar, A. D. (2015). Selenium isotopes support free O2 in the latest Archean. *Geology, 43*(3), 259-262. doi:10.1130/g36218.1

Thomazo, C., Ader, M., Farquhar, J., & Philippot, P. (2009). Methanotrophs regulated atmospheric sulfur isotope anomalies during the Mesoarchean (Tumbiana Formation, Western Australia). *Earth and Planetary Science Letters, 279*(1-2), 65-75. doi:https://doi.org/10.1016/j.epsl.2008.12.036

Van Kranendonk, M. J., Hickman, A. H., Smithies, R. H., Nelson, D. R., & Pike, G. (2002). Geology and Tectonic Evolution of the Archean North Pilbara Terrain, Pilbara Craton, Western Australia. *Economic Geology, 97*(4), 695-732. doi:https://doi.org/10.2113/gsecongeo.97.4.695

Vaughan, D. J. (1978). *Mineral chemistry of metal sulfides*. Cambridge: Cambridge University Press.

Voegelin, A. R., Nägler, T. F., Beukes, N. J., & Lacassie, J. P. (2010). Molybdenum isotopes in late Archean carbonate rocks: Implications for early Earth oxygenation. *Precambrian Research, 182*(1), 70-82. doi:https://doi.org/10.1016/j.precamres.2010.07.001

Waldbauer, J. R., Sherman, L. S., Sumner, D. Y., & Summons, R. E. (2009). Late Archean molecular fossils from the Transvaal Supergroup record the antiquity of microbial diversity and aerobiosis. *Precambrian Research, 169*(1), 28-47. doi:https://doi.org/10.1016/j.precamres.2008.10.011

Wang, X., Ossa Ossa, F., Hofmann, A., Agangi, A., Paprika, D., & Planavsky, N. J. (2020). Uranium isotope evidence for Mesoarchean biological oxygen production in shallow marine and continental settings. *Earth and Planetary Science Letters, 551*, 8. doi:https://doi.org/10.1016/j.epsl.2020.116583

Wang, X., Planavsky, N. J., Hofmann, A., Saupe, E. E., De Corte, B. P., Philippot, P., . . . Konhauser, K. O. (2018). A Mesoarchean shift in uranium isotope systematics. *Geochimica et Cosmochimica Acta, 238*, 438-452. doi:https://doi.org/10.1016/j.gca.2018.07.024

Wille, M., Kramers, J. D., Nägler, T. F., Beukes, N. J., Schröder, S., Meisel, T., . . . Voegelin, A. R. (2007). Evidence for a gradual rise of oxygen between 2.6 and 2.5 Ga from Mo isotopes and Re-PGE signatures in shales. *Geochimica et Cosmochimica Acta, 71*(10), 2417-2435. doi:https://doi.org/10.1016/j.gca.2007.02.019

Wilmeth, D. T., Corsetti, F. A., Beukes, N. J., Awramik, S. M., Petryshyn, V., Spear, J. R., & Celestian, A. J. (2019). Neoarchean (2.7 Ga) lacustrine stromatolite deposits in the Hartbeesfontein Basin, Ventersdorp Supergroup, South Africa: Implications for oxygen oases. *Precambrian Research, 320*, 291-302. doi:https://doi.org/10.1016/j.precamres.2018.11.009

Wolery, T. J. (1992). *EQ3NR, a computer program for geochemical aqueous speciation-solubility calculations: theoretical manual, users guide, and related documentation (Version 7.0); Part 3*. Retrieved from CA (United States):

3197 Appendix 4.1 – Compilation of studies purporting to show evidence of
3198 Archean oxygen oases

Age (Ma)	Lithostratigraphic unit	Terrane	Method/evidence	Reference
2500	Mount McRae Shale, Hamersley Group	Hamersley Basin, Pilbara Craton	C and S isotopes, wt. % C and S	(Kaufman et al., 2007)
2500	Mount McRae Shale, Hamersley Group	Hamersley Basin, Pilbara Craton	C and N isotopes, wt. % N, TOC, Fe and Mo concentrations	(Garvin, Buick, Anbar, Arnold, & Kaufman, 2009)
2500	Mount McRae Shale, Hamersley Group	Hamersley Basin, Pilbara Craton	Mo isotopes	(Duan et al., 2010)
2500	Mount McRae Shale, Hamersley Group	Hamersley Basin, Pilbara Craton	Re-Os isotopes	(Kendall, Creaser, Reinhard, Lyons, & Anbar, 2015)
2500	Mount McRae Shale, Hamersley Group	Hamersley Basin, Pilbara Craton	U isotopes	(Kendall, Brennecka, Weyer, & Anbar, 2013)
2500	Mount McRae Shale, Hamersley Group	Hamersley Basin, Pilbara Craton	Se isotopes	(Stüeken, Buick, & Anbar, 2015)
2500	Mount McRae Shale, Hamersley Group	Hamersley Basin, Pilbara Craton	Re-Os isotopes, TOC, wt. % S, major and trace metal concentrations	(Anbar et al., 2007)
2590	Ghaap Group, Traansvaal Supergroup	Griqualand West Basin, Kaapvaal Craton	Fe speciation, trace metal concentrations, wt. % C and S, TOC, S isotopes	(Kendall et al., 2010)
2640	Ghaap & Pretoria Groups, Transvaal Supergroup	Griqualand West Basin, Kaapvaal Craton	Mo concentrations and isotopes	(Wille et al., 2007)
2640	Ghaap Group, Transvaal Supergroup	Griqualand West Basin, Kaapvaal Craton	Mo isotopes	(Voegelin, Nägler, Beukes, & Lacassie, 2010)
2670	Ghaap Group, Transvaal Supergroup	Griqualand West Basin, Kaapvaal Craton	Fossil biomarkers	(Waldbauer, Sherman, Sumner, & Summons, 2009)
2680	Ghaap Group, Transvaal Supergroup	Griqualand West Basin, Kaapvaal Craton	Fe and Mo isotopes, Fe wt. %, Mo concentrations	(Czaja et al., 2012)

2700	Marra Mamba Formation, Hamersley Group and Maddina and Jeerinah Formations, Fortescue Group	Hamersley and Fortescue Basins, Pilbara Craton	Fossil biomarkers	(Brocks, Logan, Buick, & Summons, 1999)
~2700	Carajas Formation, Grão Pará Group	Carajas Province	Mo isotopes	(Cabral et al., 2013)
2700	Platberg Group, Ventersdorp Supergroup	Hartbeesfontein Basin, Kaapvaal Craton	Bacterial microfossils	(Wilmeth et al., 2019)
2700	Unnamed exhalite proximal to Hart Ni-Cu-PGE deposit	Shaw Dome, Abitibi greenstone belt	S and Fe isotopes, whole rock geochemistry (Mn enrichment)	(Hiebert, Bekker, Houlé, & Rouxel, 2018)
<2720	Hamersley and Fortescue Groups	Hamersley Basin, Pilbara Craton	Fossil biomarkers	(Eigenbrode, Freeman, & Summons, 2008)
2763	Apex basalt, Warrawoona Group	Marble Bar greenstone belt, Pilbara Craton	Primary hematite	(Kato et al., 2009)
<2800	Various banded iron formations	Various global localities	Cr isotopes	(Frei et al., 2009)
2800	Mosher Carbonate Formation, Steep Rock Group	Wabigoon Subprovince, Canadian Shield	REE analyses	(Riding, Fralick, & Liang, 2014)
2760-2920	Hardey and Mosquito Creek Formations, Fortescue, and Nullagine Groups	Fortescue and Mosquito Creek Basins, Pilbara Craton	S isotopes	(Ohmoto et al., 2006)
2950	Sinqeni Formation, Mozaan Group	Pongola Basin, Kaapvaal Craton	Mo and Fe isotopes	(Planavsky et al., 2014)
2950	Several formations, Mozaan Group	Pongola Basin, Kaapvaal Craton	C and S isotopes	(Ono et al., 2006)
2950	Sinqeni and Ntombe Formations, Mozaan Group	Pongola Basin, Kaapvaal Craton	Primary Mn	(Ossa Ossa et al., 2016)
2950	Sinqeni Formation, Mozaan Group	Pongola Basin, Kaapvaal Craton	Mo, Fe, and U isotopes	(Albut et al., 2019)
2950	Several formations, Mozaan Group	Pongola Basin, Kaapvaal Craton	U isotopes	(Wang et al., 2020)
2950	Several formations, Mozaan Group	Pongola Basin, Kaapvaal Craton	C, O, Fe, Mo isotopes	(Ossa Ossa et al., 2018)
2960	Gabarintha Formation, Luke Creek Group	Youanmi Terrane, Yilgarn Craton	Ce anomalies	(Kerrich & Said, 2011)
2970	Chobeni Formation, Nzuse Group	Pongola Basin, Kaapvaal Craton	Fe & S isotopes	(Eickmann et al., 2018)
2980	Sinqeni and Agatha Formations, Mozaan and Nzuse Groups	Pongola Basin, Kaapvaal Craton	Cr isotopes	(Crowe et al., 2013)

3200	Various marine halites and black shales	Various global localities	Oxygen in halite fluid inclusions and Se/Co ratios in sedimentary pyrite	(Steadman et al., 2020)
3460	Marble Bar Chert, Warrawoona Group	Marble Bar greenstone belt, Pilbara Craton	Primary hematite	(Hoashi et al., 2009)
>3700	Turbiditic and pelagic sedimentary rocks	Isua supracrustal belt, West Greenland	Pb isotopes	(Rosing & Frei, 2004)
3800	Various submarine hydrothermal deposits	Various global localities	S isotope mass balance calculations and modelling	(Ohmoto, 2020)

3199

3200

Appendix 4.2 – Carlow Castle multiple sulfur isotope data

Appendix 4.2 is accessible via this link and provides an .xlsx file containing SIMS multiple sulfur isotope data of four analysed samples from Carlow Castle.

Appendix 4.3 – Compilation of multiple isotope data from various ore deposits in Archean greenstone belts

Appendix 4.3 is accessible via this link and provides an .xlsx file containing a compiled data set of multiple sulfur isotope data from various Archean hydrothermal and magmatic ore deposits, used to construct Figure 4.5.

Appendix 4.4 – Analyzed samples from Carlow Castle Cu-Co-Au deposit

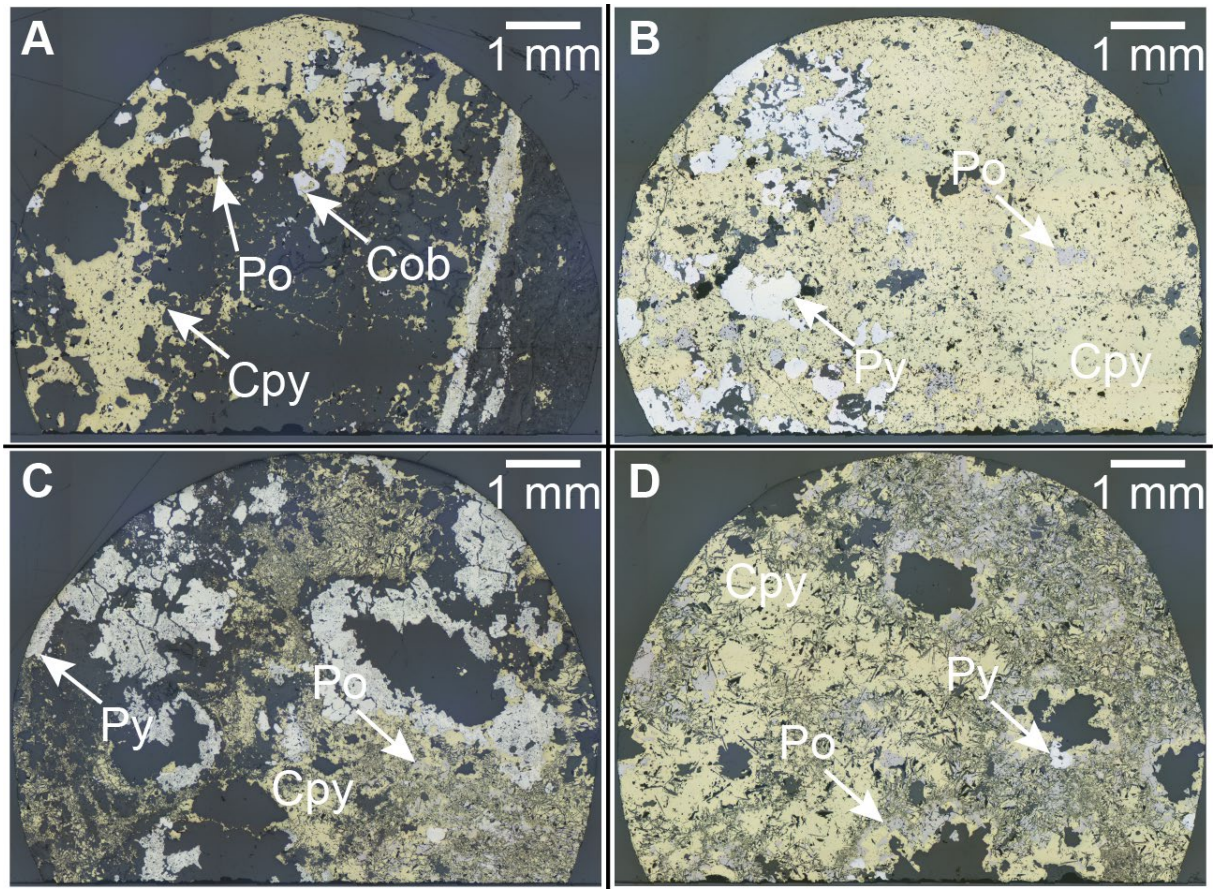

Appendix 4.4 - Carlow Castle deposit sulphide ore sample mounts prepared for secondary-ion mass spectrometry (SIMS) sulfur isotope analysis. Sample numbers are as follows: a. CC003_61, b. CC012_67, c. CC007_102a, d. CC007_102b.

Chapter 5
Copper isotopes in Archean hydrothermal systems: A case study from the Mesoarchean Carlow Castle Cu-Co-Au deposit

This chapter is currently under review for publication in *Geochimica et Cosmochimica Acta*.

5.1 Abstract

Copper isotope analysis of ore minerals has emerged as a promising tool for understanding genetic processes in Cu ore deposits. However, applications of this analytical technique to Archean Cu deposits have been very limited, even though Archean terranes are among some of the most economically endowed on Earth. As such, this study presents the first Cu isotope analysis of an Archean Cu deposit; the Mesoarchean Carlow Castle hydrothermal Cu-Co-Au deposit. In this study, 19 Archean primary Cu sulphide ore samples and 11 secondary supergene Cu ore samples were analysed. Primary ore samples are isotopically light, with δ^{65}Cu values ranging between -0.80 and 0.00‰, whilst supergene samples are isotopically heavier and range between -0.50 and 0.62‰. In primary ore samples, a relationship is observed between Cu isotope signature, ore grade, and alteration assemblage that records the isotopic and physicochemical evolution of the Carlow Castle deposit's hydrothermal ore-forming system. This isotopic evolution is suggested to reflect a Rayleigh fractionation process due to the preferential precipitation of ^{63}Cu during ore formation, which is modelled using isotopic and Cu ore grade data. Based on this modelling, a mafic igneous source is suggested as a likely metal source in the Carlow Castle Cu-Co-Au deposit. The relatively limited heavy isotopic fractionation of supergene Cu ore samples in this study is interpreted to reflect limited redox

cycling of Cu due to in-situ oxidative weathering of vein-hosted Cu sulphides in the overlying supergene system. This differs from previously studied deposits where significant Cu transport and multiple stages of isotopic enrichment that are often evident in supergene Cu enrichment layers. The results of this study suggest that Cu isotope analysis could be valuable in understanding genetic processes in hydrothermal Cu deposits, including in Archean ore deposits and terranes.

5.2 Introduction

Copper isotope analysis has emerged as a novel geochemical tool in understanding Cu mobility and cycling in geological systems (Mathur et al., 2009; Zhu et al., 2002; Zhu, O'Nions, Guo, Belshaw, & Rickard, 2000). Because Cu is a redox-sensitive base-metal, Cu isotope analysis is particularly promising as a potential palaeoredox proxy and for understanding ore-forming processes (Asael, Matthews, Bar-Matthews, & Halicz, 2007; Kendall, 2021). However, significant gaps remain in the current understanding of Cu isotope systematics and applications of Cu isotope analysis in different geological environments. This includes the understanding of processes that may induce Cu isotope fractionation in Archean geological environments, where the study of Cu isotope systematics has been very limited. This is most likely due to the fact that the most significant Cu isotope fractionation in geological environments is typically a product of redox processes, during changes in oxidation state between Cu^{+} and Cu^{2+} (Markl, Lahaye, & Schwinn, 2006). Since the availability of oxidising agents was limited throughout most of the Archean, it is reasonable to expect that Cu isotope fractionation should be minimal in Archean Cu deposits and that any Cu ore minerals in these deposits should record an unfractionated Cu isotope signature characteristic of the bulk silicate Earth, around $\delta^{65}Cu$ = 0‰ (Liu et al., 2015). However, because Cu isotope studies in Archean ore-forming systems have been very limited in comparison to younger deposits, this hypothesis has not been tested to any significant extent.

In this study we provide the first Cu isotope characterisation of an Archean Cu deposit by analysing hydrothermal chalcopyrite and chalcocite in the Mesoarchean Carlow Castle Cu-Co-Au deposit in the Pilbara Craton of northwestern Australia (Fox et al., 2021; 2019). In addition to this, we also analyse the younger supergene Cu-bearing layer that overlies Carlow Castle's sulphide mineralisation. This was done to determine whether the previously established exploration applications of Cu isotope analysis could still be applied to Cu mineralisation in Archean terranes (Braxton & Mathur, 2011; Mathur et al., 2009; Mathur & Wang, 2019). Given

that Archean terranes are among the most economically endowed on Earth (Goldfarb et al., 2010), understanding how Cu isotope exploration methods can be applied in these terranes could enhance exploration efforts for Archean Cu-rich ore deposits. In addition, given the paucity of Cu isotope data from Archean Cu ore deposits, this study was also conducted to determine whether Cu isotope analysis may have potential for understanding geological processes in Archean hydrothermal systems given the comparably limited potential for redox fractionation.

5.3 Geological Setting

Carlow Castle is a structurally-hosted hydrothermal Cu-Co-Au deposit situated in the Archean Pilbara Craton of northwest Western Australia (Hickman, 2016). Specifically, Carlow Castle is hosted in the West Pilbara Superterrane (3280–3066 Ma) of the northwest Pilbara Craton; a superterrane produced through the accretion of the Karratha (c. 3280 Ma), Regal (c. 3200 Ma), and Sholl (3130–3110 Ma) terranes during the Prinsep Orogeny (c. 3070 Ma) following ~90 Myr of crustal convergence (Hickman, 2016; Van Kranendonk et al., 2007). These terranes are composed dominantly of a series of greenstone belts and several large intrusive granitic complexes (Hickman et al., 2010). During the accretion of the West Pilbara Superterrane, the Regal Terrane was thrust over the Karratha Terrane along the Regal Thrust. As such, the Regal Thrust defines the boundary between these terranes across the northwest Pilbara Craton (Hickman, 2016). A heavily tectonised portion of the Regal Thrust, within the Roebourne greenstone belt, acts as the key host structure for Carlow Castle's Cu-Co-Au mineralization (Fox et al., 2019; Hickman, 2016). Due to its occurrence within the Regal Thrust, an orogenic crustal structure, Carlow Castle was initially interpreted to be a Cu-Co enriched orogenic Au deposit produced by the Prinsep Orogeny (Fox et al., 2019; Hickman, 2016). However, recent U-Pb dating of syn-ore apatite from Carlow Castle has revealed that it is significantly younger than initially thought. Carlow Castle most likely formed via the reactivation of the Regal Thrust around c. 2955 Ma, coinciding with a period of major precious- and base-metal volcanogenic massive sulphide (VMS) mineralisation during rifting and formation of the proximal De Grey Superbasin (3066–2919 Ma; Figure 5.1; Fox et al., 2021). The De Grey Superbasin is composed of three distinct sub-basins; (i) the Gorge Creek Basin (3066-3015 Ma), (ii) Whim Creek Basin (3009-2991 Ma), and (iii) Mallina Basin (3015-2919) (Hickman, 2016). Carlow Castle's formation is interpreted to have been contemporaneous with the evolution of the

Mallina Basin as a back-arc basin to the southeast of the West Pilbara Superterrane (Fox et al., 2021).

On a deposit-scale, Carlow Castle's mineralisation is hosted by a series of faults through a hydrothermally altered (chlorite, actinolite, and epidote dominated) section of the Ruth Well (c. 3280 Ma) and Nickol River (3220–3160 Ma) formations on the south-eastern footwall of the Regal Thrust (Figure 5.1; Fox et al., 2021; Hickman, 2016). The Ruth Well Formation is a sub-unit of the Roebourne Group in the Karratha Terrane and is a typical greenstone succession; composed primarily of extrusive mafic rocks, carbonaceous shale, and chert (Hickman & Van Kranendonk, 2012). The Roebourne Group is unconformably overlain by the predominantly fine-grained clastic marine sedimentary rocks of the Nickel River Formation (Hickman, 2016). The Roebourne Group and Nickel River Formation significantly pre-date the De Grey Superbasin, and are interpreted to have formed during volcanism on and rifting of a nascent Paleoarchean Pilbara Craton (Hickman, 2016). Carlow Castle's mineralisation occurs as a stockwork of quartz-carbonate veins hosting Cu-Co-Au bearing base-metal sulphides and sulphosalts (Fox et al., 2019). Fox et al. (2019) identified that Carlow Castle's mineralisation occurs in two distinct ore mineral assemblages. The first and more abundant assemblage is composed predominantly of chalcopyrite and pyrite with minor pyrrhotite and cobaltite, and trace electrum. Assemblage Two contains a significantly higher abundance of cobaltite which co-occurs with chalcocite, rather than chalcopyrite, and a slightly higher abundance of electrum. Based on analyses of its characteristically propylitic hydrothermal alteration assemblage, it has been established that Carlow Castle's hydrothermal ore fluid was most likely neutral to slightly alkaline in pH, reaching peak temperatures of ~300°C (Fox et al., 2021). However, a transition in the temperature of this propylitic alteration assemblage is evident and defined by a decrease in actinolite and epidote relative to chlorite. Fox et al. (2021) interpreted that this may reflect zoning of the alteration assemblage within the Carlow Castle deposit associated with fluid cooling at the periphery of the deposit during the evolution of the hydrothermal system. Fox et al. (2019) suggested that within this fluid Cu, Co, and Au were most likely transported in chloride complexes, before they co-precipitated at the site of Carlow Castle's ore mineralisation due to the reaction of this hydrothermal fluid with wall-rocks within the Regal Thrust. Additionally, supergene Cu mineralisation occurs primarily within 50 metres of the present-day surface at Carlow Castle and generally overlies the primary sulphide ore. However, due to the structurally complex nature of Carlow Castle, this supergene

mineralisation does not necessarily occur at uniform depths and some oxidised altered sulphide veins are observed as deep as ~75 metres in drill core. This supergene Cu mineralisation is mineralogically diverse; containing native Cu, secondary chalcocite, plancheite ($Cu_8Si_8O_{22}(OH)_4 \cdot (H_2O)$), agardite ($(REE, Ca)Cu_6(AsO_4)_3(OH)_6 \cdot 3H_2O$), and Cu-bearing pyrolusite (MnO_2).

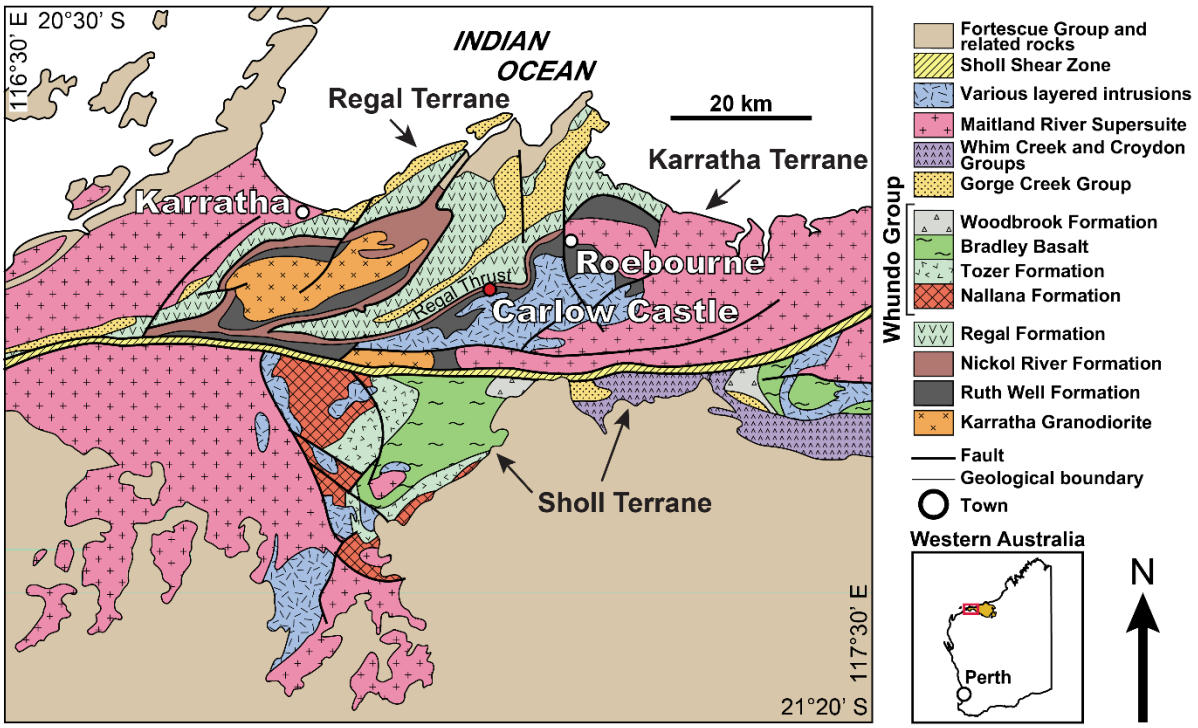

Figure 5.1 - Geological map of northwest Pilbara Craton near Carlow Castle Cu-Co-Au deposit, modified after Van Kranendonk et al. (2002). Inset map of Western Australia depicts portion of Pilbara Craton shown in main image.

5.4 Methods and materials

5.4.1 Analysed samples

A total of 30 samples were analysed in this study, with 19 samples from Carlow Castle's deep primary sulphide mineralisation, and 11 samples from supergene Cu mineralisation (sample list in results). The majority of these samples were retrieved from drill core, with the exception of four which were retrieved from mine tailings at the present-day surface of Carlow Castle. Some mineralogically or texturally heterogeneous drill core samples were sub-sampled twice to account for potential isotopic variation within a given sample, e.g., samples CC012_67(1) and CC012_67(2).

Sulphide samples were taken from core by drilling and then weighing out ~10 mg of material using a small handheld rotary multi-tool equipped with a diamond drill bit and a precision balance. These 10 mg samples were dissolved in 4 mL aqua regia solution (3.2 mL 12M HCl + 0.8 mL 15M HNO_3) at room temperature, or in concentrated HF + 7M HNO_3 at 140ºC for samples containing SiO_2 (USGS rock standards and plancheite). Samples were evaporated on a hotplate once the material was completely dissolved. These samples were then redissolved in 6M HCl to create a sample solution and diluted to a concentration of approximately 10 μg Cu in 1.5 ml of 6M HCl + 0.001% H_2O_2 to load onto the columns. Dilution factors varied between phases, depending on the stoichiometric Cu concentration in each mineral.

5.4.2 Copper isotope analysis

In order to develop a robust method for Cu isotope analysis of Cu sulphides, experiments were conducted by varying the concentration of Cu in the loading solution, volume of loading solution, volume of resin, column size, and acid volume in each step of the matrix and Cu elution. To observe how effective the elution of Cu from other elements under these different parameters was, the eluate was collected every 1-2 mL for each of these experiments. The successful calibrations are shown in Appendix 5.1.

Upon evaluation of the results for the different experiments, the final parameters and methodology chosen for Cu separation from Cu sulphides and Cu-bearing silicates are listed in Appendix 5.1. As only Cu isotopes were being analysed in this study, the final methodology did not involve any further elution stages for collection of Fe or Zn, these additional stages were only undertaken in the previous experiments to test how effective the separation of Cu from these elements was. As such, they were deemed unnecessary for the final method.

5.4.3 Multicollector-inductively coupled plasma mass spectrometry for isotopic analysis

Samples were diluted to 200 ppb Cu in 3 mL 2% HNO_3 for analysis on a Thermo Scientific Neptune multi collector inductively coupled plasma mass spectrometer (MC-ICP-MS) with an autosampler at CSIRO Land and Water on the University of Adelaide Waite Campus. Standard sample bracketing with NIST976 was used for all analyses, and this was diluted to 200 ppb with the same batch of 2% HNO_3 as the samples. Delta values in per mil for Cu isotopes are calculated as follows:

$$\delta 65Cu\ ‰ = [\frac{\left(\frac{65Cu}{63Cu}\right) sample}{\left(\frac{65Cu}{63Cu}\right) NIST976} - 1] \cdot 1000$$

Part way through this study, Ga spiking of samples (after Hou et al. (2016)) was introduced into the measurement routine to improve precision (see Appendix 5.1). The sample introduction system used was a dual Scott/cyclonic spray chamber with a 100 µl/min nebulizer, Ni sampler cone, and Ni X skimmer cone. Analyses used low resolution mode, with a typical signal strength of 12V on samples and NIST976. A single block of 60 four second integrations was run for each analysis. Raw $^{65}Cu/^{63}Cu$ and Ga mass bias corrected $^{65}Cu/^{63}Cu$ ratios were returned with mass bias correction undertaken for each integration within the block. The mean of the analysis was used for sample-standard bracketing. At least two analyses of each sample were obtained, and the precision calculated as the standard deviation between these (2SD). A procedural blank was prepared with each sample batch and contained less than 3 mV ^{65}Cu.

Internal reference materials were developed from a supergene native Cu sample (BHNatCop) from Broken Hill Pb-Zn-Ag deposit (long term average $\delta^{65}Cu$ = 1.20‰ ± 0.16) and a coarse-grained massive chalcopyrite sample from Carlow Castle (DFCu) (long term average $\delta^{65}Cu$ = -0.79‰ ± 0.09). The long-term repeatability of these reference materials is demonstrated in data from multiple analytical sessions over the course of roughly two years. These data are provided in Appendix 5.2. However, as these materials do not yet have consensus values, two digestions each of USGS BIR-1 basalt and AGV-2 andesite reference materials were also used to monitor Cu isotope analyses after development by Liu et al. (2014a). BIR-1 was measured as -0.01 ± 0.02 and AGV-2 as -0.01 ± 0.05, which are within uncertainty of the values for a recent compilation of reference materials by Wang et al. (2019) (BIR-1: 0.02 ± 0.02, AGV-2: 0.05 ± 0.02).

5.5 Results

5.5.1 Copper isotope signature of Carlow Castle

The results of Cu isotope analyses from Carlow Castle's primary and supergene Cu mineralisation are summarised in Table 5.1 and Figure 5.2. Primary mineralisation is lightly fractionated, whilst the supergene mineralisation is predominantly heavily fractionated, with some lightly fractionated values. The 19 primary samples exhibit light $\delta^{65}Cu$ values: ranging between -0.80 and 0.00‰, with a mean of -0.36‰. The 11 supergene samples exhibit predominantly heavy $\delta^{65}Cu$ values but range between -0.50 and 0.62‰, with a mean of 0.12‰.

3415 The values of both primary and supergene Cu mineralisation appear fractionated relative to the
3416 near 0‰ values that characterise unfractionated igneous rock reservoirs (Liu et al., 2015).

3417

3418 Asael, D., Matthews, A., Bar-Matthews, M., & Halicz, L. (2007). Copper isotope fractionation
3419 in sedimentary copper mineralization (Timna Valley, Israel). *Chemical Geology,*
3420 *243*(3), 238-254. doi:https://doi.org/10.1016/j.chemgeo.2007.06.007
3421 Braxton, D., & Mathur, R. (2011). Exploration Applications of Copper Isotopes in the
3422 Supergene Environment: A Case Study of the Bayugo Porphyry Copper-Gold Deposit,
3423 Southern Philippines. *Economic Geology, 106*(8), 1447-1463.
3424 doi:https://doi.org/10.2113/econgeo.106.8.1447
3425 Fox, D., Spinks, S., Barham, M., Kirkland, C. L., Pearce, M. A., Aspandiar, M., . . . Mead, E.
3426 (2021). Working up an apatite: Enigmatic Mesoarchean hydrothermal Cu-Co-Au
3427 mineralization in the Pilbara Craton. *Economic Geology, 116*(7), 1561-1573.
3428 doi:https://doi.org/10.5382/econgeo.4842
3429 Fox, D., Spinks, S., Pearce, M. A., Barham, M., Le Vaillant, M., Thorne, R., . . . Verrall, M.
3430 (2019). Plundering Carlow Castle: First Look at a Unique Mesoarchean-Hosted Cu-Co-
3431 Au Deposit. *Economic Geology, 114*(6), 1021-1031.
3432 doi:https://doi.org/10.5382/econgeo.4672
3433 Goldfarb, R. J., Bradley, D. W., & Leach, D. L. (2010). Secular Variation in Economic
3434 Geology. *Economic Geology, 105*(3), 459-465.
3435 Hickman, A. H. (2016). *Northwest Pilbara Craton: a record of 450 million years in the growth*
3436 *of Archean continential crust*. Retrieved from Perth:
3437 Hickman, A. H., Smithies, R. H., & Tyler, I. M. (2010). *Evolution of active plate margins:*
3438 *West Pilbara Superterrane, De Grey Superbasin, and the Fortescue and Hamersley*
3439 *Basins — a field guide*. Retrieved from Perth:
3440 Hickman, A. H., & Van Kranendonk, M. J. (2012). Early Earth evolution: Evidence from the
3441 3.5-1.8 Ga geological history of the Pilbara region of Western Australia. *Episodes,*
3442 *35*(1), 283-297. doi:https://doi.org/10.18814/epiiugs/2012/v35i1/028
3443 Hou, Q., Zhou, L., Gao, S., Zhang, T., Feng, L., & Yang, L. (2016). Use of Ga for mass bias
3444 correction for the accurate determination of copper isotope ratio in the NIST SRM 3114
3445 Cu standard and geological samples by MC-ICPMS. *Journal of Analytical Atomic*
3446 *Spectrometry, 31*(1), 280-287. doi:10.1039/C4JA00488D

Kendall, B. (2021). Recent Advances in Geochemical Paleo-Oxybarometers. *The Annual Review of Earth and Planetary Sciences, 49*(1), 399-433. doi:https://doi.org/10.1146/annurev-earth-071520-051637

Liu, S.-A., Huang, J., Liu, J., Wörner, G., Yang, W., Tang, Y.-J., . . . Li, S. (2015). Copper isotopic composition of the silicate Earth. *Earth and Planetary Science Letters, 427*, 95-103. doi:https://doi.org/10.1016/j.epsl.2015.06.061

Liu, S., Li, D., Li, S., Teng, F., Ke, S., He, Y., & Lu, Y. (2014a). High-precision copper and iron isotope analysis of igneous rock standards by MC-ICP-MS. *Journal of Analytical Atomic Spectrometry, 29*, 122-133. doi:https://doi.org/10.1039/C3JA50232E

Markl, G., Lahaye, Y., & Schwinn, G. (2006). Copper isotopes as monitors of redox processes in hydrothermal mineralization. *Geochimica et Cosmochimica Acta, 70*(16), 4215-4228. doi:https://doi.org/10.1016/j.gca.2006.06.1369

Mathur, R., Titley, S., Barra, F., Brantley, S., Wilson, M., Philips, A., . . . Hart, G. (2009). Exploration potential of Cu isotope fractionation in porphyry copper deposits. *Journal of Geochemical Exploration, 102*, 1-6.

Mathur, R., & Wang, D. (2019). Transition Metal Isotopes Applied to Exploration Geochemistry. In S. Decrée & L. Robb (Eds.), *Ore Deposits: Origin, Exploration, and Exploitation* (1 ed., Vol. 242): American Geophysical Union and John Wiley and Sons.

Van Kranendonk, M. J., Hickman, A. H., Smithies, R. H., Nelson, D. R., & Pike, G. (2002). Geology and Tectonic Evolution of the Archean North Pilbara Terrain, Pilbara Craton, Western Australia. *Economic Geology, 97*(4), 695-732. doi:https://doi.org/10.2113/gsecongeo.97.4.695

Van Kranendonk, M. J., Smithies, R. H., Hickman, A. H., & Champion, D. (2007). Review: secular tectonic evolution of Archean continental crust: interplay between horizontal and vertical processes in the formation of the Pilbara Craton, Australia. *Terra Nova, 19*(1), 1-38.

Wang, Z., Park, J.-W., Wang, X., Zou, Z., Kim, J., Zhang, P., & Li, M. (2019). Evolution of copper isotopes in arc systems: Insights from lavas and molten sulfur in Niuatahi volcano, Tonga rear arc. *Geochimica et Cosmochimica Acta, 250*, 18-33. doi:https://doi.org/10.1016/j.gca.2019.01.040

Zhu, X. K., Guo, Y., Williams, R. J. P., O'Nions, R. K., Matthews, A., Belshaw, N. S., . . . Salvato, B. (2002). Mass fractionation processes of transition metal isotopes. *Earth and*

Planetary Science Letters, 200(1-2), 47-62. doi:https://doi.org/10.1016/S0012-821X(02)00615-5

Zhu, X. K., O'Nions, R. K., Guo, Y., Belshaw, N. S., & Rickard, D. (2000). Determination of natural Cu-isotope variation by plasma-sourcem ass spectrometry: implications for use as geochemical tracers. *Chemical Geology, 163*(1-4), 139-149. doi:https://doi.org/10.1016/S0009-2541(99)00076-5

Table 5.1 - Sample details and Cu isotope composition of mineralised samples from Carlow Castle. Note that Cu, Co, and Au grades (ppm) here are for the metre intersection from which a given sample was taken and are sourced from publicly available JORC (2012) compliant exploration drill core data released to the Australian Securities Exchange (Artemis Resources Limited, 2018c). Note: Samples analysed with Ga mass bias correction are marked with an asterisk (*).

Sample	Drill hole	Drill hole easting (MGA 50)	Drill hole northing (MGA 50)	Measured sample depth (m)	Drill hole plunge (°)	True vertical depth (TVD) (m)	Cu (ppm)	Co (ppm)	Au (ppm)	Analysed phase	δ^{65}Cu (‰)	2σ error
Primary mineralisation												
DF2 (CC012_67(2))	18CCAD012	506935	7698900	67	60	58	95,600	338	1.41	Chalcopyrite	-0.63	0.03
DFCu (CC012_67(1))*	18CCAD012	506935	7698900	67	60	58	95,600	338	1.41	Chalcopyrite	-0.79	0.09
DF3 (CC007_102)	18CCAD007	506857.87	7698633.3	102	60	89	33,300	496	7.21	Chalcopyrite	-0.33	0.001
DF4 (CC003_61)(1)	18CCAD003	506698.19	7698681	61	75	59	13,900	6800	8.13	Chalcopyrite	-0.22	0.001
DF5 (CC009_52)	18CCAD009	506942.27	7698937.2	52	60	45	66,300	16,000	29	Chalcopyrite	-0.31	0.11
DF6 (CC007_41)	18CCAD007	506857.87	7698633.3	41	60	36	17,550	18,900	18.45	Chalcocite	-0.80	0.02
DF7 (CC000_2)	_	-	-	- (Surface	-	-	_	_	_	Chalcocite	-0.21	0.05

				sample)								
DF8 (CC000_3)	_	-	-	- (Surface sample)	-	-	_	_	_	Chalcocite	-0.27	0.09
DF9 (CC007_62)*	18CCAD007	506857.87	7698633.3	62	60	53	21,800	365	4.7	Chalcopyrite	-0.42	0.027
DF10 (CC003_85)*	18CCAD003	506698.19	7698681	85	75	82	17,000	190	0.45	Chalcopyrite	-0.21	0.008
DF11 (CC010_154)*	18CCAD010	507480.5	7698641.4	154	60	133	3240	18,500	5.15	Chalcopyrite	0.00	0.007
DF12 (CC001_55)*	18CCAD001	506701.45	7698757.3	55	60	47	27,700	69	0.21	Chalcopyrite	-0.61	0.017
DF13 (CC005_102)*	18CCAD005	506863.16	7698712.4	102	60	89	12,700	167	0.59	Chalcopyrite	-0.17	0.010
DF14 (CC010_137)*	18CCAD010	507480.5	7698641.4	137	60	118	23,200	367	0.35	Chalcopyrite	-0.44	0.003
DF15 (CC009_50)*	18CCAD009	506942.27	7698937.2	50	60	43	41,500	29,200	26.2	Chalcopyrite	-0.25	0.003
DF16 (CC003_61)(2)*	18CCAD003	506698.19	7698681	61	75	59	13,900	6800	8.13	Chalcopyrite	-0.20	0.034
DF17 (CC001_95)*	18CCAD001	506701.45	7698757.3	95	60	82	7160	192	1.84	Chalcopyrite	-0.09	0.002
DF18 (CC009_48)*	18CCAD009	506942.27	7698937.2	48	60	41	74,900	13,500	13.05	Chalcopyrite	-0.27	0.011
DF19	18CCAD008	506932.99	7698937.9	25	60	22	33,500	13,500	9.25	Chalcocite	-0.56	0.031

(CC008_25)												
Supergene mineralisation												
DF20 (CC000_1)	_	_	_	- (Surface sample)	-	-	_	_	_	Native Cu	0.20	0.01
DF21 (CC006_14)(1)*	18CCAD006	506901.24	7698720.4	14	60	12	7410	909	0.33	Pyrolusite (15% Cu)	0.43	0.005
DF22 (CC006_14)(2)*	18CCAD006	506901.24	7698720.4	14	60	12	7410	909	0.33	Plancheite	0.62	0.005
DF23 (CC000_4)*	_	_	_	- (Surface sample)	-	-	_	_	_	Native Cu	0.15	0.029
DF24 (CC011_97)*	18CCAD011	507476.27	7698549.7	97	50	74	10,250	1260	2.85	Plancheite + Agardite-(Ce)	0.19	0.037
DF25 (CC011_56)*	18CCAD011	507476.27	7698549.7	56	50	42	3590	186	0.07	Plancheite	0.24	0.007
DF26 (CC010_44)*	18CCAD010	507480.5	7698641.4	44	60	38	2830	351	0.2	Chalcocite	0.51	0.057
DF27 (CC001_50)*	18CCAD001	506701.45	7698757.3	50	60	43	3200	560	0.42	Plancheite + Agardite-(Ce)	-0.10	0.015
DF28 (CC002_16)*	18CCAD002	506778.93	7698694.9	16	60	13	17,100	1120	0.88	Plancheite	-0.32	0.008
DF29	18CCAD006	506901.24	7698720.4	52	60	45	7260	259	0.87	Plancheite	-0.50	0.014

(CC006_52)(1)*												
DF30 (CC006_52)(2)*	18CCAD006	506901.24	7698720.4	52	60	45	7260	259	0.87	Agardite-(Ce)	-0.06	0.034

3490

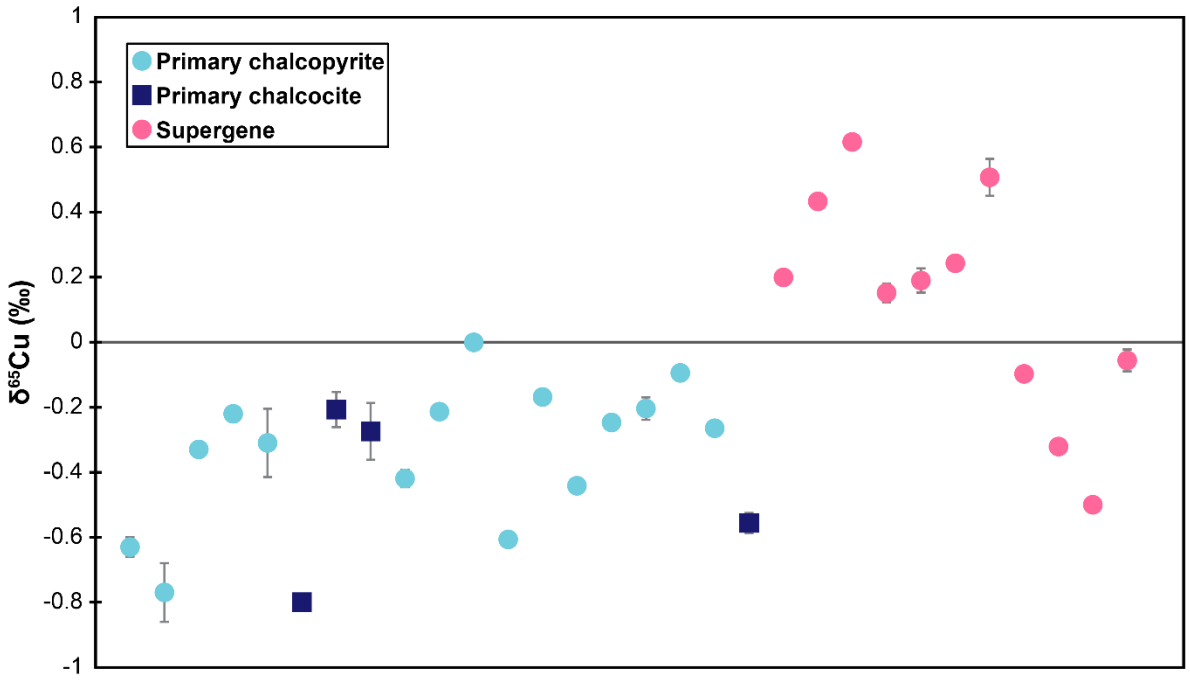

Figure 5.2 - Copper isotope composition of primary Cu sulphides (blue) and supergene Cu minerals (pink) from Carlow Castle. Note errors bars are 2σ.

5.6 Discussion

5.6.1 Carlow Castle Cu-Co-Au deposit copper isotope composition

Carlow Castle's primary Cu sulphide mineralisation is lightly fractionated; with δ^{65}Cu values ranging between -0.80‰ and 0.00‰ across 19 samples. Across this sample suite there is minimal difference in isotopic signature between different phases, chalcocite ranges between -0.80‰ and -0.21‰, whilst chalcopyrite ranges between -0.79‰ and 0.00‰ (Figure 5.2). Similarly, there is no systematic variation in isotopic signature between those samples from Co-poor and Co-rich intersections of the mineralization (Figure 5.3), designated A*ssemblage One* and A*ssemblage Two* by Fox et al. (2019). Note that Cu, Co, and Au grade values are taken from the one metre intersection of a given sample as reported by Artemis Resources Limited (2018c). Given the lack of observed spatial association between these mineral assemblages it has previously been difficult to determine whether they are cogenetic or if they represent two distinct stages of mineralisation in a multiphase mineral system. The similar Cu isotope signatures of the distinct Co-poor and Co-rich mineral assemblages suggests that they represent mineralogically distinct portions of a single evolving ore-forming system, or that at very least they represent ore formation from a similar Cu source and under a comparable precipitation mechanism. Comparable Cu isotope signatures within the analysed chalcocite and

chalcopyrite imply a common genesis with a similar metal source rather than derivation from two distinct stages of mineralisation in a complex multiphase ore-forming system. There is no clear systematic spatial zonation in Cu isotope composition evident in this data set, as has previously been reported in some porphyry Cu deposits (Gregory & Mathur, 2017; Li, Jackson, Pearson, & Graham, 2010). However, the structurally-controlled vein-hosted nature of Carlow Castle's Cu mineralisation, and potential for subsequent deformation of this mineralisation along these structures would make discerning any spatial zonation in Cu isotope signatures highly complex.

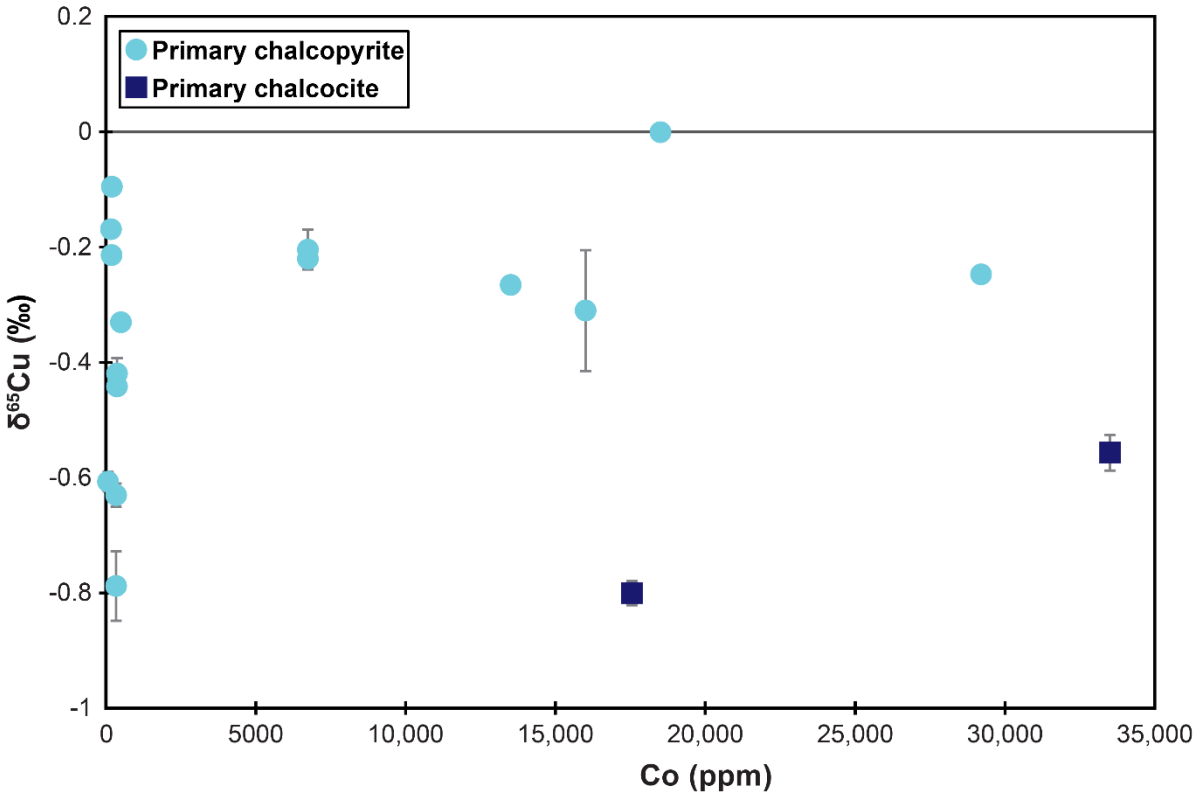

Figure 5.3 - Cross-plot of Cu isotope signature and Co grade in analysed primary Cu samples. Note errors bars are 2σ.

The isotopically light Cu isotope signature of Carlow Castle's Cu sulphide mineralisation is broadly consistent with known pathways of Cu isotope fractionation based on Cu isotope data from other hydrothermal Cu sulphide ore deposits and experimental studies. It is generally established that hydrothermal ore-forming processes tend to induce preferential incorporation of the lighter (^{63}Cu) isotope into solid Cu sulphide phases during reductive ore precipitation (Asael et al., 2007; Fujii, Moynier, Abe, Nemoto, & Albarède, 2013; Mathur et al., 2018; Pękala, Asael, Butler, Matthews, & Rickard, 2011; Zhu et al., 2002). The broadly normally

distributed (Figure 5.4) Cu isotope signature of these Cu sulphide phases is consistent with formation in an ore system with a single Cu source progressively evolving toward $\delta^{65}Cu = 0‰$, rather than from the mixing of several Cu-bearing fluids of different isotopic composition or episodic input of isotopically distinct Cu-bearing fluids. Additionally, the lack of any heavy Cu fractionation in Carlow Castle's mineralisation is somewhat striking, as it is relatively common for Cu isotope signatures in hydrothermal Cu deposits of many varieties to display a range of isotopic compositions; including some $\delta^{65}Cu$ values >0‰ (see Kim, Lee, Oyungerel, Jargal, and Tsedenbal (2019) for a recent review and comprehensive compilation of Cu isotope data from various ore deposits). Nonetheless, Carlow Castle's Cu isotope signature is within the established constraints of most hypogene (>150°C) ore deposits which typically cluster around 0‰ (Mathur et al., 2018). This is consistent with Carlow Castle's ore formation at peak temperatures of ~300°C (Fox et al., 2021).

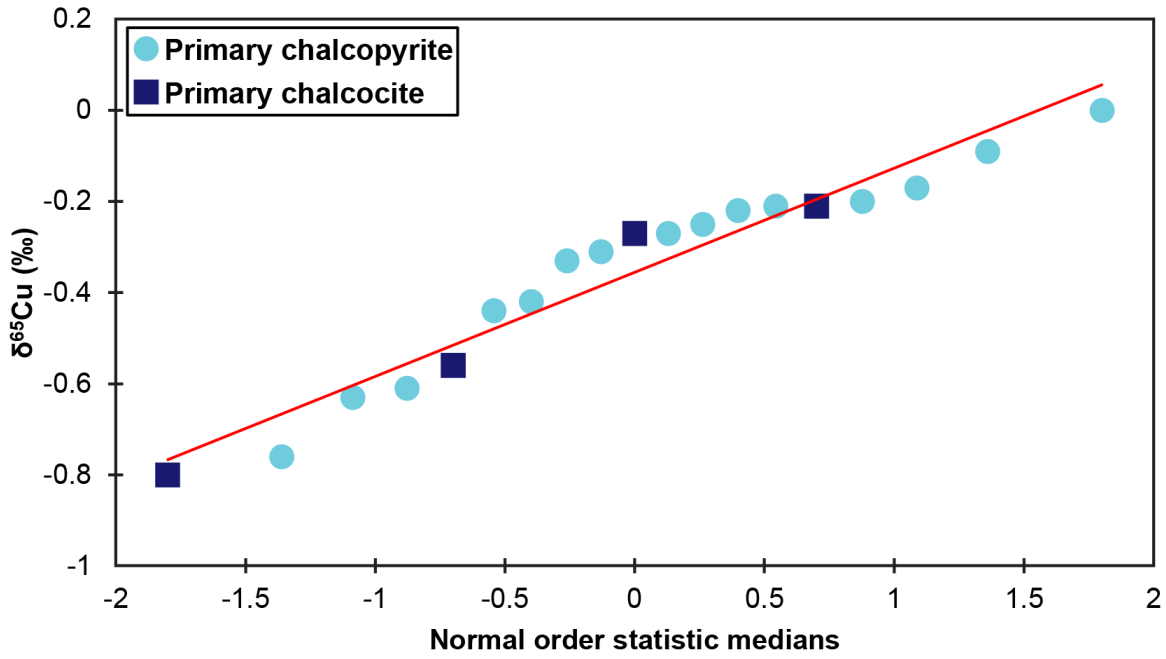

Figure 5.4 - Normal probability plot of Cu isotopes composition of primary Cu sulphide mineralisation from Carlow Castle, showing a broadly normal distribution indicative of a single homogenous Cu source.

5.6.2 Copper isotope fractionation in Archean ore-forming systems

Although the application of Cu isotopic analysis in ore-forming systems has expanded significantly in recent years with improvements in analytical capabilities (Zhu et al., 2000), studies of Archean ore deposits have been extremely sparse. As such, very little is known about if and how Archean ore-forming processes induce Cu isotope fractionation. This is also true of

Archean Earth systems more broadly due to the limited number of studies applying Cu isotopic analysis in Archean terranes generally, with some exceptions where Cu isotopic analysis has been applied as a palaeoredox proxy due to the manner in which redox processes induce significant Cu isotope fractionation (Chi Fru et al., 2016; Zavina-James et al., 2021). Given the globally anoxic conditions that prevailed for much of the Archean and the consequently limited role of redox processes in most Archean ore-forming systems, it may previously have been assumed that Cu isotopic analysis would be of limited utility when applied to these systems. As such, the fractionated and consistently observable pattern of light $\delta^{65}Cu$ in Carlow Castle's Cu sulphide mineralisation relative to an unfractionated mantle reservoir (0.06 ± 0.20‰ based on estimates by Liu et al. (2015)) is notable. This suggests that Cu isotopic analysis could have novel applications in understanding Archean ore-forming systems and that previously proposed exploration techniques utilising this analytical technique may be similarly applicable in Archean terranes (Mathur & Wang, 2019). However, Carlow Castle's Cu isotope fractionation is still relatively limited by comparison to other hydrothermal Cu deposits, which have been observed to exhibit $\delta^{65}Cu$ values <-3‰ and >4‰ (Kim et al., 2019; Li et al., 2010; and references therein). (Fox et al., 2021; Fox et al., 2019)

The absence of any $\delta^{65}Cu$ values >0‰ is a relatively unique aspect of the Cu isotope signature of the primary Cu sulphide mineralisation at Carlow Castle. The current lack of knowledge of Archean Cu isotope systematics makes it challenging to explain this feature of Carlow Castle's Cu mineralisation. Nonetheless, it is well established that oxidative weathering of Cu-bearing minerals tends to preferentially mobilise ^{65}Cu; leading to enriched $\delta^{65}Cu$ values in weathering product solutions (Mathur et al., 2012; Moynier, Vance, Fujii, & Savage, 2017). Given this, Chi Fru et al. (2016) observed an evolution toward heavier $\delta^{65}Cu$ signatures in black shales across 2.66-2.08 Ga, from slightly isotopically light around 2.66 Ga ($\delta^{65}Cu$ = -0.55‰) to slightly isotopically heavy ($\delta^{65}Cu$ = 0.74‰) by 2.3 Ga. This isotopic shift is primarily explained by increased oxidative weathering and delivery of ^{65}Cu to the marine environment because of the significant increase in atmospheric oxygen following the Great Oxygenation Event (GOE) around 2.45 Ga. Following this logic, the negative $\delta^{65}Cu$ signature of Carlow Castle's Cu sulphide mineralisation may be explained by the lack of any significant ^{65}Cu-enriched crustal Cu isotope reservoirs to provide a source of isotopically heavy Cu to Carlow Castle's mineral system. This is due to the comparably limited potential for significant oxidative weathering of Cu-bearing minerals in surface environments during the Mesoarchean

to develop any fractionated and isotopically heavy surface reservoirs. Contamination by fractionated crustal material is a commonly cited source of heavy Cu isotope enrichment and heterogeneity in hypogene systems (Kim et al., 2019; Ripley, Dong, Li, & Wasylenki, 2015). By contrast, δ^{65}Cu values in modern seawater were measured to range from 0.9 to 1.5‰ by Vance et al. (2008) whilst modern oceanic sediments from the Pacific, Atlantic and, Indian oceans were reported by Dekov, Rouxel, Asael, Hålenius, and Munnik (2013) to range between 0.41 and 0.95‰. Although some evidence of oxidative weathering has been observed in terrestrial environments following the emergence of oxidative photosynthesis, most likely during the Mesoarchean (Catling & Zahnle, 2020; Wang et al., 2018), this weathering was likely produced by isolated mildly oxygenated environments during periods of transient oxygenation prior to the GOE (Johnson et al., 2021; Lyons et al., 2014). Because of the limited extent and magnitude of Archean oxidative weathering, it would have been unlikely to induce heavy Cu isotope fractionation of crustal reservoirs on a significant scale. Additionally, the intensity of such oxidative weathering processes would have been relatively limited by comparison to modern (likely Cenozoic) supergene processes and the transient nature of such conditions would preclude the multiple cycles of oxidation and reduction necessary to generate significant heavy Cu isotope fractionation in crustal reservoirs (Johnson et al., 2021; Mathur & Fantle, 2015). Similarly, given the physicochemical conditions of Carlow Castle's ore formation (Fox et al., 2021), it is unlikely that redox changes (oxidation of Cu^{1+} to Cu^{2+}) driven by hydrothermal ore-forming processes would have induced significant heavy Cu isotope fractionation as $CuCl_2^-$ is the predominant stable Cu-Cl species in solution around 300°C, even under oxidising conditions (Brugger et al., 2016; Liu, Brugger, McPhail, & Spiccia, 2002; Maher, Jackson, & Mountain, 2011; Syverson, Borrok, Niebuhr, & Seyfried, 2021; Zhu et al., 2002). Whilst aspects of the Archean crustal environment may account for the notable lack of any >0‰ fractionation of Carlow Castle's Cu isotope signature, the pattern of Cu isotope fractionation in Carlow Castle's mineralisation most clearly reflects the evolution of an ore system defined by Rayleigh-type fractionation due to preferential incorporation of ^{63}Cu into solid Cu phases during ore precipitation. This was associated with a consequent increase in δ^{65}Cu in the fluid phase from an initially isotopically light composition (δ^{65}Cu = <0‰); evolving toward a progressively heavier composition around δ^{65}Cu = 0‰. Similar behaviour has previously been invoked to account for Cu isotope fractionation in various hypogene Cu ore systems (Gregory & Mathur, 2017; Li et al., 2010; Wu, Zheng, Wang, Chang, & Tan, 2017).

5.6.3 Copper isotope record of ore system evolution and Rayleigh fractionation

The $\delta^{65}Cu$ values of the analysed Cu sulphide samples in this study appear to record the isotopic and physicochemical evolution of Carlow Castle's hydrothermal ore-forming system. In these data, there is a negative relationship between $\delta^{65}Cu$ of a given sample and the Cu grade (measured as Cu ppm for a given intersection of drill core as reported within (Artemis Resources Limited, 2018c)) within chalcopyrite-bearing samples (Figure 5.5). However, no such relationship is evident for $\delta^{65}Cu$ and Co or Au grade in the same samples. Additionally, the relationship between $\delta^{65}Cu$ and Cu grade doesn't seem to extend to primary chalcocite samples that were analysed, though the number of chalcocite analyses is comparably limited. This may be due to the influence of different stoichiometric Cu contents of chalcocite and chalcopyrite and differences in Cu isotope fractionation during Cu precipitation into chalcopyrite and chalcocite (Liu et al., 2021). Phase-based differences in Cu isotope fractionation are certainly evident in the reverse case; where oxidation of chalcocite produces heavier Cu isotope signatures in solution than chalcopyrite (Mathur et al., 2005; Mathur & Wang, 2019). Similar behaviour can also be observed during comparisons of bornite and chalcocite weathering (Wall et al., 2011a; Wall, Mathur, Post, & Heaney, 2011b). In addition, the different chemical and thermodynamic stability conditions between chalcocite and chalcopyrite almost certainly influence Cu isotope fractionation behaviour between the fluid and solid mineral phases (Maher et al., 2011). As such, it is likely that chalcocite and chalcopyrite within the deposit do not necessarily record the isotopic evolution of this ore system in a comparable manner and, in general, different phases should be considered separately.

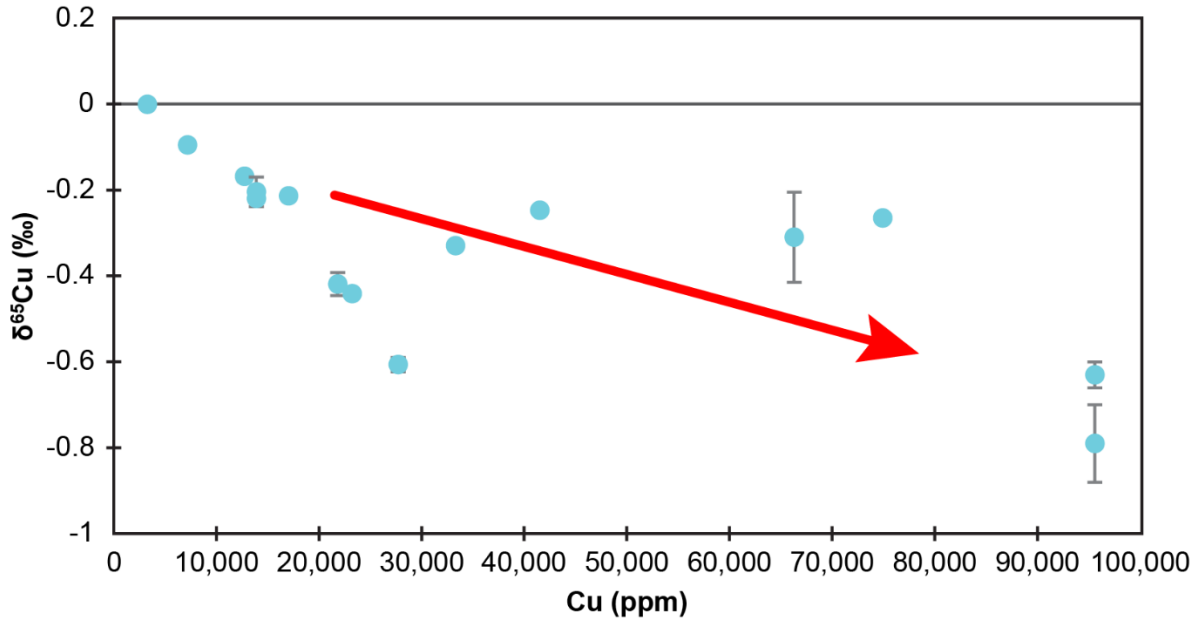

Figure 5.5 - Cross-plot of Cu grade and Cu isotope signature of primary chalcopyrite samples from Carlow Castle (r = -0.7, r^2 = 0.49, p = 0.004). Note errors bars are 2σ.

A linear least squares regression (Figure 5.5) of Cu (ppm) and δ^{65}Cu for the analysed chalcopyrite samples produces a moderate negative correlation (r = -0.7, r^2 = 0.49, p = 0.004). This relationship is interpreted to represent a record of the evolution of Carlow Castle's hypogene ore system following a Rayleigh-type fractionation process. It is interpreted that sample CC012_67(1) (Cu (ppm) = 95,600; δ^{65}Cu = 0.79‰), as the most Cu-rich and isotopically lightest sample, represents an early stage in the evolution of this ore system and the initiation of Cu-sulphide precipitation. As it is well established that ^{63}Cu preferentially precipitates into the solid phase during Cu sulphide ore formation within hydrothermal systems (Asael et al., 2007; Bornhorst & Mathur, 2017; Ehrlich et al., 2004; Zhu et al., 2002), it is reasonable to interpret that the initial stages of mineralisation would be both the lightest isotopically and most Cu-rich. As the system evolved according to a Rayleigh fractionation process, progressive removal of total dissolved Cu and specifically ^{63}Cu from the fluid phase and into the ore would be reflected in a concomitant decrease in ore grade and increase in δ^{65}Cu over time. It should be noted however that this hypothetical model with a finite Cu-bearing fluid reservoir that is almost certainly a broad simplification of the evolution of what was no doubt a complex hydrothermal system.

Fox et al. (2021) suggested that changing abundances of actinolite, chlorite and epidote across the deposit's propylitic alteration assemblage indicated variations in alteration temperatures.

Higher abundances of actinolite were taken to indicate higher peak temperatures of alteration (Corbett & Leach, 1997). Notably, these variations in alteration assemblage also appear to broadly correlate with the relationship observed in this study between Cu grade and δ^{65}Cu. Fox et al. (2021) observed that sample CC012_67 displays the highest temperature propylitic (most actinolite-rich) alteration assemblage of those samples analysed and therefore posited that it may represent a high-temperature portion of a thermally-zoned deposit compared to lower-temperature (actinolite and epidote-poor, chlorite-rich) mineralisation, e.g., samples CC009_48 and CC003_61. This observation supports the interpretation in the current study; that the trend in Cu grade and δ^{65}Cu reflects the progressive evolution of Carlow Castle's hydrothermal system during ore precipitation. There are three lines of converging evidence from alteration temperatures, Cu grade of the samples, and Cu isotope compositions that support this interpretation. In this case, the early stages of mineralisation characterised by an isotopically light and Cu-rich fluid would also be expected to have been the hottest. This is supported by the comparably high temperature alteration assemblage of CC012_67. Here the isotopic evolution of this ore fluid may reflect its coeval physicochemical evolution, precipitating Cu as it equilibrated with the host wall-rock of the Ruth Well and Nickol River Formations; becoming progressively cooler and more reduced. This is suggested by the decreased abundance of actinolite and epidote relative to chlorite in isotopically heavier and lower Cu grade samples, e.g., CC009_48 and CC003_61. The alteration assemblage here appears to be evolving from a relatively high-temperature to comparably low-temperature propylitic assemblage dominated by calc-silicate minerals formed at neutral to slightly alkaline pH (6.0 at 300°C) (Reed, 1997). Therefore, the primary physicochemical control on Cu isotope fractionation appears to be temperature (Corbett & Leach, 1997; Pirajno, 2009). As such, changes in pH can be ruled out as a significant influence on Cu isotope fractionation in this system. This is important to note given the influence that pH can have on Cu isotope fractionation, due to the impact of pH on Cu solubility and fluid-mineral fractionation factors (Gregory & Mathur, 2017; Maher et al., 2011; Mathur et al., 2013).

The parameters of Carlow Castle's Rayleigh fractionation process can be estimated using the chalcopyrite Cu grade and δ^{65}Cu data in this study as a record of this process. It is assumed that the chalcopyrite samples analysed in this study represent the full spectrum of Carlow Castle's ore system evolution with isotopically lightest/heaviest and most Cu-rich/poor samples representing the initial and final stages of this ore fluid evolution process respectively.

Therefore, $\boldsymbol{\alpha}$ (fractionation factor) and $\boldsymbol{\delta_o}$ (initial isotopic composition) can be estimated relatively simply with a logarithmic regression through these data using a similar method to Scott, Lu, Cavanaugh, and Liu (2004). Within this Rayleigh fractionation model the Cu grade of the samples is used to represent **F** (fraction of remaining dissolved Cu). As sample CC012_67 is interpreted to represent the earliest phase of mineralisation in this system (Figure 5.6), when the ore fluid was most Cu-rich, Cu grades of all samples are normalised relative to sample CC012_67's Cu grade (95,600 ppm) by the formula; $\boldsymbol{F} = \frac{Sample\ grade}{Sample\ CC012\_67\ grade}$. A logarithmic expression that defines the Rayleigh fractionation model of Carlow Castle's chalcopyrite can then be simply derived through a least squares linear regression of the δ^{65}Cu data and corresponding values for $\ln(\boldsymbol{F})$. This gives a best fit line defined by the expression $y = -0.164x - 0.55$ or $\delta^{65}\mathrm{Cu} = -0.164(\mathbf{F}) - 0.55$. From this $\boldsymbol{\alpha - 1}$ can be derived as $\frac{-0.164}{1000} = -0.000164$ and $\boldsymbol{\delta_o} = -0.55‰$. This defines a best fit (r = -0.75, r^2 = 0.56, p = 0.0014) Rayleigh fractionation model for Carlow Castle's Cu mineralisation of $\delta^{65}\mathrm{Cu} = (1000 - 0.55) \cdot F^{-0.000164} - 1000$. Whilst this method allows for estimation of the Rayleigh fractionation model for Carlow Castle's chalcopyrite mineralisation, it is necessary to know the degree of isotopic fractionation between dissolved Cu in the fluid phase and precipitated Cu in chalcopyrite, given as $\Delta^{65}\mathrm{Cu}_{(\text{chalcopyrite-Cu(aq)})}$. It has previously been assumed in some studies that isotopic compositions of Cu-sulphides closely reflect the isotopic composition of their parent ore fluid, i.e., $\Delta^{65}\mathrm{Cu}_{(\text{chalcopyrite-Cu(aq)})} \approx 0$ (Asael, Matthews, Oszczepalski, Bar-Matthews, & Halicz, 2009). However, Syverson et al. (2021) recently used experimental data and natural analogues from submarine hydrothermal vent systems to demonstrate that $\Delta^{65}\mathrm{Cu}_{(\text{chalcopyrite-Cu(aq)})}$ = -0.22 ± 0.16‰ under comparable hydrothermal conditions to Carlow Castle's formation. If it is assumed that a similar value for $\Delta^{65}\mathrm{Cu}_{(\text{chalcopyrite-Cu(aq)})}$ applies for Carlow Castle, this would give a starting fluid composition as $\boldsymbol{\delta_o} = -0.55 + 0.22 = -0.33‰$ (Figure 5.6).

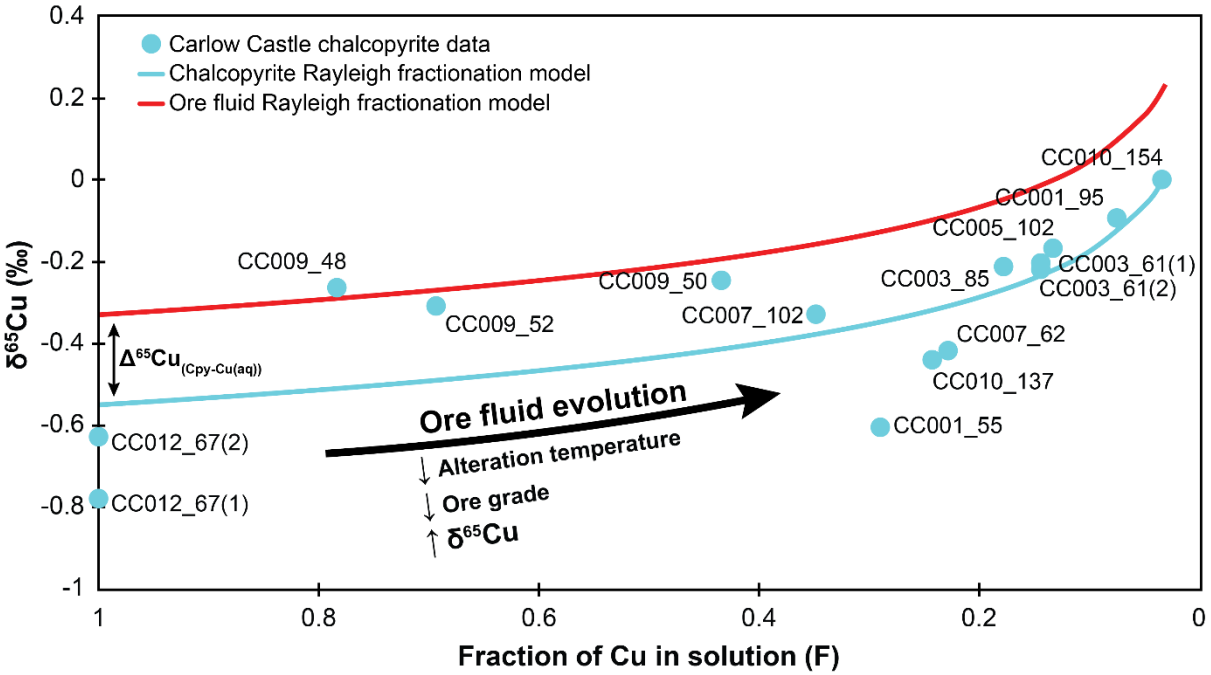

Figure 5.6 - Rayleigh fractionation model for Carlow Castle chalcopyrite and ore fluid based on estimated best-fit logarithmic regression of chalcopyrite data.

Though generally the goodness-of-fit for the logarithmic regression used to construct the above Rayleigh fraction model for Carlow Castle's chalcopyrite Cu isotope data is acceptable (r^2 = *0.56*), some outlier data points exist, e.g., CC009_48 or CC001_55. Whilst it may be tempting to remove these outliers and consider them as part of a separate system, there is little compelling geological evidence to suggest that this is valid. Instead, these deviations are more likely to reflect a variety of possible limitations of the method utilised here and associated assumptions. For example, the vein-hosted nature of Carlow Castle's mineralisation means that Cu grade measurements over a given metre sample of mineralised core are likely to vary significantly due to a 'nugget effect' that arises from the heterogeneous distribution of this mineralisation. This effect would be less pronounced if this mineralisation was instead evenly disseminated over a given mineralised intersection. This is illustrated by the difference in Cu grade between samples CC009_48 (74,900 ppm Cu) and CC009_50 (41,500 ppm Cu) which occur 2 metres in depth apart in the same drill hole but vary in Cu grade by 33,400 ppm (~80.5%) whilst only varying 0.02‰ in δ^{65}Cu. Additionally, the complex mineralogy of some samples, which may contain several different Cu-bearing phases with different stoichiometric Cu concentrations (e.g., chalcocite and chalcopyrite), may complicate these grade measurements over a given metre intersection. Finally, it may simply be that the Rayleigh fractionation model developed here to represent Carlow Castle's ore-forming system is a

necessarily idealised model of a complex natural system and as such fails to account for isotopic fractionation in all samples perfectly. Nonetheless, this still provides an approximate model of Carlow Castle's ore system evolution through the lens of Cu isotopes.

The initial Cu isotopic composition of Carlow Castle's ore fluid ($\delta^{65}Cu$ = -0.304‰) is broadly consistent with derivation of Cu from a minimally fractionated igneous source, which would be expected to display an isotopic composition in the range of $\delta^{65}Cu = 0.06 \pm 0.20$‰ (Liu et al., 2015). In this instance, derivation from an unfractionated and homogeneous igneous source may account for the relatively limited fractionation and broadly normally distributed Cu isotope signature evident in Carlow Castle's Cu sulphide mineralisation. However, there is no evidence of large-scale magmatic activity in the West Pilbara Superterrane that was both coeval with Carlow Castle's ore formation (c. 2.95 Ga) and proximal to the deposit to provide an igneous driver of ore formation and source of metal (Fox et al., 2021). Nonetheless, an igneous metal source would be consistent with previous hypotheses, as it has been suggested that the greenstone belts that form much of the surrounding terranes could provide a potential source of metalliferous mafic rocks from which ore metals could be liberated (Fox et al., 2021; Fox et al., 2019). This is consistent with the established association between mafic igneous rocks and significant hydrothermal Co deposits, including in non-magmatic-hydrothermal deposits (Hitzman et al., 2017). In this regard, the Cu isotopic signature of Carlow Castle's ore is potential evidence of a mafic igneous metal source, most likely from the surrounding greenstone belts which are rich in mafic and ultramafic igneous rocks.

5.6.4 Copper isotope fractionation in supergene Cu samples

Generally, the most significant fractionation of Cu isotopes in ore-forming systems is observed in secondary minerals produced through oxidative weathering of underlying primary ore sulphides (Larson et al., 2003; Sherman, 2013), where redox reactions generate significant enrichment of ^{65}Cu ($\Delta^{65}Cu_{(\text{supergene Cu-primary Cu})}$) in resulting supergene Cu minerals up to >10‰ (Kim et al., 2019). This is due to preferential mobilisation of ^{65}Cu into solution during oxidative weathering of primary Cu sulphide minerals (Markl et al., 2006; Mathur et al., 2005; Mathur & Wang, 2019). However, in the current study the enrichment of ^{65}Cu in supergene phases is somewhat limited, only ranging up to a maximum of 0.62‰ in sample CC006_14(2). Between the isotopically lightest primary Cu sample (CC007_41, $\delta^{65}Cu$ = -0.80‰) and the isotopically heaviest supergene Cu sample this gives a relatively limited $\Delta^{65}Cu_{(\text{supergene Cu-primary Cu})}$ = 0.62‰ – -0.80‰ = 1.42‰. Generally, large magnitude isotopic fractionation of supergene Cu minerals

is interpreted to result from multiple cycles of isotopic enrichment from successive oxidative weathering and reprecipitation of Cu, due to the comparably limited isotopic fractionation produced by single-cycle weathering experiments (Braxton & Mathur, 2011; Mathur, Dendas, Titley, & Phillips, 2010; Mathur et al., 2005; Moynier et al., 2017). Reflecting this, the limited Cu isotope fractionation within Carlow Castle's supergene Cu mineralisation suggests that this supergene Cu has undergone limited redox cycling (Mathur et al., 2010). Although the ^{65}Cu enrichment in these supergene phases is relatively moderate by comparison to other studies, these supergene phases are isotopically distinct from Carlow Castle's primary Cu mineralisation as the majority of the supergene Cu isotope data display $\delta^{65}Cu$ values >0‰. In contrast, Carlow Castle's primary mineralisation exclusively displays $\delta^{65}Cu$ values ≤0‰. Additionally, it is likely that even the isotopically lightest supergene sample in this study (CC006_52(1); $\delta^{65}Cu$ = -0.50‰) is still heavily fractionated relative to the primary Cu sulphide ore from which it was derived. This is reflected by the fact that the lightest supergene sample is still isotopically heavier than the lightest primary Cu sulphide sample (CC007_41; $\delta^{65}Cu$ = -0.80‰), though the magnitude of heavy fractionation is clearly relatively limited.

A significant portion of the existing literature on Cu isotope analysis of supergene materials in ore deposit settings has focussed on porphyry Cu deposits. Here spatially distinct Fe-oxide leach caps, underlying supergene Cu enrichment zones, and deep-lying hypogene Cu sulphide mineralisation form well-developed, spatially extensive, discrete Cu isotope reservoirs (Asadi, Mathur, Moore, & Zarasvandi, 2015; Braxton & Mathur, 2011; Mathur et al., 2010; Mathur et al., 2009; Palacios, Rouxel, Reich, Cameron, & Leybourne, 2011). Very little of this literature is focused on the effect of supergene processes on Cu isotope fractionation in structurally complex vein-hosted Cu ore systems and even less literature is focused on Cu fractionation between Archean Cu sulphide ores and contemporary supergene Cu mineralisation in Archean terranes. The complex structurally-hosted nature of Carlow Castle's mineralisation means that the development of discrete supergene and hypogene sub-zones is less spatially uniform. The development of these zones is likely to be strongly influenced by the effect of individual structures on regional permeability and groundwater flow, which would have preferentially focussed fluids and therefore chemical weathering along certain permeable structures (Babiker & Gudmundsson, 2004; Ferrill et al., 1999). As a result, the depth of supergene Cu samples varies significantly across different drill holes. To illustrate this, samples CC011_97 and CC002_16 are both supergene Cu samples that contain plancheite; however, they were sampled

from different drill holes and occur 61 metres apart in true vertical depth (TVD). Further, sample CC008_25 is a primary chalcocite sample and occurs at only 22 metres TVD; 52 metres shallower than the deepest supergene sample. Reflecting this, there is no discernible trend evident between the δ^{65}Cu values and depths of different samples in this study (Figure 5.7).

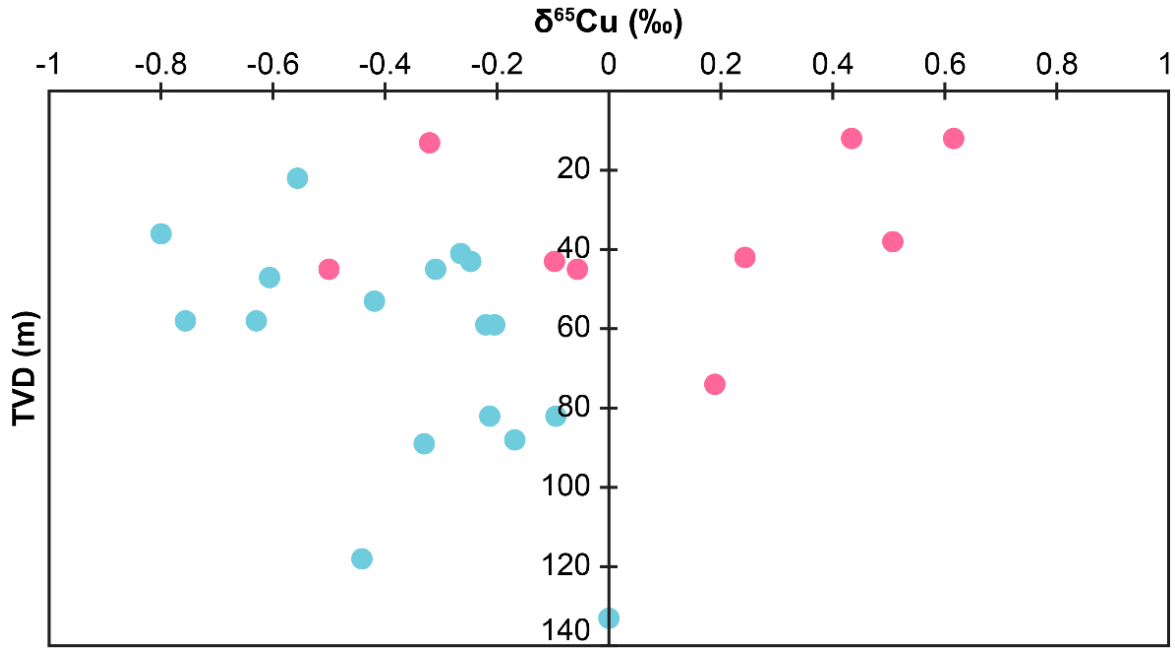

Figure 5.7 - Cross-plot of Cu isotope signature and true vertical depth of analysed samples. There appears to be no clear correlation between sample depth and isotopic signature for supergene samples. Also, some supergene Cu samples were retrieved from greater depths than some of the primary Cu ore samples, reflecting Carlow Castle's structurally complex vein-hosted mineralisation. Note that samples that were not retrieved from drill core have an unknown original depth and therefore are not presented here.

Unlike the clear relationship between Cu grade and δ^{65}Cu that is evident across the primary chalcopyrite data from Carlow Castle, no comparable relationship is evident across the supergene Cu isotope data in this study (Figure 5.8). This precludes the construction of a Rayleigh fractionation model for the supergene data set. These supergene data are complicated by mineralogical complexity comprising several different Cu-bearing phases, which almost certainly undergo distinct phase-specific isotopic fractionation processes during Cu precipitation and contain different stoichiometric proportions of Cu (Liu et al., 2021). This is exemplified by the relatively significant difference in isotopic composition between plancheite in sample CC006_52(1) (δ^{65}Cu = -0.50‰) and agardite in sample CC006_52(2) (δ^{65}Cu = -

0.06‰), even though these samples were extracted from the same core sample. In addition, it is likely that the range of supergene samples essentially represent several independent, small-scale supergene systems along a given fluid pathway via in-situ alteration of primary sulphide ore in a given vein with spatially limited Cu transport. This is implied by (i) the significant difference in depth between supergene samples analysed in this study due to in-situ alteration of primary sulphide veins with limited lateral Cu transport, (ii) spatially distinct and disconnected supergene Cu isotope reservoirs, (iii) probable channelling of regional oxidised groundwater flow along permeable mineralised structures with minimal fluid interaction between hydrogeologically distinct structures. If these supergene samples represent multiple small hydrogeologically heterogeneous oxidised vein systems, it is not geologically valid to attempt to construct a Rayleigh fractionation model based on these data. The spatial restriction of these supergene Cu minerals to small vein-hosted systems rather than an extensive supergene enrichment blanket, as is commonly observed in analyses of supergene Cu minerals from porphyry deposits (Asadi et al., 2015; Braxton & Mathur, 2011), may have limited repeated Cu transport and redox cycling in these supergene minerals. This most likely accounts for the limited isotopic enrichment in Carlow Castle's supergene Cu mineralisation. Given the wide interest in the potential use of Cu isotope analysis of ore minerals for potential exploration applications (Braxton & Mathur, 2011; Mathur et al., 2013; Mathur et al., 2009; Mathur & Wang, 2019), this may be an important consideration when exploring in structurally complex terranes or for structurally-hosted ore deposits.

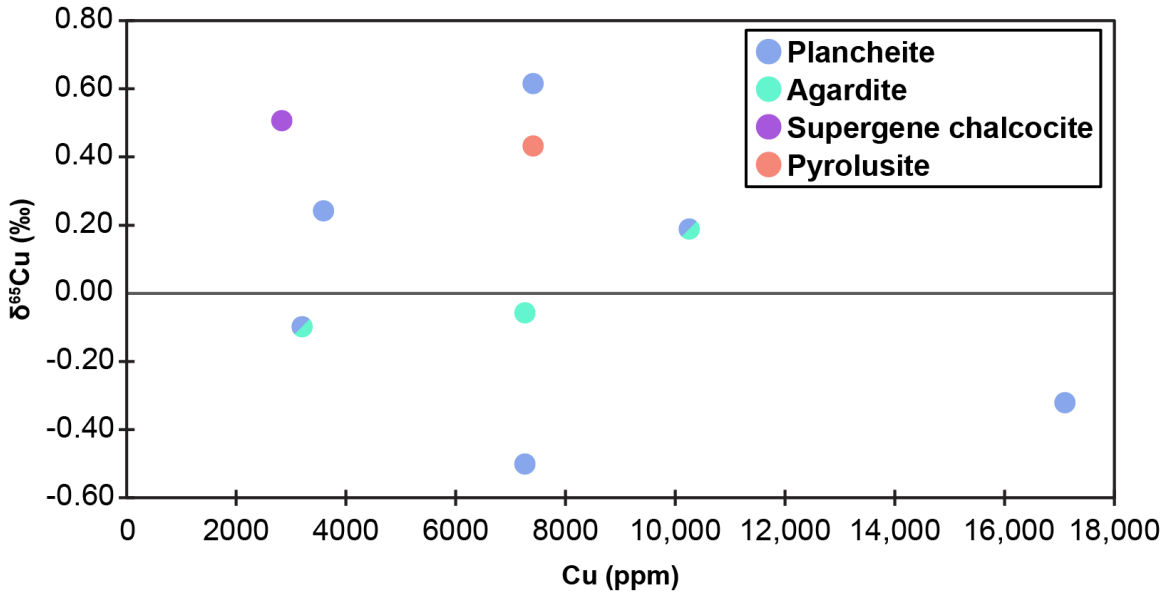

Figure 5.8 - Cross-plot of Cu grade (ppm) and isotopic signature of supergene Cu samples. Note that error bars are not visible as they are smaller than the sample symbols.

5.7 Conclusions and implications

In this study we provide the first Cu isotope analysis of an Archean Cu ore deposit; the Mesoarchean Carlow Castle Cu-Co-Au deposit in the Pilbara Craton, Western Australia. Copper isotope fractionation in Carlow Castle's primary Cu sulphide ore is relatively limited, consistent with its Archean age and hypogene origin; ranging between $\delta^{65}Cu$ = -0.8 and 0‰. Nonetheless, these values are fractionated beyond the bounds of a bulk silicate Earth composition. This isotopic fractionation is attributed to Rayleigh fractionation due to preferential incorporation of ^{63}Cu into the solid phase during Cu sulphide precipitation. We observe that, based on an apparent relationship with Cu grade in analysed ore samples, the Cu isotopic signature of chalcopyrite samples appear to record the physicochemical evolution of Carlow Castle's ore system during this process. This is further supported by an apparent relationship between alteration mineral assemblage and Cu isotope signature in the analysed samples. Modelling of this Rayleigh fractionation process based on the isotopic composition of analysed chalcopyrite gives an estimated initial fluid Cu isotopic composition around $\delta^{65}Cu$ = -0.3‰. This is interpreted as evidence of a probable mafic igneous metal source with minimal input from a fractionated crustal source and supports previous hypotheses for deposit formation. These findings suggest that Cu isotope analysis also has potential utility in understanding genetic processes in Archean ore-forming systems and Cu transport in Archean Earth systems more broadly. However, the current understanding of Archean Cu isotope

systematics suffers from a relatively small body of existing literature. In addition, Carlow Castle represents a relatively unique variety of Archean structurally-hosted hydrothermal Cu-Co-Au deposit (Fox et al., 2021; Fox et al., 2019). As such, this may limit the wider applicability of these findings. Nonetheless, this underlines the importance of expanding the existing literature applying copper isotopes to understand Archean geological processes. Analysis of supergene Cu minerals from Carlow Castle display relatively limited heavy fractionation from their primary Cu sulphide source; ranging between $\delta^{65}Cu$ = -0.50 to 0.62‰. This is suggestive of limited redox cycling of Cu during the formation of these supergene Cu minerals and is interpreted to reflect the lack of a large, shallow, hydrogeologically uniform supergene enrichment blanket produced by multiple cycles of Cu enrichment due to oxidative groundwater flux. Instead, the occurrence of these supergene Cu minerals within primary ore veins due to partial or complete in-situ replacement of primary Cu sulphide minerals suggests that they represent several hydrogeologically disconnected supergene systems with minimal intermixing. This may be an important consideration when utilising Cu isotopes for exploration for structurally complex Cu ore deposits and potentially warrants further study. Nonetheless the fractionation of these supergene phases relative to their primary Cu ore may still suggest that Cu isotope analysis could be a promising tool for exploration in Archean terranes.

Acknowledgements

This research was supported by an Australian Government Research Training Program Scholarship and a CSIRO Mineral Resources postgraduate student scholarship. Artemis Resources Limited are acknowledged for support of this study through provision of sample material. LEM, JF, and JP acknowledge assistance from the MinEx CRC for development of the Cu isotope techniques at University of Adelaide. The Tate Museum at the University of Adelaide is acknowledged for donating a sample for development of the internal standard BHNatCop. Claire Wright at CSIRO Waite Campus is acknowledged for assistance with MC-ICP-MS.

References

Artemis Resources Limited. (2018c). High Grade Cobalt Drilled over 1.2km at Carlow Castle [Press release]. Retrieved from https://www.asx.com.au/asxpdf/20181015/pdf/43z7lvpq8r2kvt.pdf

Asadi, S., Mathur, R., Moore, F., & Zarasvandi, A. (2015). Copper isotope fractionation in the Meiduk porphyry copper deposit, Northwest of Kerman Cenozoic magmatic arc, Iran. *Terra Nova, 27*(1), 36-41. doi:https://doi.org/10.1111/ter.12128

Asael, D., Matthews, A., Bar-Matthews, M., & Halicz, L. (2007). Copper isotope fractionation in sedimentary copper mineralization (Timna Valley, Israel). *Chemical Geology, 243*(3), 238-254. doi:https://doi.org/10.1016/j.chemgeo.2007.06.007

Asael, D., Matthews, A., Oszczepalski, S., Bar-Matthews, M., & Halicz, L. (2009). Fluid speciation controls of low temperature copper isotope fractionation applied to the Kupferschiefer and Timna ore deposits. *Chemical Geology, 262*(3), 147-158. doi:https://doi.org/10.1016/j.chemgeo.2009.01.015

Babiker, M., & Gudmundsson, A. (2004). The effects of dykes and faults on groundwater flow in an arid land: the Red Sea Hills, Sudan. *Journal of Hydrology, 297*(1), 256-273. doi:https://doi.org/10.1016/j.jhydrol.2004.04.018

Bornhorst, T. J., & Mathur, R. (2017). Copper Isotope Constraints on the Genesis of the Keweenaw Peninsula Native Copper District, Michigan, USA. *Minerals, 7*(10). doi:10.3390/min7100185

Braxton, D., & Mathur, R. (2011). Exploration Applications of Copper Isotopes in the Supergene Environment: A Case Study of the Bayugo Porphyry Copper-Gold Deposit, Southern Philippines. *Economic Geology, 106*(8), 1447-1463. doi:https://doi.org/10.2113/econgeo.106.8.1447

Brugger, J., Liu, W., Etschmann, B., Mei, Y., Sherman, D. M., & Testemale, D. (2016). A review of the coordination chemistry of hydrothermal systems, or do coordination changes make ore deposits? *Chemical Geology, 447*, 219-253. doi:https://doi.org/10.1016/j.chemgeo.2016.10.021

Catling, D. C., & Zahnle, K. J. (2020). The Archean Atmosphere. *Science Advances, 6*(9), 1-16. doi:https://doi.org/10.1126/sciadv.aax1420

Chi Fru, E., Rodríguez, N. P., Partin, C. A., Lalonde, S. V., Andersson, P., Weiss, D. J., . . . Konhauser, K. O. (2016). Cu isotopes in marine black shales record the Great Oxidation

Event. *Proceedings of the National Academy of Sciences, 113*(18), 4941. doi:10.1073/pnas.1523544113

Corbett, G. J., & Leach, T. M. (1997). Southwest Pacific Rim gold-copper systems: Structure, alteration and mineralization. *Society of Economic Geologists Special Publication, 6*, 240. doi:https://doi.org/10.5382/SP.06

Dekov, V. M., Rouxel, O., Asael, D., Hålenius, U., & Munnik, F. (2013). Native Cu from the oceanic crust: Isotopic insights into native metal origin. *Chemical Geology, 359*, 136-149. doi:https://doi.org/10.1016/j.chemgeo.2013.10.001

Ehrlich, S., Butler, I., Halicz, L., Rickard, D., Oldroyd, A., & Matthews, A. (2004). Experimental study of the copper isotope fractionation between aqueous Cu(II) and covellite, CuS. *Chemical Geology, 209*(3), 259-269. doi:https://doi.org/10.1016/j.chemgeo.2004.06.010

Ferrill, D. A., Winterle, J., Wittmeyer, G. W., Sims, D., Colton, S. L., & Armstrong, A. (1999). *Stressed Rock Strains Groundwater at Yucca Mountain, Nevada*.

Fox, D., Spinks, S., Barham, M., Kirkland, C. L., Pearce, M. A., Aspandiar, M., . . . Mead, E. (2021). Working up an apatite: Enigmatic Mesoarchean hydrothermal Cu-Co-Au mineralization in the Pilbara Craton. *Economic Geology, 116*(7), 1561-1573. doi:https://doi.org/10.5382/econgeo.4842

Fox, D., Spinks, S., Pearce, M. A., Barham, M., Le Vaillant, M., Thorne, R., . . . Verrall, M. (2019). Plundering Carlow Castle: First Look at a Unique Mesoarchean-Hosted Cu-Co-Au Deposit. *Economic Geology, 114*(6), 1021-1031. doi:https://doi.org/10.5382/econgeo.4672

Fujii, T., Moynier, F., Abe, M., Nemoto, K., & Albarède, F. (2013). Copper isotope fractionation between aqueous compounds relevant to low temperature geochemistry and biology. *Geochimica et Cosmochimica Acta, 110*, 29-44. doi:https://doi.org/10.1016/j.gca.2013.02.007

Goldfarb, R. J., Bradley, D. W., & Leach, D. L. (2010). Secular Variation in Economic Geology. *Economic Geology, 105*(3), 459-465.

Gregory, M. J., & Mathur, R. (2017). Understanding Copper Isotope Behavior in the High Temperature Magmatic-Hydrothermal Porphyry Environment. *Geochemistry, Geophysics, Geosystems, 18*(11), 4000-4015. doi:https://doi.org/10.1002/2017GC007026

Hickman, A. H. (2016). *Northwest Pilbara Craton: a record of 450 million years in the growth of Archean continential crust*. Retrieved from Perth:

Hickman, A. H., Smithies, R. H., & Tyler, I. M. (2010). *Evolution of active plate margins: West Pilbara Superterrane, De Grey Superbasin, and the Fortescue and Hamersley Basins — a field guide*. Retrieved from Perth:

Hickman, A. H., & Van Kranendonk, M. J. (2012). Early Earth evolution: Evidence from the 3.5-1.8 Ga geological history of the Pilbara region of Western Australia. *Episodes, 35*(1), 283-297. doi:https://doi.org/10.18814/epiiugs/2012/v35i1/028

Hitzman, M., Bookstrom, A. A., Slack, J. F., & Zientek, M. L. (2017). *Cobalt—Styles of Deposits and the Search for Primary Deposits*. Retrieved from Virginia: https://doi.org/10.3133/ofr20171155

Hou, Q., Zhou, L., Gao, S., Zhang, T., Feng, L., & Yang, L. (2016). Use of Ga for mass bias correction for the accurate determination of copper isotope ratio in the NIST SRM 3114 Cu standard and geological samples by MC-ICPMS. *Journal of Analytical Atomic Spectrometry, 31*(1), 280-287. doi:10.1039/C4JA00488D

Johnson, A. C., Ostrander, C. M., Romaniello, S. J., Reinhard, C. T., Greaney, A. T., Lyons, T. W., & Anbar, A. D. (2021). Reconciling evidence of oxidative weathering and atmospheric anoxia on Archean Earth. *Science Advances, 7*(40), eabj0108. doi:doi:10.1126/sciadv.abj0108

JORC. (2012). *Australasian Code for Reporting of Exploration Results, Mineral Resources and Ore Reserves*. Retrieved from

Kendall, B. (2021). Recent Advances in Geochemical Paleo-Oxybarometers. *The Annual Review of Earth and Planetary Sciences, 49*(1), 399-433. doi:https://doi.org/10.1146/annurev-earth-071520-051637

Kim, Y., Lee, I., Oyungerel, S., Jargal, L., & Tsedenbal, T. (2019). Cu and S isotopic signatures of the Erdenetiin Ovoo porphyry Cu-Mo deposit, northern Mongolia: Implications for their origin and mineral exploration. *Ore Geology Reviews, 104*, 656-669. doi:https://doi.org/10.1016/j.oregeorev.2018.11.025

Larson, P. B., Maher, K., Ramos, F. C., Chang, Z., Gaspar, M., & Meinert, L. D. (2003). Copper isotope ratios in magmatic and hydrothermal ore-forming environments. *Chemical Geology, 201*(3), 337-350. doi:https://doi.org/10.1016/j.chemgeo.2003.08.006

Li, W., Jackson, S. E., Pearson, N. J., & Graham, S. (2010). Copper isotopic zonation in the Northparkes porphyry Cu–Au deposit, SE Australia. *Geochimica et Cosmochimica Acta, 74*(14), 4078-4096. doi:https://doi.org/10.1016/j.gca.2010.04.003

Liu, S.-A., Huang, J., Liu, J., Wörner, G., Yang, W., Tang, Y.-J., . . . Li, S. (2015). Copper isotopic composition of the silicate Earth. *Earth and Planetary Science Letters, 427*, 95-103. doi:https://doi.org/10.1016/j.epsl.2015.06.061

Liu, S., Li, D., Li, S., Teng, F., Ke, S., He, Y., & Lu, Y. (2014a). High-precision copper and iron isotope analysis of igneous rock standards by MC-ICP-MS. *Journal of Analytical Atomic Spectrometry, 29*, 122-133. doi:https://doi.org/10.1039/C3JA50232E

Liu, S., Li, Y., Liu, J., Yang, Z., Liu, J., & Shi, Y. (2021). Equilibrium Cu isotope fractionation in copper minerals: a first-principles study. *Chemical Geology, 564*, 120060. doi:https://doi.org/10.1016/j.chemgeo.2021.120060

Liu, W., Brugger, J., McPhail, D. C., & Spiccia, L. (2002). A spectrophotometric study of aqueous copper(I)–chloride complexes in LiCl solutions between 100 °C and 250 °C. *Geochimica et Cosmochimica Acta, 66*(20), 3615-3633. doi:https://doi.org/10.1016/S0016-7037(02)00942-0

Lyons, T. W., Reinhard, C. T., & Planavsky, N. J. (2014). The rise of oxygen in Earth's early ocean and atmosphere. *Nature, 506*, 307-315. doi:https://doi.org/10.1038/nature13068

Maher, K. C., Jackson, S., & Mountain, B. (2011). Experimental evaluation of the fluid–mineral fractionation of Cu isotopes at 250°C and 300°C. *Chemical Geology, 286*(3), 229-239. doi:https://doi.org/10.1016/j.chemgeo.2011.05.008

Markl, G., Lahaye, Y., & Schwinn, G. (2006). Copper isotopes as monitors of redox processes in hydrothermal mineralization. *Geochimica et Cosmochimica Acta, 70*(16), 4215-4228. doi:https://doi.org/10.1016/j.gca.2006.06.1369

Mathur, R., Dendas, M., Titley, S., & Phillips, A. (2010). Patterns in the Copper Isotope Composition of Minerals in Porphyry Copper Deposits in Southwestern United States. *Economic Geology, 105*(8), 1457-1467. doi:10.2113/econgeo.105.8.1457

Mathur, R., Falck, H., Belogub, E., Milton, J. E., Wilson, M., Rose, A., & Powell, W. (2018). Origins of Chalcocite Defined by Copper Isotope Values. *Geofluids, 2018*, 1-9.

Mathur, R., & Fantle, M. S. (2015). Copper Isotopic Perspectives on Supergene Processes: Implications for the Global Cu Cycle. *Elements, 11*(5), 323-329. doi:10.2113/gselements.11.5.323

Mathur, R., Jin, L., Prush, V., Paul, J., Ebersole, C., Fornadel, A., . . . Brantley, S. (2012). Cu isotopes and concentrations during weathering of black shale of the Marcellus Formation, Huntingdon County, Pennsylvania (USA). *Chemical Geology, 304-305*, 175-184. doi:https://doi.org/10.1016/j.chemgeo.2012.02.015

Mathur, R., Munk, L., Nguyen, M., Gregory, M., Annell, H., & Lang, J. (2013). Modern and Paleofluid Pathways Revealed by Cu Isotope Compositions in Surface Waters and Ores of the Pebble Porphyry Cu-Au-Mo Deposit, Alaska. *Economic Geology, 108*(3), 529-541. doi:10.2113/econgeo.108.3.529

Mathur, R., Ruiz, J., Titley, S., Liermann, L., Buss, H., & Brantley, S. (2005). Cu isotopic fractionation in the supergene environment with and without bacteria. *Geochimica et Cosmochimica Acta, 69*(22), 5233-5246. doi:https://doi.org/10.1016/j.gca.2005.06.022

Mathur, R., Titley, S., Barra, F., Brantley, S., Wilson, M., Philips, A., . . . Hart, G. (2009). Exploration potential of Cu isotope fractionation in porphyry copper deposits. *Journal of Geochemical Exploration, 102*, 1-6.

Mathur, R., & Wang, D. (2019). Transition Metal Isotopes Applied to Exploration Geochemistry. In S. Decrée & L. Robb (Eds.), *Ore Deposits: Origin, Exploration, and Exploitation* (1 ed., Vol. 242): American Geophysical Union and John Wiley and Sons.

Moynier, F., Vance, D., Fujii, T., & Savage, P. (2017). The Isotope Geochemistry of Zinc and Copper. *Reviews in Mineralogy and Geochemistry, 82*(1), 543-600. doi:10.2138/rmg.2017.82.13

Palacios, C., Rouxel, O., Reich, M., Cameron, E. M., & Leybourne, M. I. (2011). Pleistocene recycling of copper at a porphyry system, Atacama Desert, Chile: Cu isotope evidence. *Mineralium Deposita, 46*(1), 1-7. doi:10.1007/s00126-010-0315-6

Pękala, M., Asael, D., Butler, I. B., Matthews, A., & Rickard, D. (2011). Experimental study of Cu isotope fractionation during the reaction of aqueous Cu(II) with Fe(II) sulphides at temperatures between 40 and 200°C. *Chemical Geology, 289*(1), 31-38. doi:https://doi.org/10.1016/j.chemgeo.2011.07.004

Pirajno, F. (2009). Hydrothermal Processes and Wall Rock Alteration. In F. Pirajno (Ed.), *Hydrothermal Processes and Mineral Systems* (Vol. 1, pp. 73-164). Dordrecht: Springer.

Reed, M. H. (1997). Hydrothermal Alteration and Its Relationship to Ore Fluid Composition. In H. L. Barnes (Ed.), *Geochemistry of Hydrothermal Ore Deposits* (3 ed., pp. 303-365). New York: Wiley.

Ripley, E. M., Dong, S., Li, C., & Wasylenki, L. E. (2015). Cu isotope variations between conduit and sheet-style Ni–Cu–PGE sulfide mineralization in the Midcontinent Rift System, North America. *Chemical Geology, 414*, 59-68. doi:https://doi.org/10.1016/j.chemgeo.2015.09.007

Scott, K. M., Lu, X., Cavanaugh, C. M., & Liu, J. S. (2004). Optimal methods for estimating kinetic isotope effects from different forms of the Rayleigh distillation equation 1 1Associate editor: J. Horita. *Geochimica et Cosmochimica Acta, 68*(3), 433-442. doi:https://doi.org/10.1016/S0016-7037(03)00459-9

Sherman, D. M. (2013). Equilibrium isotopic fractionation of copper during oxidation/reduction, aqueous complexation and ore-forming processes: Predictions from hybrid density functional theory. *Geochimica et Cosmochimica Acta, 118*, 85-97. doi:https://doi.org/10.1016/j.gca.2013.04.030

Syverson, D. D., Borrok, D. M., Niebuhr, S., & Seyfried, W. E. (2021). Chalcopyrite-dissolved Cu isotope exchange at hydrothermal conditions: Experimental constraints at 350 °C and 50 MPa. *Geochimica et Cosmochimica Acta, 298*, 191-206. doi:https://doi.org/10.1016/j.gca.2021.02.005

Van Kranendonk, M. J., Hickman, A. H., Smithies, R. H., Nelson, D. R., & Pike, G. (2002). Geology and Tectonic Evolution of the Archean North Pilbara Terrain, Pilbara Craton, Western Australia. *Economic Geology, 97*(4), 695-732. doi:https://doi.org/10.2113/gsecongeo.97.4.695

Van Kranendonk, M. J., Smithies, R. H., Hickman, A. H., & Champion, D. (2007). Review: secular tectonic evolution of Archean continental crust: interplay between horizontal and vertical processes in the formation of the Pilbara Craton, Australia. *Terra Nova, 19*(1), 1-38.

Vance, D., Archer, C., Bermin, J., Perkins, J., Statham, P. J., Lohan, M. C., . . . Mills, R. A. (2008). The copper isotope geochemistry of rivers and the oceans. *Earth and Planetary Science Letters, 274*(1), 204-213. doi:https://doi.org/10.1016/j.epsl.2008.07.026

Wall, A. J., Heaney, P. J., Mathur, R., Post, J. E., Hanson, J. C., & Eng, P. J. (2011a). A flow-through reaction cell that couples time-resolved X-ray diffraction with stable isotope analysis. *Journal of Applied Crystallography, 44*(2), 429-432. doi:doi:10.1107/S0021889811000525

Wall, A. J., Mathur, R., Post, J. E., & Heaney, P. J. (2011b). Cu isotope fractionation during bornite dissolution: An in situ X-ray diffraction analysis. *Ore Geology Reviews, 42*(1), 62-70. doi:https://doi.org/10.1016/j.oregeorev.2011.01.001

Wang, X., Planavsky, N. J., Hofmann, A., Saupe, E. E., De Corte, B. P., Philippot, P., . . . Konhauser, K. O. (2018). A Mesoarchean shift in uranium isotope systematics. *Geochimica et Cosmochimica Acta, 238*, 438-452. doi:https://doi.org/10.1016/j.gca.2018.07.024

Wang, Z., Park, J.-W., Wang, X., Zou, Z., Kim, J., Zhang, P., & Li, M. (2019). Evolution of copper isotopes in arc systems: Insights from lavas and molten sulfur in Niuatahi volcano, Tonga rear arc. *Geochimica et Cosmochimica Acta, 250*, 18-33. doi:https://doi.org/10.1016/j.gca.2019.01.040

Wu, S., Zheng, Y., Wang, D., Chang, H., & Tan, M. (2017). Variation of copper isotopes in chalcopyrite from Dabu porphyry Cu-Mo deposit in Tibet and implications for mineral exploration. *Ore Geology Reviews, 90*, 14-24. doi:https://doi.org/10.1016/j.oregeorev.2017.10.001

Zavina-James, N. A. V., Zerkle, A. L., Steele, R. C. J., Warke, M. R., Izon, G., & Savage, P. S. (2021). A copper isotope investigation of methane cycling in Late Archaean sediments. *Precambrian Research, 362*, 106267. doi:https://doi.org/10.1016/j.precamres.2021.106267

Zhu, X. K., Guo, Y., Williams, R. J. P., O'Nions, R. K., Matthews, A., Belshaw, N. S., . . . Salvato, B. (2002). Mass fractionation processes of transition metal isotopes. *Earth and Planetary Science Letters, 200*(1-2), 47-62. doi:https://doi.org/10.1016/S0012-821X(02)00615-5

Zhu, X. K., O'Nions, R. K., Guo, Y., Belshaw, N. S., & Rickard, D. (2000). Determination of natural Cu-isotope variation by plasma-sourcem ass spectrometry: implications for use as geochemical tracers. *Chemical Geology, 163*(1-4), 139-149. doi:https://doi.org/10.1016/S0009-2541(99)00076-5

Appendix 5.1 – Chromatography procedure

Appendix 5.1 is accessible via this link and provides an .xlsx file containing the final procedure, with results, used for Cu separation for Cu isotope analysis.

Appendix 5.2 – Long term analyses of reference materials

Appendix 5.2 is accessible via this link and provides an .xlsx file containing results of analyses of reference materials DFCu and BHNatCop from several analytical sessions between February 2020 and October 2022, demonstrating the long-term reproducibility of reference values.

Chapter 6

Synthesis and conclusions

The primary objective of this research project was to provide insights into the nature and genesis of the recently discovered Carlow Castle Cu-Co-Au ore system. Whilst a secondary objective was to establish a working methodology for Cu isotope analysis in collaboration with the Metal Isotopes Group, University of Adelaide and use Carlow Castle as a case study to test this methodology. As this thesis is presented as a series of individual papers, each chapter has dealt with different aspects of these objectives, with the conclusions and implications of each chapter stated at the end of that chapter. As such, this concluding chapter focusses on synthesising these findings to construct a simplified mineral system model for Carlow Castle, along with a discussion of the broader implications of this research for the understanding of Cu-Co-Au metallogenesis through geological time, the Mesoarchean sulphur isotope record, and the application of Cu isotope analysis to understanding the genesis of and exploring for Archean hydrothermal Cu deposits. This is accompanied by discussion of limitations of the research along with avenues for future research.

6.1 New constraints on the genesis of Carlow Castle Cu-Co-Au deposit

The mineral systems approach to holistically defining the confluence of geological processes at various scales that produce significant ore deposits was first formally proposed by Wyborn, Heinrich, and Jaques (1994), though elements of this approach predate formalisation in the cited study (Hayes & Einaudi, 1986). This concept has since become the standard framework to define ore-forming systems in studies of ore deposit petrology (Hagemann, Lisitsin, & Huston, 2016; Huston et al., 2016; McCuaig, Beresford, & Hronsky, 2010; McCuaig et al., 2014). Therefore, the findings of the different analytical approaches utilised to investigate

Carlow Castle Cu-Co-Au deposit in this thesis are most logically synthesised through the development of a Carlow Castle Cu-Co-Au mineral system model. Although the components of the mineral systems framework vary slightly depending on mineralisation style, there are generally five key elements; (i) an energy source to drive the formation of the mineral system, (ii) ligands to complex with dissolved metals and allow for hydrothermal metal mobility, (iii) a fertile metalliferous source to provide ore metals for concentration into the ore deposit, (iv) a pathway through which ore fluids can be focussed and metals transported to their site of deposition, and (v) a physical or chemical trap to induce metal deposition and ore formation (Hagemann, Cassidy, Hagemann, & Brown, 2000; Hagemann et al., 2016; Huston, Stevens, Southgate, Muhling, & Wyborn, 2006). The components of this mineral systems model follow in the proceeding text and are summarised in Table 6.1 at the end of this section.

Apatite U-Pb geochronology (Chapter Three) suggests that Carlow Castle formed around 2955 Ma during the late stages of formation of the De Grey Superbasin (3066-2919 Ma). Specifically, this age of mineralisation coincided with the final stages of extension during the formation of the Mallina Basin (3015-2931), following subduction at the northwest margin of the Pilbara Craton. Whilst a genetic connection to the Prinsep Orogeny (~3070 Ma) had previously been suggested (Hickman, 2016), the age constraints provided in this thesis indicate that Carlow Castle significantly post-dates this orogenic event. As such, it is likely that the underlying energy source that drove the formation of Carlow Castle was related to increased heat flow during proximal rifting of the De Grey Superbasin and extensional reactivation of the Regal Thrust. Ultimately a magmatic source for the Carlow Castle mineral system is not evident, unlike coeval base-metal VMS mineralisation in the Whim Creek Basin, which is contemporaneous with proximal granitic magmatism of the Sisters Supersuite (2954-2919 Ma). Consequently, large-scale convective flow of hydrothermal fluids driven by increased

4165 geothermal gradients due to regional extension and rifting are likely to have been the primary
4166 driver of the Carlow Castle mineral system.

4167 The source and nature of metal complexing ligands in the Carlow Castle ore system is difficult
4168 to constrain without detailed analyses of ore-stage fluid inclusions. However, the most likely
4169 ligand for complexation with Cu and Co, was Cl^-, in addition to OH^- in the case of Au. This is
4170 suggested given the predominance of Cl^- complexation to transport Cu and Co in hydrothermal
4171 ore systems (Heinrich & Candela, 2014; Seward et al., 2014), and absence of evidence of
4172 alternative halide ligands such as F- (Chapter Two). Although reduced sulphur species, such
4173 as HS^-, commonly transport Au in hydrothermal solutions, the coeval paragenesis of Cu and
4174 Co with Au mineralisation within Carlow Castle imply synchronous transport of these ore
4175 metals. As it is unlikely that Cu and Co would be simultaneously soluble with Au in a HS^--rich
4176 fluid (Heinrich & Candela, 2014), also evidenced by the thermodynamic modelling conducted
4177 in Chapter Four, Cl^- and/or OH^- is suggested as the most likely ligand to complex with Au.
4178 Additionally, considering that Carlow Castle would most likely have been situated at the base
4179 of the Gorge Creek Basin at the time of ore formation, saline basinal fluids from the overlying
4180 sedimentary sequence may have contributed significantly to the Carlow Castle ore system. Any
4181 seawater contribution to such basinal fluids would have been relatively saline (6-24 wt. % NaCl
4182 equiv.), given the comparably greater salinity of Archean and Proterozoic seawaters relative to
4183 those of the Phanerozoic (Huston et al., 2010). This interpretation is supported by the slightly
4184 heavy $\delta^{34}S$ values of sulphide mineralisation at Carlow Castle (Chapter Four), which may be
4185 indicative of an isotopically heavy Archean seawater sulphate ($\delta^{34}S$ = 3-8‰) contribution from
4186 a basinal brine to the hydrothermal system (Crowe et al., 2013). The propylitic alteration
4187 assemblage that characterises the Carlow Castle deposit is interpreted to reflect a neutral pH
4188 (~6.0) ore fluid and peak fluid temperatures of ~300°C (Chapter Three). In consideration of

this evidence and thermodynamic modelling of the hydrothermal mobility of Cu and Co, it is argued that these conditions would have been consistent with metal mobilisation under oxidised conditions (Chapter Four). These relatively moderate fluid conditions (T ≈ 300°C, pH ≈ 6.0) further support the above interpretation of derivation of the Carlow Castle ore fluid from a basinal brine.

Unequivocally constraining metal sources in ore-forming systems is often challenging (Goldfarb & Groves, 2015; Groves et al., 2022). However, it is suggested herein that the mafic rocks that constitute a significant portion of the Roebourne greenstone belt surrounding Carlow Castle are the most probable source of ore metals for the Carlow Castle mineral system. This was initially suggested based on the strong metallogenic relationship between mafic igneous rocks and Co-rich ore deposits (Chapter Two), due to the significantly greater concentration of Co in mafic and ultramafic igneous rocks relative to other lithologies (Slack, Kimball, & Shedd, 2017b). This interpretation is also supported by Cu isotope analysis and Rayleigh fractionation modelling (Chapter Five). This Rayleigh fractionation modelling gave an estimated initial ore fluid Cu isotope composition of $\delta^{65}Cu$ = 0.33‰, which is consistent with an igneous rock reservoir (Liu et al., 2015). The lack of significant variation in Cu isotope composition between Co-rich and Co-poor ore mineral assemblages within the Carlow Castle ore body was interpreted to reflect a consistent metal source between these assemblages.

Given the occurrence of Carlow Castle through higher-order structures of the crustal-scale Regal Thrust, it is suggested to represent the critical fluid pathway that facilitated metal transport and concentration. Given the significant spatial extent of the Regal Thrust over the present-day northwest Pilbara Craton (Hickman, 2016), it is likely that it acted as a major regional conduit for fluid flow following extensional reactivation during formation of the De Grey Superbasin. Channelling of regional fluid flow, potentially from the overlying Gorge

Creek Basin, along the Regal Thrust and through metal-rich mafic rocks of the Roebourne greenstone belt would have allowed these ore fluids to be focussed into the mylonitised Carlow Castle shear zone. Following migration into the heavily tectonised Carlow Castle shear zone, metal precipitation most likely resulted from gradual equilibration of the Carlow Castle ore fluid with the cold, reduced wall-rocks of the Ruth Well and Nickol River Formations (Chapters Three and Five). This process is recorded through the lens of Cu isotopes analysis (Chapter Five), from an initially high alteration temperature (~300°C), isotopically light, and Cu-rich fluid to a comparably low temperature (<300°C), isotopically heavy, and Cu-poor fluid. This is evidenced by a transition from actinolite- and epidote-dominated to chlorite-dominated alteration assemblages, with a corresponding increase in δ^{65}Cu and decrease in Cu grade (ppm) in analysed samples due to Rayleigh isotope fractionation. Additionally, the progressive increase in sulphur fugacity within the ore mineral paragenetic sequence noted in Chapter Two may also be a symptom of this fluid evolution process. A progressive decline in temperature and oxygen fugacity and consequent decline in sulphur solubility within the system (Tornos & Heinrich, 2008), especially during the transition from sulphate- to sulphide-stable conditions, would be reflected in an apparent increase in sulphur precipitation into solid mineral phases. Whilst it was initially suggested that this observed increase in sulphur fugacity could reflect mixing with a sulphide-bearing sulphur source at the site of mineralisation, this is not evident in the sulphur isotope analysis conducted in Chapter Four. If this increase in sulphur fugacity was a product of the progressive addition of externally derived reduced sulphur to the system, this would most likely be reflected in distinct sulphur isotope compositions for low sulphur fugacity and high sulphur fugacity ore minerals. However, the indistinguishable sulphur isotope compositions of pyrrhotite (lower fS_2) and pyrite (higher fS_2) analysed in Chapter Four suggest that the progressive increase in sulphur fugacity within solid mineral

4237 phases reflects declining sulphur solubility due to declining temperature and oxygen fugacity,
4238 rather than the progressive addition of external sulphur to the hydrothermal system.

4239 Table 6.1 - Summary of mineral system model components for Carlow Castle Cu-Co-Au deposit.

Mineral system component	**Carlow Castle Cu-Co-Au deposit**	**Rationale**
Driver/energy source	• Major crustal extension and rifting of the proximal/overlying De Grey Superbasin. • Reactivation of crustal-scale Regal Thrust host structure around 2950 Ma. • Enhanced geothermal gradient related to crustal rifting, driving fluid flow. • Lack of proximal magmatic driver, unlike contemporaneous base-metal deposits in the Mallina and Whim Creek basins.	• Syn-ore apatite U-Pb dating, suggests a probable age around 2950 Ma, significantly post-dating Prinsep Orogeny (~3070 Ma). • Coincident crustal extension and formation of De Grey Superbasin. • Moderate peak alteration temperature (~300°C), not consistent with high temperature magmatic system. • Lack of proximal contemporaneous magmatic rocks associated with ore-formation in other deposits, i.e., Sisters Supersuite (2954-2919 Ma).
Metal complexing ligands	• Cu, Co, and Au complexation with Cl^- the most likely pathway for metal mobilization. • OH^- also a viable ligand for Au. • Complexation of metals with reduced sulphur species (HS^-) or alternative halide (F^-) ligands unlikely. • Cl^- potentially sourced from basinal brines of proximal/overlying De Grey Superbasin.	• Predominance of Cl- complexation as the primary pathway for metal mobilization in hydrothermal Cu-Co deposits. • Evidence from thermodynamic and experimental data on hydrothermal Cu, Co, and Au mobility. • Coeval mineralization of Cu, Co, and Au precludes transportation of Au within reduced sulphur complexes. • Ore formation coincident with formation of De Grey Superbasin; potential source of saline basinal brines.

		• Moderate temperature, neutral pH ore fluid consistent with basinal brine.
Metal source	• Mafic igneous rocks in surrounding Roebourne greenstone belt.	• Established association between mafic/ultramafic rocks and Co deposits due to Co-rich composition. • Significant volume of mafic and ultramafic igneous rocks is surrounding host terrane and host formation. • Cu isotope data suggest an initial fluid isotopic signature consistent with a mafic igneous source.
Fluid pathway	• Regal Thrust and connecting higher-order structures within Carlow Castle shear zone.	• Occurrence of Carlow Castle Cu-Co-Au deposit through shear zone within Regal Thrust. • Strongly structurally-controlled nature of Cu-Co-Au mineralisation. • Significant regional extent and crustal-scale of Regal Thrust, through mafic rocks of Roebourne greenstone belt.
Metal trap	• Channeling of ore fluids into complex trap structures within Carlow Castle shear zone. • Interaction between Carlow Castle ore fluid and wall-rocks. • Equilibration of hot (~300°C) oxidised metal-bearing ore fluid with cold and reduced host rocks within Carlow Castle shear zone.	• Transition in propylitic alteration assemblage from actinolite and epidote dominated to chlorite dominated records change in temperature but not fluid pH or composition. • Progressive ore fluid evolution recorded by correlation between Cu isotope signature, Cu grade, and alteration assemblage.

	• Transition from oxidised $SO4^{2-}$-stable to reduced HS^{-}-stable fluid conditions.	• Progressive increase in sulphur fugacity reflecting decreasing sulphur solubility during cooling and declining oxygen fugacity from $SO4^{2-}$-stable to HS^{-}-stable conditions. • Thermodynamic modelling supports a transition from oxidised to reduced fluid conditions to induce metal precipitation.

4240

6.2 Research implications, limitations, and outlook

Whilst Carlow Castle bears some similarities to previously observed Cu-Co(-Au) deposits, especially those of the relatively obscure polymetallic/Co-rich vein and metasedimentary rock-hosted Co-Cu-Au deposit types, e.g., Bou Azzer, Morocco; Cobalt, Ontario; Blackbird district, Idaho (Slack et al., 2017b). The Archean age of Carlow Castle clearly distinguishes it from these deposit types, of which no Archean examples are known. In fact, Carlow Castle is the oldest dated Cu-Co(-Au) deposit on Earth. As such, it is suggested that Carlow Castle may represent a distinct Archean analogue of the polymetallic/Co-rich vein deposit class due to similarities in geological characteristics between Carlow Castle and deposits of this class.

The rarity of Archean Cu-Co deposits in general is primarily due to the previously noted redox-sensitive nature of Cu and Co stability in hydrothermal environments and the limited supply of necessary oxidative fluids to crustal environments to mobilise these metals during the Archean. Therefore, the Mesoarchean age of Carlow Castle is significant as it suggests that the onset of hydrothermal Cu-Co ore-forming processes under relatively moderate hydrothermal conditions stretches back into the Archean, rather than from the Proterozoic following the Great Oxygenation Event. Importantly, this implies that analogous Cu-Co-Au deposits could exist throughout Archean terranes. However, the understanding of ore-forming processes in many of the more obscure hydrothermal Co-rich deposit types, i.e., non-sediment-hosted Cu-Co deposits, is currently relatively lacking. Whilst this thesis attempts to provide some insights into the genesis of a single Archean hydrothermal Cu-Co-Au deposit, further study of the relatively rare processes that produce significant Co enrichment in some hydrothermal ore deposits is still required, especially amongst Archean examples. Further study of the genesis of obscure Co-rich deposit classes (e.g., polymetallic/Co-rich vein, black shale-hosted Ni-Cu-Zn-Co, and metasedimentary rock-hosted Co-Cu-Au deposits) may provide insights into the

nature of these ore-forming processes. This may also include further study of the Carlow Castle mineral system, as there are still aspects of the mineral system to which further study would be beneficial. To this end, a fluid inclusion study of Carlow Castle would form a logical progression of the analysis conducted in this thesis and enhance the understanding of the Carlow Castle mineral system, particularly regarding the nature of the ligands and ore fluid that enabled metal mobilisation. However, comparative analysis of critical genetic differences between Co-poor and Co-rich deposits amongst relatively well understood mineralisation styles (e.g., sediment-hosted deposits and volcanogenic massive sulphide deposits) may also be effective in identifying the distinct ore-forming processes that impart significant Co endowments in some hydrothermal ore deposits of a given class, but not others.

On a more regional-scale, the probable genetic relationship of Carlow Castle Cu-Co-Au deposit to the latter stages of development of the Mallina Basin within the De Grey Superbasin around 2950 Ma reaffirm previous observations that this period produced the greatest variety of mineralization of any period in the development of the north west Pilbara Craton (Hickman, 2016). This observation is also strengthened by recent discoveries of significant Au mineralisation within the Mallina Basin; most notably the 6.8 million ounce Hemi Au deposit discovered in 2019 (De Grey Mining Limited, 2021). This may be of significance for the purpose of understanding regional metallogenesis during the formation of the Pilbara Craton and for broad-scale exploration targeting. However, this thesis has focussed primarily on the mineralogy, geochronology, and geochemistry of the Carlow Castle ore deposit. A study centred around both the broad structure and microstructural evidence for potential late deformation within the Carlow Castle, that could be correlated with regional studies on the structural evolution of the Pilbara Craton (Kiyokawa, Aihara, Takehara, & Horie, 2019;

Kiyokawa et al., 2002), would potentially provide useful insights into the formation of Carlow Castle and metallogenesis within the Pilbara Craton more broadly.

Results from multiple sulphur isotope analysis and thermodynamic modelling conducted in Chapter Four inform the understanding of the evolution of the Archean atmosphere and its potential relationship with Archean metallogeny. In particular, the notable absence of evidence of mass-independent sulphur isotope fractionation (MIF-S) supports the potential existence of a MIF-S minimum within during the Mesoarchean (Kasting & Ono, 2006). This is believed to have coincided with the early evolution of oxygenic photosynthesis and the development of one of Earth's first weakly ephemerally oxygenated surface environments, within the Pongola Basin around 2950 Ma. Evidence of oxygenation in the Pongola Basin has been implicated in triggering the Pongola Glaciation through oxidation of the methane-rich Archean atmosphere (Crowe et al., 2013; Eickmann et al., 2018; Ono et al., 2006; Planavsky et al., 2014). An oxidative origin for Carlow Castle is further supported through thermodynamic modelling of Cu-Co solubility under the established conditions of ore formation and consideration of the geological context of the deposit. As such, Carlow Castle could contribute distal evidence of a partially oxygenated atmosphere. The coincident timing of the formation of Carlow Castle and the Pongola Glaciation could demonstrate that oxygenic photosynthesis was already relatively widespread by the Mesoarchean. Though a potential mantle model is discussed and contrary reasoning presented in Chapter Four, some readers may find the oxidative model for the origin of Carlow Castle to be contentious as the potential for ephemeral oxygenation of surface environments prior to the Great Oxygenation Event is a relatively modern concept (Lyons et al., 2014). This interpretation reflects an evolution of ideas from Chapter Three, where a magmatic origin for Carlow Castle was tentatively suggested. Further research could focus on characterising the multiple sulphur isotope composition of broadly coeval hydrothermal ore

deposits and sedimentary rocks across the northwest Pilbara Craton and particularly within the Mallina Basin. Whilst several studies of Archean hydrothermal ore deposits within the adjacent Yilgarn Craton have focussed on utilising multiple sulphur isotopes to understand ore-forming processes, research applying this technique to understanding ore genesis within the Pilbara Craton is non-existent beyond the study presented here. As such, the application of multiple sulphur isotope analysis to understanding ore formation within the northwest Pilbara Craton would be novel and would provide useful insights into the crustal development of the northwest Pilbara Craton and regional metallogeny through the Archean.

Whilst the potential of Cu isotope analysis to understand Cu ore-forming processes and for Cu ore deposit exploration has been demonstrated in previous studies (Asael et al., 2007; Gregory & Mathur, 2017; Mathur & Wang, 2019), Chapter Five presents the first application of Cu isotope analysis to an Archean Cu ore deposit. Critically, the limited potential for redox cycling to induce isotopic fractionation in Archean ore-forming systems may imply that the isotopic signature of Archean Cu ores should display an unfractionated signature consistent with a bulk silicate Earth composition (Liu et al., 2015; Zhu et al., 2002). However, Cu mineralisation from Carlow Castle display a fractionated isotopically light composition relative to the bulk silicate Earth reservoir. Additionally, a correlation between Cu isotope signature, Cu ore grade, and hydrothermal alteration assemblage appears to record the physicochemical evolution of the Carlow Castle ore system. This suggests that Cu isotope analysis may be a useful tool in understanding Archean Cu ore systems and analysis of Cu ore minerals could be a novel tool to record the evolution of hydrothermal systems, especially when coupled with existing mineralogical and geochemical tools. However, the existing literature applying Cu isotope analysis to Archean geological systems is scant and the current understanding of the Cu isotope systematics of the Archean Earth is very limited. Therefore, whilst this study provides a

compelling proof of concept for the use of Cu isotope analysis to understand Archean Cu ore-forming systems, there is a need for further research in this space. Additionally, the relatively limited heavy isotopic fractionation of supergene Cu mineralisation from Carlow Castle bears implications for the use of Cu isotope analysis as a geochemical exploration tool. Previous studies primarily relied upon the significant heavy isotopic fractionation of Cu during weathering of Cu sulphide ores as a potential means to vector towards primary Cu ore deposits (Mathur & Wang, 2019). However, the majority of these studies focussed on porphyry Cu deposits with well-developed supergene leach caps and enrichment zones overlying primary Cu mineralisation. As such, the limited supergene isotopic fractionation reported here is an important consideration for future studies implementing Cu isotope analysis of supergene materials in structurally complex terranes, where supergene zonation around Cu sulphide deposits may be less defined. However, the study presented here is only focussed on a single case study area. The wider applicability of these interpretations would be strengthened by further research on supergene Cu isotope systematics in a wider variety of ore deposit settings.

References

Asael, D., Matthews, A., Bar-Matthews, M., & Halicz, L. (2007). Copper isotope fractionation in sedimentary copper mineralization (Timna Valley, Israel). *Chemical Geology, 243*(3), 238-254. doi:https://doi.org/10.1016/j.chemgeo.2007.06.007

Crowe, S. A., Døssing, L. N., Beukes, N. J., Bau, M., Kruger, S. J., Frei, R., & Canfield, D. E. (2013). Atmospheric oxygenation three billion years ago. *Nature, 501*, 535-538. doi:https://doi.org/10.1038/nature12426

De Grey Mining Limited. (2021). 6.8Moz Hemi Maiden Mineral Resource drives Mallina Gold Project [Press release]. Retrieved from https://www.asx.com.au/asxpdf/20210803/pdf/44yzld3b2kwz40.pdf

Eickmann, B., Hofmann, A., Wille, M., Bui, T., Wing, B. A., & Schoenberg, R. (2018). Isotopic evidence for oxygenated Mesoarchaean shallow oceans. *Nature Geoscience, 11*, 133-138. doi:https://doi.org/10.1038/s41561-017-0036-x

Goldfarb, R. J., & Groves, D. I. (2015). Orogenic gold: Common or evolving fluid and metal sources through time. *Lithos, 233*, 2-26. doi:https://doi.org/10.1016/j.lithos.2015.07.011

Gregory, M. J., & Mathur, R. (2017). Understanding Copper Isotope Behavior in the High Temperature Magmatic-Hydrothermal Porphyry Environment. *Geochemistry, Geophysics, Geosystems, 18*(11), 4000-4015. doi:https://doi.org/10.1002/2017GC007026

Groves, D. I., Santosh, M., Müller, D., Zhang, L., Deng, J., Yang, L.-Q., & Wang, Q.-F. (2022). Mineral systems: Their advantages in terms of developing holistic genetic models and for target generation in global mineral exploration. *Geosystems and Geoenvironment, 1*(1), 100001. doi:https://doi.org/10.1016/j.geogeo.2021.09.001

Hagemann, S. G., Cassidy, K. F., Hagemann, S. G., & Brown, P. E. (2000). Archean Orogenic Lode Gold Deposits. In *Gold in 2000* (Vol. 13, pp. 0): Society of Economic Geologists.

Hagemann, S. G., Lisitsin, V. A., & Huston, D. L. (2016). Mineral system analysis: Quo vadis. *Ore Geology Reviews, 76*, 504-522. doi:https://doi.org/10.1016/j.oregeorev.2015.12.012

Hayes, T. S., & Einaudi, M. T. (1986). Genesis of the Spar Lake strata-bound copper- silver deposit, Montana: part I. Controls inherited from sedimentation and preore diagenesis (USA). *Economic Geology, 81*(8), 1899-1931.

4382 Heinrich, C. A., & Candela, P. A. (2014). 13.1 - Fluids and Ore Formation in the Earth's Crust.
4383 In H. Holland & K. Turekian (Eds.), *Treatise on Geochemistry (Second Edition)* (Vol.
4384 13, pp. 1-28). Amsterdam: Elsevier Science.
4385 Hickman, A. H. (2016). *Northwest Pilbara Craton: a record of 450 million years in the growth*
4386 *of Archean continential crust*. Retrieved from Perth:
4387 Huston, D., Pehrsson, S., Eglington, B. M., & Zaw, K. (2010). The Geology and Metallogeny
4388 of Volcanic-Hosted Massive Sulfide Deposits: Variations through Geologic Time and
4389 with Tectonic Setting. *Economic Geology, 105*(3), 571-591.
4390 Huston, D. L., Mernagh, T. P., Hagemann, S. G., Doublier, M. P., Fiorentini, M., Champion,
4391 D. C., . . . Bastrakov, E. (2016). Tectono-metallogenic systems — The place of mineral
4392 systems within tectonic evolution, with an emphasis on Australian examples. *Ore*
4393 *Geology Reviews, 76*, 168-210. doi:https://doi.org/10.1016/j.oregeorev.2015.09.005
4394 Huston, D. L., Stevens, B., Southgate, P. N., Muhling, P., & Wyborn, L. (2006). Australian
4395 Zn-Pb-Ag Ore-Forming Systems: A Review and Analysis. *Economic Geology, 101*(6),
4396 1117-1157. doi:10.2113/gsecongeo.101.6.1117
4397 Kasting, J. F., & Ono, S. (2006). Palaeoclimates: the first two billion years. *Philosophical*
4398 *transactions of the Royal Society of London, 361*(1470), 917-929.
4399 doi:https://doi.org/10.1098/rstb.2006.1839
4400 Kiyokawa, S., Aihara, Y., Takehara, M., & Horie, K. (2019). Timing and development of
4401 sedimentation of the Cleaverville Formation and a post-accretion pull-apart system in
4402 the Cleaverville area, coastal Pilbara Terrane, Pilbara, Western Australia. *Island Arc,*
4403 *28*(6), e12324. doi:https://doi.org/10.1111/iar.12324
4404 Kiyokawa, S., Taira, A., Byrne, T., Bowring, S., & Sano, Y. (2002). Structural evolution of the
4405 middle Archean coastal Pilbara terrane, Western Australia. *Tectonics, 21*(5), 1-24.
4406 Liu, S.-A., Huang, J., Liu, J., Wörner, G., Yang, W., Tang, Y.-J., . . . Li, S. (2015). Copper
4407 isotopic composition of the silicate Earth. *Earth and Planetary Science Letters, 427*,
4408 95-103. doi:https://doi.org/10.1016/j.epsl.2015.06.061
4409 Lyons, T. W., Reinhard, C. T., & Planavsky, N. J. (2014). The rise of oxygen in Earth's early
4410 ocean and atmosphere. *Nature, 506*, 307-315. doi:https://doi.org/10.1038/nature13068
4411 Mathur, R., & Wang, D. (2019). Transition Metal Isotopes Applied to Exploration
4412 Geochemistry. In S. Decrée & L. Robb (Eds.), *Ore Deposits: Origin, Exploration, and*
4413 *Exploitation* (1 ed., Vol. 242): American Geophysical Union and John Wiley and Sons.

McCuaig, T. C., Beresford, S., & Hronsky, J. (2010). Translating the mineral systems approach into an effective exploration targeting system. *Ore Geology Reviews, 38*(3), 128-138. doi:https://doi.org/10.1016/j.oregeorev.2010.05.008

McCuaig, T. C., Hronsky, J. M. A., Kelley, K. D., & Golden, H. C. (2014). The Mineral System Concept: The Key to Exploration Targeting. In *Building Exploration Capability for the 21st Century* (Vol. 18, pp. 0): Society of Economic Geologists.

Ono, S., Beukes, N. J., Rumble, D., & Fogel, M. L. (2006). Early evolution of atmospheric oxygen from multiple-sulfur and carbon isotope records of the 2.9 Ga Mozaan Group of the Pongola Supergroup, Southern Africa. *South African Journal of Geology, 109*(1-2), 97-108. doi:https://doi.org/10.2113/gssajg.109.1-2.97

Planavsky, N. J., Asael, D., Hofmann, A., Reinhard, C. T., LaLonde, S. V., Knudsen, A. C., . . . Rouxel, O. (2014). Evidence for oxygenic photosynthesis half a billion years before the Great Oxidation Event. *Nature Geoscience, 7*, 283-286. doi:https://doi.org/10.1038/ngeo2122

Seward, T. M., Williams-Jones, A. E., & Migdisov, A. A. (2014). 13.2 - The Chemistry of Metal Transport and Deposition by Ore-Forming Hydrothermal Fluids. In H. Holland & K. Turekian (Eds.), *Treatise on Geochemistry (Second Edition)* (Vol. 13, pp. 29-57). Amsterdam: Elsevier Science.

Slack, J. F., Kimball, B. E., & Shedd, K. B. (2017a). *Cobalt* (1802F). Retrieved from Reston, VA: http://pubs.er.usgs.gov/publication/pp1802F

Tornos, F., & Heinrich, C. A. (2008). Shale basins, sulfur-deficient ore brines and the formation of exhalative base metal deposits. *Chemical Geology, 247*(1), 195-207. doi:https://doi.org/10.1016/j.chemgeo.2007.10.011

Wyborn, L. A. I., Heinrich, C. A., & Jaques, A. L. (1994). Australian Proterozoic mineral systems: essential ingredients and mappable criteria. *Australian Institute of Mining and Metallurgy Publication Series*(94), 109-115.

Zhu, X. K., Guo, Y., Williams, R. J. P., O'Nions, R. K., Matthews, A., Belshaw, N. S., . . . Salvato, B. (2002). Mass fractionation processes of transition metal isotopes. *Earth and Planetary Science Letters, 200*(1-2), 47-62. doi:https://doi.org/10.1016/S0012-821X(02)00615-5

Bibliography

Ahmed, H. A., Arai, S., & Ikenne, M. (2009). Mineralogy and Paragenesis of the Co-Ni Arsenide Ores of Bou Azzer, Anti-Atlas, Morocco. *Economic Geology, 104*(2), 249-266.

Albut, G., Kamber, B. S., Brüske, A., Beukes, N. J., Smith, A. J. B., & Schoenberg, R. (2019). Modern weathering in outcrop samples versus ancient paleoredox information in drill core samples from a Mesoarchaean marine oxygen oasis in Pongola Supergroup, South Africa. *Geochimica et Cosmochimica Acta, 265*, 330-353. doi:https://doi.org/10.1016/j.gca.2019.09.001

Anbar, A. D., Duan, Y., Lyons, T. W., Arnold, G. L., Kendall, B., Creaser, R. A., . . . Buick, R. (2007). A Whiff of Oxygen Before the Great Oxidation Event? *Science, 317*(5846), 1903-1906. doi:https://doi.org/10.1126/science.1140325

Arrobas, D. L. P., Hund, K. L., McCormick, M. S., Ningthoujam, J., & Drexhage, J. R. (2017). *The Growing Role of Minerals and Metals for a Low Carbon Future*. Retrieved from Washington, D.C.: http://documents.worldbank.org/curated/en/207371500386458722/The-Growing-Role-of-Minerals-and-Metals-for-a-Low-Carbon-Future

Artemis Resources Limited. (2017). Cobalt Update - Carlow Castle Project [Press release]. Retrieved from https://artemisresources.com.au/investors-relations/announcements

Artemis Resources Limited. (2018a). 2.32% Cobalt in Shallow Drilling at Carlow Castle [Press release]. Retrieved from https://artemisresources.com.au/investors-relations/announcements

Artemis Resources Limited. (2018b). 4.5 Mt of Cobalt/Copper/Gold JORC Resources at Carlow Castle - Karratha, Western Australia [Press release]. Retrieved from https://artemisresources.com.au/investors-relations/announcements

Artemis Resources Limited. (2018c). High Grade Cobalt Drilled over 1.2km at Carlow Castle [Press release]. Retrieved from https://www.asx.com.au/asxpdf/20181015/pdf/43z7lvpq8r2kvt.pdf

Artemis Resources Limited. (2019a). 5,000m Diamond Drilling Programme for Carlow Castle [Press release]. Retrieved from https://artemisresources.com.au/investors-relations/announcements

Artemis Resources Limited. (2019b). Carlow Castle Au-Cu-Co Resource Grows by 71% to 7.7Mt [Press release]. Retrieved from https://artemisresources.com.au/investors-relations/announcements

Artemis Resources Limited. (2019c). Significant Resource Increase for Carlow Castle [Press release]. Retrieved from https://www.asx.com.au/asxpdf/20191120/pdf/44brd03vh31ncw.pdf

Artemis Resources Limited. (2021). June 2021 Quarterly Report [Press release]. Retrieved from https://wcsecure.weblink.com.au/pdf/ARV/02400741.pdf

Asadi, S., Mathur, R., Moore, F., & Zarasvandi, A. (2015). Copper isotope fractionation in the Meiduk porphyry copper deposit, Northwest of Kerman Cenozoic magmatic arc, Iran. *Terra Nova, 27*(1), 36-41. doi:https://doi.org/10.1111/ter.12128

Asael, D., Matthews, A., Bar-Matthews, M., & Halicz, L. (2007). Copper isotope fractionation in sedimentary copper mineralization (Timna Valley, Israel). *Chemical Geology, 243*(3), 238-254. doi:https://doi.org/10.1016/j.chemgeo.2007.06.007

Asael, D., Matthews, A., Oszczepalski, S., Bar-Matthews, M., & Halicz, L. (2009). Fluid speciation controls of low temperature copper isotope fractionation applied to the Kupferschiefer and Timna ore deposits. *Chemical Geology, 262*(3), 147-158. doi:https://doi.org/10.1016/j.chemgeo.2009.01.015

Babiker, M., & Gudmundsson, A. (2004). The effects of dykes and faults on groundwater flow in an arid land: the Red Sea Hills, Sudan. *Journal of Hydrology, 297*(1), 256-273. doi:https://doi.org/10.1016/j.jhydrol.2004.04.018

Barrett, T. J., Maclean, W. H., & Cattalani, S. (1991). Massive sulfide deposits of the Noranda area, Quebec. III. The Ansil mine *Canadian Journal of Earth Sciences, 28*(11), 1699-1730.

Bethke, C. M. (1996). *Geochemical Reaction Modeling: concepts and applications*. Oxford, UK: Oxford University Press.

Bookstrom, A. A. (2013). The Idaho cobalt belt. *Northwest Geology, 42*, 149-162.

Bookstrom, A. A., Box, S. E., Cossette, P. M., Frost, T. P., Gillerman, V. S., King, G. R., & Zirakparvar, N. A. (2016). Geologic history of the Blackbird Co-Cu district in the Lemhi subbasin of the Belt-Purcell Basin. In J. S. MacLean & J. W. Sears (Eds.), *Belt Basin: Window to Mesoproterozoic Earth: Geological Society of America Special Paper* (Vol. 522, pp. 185-219). United States: Geological Society of America.

Bornhorst, T. J., & Mathur, R. (2017). Copper Isotope Constraints on the Genesis of the Keweenaw Peninsula Native Copper District, Michigan, USA. *Minerals, 7*(10). doi:10.3390/min7100185

Bouabdellah, M., Maacha, L., Levresse, G., & Saddiqi, O. (2016). The Bou Azzer Co–Ni–Fe–As(±Au ± Ag) District of Central Anti-Atlas (Morocco): A Long-Lived Late Hercynian to Triassic Magmatic-Hydrothermal to Low-Sulphidation Epithermal System. In M. Bouabdellah & J. F. Slack (Eds.), *Mineral Deposits of North Africa* (pp. 229-247). Cham: Springer International Publishing.

Boucher, S. M. (2011). *Ore Petrology and Alteration of the West Ansil Volcanic-hosted Massive Sulphide Deposit of the Noranda Mining Camp, Rouyn-Noranda, Québec.* (Master of Science Degree in Earth Sciences Master of Science), University of Ottawa, Ottawa.

Braxton, D., & Mathur, R. (2011). Exploration Applications of Copper Isotopes in the Supergene Environment: A Case Study of the Bayugo Porphyry Copper-Gold Deposit, Southern Philippines. *Economic Geology, 106*(8), 1447-1463. doi:https://doi.org/10.2113/econgeo.106.8.1447

British Geological Survey. (2015). *Risk List 2015*. Retrieved from Nottingham, United Kingdom:

Britt, A., Summerfield, D., Senior, A., Kay, P., Huston, D., Hitchman, A., . . . Schofield, A. (2017). *Australia's Identified Mineral Resources 2017*. Retrieved from Canberra:

Brocks, J. J., Logan, G. A., Buick, R., & Summons, R. E. (1999). Archean Molecular Fossils and the Early Rise of Eukaryotes. *Science, 285*(5430), 1033-1036. doi:10.1126/science.285.5430.1033

Brown, A. C. (2014). Low-Temperature Sediment-Hosted Copper Deposits. In K. Turekian & H. Holland (Eds.), *Treatise on Geochemistry* (2nd ed., Vol. 13, pp. 251-271). Oxford: Elsevier Science.

Brugger, J., Etschmann, B., Liu, W., Testemale, D., Hazemann, J., Emerich, H., & Beek, W. (2007). An XAFS study of the structure and thermodynamics of Cu(I) chloride complexes in brines up to supercritical conditions (400°C, 600 bars). *Geochimica et Cosmochimica Acta, 71*(20), 4920-4941. doi:https://doi.org/10.1016/j.gca.2007.08.003

Brugger, J., Liu, W., Etschmann, B., Mei, Y., Sherman, D. M., & Testemale, D. (2016). A review of the coordination chemistry of hydrothermal systems, or do coordination

changes make ore deposits? *Chemical Geology, 447*, 219-253. doi:https://doi.org/10.1016/j.chemgeo.2016.10.021

Cabral, A. R., Creaser, R. A., Nägler, T., Lehmann, B., Voegelin, A. R., Belyatsky, B., . . . Escher, P. (2013). Trace-element and multi-isotope geochemistry of Late-Archean black shales in the Carajás iron-ore district, Brazil. *Chemical Geology, 362*, 91-104. doi:https://doi.org/10.1016/j.chemgeo.2013.08.041

Canfield, D. E. (2004). The evolution of the Earth surface sulfur reservoir. *American Journal of Science, 304*(10), 839-861. doi:https://doi.org/10.2475/ajs.304.10.839

Catling, D. C., & Zahnle, K. J. (2020). The Archean Atmosphere. *Science Advances, 6*(9), 1-16. doi:https://doi.org/10.1126/sciadv.aax1420

Cherniak, D. J. (2005). Uranium and manganese diffusion in apatite. *Chemical Geology, 219*(1-4), 297-308.

Cherniak, D. J., Lanford, W. A., & Ryerson, F. J. (1991). Lead diffusion in apatite and zircon using ion implantation and Rutherford Backscattering techniques. *Geochimica et Cosmochimica Acta, 55*(6), 1663-1673.

Chi Fru, E., Rodríguez, N. P., Partin, C. A., Lalonde, S. V., Andersson, P., Weiss, D. J., . . . Konhauser, K. O. (2016). Cu isotopes in marine black shales record the Great Oxidation Event. *Proceedings of the National Academy of Sciences, 113*(18), 4941. doi:10.1073/pnas.1523544113

Chi, G., Liu, Y., & Dube, B. (2009). Relationship between CO2-dominated fluids, hydrothermal alterations and gold mineralization in the Red Lake greenstone belt, Canada. *Applied Geochemistry, 24*, 504-516.

Corbett, G. J., & Leach, T. M. (1997). Southwest Pacific Rim gold-copper systems: Structure, alteration and mineralization. *Society of Economic Geologists Special Publication, 6*, 240. doi:https://doi.org/10.5382/SP.06

Cox, D. P., Lindsey, D. A., Singer, D. A., & Diggles, M. F. (2003). *Sediment-hosted copper deposits of the world: Deposit models and database* (2003-107). Retrieved from http://pubs.er.usgs.gov/publication/ofr2003107

Crerar, D., & Barnes, H. (1976). Ore solution chemistry; V, Solubilities of chalcopyrite and chalcocite assemblages in hydrothermal solution at 200 degrees to 350 degrees C. *Economic Geology, 71*(4), 772-794.

4571 Crowe, S. A., Døssing, L. N., Beukes, N. J., Bau, M., Kruger, S. J., Frei, R., & Canfield, D. E.
4572 (2013). Atmospheric oxygenation three billion years ago. *Nature, 501*, 535-538.
4573 doi:https://doi.org/10.1038/nature12426
4574 Czaja, A. D., Johnson, C. M., Roden, E. E., Beard, B. L., Voegelin, A. R., Nägler, T. F., . . .
4575 Wille, M. (2012). Evidence for free oxygen in the Neoarchean ocean based on coupled
4576 iron–molybdenum isotope fractionation. *Geochimica et Cosmochimica Acta, 86*, 118-
4577 137. doi:https://doi.org/10.1016/j.gca.2012.03.007
4578 De Caritat, P., Hutcheon, I., & Walshe, J. L. (1993). Chlorite Geothermometry: A Review.
4579 *Clays and Clay Minerals, 41*(2), 219-239.
4580 De Grey Mining Limited. (2021). 6.8Moz Hemi Maiden Mineral Resource drives Mallina Gold
4581 Project [Press release]. Retrieved from
4582 https://www.asx.com.au/asxpdf/20210803/pdf/44yzld3b2kwz40.pdf
4583 de Kock, M. O., Evans, D. A. D., & Beukes, N. J. (2009). Validating the existence of Vaalbara
4584 in the Neoarchean. *Precambrian Research, 174*(1-2), 145-154.
4585 doi:https://doi.org/10.1016/j.precamres.2009.07.002
4586 de Melo, G. H. C., Monteiro, L. V. S., Xavier, R. P., Moreto, C. P. N., & Santiago, E. (2019).
4587 Tracing Fluid Sources for the Salobo and Igarapé Bahia Deposits: Implications for the
4588 Genesis of the Iron Oxide Copper-Gold Deposits in the Carajás Province, Brazil.
4589 *Economic Geology, 114*(4), 697-718.
4590 de Melo, G. H. C., Monteiro, L. V. S., Xavier, R. P., Moreto, C. P. N., Santiago, E., Dufrane,
4591 S. A., . . . Santos, A. F. F. (2017). Temporal evolution of the giant Salobo IOCG deposit,
4592 Carajás Province (Brazil): constraints from paragenesis of hydrothermal alteration and
4593 U-Pb geochronology. *Mineralium Deposita, 52*, 709-732.
4594 Dekov, V. M., Rouxel, O., Asael, D., Hålenius, U., & Munnik, F. (2013). Native Cu from the
4595 oceanic crust: Isotopic insights into native metal origin. *Chemical Geology, 359*, 136-
4596 149. doi:https://doi.org/10.1016/j.chemgeo.2013.10.001
4597 Domagal-Goldman, S. D., Kasting, J. F., Johnston, D. T., & Farquhar, J. (2008). Organic haze,
4598 glaciations and multiple sulfur isotopes in the Mid-Archean Era. *Earth and Planetary*
4599 *Science Letters, 265*(1-2), 29-40. doi:https://doi.org/10.1016/j.epsl.2008.01.040
4600 Duan, Y., Anbar, A. D., Arnold, G. L., Lyons, T. W., Gordon, G. W., & Kendall, B. (2010).
4601 Molybdenum isotope evidence for mild environmental oxygenation before the Great
4602 Oxidation Event. *Geochimica et Cosmochimica Acta, 74*(23), 6655-6668.
4603 doi:https://doi.org/10.1016/j.gca.2010.08.035

Ehrlich, S., Butler, I., Halicz, L., Rickard, D., Oldroyd, A., & Matthews, A. (2004). Experimental study of the copper isotope fractionation between aqueous Cu(II) and covellite, CuS. *Chemical Geology, 209*(3), 259-269. doi:https://doi.org/10.1016/j.chemgeo.2004.06.010

Eickmann, B., Hofmann, A., Wille, M., Bui, T., Wing, B. A., & Schoenberg, R. (2018). Isotopic evidence for oxygenated Mesoarchaean shallow oceans. *Nature Geoscience, 11*, 133-138. doi:https://doi.org/10.1038/s41561-017-0036-x

Eigenbrode, J. L., Freeman, K. H., & Summons, R. E. (2008). Methylhopane biomarker hydrocarbons in Hamersley Province sediments provide evidence for Neoarchean aerobiosis. *Earth and Planetary Science Letters, 273*(3), 323-331. doi:https://doi.org/10.1016/j.epsl.2008.06.037

En-Naciri, A., Barbanson, L., & Touray, J. (1997). Brine inclusions from the Co-As(Au) Bou Azzer District, Anti-Atlas Mountains, Morocco. *Economic Geology, 92*(3), 360-367.

Eremenco, D., Mortimer, R., & Mead, E. (2019). Delineating cobalt targets from a galvanic and inductive source Sub-Audio Magnetics (SAM) at the Carlow Castle project, Western Australia. *ASEG Extended Abstracts, 2019*(1), 1-4. doi:10.1080/22020586.2019.12072960

Eriksson, K. A. (1982). Geometry and internal characteristics of Archaean submarine channel deposits, Pilbara Block, Western Australia. *Journal of Sedimentary Research, 52*(2), 383-393. doi:10.1306/212F7F5E-2B24-11D7-8648000102C1865D

Essaraj, S., Boiron, M., Cathelineau, M., Banks, D. A., & Benharref, M. (2005). Penetration of surface-evaporated brines into the Proterozoic basement and deposition of Co and Ag at Bou Azzer (Morocco): Evidence from fluid inclusions. *Journal of African Earth Sciences, 41*(1-2), 25-39.

European Commission. (2017). *The 2017 List of Critical Raw Materials for the EU*. Retrieved from Brussels, Belgium:

Evans, M. E., & Muxworthy, A. R. (2018). Vaalbara Palaeomagnetism. *Canadian Journal of Earth Sciences, 56*(9), 912-916. doi:https://doi.org/10.1139/cjes-2018-0081

Farquhar, J., Bao, H., & Thiemens, M. (2000). Atmospheric Influence of Earth's Earliest Sulfur Cycle. *Science, 289*(5480), 756-758. doi:https://doi.org/10.1126/science.289.5480.756

Farquhar, J., Peters, M., Johnston, D. T., Strauss, H., Masterson, A. L., Wiechert, U., & Kaufman, A. J. (2007). Isotopic evidence for Mesoarchaean anoxia and changing

4636 atmospheric sulphur chemistry. *Nature, 449*, 706-709.
4637 doi:https://doi.org/10.1038/nature06202
4638 Farquhar, J., & Wing, B. A. (2003). Multiple sulfur isotopes and the evolution of the
4639 atmosphere. *Earth and Planetary Science Letters, 213*(1-2), 1-13.
4640 doi:https://doi.org/10.1016/S0012-821X(03)00296-6
4641 Farquhar, J., Wu, N., Canfield, D. E., & Oduro, H. (2010). Connections between Sulfur Cycle
4642 Evolution, Sulfur Isotopes, Sediments, and Base Metal Sulfide Deposits. *Economic*
4643 *Geology, 105*(3), 509-533. doi:10.2113/gsecongeo.105.3.509
4644 Ferrill, D. A., Winterle, J., Wittmeyer, G. W., Sims, D., Colton, S. L., & Armstrong, A. (1999).
4645 *Stressed Rock Strains Groundwater at Yucca Mountain, Nevada*.
4646 Fox, D., Spinks, S., Barham, M., Kirkland, C. L., Pearce, M. A., Aspandiar, M., . . . Mead, E.
4647 (2021). Working up an apatite: Enigmatic Mesoarchean hydrothermal Cu-Co-Au
4648 mineralization in the Pilbara Craton. *Economic Geology, 116*(7), 1561-1573.
4649 doi:https://doi.org/10.5382/econgeo.4842
4650 Fox, D., Spinks, S., Pearce, M. A., Barham, M., Le Vaillant, M., Thorne, R., . . . Verrall, M.
4651 (2019). Plundering Carlow Castle: First Look at a Unique Mesoarchean-Hosted Cu-Co-
4652 Au Deposit. *Economic Geology, 114*(6), 1021-1031.
4653 doi:https://doi.org/10.5382/econgeo.4672
4654 Franklin, J. M., Gibson, H. L., Jonasson, I. R., & Galley, A. G. (2005). Volcanogenic Massive
4655 Sulfide Deposits. In J. W. Hedenquist, J. F. H. Thompson, R. J. Goldfarb, & J. P.
4656 Richards (Eds.), *Economic Geology One Hundredth Anniversary Volume* (pp. 523-
4657 560). Littleton, Colorado: Society of Economic Geologists.
4658 Frei, R., Gaucher, C., Poulton, S. W., & Canfield, D. E. (2009). Fluctuations in Precambrian
4659 atmospheric oxygenation recorded by chromium isotopes. *Nature, 461*, 250–253.
4660 doi:https://doi.org/10.1038/nature08266
4661 Fryer, B. J., & Taylor, R. P. (1987). Rare-earth element distributions in uraninites: Implications
4662 for ore genesis. *Chemical Geology, 63*(1-2), 101-108.
4663 Fujii, T., Moynier, F., Abe, M., Nemoto, K., & Albarède, F. (2013). Copper isotope
4664 fractionation between aqueous compounds relevant to low temperature geochemistry
4665 and biology. *Geochimica et Cosmochimica Acta, 110*, 29-44.
4666 doi:https://doi.org/10.1016/j.gca.2013.02.007
4667 Gaboury, D. (2019). Parameters for the formation of orogenic gold deposits. *Applied Earth*
4668 *Science*, 1-10.

Galley, A. G., Jonasson, I. R., & Watkinson, D. H. (2000). Magnetite-rich calc-silicate alteration in relation to synvolcanic intrusion at the Ansil volcanogenic massive sulfide deposit, Rouyn-Noranda, Quebec, Canada. *Mineralium Deposita, 35*, 619-637.

Galley, A. G., Watkinson, D. H., Jonasson, I. R., & Riverin, G. (1995). The Subsea-Floor Formation of Volcanic-Hosted Massive Sulfide: Evidence from the Ansil Deposit, Rouyn-Noranda, Canada. *Economic Geology, 90*(7), 2006–2017.

Garvin, J., Buick, R., Anbar, A. D., Arnold, G. L., & Kaufman, A. J. (2009). Isotopic Evidence for an Aerobic Nitrogen Cycle in the Latest Archean. *Science, 323*(5917), 1045-1048. doi:https://doi.org/10.1126/science.1165675

Goldfarb, R. J., Bradley, D. W., & Leach, D. L. (2010). Secular Variation in Economic Geology. *Economic Geology, 105*(3), 459-465.

Goldfarb, R. J., & Groves, D. I. (2015). Orogenic gold: Common or evolving fluid and metal sources through time. *Lithos, 233*, 2-26. doi:https://doi.org/10.1016/j.lithos.2015.07.011

Golubev, S. V., Benezeth, P., Schott, J., Dandurand, J. L., & Castillo, A. (2009). Siderite dissolution kinetics in acidic aqueous solutions from 25 to 100 °C and 0 to 50 atm pCO2. *Chemical Geology, 265*(1-2), 13-19.

Gregory, M. J., & Mathur, R. (2017). Understanding Copper Isotope Behavior in the High Temperature Magmatic-Hydrothermal Porphyry Environment. *Geochemistry, Geophysics, Geosystems, 18*(11), 4000-4015. doi:https://doi.org/10.1002/2017GC007026

Groves, D. I., Goldfarb, R. J., Gebre-Mariam, M., Hagemann, S. G., & Robert, F. (1998). Orogenic gold deposits: A proposed classification in the context of their crustal distribution and relationship to other gold deposit types. *Ore Geology Reviews, 13*, 7-27.

Groves, D. I., & Santosh, M. (2015). Province-scale commonalities of some world-class gold deposits: Implications for mineral exploration. *Geoscience Frontiers, 6*(3), 389-399. doi:https://doi.org/10.1016/j.gsf.2014.12.007

Groves, D. I., Santosh, M., Müller, D., Zhang, L., Deng, J., Yang, L.-Q., & Wang, Q.-F. (2022). Mineral systems: Their advantages in terms of developing holistic genetic models and for target generation in global mineral exploration. *Geosystems and Geoenvironment, 1*(1), 100001. doi:https://doi.org/10.1016/j.geogeo.2021.09.001

Grundler, P. V., Brugger, J., Etschmann, B., Helm, L., Liu, W., Spry, P. G., . . . Pring, A. (2013). Speciation of aqueous tellurium(IV) in hydrothermal solutions and vapors, and the role of oxidized tellurium species in Te transport and gold deposition. *Geochimica et Cosmochimica Acta, 120*.

Guy, B. M., Ono, S., Gutzmer, J., Kaufman, A. J., Lin, Y., Fogel, M. L., & Beukes, N. J. (2012). A multiple sulfur and organic carbon isotope record from non-conglomeratic sedimentary rocks of the Mesoarchean Witwatersrand Supergroup, South Africa. *Precambrian Research, 216-219*, 208-231. doi:https://doi.org/10.1016/j.precamres.2012.06.018

Hagemann, S. G., Cassidy, K. F., Hagemann, S. G., & Brown, P. E. (2000). Archean Orogenic Lode Gold Deposits. In *Gold in 2000* (Vol. 13, pp. 0): Society of Economic Geologists.

Hagemann, S. G., Lisitsin, V. A., & Huston, D. L. (2016). Mineral system analysis: Quo vadis. *Ore Geology Reviews, 76*, 504-522. doi:https://doi.org/10.1016/j.oregeorev.2015.12.012

Halevy, I., Johnston, D. T., & Schrag, D. P. (2010). Explaining the Structure of the Archean Mass-Independent Sulfur Isotope Record. *Science, 329*(5988), 204-207. doi:https://doi.org/10.1126/science.1190298

Hayes, T. S., Cox, D. P., Bliss, J. D., Piatak, N. M., & Seal Ii, R. R. (2015). *Sediment-hosted stratabound copper deposit model* (2010-5070M). Retrieved from Reston, VA: http://pubs.er.usgs.gov/publication/sir20105070M

Hayes, T. S., & Einaudi, M. T. (1986). Genesis of the Spar Lake strata-bound copper- silver deposit, Montana: part I. Controls inherited from sedimentation and preore diagenesis (USA). *Economic Geology, 81*(8), 1899-1931.

Hedenquist, J. W., Arribas, A., & Gonzalez-Urien, E. (2000). Exploration for Epithermal Gold Deposits *SEG Reviews, 13*, 245-277.

Heinrich, C. A., & Candela, P. A. (2014). 13.1 - Fluids and Ore Formation in the Earth's Crust. In H. Holland & K. Turekian (Eds.), *Treatise on Geochemistry (Second Edition)* (Vol. 13, pp. 1-28). Amsterdam: Elsevier Science.

Helgeson, H. C., Delany, J. M., Nesbitt, H. W., & Bird, D. K. (1978). Summary and critique of the thermodynamic properties of rock-forming minerals. *American Journal of Science, 278A*, 229.

Henley, R. W., & Ellis, A. J. (1983). Geothermal Systems Ancient and Modern: A Geochemical Review. *Earth-Science Reviews, 19*(1), 1-50. doi:https://doi.org/10.1016/0012-8252(83)90075-2

Hickman, A. H. (1983). *Geology of the Pilbara Block and its environs / by Arthur H. Hickman*. Perth [W.A.]: Geological Survey of Western Australia.

Hickman, A. H. (2002). *Geology of the Roebourne 1:100 000 sheet*. Retrieved from

Hickman, A. H. (2004a). Two contrasting granite−greenstone terranes in the Pilbara Craton, Australia: evidence for vertical and horizontal tectonic regimes prior to 2900 Ma. *Precambrian Research, 131*(3-4), 153-172.

Hickman, A. H. (2004b). Two contrasting granite−greenstone terranes in the Pilbara Craton, Australia: evidence for vertical and horizontal tectonic regimes prior to 2900Ma. *Precambrian Research, 131*(3), 153-172. doi:https://doi.org/10.1016/j.precamres.2003.12.009

Hickman, A. H. (2012). Review of the Pilbara Craton and Fortescue Basin, Western Austrlia: Crustal evolution providing environments for early life. *Island Arc, 21*(1), 1-31.

Hickman, A. H. (2016). *Northwest Pilbara Craton: a record of 450 million years in the growth of Archean continential crust*. Retrieved from Perth:

Hickman, A. H. (2021). *East Pilbara Craton: a record of one billion years in the growth of Archean continental crust*. Retrieved from

Hickman, A. H., Huston, D., Van Kranendonk, M. J., & Smithies, R. H. (2006). *Geology and mineralization of the west Pilbara - a field guide*. Retrieved from

Hickman, A. H., Smithies, R. H., & Tyler, I. M. (2010). *Evolution of active plate margins: West Pilbara Superterrane, De Grey Superbasin, and the Fortescue and Hamersley Basins — a field guide*. Retrieved from Perth:

Hickman, A. H., & Van Kranendonk, M. J. (2012). Early Earth evolution: Evidence from the 3.5-1.8 Ga geological history of the Pilbara region of Western Australia. *Episodes, 35*(1), 283-297. doi:https://doi.org/10.18814/epiiugs/2012/v35i1/028

Hiebert, R. S., Bekker, A., Houlé, M. G., & Rouxel, O. J. (2018). Depositional setting of the Late Archean Fe oxide- and sulfide-bearing chert and graphitic argillite in the Shaw Dome, Abitibi greenstone belt, Canada. *Precambrian Research, 311*, 98-116. doi:https://doi.org/10.1016/j.precamres.2018.04.004

Hitzman, M., Bookstrom, A. A., Slack, J. F., & Zientek, M. L. (2017). *Cobalt—Styles of Deposits and the Search for Primary Deposits*. Retrieved from Virginia: https://doi.org/10.3133/ofr20171155

Hitzman, M., Kirkham, R. V., Broughton, D., Thorson, J., & Selley, D. (2005). The Sediment-Hosted Stratiform Copper Ore System. *Economic Geology, 100th Anniversary Volume*, 609-642. doi:https://doi.org/10.5382/AV100.19

Hitzman, M., Selley, D., & Bull, S. (2010). Formation of Sedimentary Rock-Hosted Stratiform Copper Deposits through Earth History. *Economic Geology, 105*(3), 627-639. doi:https://doi.org/10.2113/gsecongeo.105.3.627

Hoashi, M., Bevacqua, D. C., Otake, T., Watanabe, Y., Hickman, A. H., Utsunomiya, S., & Ohmoto, H. (2009). Primary haematite formation in an oxygenated sea 3.46 billion years ago. *Nature Geoscience, 2*, 301-306. doi:https://doi.org/10.1038/ngeo465

Hoatson, D. M., & Sun, S. (2002). Archean Layered Mafic-Ultramafic Intrusions in the West Pilbara Craton, Western Australia: A Synthesis of Some of the Oldest Orthomagmatic Mineralizing Systems in the World. *Economic Geology, 97*(4), 847-872.

Hofmann, B. A. (1999). *Geochemistry of Natural Redox Fronts - A Review*. Retrieved from Wettingen, Switzerland:

Horn, S., Gunn, A. G., Petavratzi, E., Shaw, R. A., Eilu, P., Törmänen, T., . . . Wall, F. (2021). Cobalt resources in Europe and the potential for new discoveries. *Ore Geology Reviews, 130*, 103915. doi:https://doi.org/10.1016/j.oregeorev.2020.103915

Hou, Q., Zhou, L., Gao, S., Zhang, T., Feng, L., & Yang, L. (2016). Use of Ga for mass bias correction for the accurate determination of copper isotope ratio in the NIST SRM 3114 Cu standard and geological samples by MC-ICPMS. *Journal of Analytical Atomic Spectrometry, 31*(1), 280-287. doi:10.1039/C4JA00488D

Hughes, J. M., & Rakovan, J. F. (2015). Structurally Robust, Chemically Diverse: Apatite and Apatite Supergroup Minerals. *Elements, 11*(3), 165-170.

Huston, D. (2006). Mineralization and regional alteration at the Mons Cupri stratiform Cu–Zn–Pb deposit, Pilbara Craton, Western Australia. *Mineralium Deposita, 41*, 17-32. doi:https://doi.org/10.1007/s00126-005-0036-4

Huston, D., Blewett, R., Keillor, B., Standing, J., Smithies, R. H., Marshall, A., . . . Kamprad, J. (2002a). Lode Gold and Epithermal Deposits of the Mallina Basin, North Pilbara Terrain, Western Australia. *Economic Geology, 97*(4), 801-818.

Huston, D., Blewett, R., Mernagh, T., Sun, S., & Kamprad, J. (2001). *Gold Deposits of the Pilbara Craton: Results of AGSO Research*. Retrieved from Canberra:

Huston, D., Pehrsson, S., Eglington, B. M., & Zaw, K. (2010). The Geology and Metallogeny of Volcanic-Hosted Massive Sulfide Deposits: Variations through Geologic Time and with Tectonic Setting. *Economic Geology, 105*(3), 571-591.

Huston, D., Smithies, R. H., & Sun, S. (2000). Correlation of the Archaean Mallina ‐ Whim Creek Basin: Implications for base ‐ metal potential of the central part of the Pilbara granite ‐ greenstone terrane. *Australian Journal of Earth Sciences, 47*(2), 217-230.

Huston, D., Sun, S., Blewett, R., Hickman, A. H., Van Kranendonk, M. J., Philips, D., . . . Brauhart, C. (2002b). The Timing of Mineralization in the Archean North Pilbara Terrain, Western Australia. *Economic Geology, 97*(4), 733-755.

Huston, D. L., Mernagh, T. P., Hagemann, S. G., Doublier, M. P., Fiorentini, M., Champion, D. C., . . . Bastrakov, E. (2016). Tectono-metallogenic systems — The place of mineral systems within tectonic evolution, with an emphasis on Australian examples. *Ore Geology Reviews, 76*, 168-210. doi:https://doi.org/10.1016/j.oregeorev.2015.09.005

Huston, D. L., Stevens, B., Southgate, P. N., Muhling, P., & Wyborn, L. (2006). Australian Zn-Pb-Ag Ore-Forming Systems: A Review and Analysis. *Economic Geology, 101*(6), 1117-1157. doi:10.2113/gsecongeo.101.6.1117

Jansson, N. F., & Liu, W. (2020). Controls on cobalt and nickel distribution in hydrothermal sulphide deposits in Bergslagen, Sweden - constraints from solubility modelling. *GFF, 142*(2), 87-95. doi:https://doi.org/10.1080/11035897.2020.1751270

Johnson, A. C., Ostrander, C. M., Romaniello, S. J., Reinhard, C. T., Greaney, A. T., Lyons, T. W., & Anbar, A. D. (2021). Reconciling evidence of oxidative weathering and atmospheric anoxia on Archean Earth. *Science Advances, 7*(40), eabj0108. doi:doi:10.1126/sciadv.abj0108

Johnston, D. T. (2011). Multiple sulfur isotopes and the evolution of Earth's surface sulfur cycle. *Earth-Science Reviews, 106*(1-2), 161-183. doi:https://doi.org/10.1016/j.earscirev.2011.02.003

JORC. (2012). *Australasian Code for Reporting of Exploration Results, Mineral Resources and Ore Reserves*. Retrieved from

Kasting, J. F., & Ono, S. (2006). Palaeoclimates: the first two billion years. *Philosophical transactions of the Royal Society of London, 361*(1470), 917-929. doi:https://doi.org/10.1098/rstb.2006.1839

Kato, Y., Ohta, I., Tsunematsu, T., Watanabe, Y., Isozaki, Y., Maruyama, S., & Imai, N. (1998). Rare earth element variations in mid-Archean banded iron formations: implications for the chemistry of ocean and continent and plate tectonics. *Geochimica et Cosmochimica Acta, 62*(21-22), 3475-3497.

Kato, Y., Suzuki, K., Nakamura, K., Hickman, A. H., Nedachi, M., Kusakabe, M., . . . Ohmoto, H. (2009). Hematite formation by oxygenated groundwater more than 2.76 billion years ago. *Earth and Planetary Science Letters, 278*(1-2), 40-49. doi:https://doi.org/10.1016/j.epsl.2008.11.021

Kaufman, A. J., Johnston, D. T., Farquhar, J., Masterson, A. L., Lyons, T. W., Bates, S., . . . Arnold, G. L. (2007). Late Archean Biospheric Oxygenation and Atmospheric Evolution. *Science, 317*(5846), 1900-1903. doi:https://doi.org/10.1126/science.1138700

Keith, M., Smith, D. J., Jenkin, G. R. T., Holwell, D. A., & Dye, M. T. (2018). A review of Te and Se systematics in hydrothermal pyrite from precious metal deposits: Insights into ore-forming processes. *Ore Geology Reviews, 96*, 269-282.

Kemp, A. I. S., Hickman, A. H., Kirkland, C. L., & Vervoort, J. (2015). Hf isotopes in detrital and inherited zircons of the Pilbara Craton provide no evidence for Hadean continents. *Precambrian Research, 261*, 112-126.

Kendall, B. (2021). Recent Advances in Geochemical Paleo-Oxybarometers. *The Annual Review of Earth and Planetary Sciences, 49*(1), 399-433. doi:https://doi.org/10.1146/annurev-earth-071520-051637

Kendall, B., Brennecka, G. A., Weyer, S., & Anbar, A. D. (2013). Uranium isotope fractionation suggests oxidative uranium mobilization at 2.50Ga. *Chemical Geology, 362*, 105-114. doi:https://doi.org/10.1016/j.chemgeo.2013.08.010

Kendall, B., Creaser, R. A., Reinhard, C. T., Lyons, T. W., & Anbar, A. D. (2015). Transient episodes of mild environmental oxygenation and oxidative continental weathering during the late Archean. *Science Advances, 1*(10), 6. doi:https://doi.org/10.1126/sciadv.1500777

Kendall, B., Reinhard, C. T., Lyons, T. W., Kaufman, A. J., Poulton, S. W., & Anbar, A. D. (2010). Pervasive oxygenation along late Archaean ocean margins. *Nature Geoscience, 3*(9), 647-652. doi:10.1038/ngeo942

Kerrich, R., & Fyfe, W. S. (1981). The gold—carbonate association: Source of CO2, and CO2 fixation reactions in Archaean lode deposits. *Chemical Geology, 33*(1-4), 265-294.

Kerrich, R., Goldfarb, R. J., Groves, D. I., Garwin, S., & Jia, Y. (2000). The characteristics, origins, and geodynamic settings of supergiant gold metallogenic provinces. *Science in China D: Earth Sciences, 43*(1), 1-68.

Kerrich, R., & Said, N. (2011). Extreme positive Ce-anomalies in a 3.0Ga submarine volcanic sequence, Murchison Province: Oxygenated marine bottom waters. *Chemical Geology, 280*(1), 232-241. doi:https://doi.org/10.1016/j.chemgeo.2010.11.012

Killingsworth, B. A., Sansjofre, P., Philippot, P., Cartigny, P., Thomazo, C., & Lalonde, S. V. (2019). Constraining the rise of oxygen with oxygen isotopes. *Nature Communications, 10*(1), 4924. doi:10.1038/s41467-019-12883-2

Kim, Y., Lee, I., Oyungerel, S., Jargal, L., & Tsedenbal, T. (2019). Cu and S isotopic signatures of the Erdenetiin Ovoo porphyry Cu-Mo deposit, northern Mongolia: Implications for their origin and mineral exploration. *Ore Geology Reviews, 104*, 656-669. doi:https://doi.org/10.1016/j.oregeorev.2018.11.025

Kirkham, R. V. (1989). Distribution, Settings, and Genesis of Sediment-hosted Stratiform Copper Deposits. *Geological Association of Canada Special Paper, 36*, 3-38.

Kirkland, C. L., Yakymchuk, C., Szilas, K., Evans, N. J., Hollis, J., McDonald, B., & Gardiner, N. J. (2018). Apatite: a U-Pb thermochronometer or geochronometer? *Lithos, 138-139*, 143-157.

Kirschbaum, M. J., & Hitzman, M. (2016). Guelb moghrein: An unusual carbonate-hosted iron oxide copper-gold deposit in Mauritania, Northwest Africa. *Economic Geology, 111*(3), 763-770.

Kissin, S. A. (1992). Five-element (Ni-Co-As-Ag-Bi) Veins. *Geoscience Canada, 19*(3), 113-124.

Kiyokawa, S., Aihara, Y., Takehara, M., & Horie, K. (2019). Timing and development of sedimentation of the Cleaverville Formation and a post-accretion pull-apart system in the Cleaverville area, coastal Pilbara Terrane, Pilbara, Western Australia. *Island Arc, 28*(6), e12324. doi:https://doi.org/10.1111/iar.12324

Kiyokawa, S., Taira, A., Byrne, T., Bowring, S., & Sano, Y. (2002). Structural evolution of the middle Archean coastal Pilbara terrane, Western Australia. *Tectonics, 21*(5), 1-24.

Kolb, J., Meyer, F. M., Vennemann, T., Hoffbauer, R., Gerdes, A., & Sakellaris, G. A. (2008). Geological setting of the Guelb Moghrein Fe oxide-Cu-Au-Co mineralization, Akjoujt area, Mauritania. *Geological Society, London, Special Publications, 297*, 53-75.

Kolb, J., Meyer, F. M., Vennemann, T., Sindern, S., Prantl, S., Bottcher, M. E., & Sakellaris, G. A. (2010). Characterisation of the Hydrothermal Fluids of the Guelb Moghrein Iron Oxide-Cu-Au-Co Deposit, Mauritania: Ore Mineral Chemistry, Fluid Inclusions and Isotope Geochemistry. In T. M. Porter (Ed.), *Hydrothermal Iron Oxide Copper-Gold and Related Deposits: A Global Perspective - Advances in the Understanding of IOCG Deposits* (Vol. 4, pp. 553-572). Adelaide: PGC Publishing.

Kolb, J., & Petrov, N. (2016). The Guelb Moghrein Cu–Au deposit: Neoarchaean hydrothermal sulfide mineralization in carbonate-facies iron formation. *Ore Geology Reviews, 78*, 573-577.

Krneta, S., Ciobanu, C. L., Cook, N. L., Ehrig, K., & Kontonikas-Charos, A. (2017). Rare Earth Element Behaviour in Apatite from the Olympic Dam Cu–U–Au–Ag Deposit, South Australia. *Minerals, 7*(8), 135.

LaFlamme, C., Martin, L., Jeon, H., Reddy, S. M., Selvaraja, V., Caruso, S., . . . Kilburn, M. R. (2016). In situ multiple sulfur isotope analysis by SIMS of pyrite, chalcopyrite, pyrrhotite, and pentlandite to refine magmatic ore genetic models. *Chemical Geology, 444*(1), 1-15. doi:https://doi.org/10.1016/j.chemgeo.2016.09.032.

Larson, P. B., Maher, K., Ramos, F. C., Chang, Z., Gaspar, M., & Meinert, L. D. (2003). Copper isotope ratios in magmatic and hydrothermal ore-forming environments. *Chemical Geology, 201*(3), 337-350. doi:https://doi.org/10.1016/j.chemgeo.2003.08.006

Le Blanc, M., & Billaud, P. (1982). Cobalt Arsenide Orebodies Related to an Upper Proterozoic Ophiolite: Bou Azzer (Morocco). *Economic Geology, 77*(1), 162-175.

Le Vaillant, M., Barnes, S. J., Fiorentini, M. L., Barnes, S., Bath, A., & Miller, J. (2018). Platinum-group element and gold contents of arsenide and sulfarsenide minerals associated with Ni and Au deposits in Archean greenstone belts. *Mineralogical Magazine, 82*(3), 325-347.

Lefebure, D. V. (1996). Five-element Veins Ag-Ni-Co-As+/-(Bi,U). In D. V. Lefebure & T. Höy (Eds.), *Selected British Columbia Mineral Deposit Profiles* (Vol. 2, pp. 89-92). Vancouver: British Columbia Ministry of Employment and Investment.

Leonard, M. D., Michaelides, E. E., & Michaelides, D. N. (2020). Energy storage needs for the substitution of fossil fuel power plants with renewables. *Renewable Energy, 145*, 951-962. doi:https://doi.org/10.1016/j.renene.2019.06.066

Li, W., Jackson, S. E., Pearson, N. J., & Graham, S. (2010). Copper isotopic zonation in the Northparkes porphyry Cu–Au deposit, SE Australia. *Geochimica et Cosmochimica Acta, 74*(14), 4078-4096. doi:https://doi.org/10.1016/j.gca.2010.04.003

Liu, S.-A., Huang, J., Liu, J., Wörner, G., Yang, W., Tang, Y.-J., . . . Li, S. (2015). Copper isotopic composition of the silicate Earth. *Earth and Planetary Science Letters, 427*, 95-103. doi:https://doi.org/10.1016/j.epsl.2015.06.061

Liu, S., Borg, S., Testemale, D., Etschmann, B., Hazemann, J., & Brugger, J. (2011). Speciation and thermodynamic properties for cobalt chloride complexes in hydrothermal fluids at 35–440° C and 600 bar: an in-situ XAS study. *Geochimica et Cosmochimica Acta, 75*(5), 1227-1248. doi:https://doi.org/10.1016/j.gca.2010.12.002

Liu, S., Li, D., Li, S., Teng, F., Ke, S., He, Y., & Lu, Y. (2014a). High-precision copper and iron isotope analysis of igneous rock standards by MC-ICP-MS. *Journal of Analytical Atomic Spectrometry, 29*, 122-133. doi:https://doi.org/10.1039/C3JA50232E

Liu, S., Li, Y., Liu, J., Yang, Z., Liu, J., & Shi, Y. (2021). Equilibrium Cu isotope fractionation in copper minerals: a first-principles study. *Chemical Geology, 564*, 120060. doi:https://doi.org/10.1016/j.chemgeo.2021.120060

Liu, W., Brugger, J., McPhail, D. C., & Spiccia, L. (2002). A spectrophotometric study of aqueous copper(I)–chloride complexes in LiCl solutions between 100 °C and 250 °C. *Geochimica et Cosmochimica Acta, 66*(20), 3615-3633. doi:https://doi.org/10.1016/S0016-7037(02)00942-0

Liu, W., Etschmann, B., Testemale, D., Hazemann, J., Rempel, K., Muller, H., & Brugger, J. (2014b). Gold transport in hydrothermal fluids: Competition among the Cl−, Br−, HS− and NH3(aq) ligands. *Chemical Geology, 376*, 11-19.

Liu, W., & McPhail, D. C. (2005). Thermodynamic properties of copper chloride complexes and copper transport in magmatic-hydrothermal solutions. *Chemical Geology, 221*(1-2), 21-39. doi:https://doi.org/10.1016/j.chemgeo.2005.04.009

Loukola-Ruskeeniemi, K., & Lahtinen, H. (2013). Multiphase evolution in the black-shale-hosted Ni–Cu–Zn–Co deposit at Talvivaara, Finland. *Ore Geology Reviews, 52*, 85-99. doi:https://doi.org/10.1016/j.oregeorev.2012.10.006

Ludwig, K. R. (1991). *ISOPLOT: A Plotting and Regression Program for Radiogenic-Isotope Data*. Retrieved from Denver, Colorado:

Luskin, C., Wilson, A., Gold, D., & Hofmann, A. (2019). The Pongola Supergroup: Mesoarchaean Deposition Following Kaapvaal Craton Stabilization. In A. Kröner & A. Hofmann (Eds.), *The Archaean Geology of the Kaapvaal Craton, Southern Africa* (pp. 225-254). Cham: Springer International Publishing.

Lyons, T. W., & Gill, B. C. (2010). Ancient Sulfur Cycling and Oxygenation of the Early Biosphere. *Elements, 6*(2), 93-99. doi:https://doi.org/10.2113/gselements.6.2.93

Lyons, T. W., Reinhard, C. T., & Planavsky, N. J. (2014). The rise of oxygen in Earth's early ocean and atmosphere. *Nature, 506*, 307-315. doi:https://doi.org/10.1038/nature13068

Maher, K. C., Jackson, S., & Mountain, B. (2011). Experimental evaluation of the fluid–mineral fractionation of Cu isotopes at 250°C and 300°C. *Chemical Geology, 286*(3), 229-239. doi:https://doi.org/10.1016/j.chemgeo.2011.05.008

Mao, M., Rukhlov, A. S., Rowins, S. M., Spence, J., & Coogan, L. A. (2016). Apatite Trace Element Compositions: A Robust New Tool for Mineral Exploration. *Economic Geology, 111*(5), 1187-1222.

Markl, G., Lahaye, Y., & Schwinn, G. (2006). Copper isotopes as monitors of redox processes in hydrothermal mineralization. *Geochimica et Cosmochimica Acta, 70*(16), 4215-4228. doi:https://doi.org/10.1016/j.gca.2006.06.1369

Mathur, R., Dendas, M., Titley, S., & Phillips, A. (2010). Patterns in the Copper Isotope Composition of Minerals in Porphyry Copper Deposits in Southwestern United States. *Economic Geology, 105*(8), 1457-1467. doi:10.2113/econgeo.105.8.1457

Mathur, R., Falck, H., Belogub, E., Milton, J. E., Wilson, M., Rose, A., & Powell, W. (2018). Origins of Chalcocite Defined by Copper Isotope Values. *Geofluids, 2018*, 1-9.

Mathur, R., & Fantle, M. S. (2015). Copper Isotopic Perspectives on Supergene Processes: Implications for the Global Cu Cycle. *Elements, 11*(5), 323-329. doi:10.2113/gselements.11.5.323

Mathur, R., Jin, L., Prush, V., Paul, J., Ebersole, C., Fornadel, A., . . . Brantley, S. (2012). Cu isotopes and concentrations during weathering of black shale of the Marcellus Formation, Huntingdon County, Pennsylvania (USA). *Chemical Geology, 304-305*, 175-184. doi:https://doi.org/10.1016/j.chemgeo.2012.02.015

Mathur, R., Munk, L., Nguyen, M., Gregory, M., Annell, H., & Lang, J. (2013). Modern and Paleofluid Pathways Revealed by Cu Isotope Compositions in Surface Waters and Ores

of the Pebble Porphyry Cu-Au-Mo Deposit, Alaska. *Economic Geology, 108*(3), 529-541. doi:10.2113/econgeo.108.3.529

Mathur, R., Ruiz, J., Titley, S., Liermann, L., Buss, H., & Brantley, S. (2005). Cu isotopic fractionation in the supergene environment with and without bacteria. *Geochimica et Cosmochimica Acta, 69*(22), 5233-5246. doi:https://doi.org/10.1016/j.gca.2005.06.022

Mathur, R., Titley, S., Barra, F., Brantley, S., Wilson, M., Philips, A., . . . Hart, G. (2009). Exploration potential of Cu isotope fractionation in porphyry copper deposits. *Journal of Geochemical Exploration, 102*, 1-6.

Mathur, R., & Wang, D. (2019). Transition Metal Isotopes Applied to Exploration Geochemistry. In S. Decrée & L. Robb (Eds.), *Ore Deposits: Origin, Exploration, and Exploitation* (1 ed., Vol. 242): American Geophysical Union and John Wiley and Sons.

McCuaig, T. C., Beresford, S., & Hronsky, J. (2010). Translating the mineral systems approach into an effective exploration targeting system. *Ore Geology Reviews, 38*(3), 128-138. doi:https://doi.org/10.1016/j.oregeorev.2010.05.008

McCuaig, T. C., Hronsky, J. M. A., Kelley, K. D., & Golden, H. C. (2014). The Mineral System Concept: The Key to Exploration Targeting. In *Building Exploration Capability for the 21st Century* (Vol. 18, pp. 0): Society of Economic Geologists.

Meinert, L. D. (1992). Skarns and Skarn Deposits. *Geoscience Canada, 19*(4), 145-162.

Meinert, L. D., Dipple, G. M., & Nicolescu, S. (2005). World Skarn Deposits. In J. W. Hedenquist, J. F. H. Thompson, R. J. Goldfarb, & J. P. Richards (Eds.), *Economic Geology* (Vol. One Hundredth Anniversary Volume): Society of Economic Geologists.

Midgisov, A. A., Zezin, D., & Williams-Jones, A. E. (2011). An experimental study of cobalt (II) complexation in Cl− and H2S-bearing hydrothermal solutions. *Geochimica et Cosmochimica Acta, 75*(14), 4065-4079. doi:https://doi.org/10.1016/j.gca.2011.05.003

Mikucki, E. J., & Ridley, J. R. (1993). The hydrothermal fluid of Archa an lode-gold deposits at different metamorphic grades: compositional constraints from ore and wallrock alteration assemblages. *Mineralium Deposita, 28*, 469-481.

Mills, K. C. (1974). *Thermodynamic data for inorganic sulphides, selenides and tellurides*. London: Butterworths.

Misra, K. C. (2000). Skarn Deposits. In K. C. Misra (Ed.), *Understanding Mineral Deposits*. Dordrecht: Springer.

Morgan, L. A., & Schulz, K. J. (2012). Physical Volcanology of Volcanogenic Massive Sulfide Deposits. In W. C. P. Shanks, III & R. Thurston (Eds.), *Volcanogenic Massive Sulfide*

5019 *Occurrence Model* (Vol. 2010–5070–C, pp. 61-100). Reston, Virginia: U.S. Geological
5020 Survey.
5021 Moynier, F., Vance, D., Fujii, T., & Savage, P. (2017). The Isotope Geochemistry of Zinc and
5022 Copper. *Reviews in Mineralogy and Geochemistry, 82*(1), 543-600.
5023 doi:10.2138/rmg.2017.82.13
5024 Mudd, G. M., Weng, Z. H., Jowitt, S. M., Turnbull, I. D., & Graedel, T. E. (2013). Quantifying
5025 the recoverable resources of by-product metals: The case of cobalt. *Ore Geology*
5026 *Reviews, 55*, 87-98.
5027 Mudd, G. M., Werner, T. T., Weng, Z. H., Yellitshetty, M., Yuan, Y., McAlpine, S. R. B., . . .
5028 Czarnota, K. (2018). *Critical Minerals in Australia: A Review of Opportunities and*
5029 *Research Needs*. Retrieved from Canberra, Australia:
5030 Mueller, A. G., Lawrance, L. M., Muhling, J., & Pooley, G. D. (2012). Mineralogy and PTX
5031 relationships of the Archean Hannan South Au-Cu (Co-Bi) deposit, Kalgoorlie,
5032 Western Australia: Thermodynamic constraints on the formation of a zoned intrusion-
5033 related skarn. *Economic Geology, 107*(1), 1-24.
5034 Muller, E., Philippot, P., Bard-Rollion, C., & Cartigny, P. (2016). Multiple sulfur-isotope
5035 signatures in Archean sulfates and their implications for the chemistry and dynamics of
5036 the early atmosphere. *Proceedings of the National Academy of Sciences, 113*(27), 7432-
5037 7437. doi:https://doi.org/10.1073/pnas.1520522113
5038 Oberthür, T., Melcher, F., Henjes-Kunst, F., Gerdes, A., Stein, H., Zimmerman, A., & El
5039 Ghorfi, M. (2009). Hercynian age of the cobalt-nickel-arsenide-(Gold) Ores, Bou
5040 Azzer, Anti-Atlas, Morocco: Re-Os, Sm-Nd, and U-Pb age determinations. *Economic*
5041 *Geology, 104*(7), 1065-1079.
5042 Ohmoto, H. (2020). A seawater-sulfate origin for early Earth's volcanic sulfur. *Nature*
5043 *Geoscience, 13*, 576-583. doi:https://doi.org/10.1038/s41561-020-0601-6
5044 Ohmoto, H., Watanabe, Y., Ikemi, H., Poulson, S. R., & Taylor, B. E. (2006). Sulphur isotope
5045 evidence for an oxic Archaean atmosphere. *Nature, 442*, 908-911.
5046 doi:https://doi.org/10.1038/nature05044
5047 Olivetti, E. A., Ceder, G., Gaustad, G. G., & Fu, X. (2017). Lithium-Ion Battery Supply Chain
5048 Considerations: Analysis of Potential Bottlenecks in Critical Metals. *Joule, 1*(2), 229-
5049 243.
5050 Ono, S., Beukes, N. J., Rumble, D., & Fogel, M. L. (2006). Early evolution of atmospheric
5051 oxygen from multiple-sulfur and carbon isotope records of the 2.9 Ga Mozaan Group

of the Pongola Supergroup, Southern Africa. *South African Journal of Geology, 109*(1-2), 97-108. doi:https://doi.org/10.2113/gssajg.109.1-2.97

Openpit Mining Limited. (1987). *Roebourne Project Progress Report of Exploration for 1987*. Retrieved from Perth: https://geodocsget.dmirs.wa.gov.au/api/GeoDocsGet?filekey=d8f8222d-9c0f-4a7d-9cb1-3188991bf768-m7nok2ay4ykgnw2exiit357u15npjxp0wx8891s1

Ossa Ossa, F., Hofmann, A., Spangenberg, J. E., Poulson, S. W., Stüeken, E. E., Schoenberg, R., . . . Bekker, A. (2019). Limited oxygen production in the Mesoarchean ocean. *Proceedings of the National Academy of Sciences, 116*(14), 6647-6652. doi:https://doi.org/10.1073/pnas.1818762116

Ossa Ossa, F., Hofmann, A., Vidal, O., Kramers, J. D., Belyanin, G., & Cavallazi, B. (2016). Unusual manganese enrichment in the Mesoarchean Mozaan Group, Pongola Supergroup, South Africa. *Precambrian Research, 281*, 414-433. doi:https://doi.org/10.1016/j.precamres.2016.06.009

Ossa Ossa, F., Hofmann, A., Wille, M., Spangenberg, J. E., Bekker, A., Poulton, S. W., . . . Schoenberg, R. (2018). Aerobic iron and manganese cycling in a redox-stratified Mesoarchean epicontinental sea. *Earth and Planetary Science Letters, 500*, 28-40. doi:https://doi.org/10.1016/j.epsl.2018.07.044

Ostrander, C. M., Johnson, A. C., & Anbar, A. D. (2021). Earth's First Redox Revolution. *Annual Review of Earth and Planetary Sciences, 49*(1), 337-366. doi:10.1146/annurev-earth-072020-055249

Palacios, C., Rouxel, O., Reich, M., Cameron, E. M., & Leybourne, M. I. (2011). Pleistocene recycling of copper at a porphyry system, Atacama Desert, Chile: Cu isotope evidence. *Mineralium Deposita, 46*(1), 1-7. doi:10.1007/s00126-010-0315-6

Paton, C., Hellstrom, J., Paul, B., Woodhead, J., & Hergt, J. (2011). Iolite: Freeware for the visualisation and processing of mass spectrometric data. *Journal of Analytical Atomic Spectrometry, 26*(12), 2508-2518.

Pękala, M., Asael, D., Butler, I. B., Matthews, A., & Rickard, D. (2011). Experimental study of Cu isotope fractionation during the reaction of aqueous Cu(II) with Fe(II) sulphides at temperatures between 40 and 200°C. *Chemical Geology, 289*(1), 31-38. doi:https://doi.org/10.1016/j.chemgeo.2011.07.004

Petavratzi, E., Gunn, G., & Kresse, C. (2019). *Commodity Review: Cobalt*. Retrieved from

5084 Peterson, A., Kemp, A. I. S., Hickman, A. H., Whitehouse, M. J., Martin, L., & Gray, C. M.
5085 (2019). A new 3.59 Ga magmatic suite and a chondritic source to the east Pilbara
5086 Craton. *Chemical Geology, 511*, 51-70.
5087 Philippot, P., Ávila, J. N., Killingsworth, B. A., Tessalina, S., Baton, F., Caquineau, T., . . .
5088 Busigny, V. (2018). Globally asynchronous sulphur isotope signals require re-
5089 definition of the Great Oxidation Event. *Nature Communications, 9*(1), 2245.
5090 doi:10.1038/s41467-018-04621-x
5091 Pike, G., Cas, R., & Smithies, R. H. (2002). Geologic Constraints on Base Metal Mineralization
5092 of the Whim Creek Greenstone Belt, Pilbara Craton, Western Australia. *Economic*
5093 *Geology, 97*(4), 827-845. doi:https://doi.org/10.2113/gsecongeo.97.4.827
5094 Pirajno, F. (2009). Hydrothermal Processes and Wall Rock Alteration. In F. Pirajno (Ed.),
5095 *Hydrothermal Processes and Mineral Systems* (Vol. 1, pp. 73-164). Dordrecht:
5096 Springer.
5097 Planavsky, N. J., Asael, D., Hofmann, A., Reinhard, C. T., LaLonde, S. V., Knudsen, A. C., . .
5098 . Rouxel, O. (2014). Evidence for oxygenic photosynthesis half a billion years before
5099 the Great Oxidation Event. *Nature Geoscience, 7*, 283-286.
5100 doi:https://doi.org/10.1038/ngeo2122
5101 Plasil, J. (2014). Oxidation–hydration weathering of uraninite: the current state-of-knowledge.
5102 *Journal of Geosciences, 59*(2), 99-114.
5103 Pokrovski, G. S., Akinfie, V., Borisova, A. Y., Zotov, A. V., & Kouzmanov, K. (2014). Gold
5104 speciation and transport in geological fluids: insights from experiments and physical-
5105 chemical modelling. In P. S. Garofalo & J. R. Ridley (Eds.), *Gold-Transporting*
5106 *Hydrothermal Fluids in the Earth's Crust* (Vol. Special Publications 402). London:
5107 Geological Society.
5108 Postma, D. (1983). Pyrite and siderite oxidation in swamp sediments. *Journal of Soil Science,*
5109 *34*(1), 163-182.
5110 Reed, M. H. (1997). Hydrothermal Alteration and Its Relationship to Ore Fluid Composition.
5111 In H. L. Barnes (Ed.), *Geochemistry of Hydrothermal Ore Deposits* (3 ed., pp. 303-
5112 365). New York: Wiley.
5113 Reinhard, C. T., Planavsky, N. J., & Lyons, T. W. (2013). Long-term sedimentary recycling of
5114 rare sulphur isotope anomalies. *Nature, 497*(7447), 100-103. doi:10.1038/nature12021

Reinhard, C. T., Raiswell, R., Scott, C., Anbar, A. D., & Lyons, T. W. (2009). A Late Archean Sulfidic Sea Stimulated by Early Oxidative Weathering of the Continents. *Science, 326*(5953), 713-716. doi:https://doi.org/10.1126/science.1176711

Reyes, A. G. (1990). Petrology of Philippine geothermal systems and the application of alteration mineralogy to their assessment. *Journal of Volcanology and Geothermal Research, 43*(1-2), 279-309. doi:https://doi.org/10.1016/0377-0273(90)90057-M

Riding, R., Fralick, P., & Liang, L. (2014). Identification of an Archean marine oxygen oasis. *Precambrian Research, 251*, 232-237. doi:https://doi.org/10.1016/j.precamres.2014.06.017

Ripley, E. M., Dong, S., Li, C., & Wasylenki, L. E. (2015). Cu isotope variations between conduit and sheet-style Ni–Cu–PGE sulfide mineralization in the Midcontinent Rift System, North America. *Chemical Geology, 414*, 59-68. doi:https://doi.org/10.1016/j.chemgeo.2015.09.007

Rose, A. (1989). Mobility of Copper and Other Heavy Metals in Sedimentary Environments. *Special Paper - Geological Association of Canada, 36*, 97-110.

Rosing, M. T., & Frei, R. (2004). U-rich Archaean sea-floor sediments from Greenland – indications of >3700 Ma oxygenic photosynthesis. *Earth and Planetary Science Letters, 217*(3), 237-244. doi:https://doi.org/10.1016/S0012-821X(03)00609-5

Ruddock, I. (1999a). *Mineral occurences and exploration potential of the west Pilbara*. Retrieved from Perth, Western Australia:

Ruddock, I. (1999b). *Mineral occurrences and exploration potential of the West Pilbara / by I. Ruddock*. Perth, W.A: Geological Survey of Western Australia.

Saintilan, N. J., Selby, D., Creaser, R. A., & Dewaele, S. (2017). Sulphide Re-Os geochronology links orogenesis, salt and Cu-Co ores in the Central African Copperbelt. *Scientific Reports, 8*(1).

Sakellaris, G. A., & Meyer, F. M. (2008). *A metamorphic origin of the Guelb Moghrein Fe oxide-copper-gold-cobalt deposit, Mauritania.* Paper presented at the XIII International conference on thermobarogeochemistry and IVth APIFIS symposium, Moscow.

Saunders, J. A., Hofstra, A. H., Goldfarb, R. J., & Reed, M. H. (2014). 13.15 - Geochemistry of Hydrothermal Gold Deposits. In H. Holland & K. Turekian (Eds.), *Treatise on Geochemistry* (2 ed., Vol. 13, pp. 383-424). Amsterdam: Elsevier.

Saunders, J. A., & Schoenly, P. A. (1995). Boiling, colloid nucleation and aggregation, and the genesis of bonanza Au-Ag ores of the sleeper deposit, Nevada. *Mineralium Deposita, 30*(3-4), 199-210.

Schmitz, M. D., Bowring, S., & Ireland, T. R. (2003). Evaluation of Duluth complex anorthositic series (AS3) zircon as a U-Pb geochronological standard: new high-precision isotope dilution thermal ionization mass spectrometry results. *Geochimica et Cosmochimica Acta, 67*(19), 3665-3672.

Schulz, K. J. (2012). Regional Environment. In W. C. P. Shanks, III & R. Thurston (Eds.), *Volcanogenic Massive Sulfide Occurrence Model* (Vol. 2010–5070–C, pp. 37-60). Reston, Virginia: U.S. Geological Survey.

Schulz, K. J., DeYoung Jr, J. H., Seal Ii, R. R., & Bradley, D. C. (2017). *Critical mineral resources of the United States—An introduction* (1802A). Retrieved from Reston, VA: http://pubs.er.usgs.gov/publication/pp1802A

Scott, K. M., Lu, X., Cavanaugh, C. M., & Liu, J. S. (2004). Optimal methods for estimating kinetic isotope effects from different forms of the Rayleigh distillation equation 1 1Associate editor: J. Horita. *Geochimica et Cosmochimica Acta, 68*(3), 433-442. doi:https://doi.org/10.1016/S0016-7037(03)00459-9

Seal, R. R. (2006). Sulfur Isotope Geochemistry of Sulfide Minerals. *Reviews in Mineralogy and Geochemistry, 61*(1), 633-677. doi:https://doi.org/10.2138/rmg.2006.61.12

Seedorff, E., Dilles, J. H., Proffett, J. M., Jr., Einaudi, M. T., Zurcher, L., Stavast, W. J. A., . . . Barton, M. D. (2005). Porphyry Deposits: Characteristics and Origin of Hypogene Features. In J. W. Hedenquist, J. F. H. Thompson, R. J. Goldfarb, & J. P. Richards (Eds.), One Hundredth Anniversary Volume (pp. 0): Society of Economic Geologists. Retrieved from https://doi.org/10.5382/AV100.10. doi:10.5382/AV100.10

Selvaraja, V., Caruso, S., Fiorentini, M. L., & LaFlamme, C. (2017). The Global Sedimentary Sulfur Isotope Database. *The Centre for Exploration Targeting - Univeristy of Western Australia*.

Seward, T. M., Williams-Jones, A. E., & Migdisov, A. A. (2014). 13.2 - The Chemistry of Metal Transport and Deposition by Ore-Forming Hydrothermal Fluids. In H. Holland & K. Turekian (Eds.), *Treatise on Geochemistry (Second Edition)* (Vol. 13, pp. 29-57). Amsterdam: Elsevier Science.

Sharman, E. R., Taylor, B. E., Minarik, W. G., Dube, B., & Wing, B. A. (2015). Sulfur isotope and trace element data from ore sulfides in the Noranda district (Abitibi, Canada):

implications for volcanogenic massive sulfide deposit genesis. *Mineralium Deposita, 50*, 591-606.

Sherman, D. M. (2013). Equilibrium isotopic fractionation of copper during oxidation/reduction, aqueous complexation and ore-forming processes: Predictions from hybrid density functional theory. *Geochimica et Cosmochimica Acta, 118*, 85-97. doi:https://doi.org/10.1016/j.gca.2013.04.030

Shibuya, T., Kitajima, K., Komiya, T., Terabayashi, M., & Maruyama, S. (2007). Middle Archean ocean ridge hydrothermal metamorphism and alteration recorded in the Cleaverville area, Pilbara Craton, Western Australia. *Journal of Metamorphic Geology, 25*(7), 751-767.

Shock, E. I., Sassani, D. C., Willis, M., & Sverjensky, D. A. (1997). Inorganic species in geologic fluids: correlations among standard molal thermodynamic properties of aqueous ions and hydroxide complexes. *Geochimica et Cosmochimica Acta, 61*(5), 907-950. doi:https://doi.org/10.1016/S0016-7037(96)00339-0

Slack, J. F., Johnson, C. A., Causey, J. D., Lund, K., Schulz, K. J., Gray, J. E., & Eppinger, R. G. (2013). *Descriptive and geoenvironmental model for Co-Cu-Au deposits in metasedimentary rocks: Chapter G in Mineral deposit models for resource assessment* (2010-5070G). Retrieved from Reston, VA: http://pubs.er.usgs.gov/publication/sir20105070G

Slack, J. F., Kimball, B. E., & Shedd, K. B. (2017a). *Cobalt* (1802F). Retrieved from Reston, VA: http://pubs.er.usgs.gov/publication/pp1802F

Slack, J. F., Kimball, B. E., & Shedd, K. B. (2017b). Cobalt. In K. J. Schulz, J. H. DeYoung., R. R. Seal, & D. W. Bradley (Eds.), *Critical Mineral Resources of the United States—Economic and Environmental Geology and Prospects for Future Supply* (Vol. Chapter F, pp. 40 p.). Reston, Virginia: U.S. Geological Survey.

Smithies, R. H., Champion, D., Van Kranendonk, M. J., & Hickman, A. H. (2007). *Geochemistry of volcanic rocks of the northern Pilbara Craton, Western Australia*. Retrieved from Perth:

Smithies, R. H., Hickman, A. H., & Nelson, D. R. (1999). New constraints on the evolution of the Mallina Basin, and their bearing on relationships between contrasting eastern and western granite–greenstone terranes of the Archaean Pilbara Craton,Western Australia. *Precambrian Research, 94*(1-2), 11-28.

Soloviev, S. G., Kryazhev, S. G., & Dvurechenskaya, S. S. (2013). Geology, mineralization, stable isotope geochemistry, and fluid inclusion characteristics of the Novogodnee–Monto oxidized Au–(Cu) skarn and porphyry deposit, Polar Ural, Russia. *Mineralium Deposita, 48*(5), 603-627.

Stacey, J. S., & Kramers, J. D. (1975). Approximation of terrestrial lead isotope evolution by a two-stage model. *Earth and Planetary Science Letters, 26*(2), 207-221.

Steadman, J. A., Large, R. R., Blamey, N. J., Mukherjee, I., Corkrey, R., Danyushevsky, L. V., . . . Lécuyer, C. (2020). Evidence for elevated and variable atmospheric oxygen in the Precambrian. *Precambrian Research, 343*, 105722. doi:https://doi.org/10.1016/j.precamres.2020.105722

Stüeken, E. E., Buick, R., & Anbar, A. D. (2015). Selenium isotopes support free O2 in the latest Archean. *Geology, 43*(3), 259-262. doi:10.1130/g36218.1

Syverson, D. D., Borrok, D. M., Niebuhr, S., & Seyfried, W. E. (2021). Chalcopyrite-dissolved Cu isotope exchange at hydrothermal conditions: Experimental constraints at 350 °C and 50 MPa. *Geochimica et Cosmochimica Acta, 298*, 191-206. doi:https://doi.org/10.1016/j.gca.2021.02.005

Taylor, C. D., Causey, J. D., Denning, P. D., Hammartstrom, J. M., Hayes, T. S., Horton, J. D., . . . Zientek, M. L. (2013). *Descriptive Models, Grade-Tonnage Relations, and Databases for the Assessment of Sediment-Hosted Copper Deposits—With Emphasis on Deposits in the Central African Copperbelt, Democratic Republic of the Congo and Zambia*. Retrieved from Reston, Virginia:

Thomazo, C., Ader, M., Farquhar, J., & Philippot, P. (2009). Methanotrophs regulated atmospheric sulfur isotope anomalies during the Mesoarchean (Tumbiana Formation, Western Australia). *Earth and Planetary Science Letters, 279*(1-2), 65-75. doi:https://doi.org/10.1016/j.epsl.2008.12.036

Thomson, S. N., Gehrels, G. E., Ruiz, J., & Buchwaldt, R. (2012). Routine low-damage apatite U-Pb dating using laser ablation–multicollector–ICPMS. *Geochemistry, Geophysics, Geosystems, 13*(2).

Tillberg, M., Maskenskaya, O. M., Drake, H., Hogmalm, J. K., Broman, C., Fallick, A. E., & Åström, M. E. (2019). Fractionation of Rare Earth Elements in Greisen and Hydrothermal Veins Related to A-Type Magmatism. *Geofluids*, 20. doi:https://doi.org/10.1155/2019/4523214

Tornos, F., & Heinrich, C. A. (2008). Shale basins, sulfur-deficient ore brines and the formation of exhalative base metal deposits. *Chemical Geology, 247*(1), 195-207. doi:https://doi.org/10.1016/j.chemgeo.2007.10.011

U.S. Department of the Interior. (2018). *Final List of Critical Minerals 2018*. Retrieved from Washington D.C., United States of America:

US Geological Survey. (2018). *Mineral commodity summaries 2018*. Retrieved from

Van Kranendonk, M. J., Hickman, A. H., Smithies, R. H., Nelson, D. R., & Pike, G. (2002). Geology and Tectonic Evolution of the Archean North Pilbara Terrain, Pilbara Craton, Western Australia. *Economic Geology, 97*(4), 695-732. doi:https://doi.org/10.2113/gsecongeo.97.4.695

Van Kranendonk, M. J., Hickman, A. H., Smithies, R. H., Williams, I. R., Bagas, L., & Farrell, T. R. (2006). *Revised lithostratigraphy of Archean supracrustal and intrusive rocks in the northern Pilbara Craton, Western Australia*. Retrieved from

Van Kranendonk, M. J., Smithies, R. H., Hickman, A. H., & Champion, D. (2007). Review: secular tectonic evolution of Archean continental crust: interplay between horizontal and vertical processes in the formation of the Pilbara Craton, Australia. *Terra Nova, 19*(1), 1-38.

Van Kranendonk, M. J., Smithies, R. H., Hickman, A. H., Wingate, M. T. D., & Bodorkos, S. (2010). Evidence for Mesoarchean (~3.2Ga) rifting of the Pilbara Craton: The missing link in an early Precambrian Wilson cycle. *Precambrian Research, 177*, 145-161.

Vance, D., Archer, C., Bermin, J., Perkins, J., Statham, P. J., Lohan, M. C., . . . Mills, R. A. (2008). The copper isotope geochemistry of rivers and the oceans. *Earth and Planetary Science Letters, 274*(1), 204-213. doi:https://doi.org/10.1016/j.epsl.2008.07.026

Vaughan, D. J. (1978). *Mineral chemistry of metal sulfides*. Cambridge: Cambridge University Press.

Voegelin, A. R., Nägler, T. F., Beukes, N. J., & Lacassie, J. P. (2010). Molybdenum isotopes in late Archean carbonate rocks: Implications for early Earth oxygenation. *Precambrian Research, 182*(1), 70-82. doi:https://doi.org/10.1016/j.precamres.2010.07.001

Waldbauer, J. R., Sherman, L. S., Sumner, D. Y., & Summons, R. E. (2009). Late Archean molecular fossils from the Transvaal Supergroup record the antiquity of microbial diversity and aerobiosis. *Precambrian Research, 169*(1), 28-47. doi:https://doi.org/10.1016/j.precamres.2008.10.011

Wall, A. J., Heaney, P. J., Mathur, R., Post, J. E., Hanson, J. C., & Eng, P. J. (2011a). A flow-through reaction cell that couples time-resolved X-ray diffraction with stable isotope analysis. *Journal of Applied Crystallography, 44*(2), 429-432. doi:doi:10.1107/S0021889811000525

Wall, A. J., Mathur, R., Post, J. E., & Heaney, P. J. (2011b). Cu isotope fractionation during bornite dissolution: An in situ X-ray diffraction analysis. *Ore Geology Reviews, 42*(1), 62-70. doi:https://doi.org/10.1016/j.oregeorev.2011.01.001

Wang, X., Ossa Ossa, F., Hofmann, A., Agangi, A., Paprika, D., & Planavsky, N. J. (2020). Uranium isotope evidence for Mesoarchean biological oxygen production in shallow marine and continental settings. *Earth and Planetary Science Letters, 551*, 8. doi:https://doi.org/10.1016/j.epsl.2020.116583

Wang, X., Planavsky, N. J., Hofmann, A., Saupe, E. E., De Corte, B. P., Philippot, P., . . . Konhauser, K. O. (2018). A Mesoarchean shift in uranium isotope systematics. *Geochimica et Cosmochimica Acta, 238*, 438-452. doi:https://doi.org/10.1016/j.gca.2018.07.024

Wang, Z., Park, J.-W., Wang, X., Zou, Z., Kim, J., Zhang, P., & Li, M. (2019). Evolution of copper isotopes in arc systems: Insights from lavas and molten sulfur in Niuatahi volcano, Tonga rear arc. *Geochimica et Cosmochimica Acta, 250*, 18-33. doi:https://doi.org/10.1016/j.gca.2019.01.040

Westendorp, R. W., & Watkinson, D. H. (1991). Silicon-bearing zoned magnetite crystals and the evolution of hydrothermal fluids at the Ansil Cu-Zn mine, Rouyn-Noranda, Quebec. *Economic Geology, 86*(5), 1110-1114.

White, N. C., & Hedenquist, J. W. (1995). Epithermal gold deposits: styles, characteristics and exploration. *SEG Newsletter, 23*(1), 9-13.

Wille, M., Kramers, J. D., Nägler, T. F., Beukes, N. J., Schröder, S., Meisel, T., . . . Voegelin, A. R. (2007). Evidence for a gradual rise of oxygen between 2.6 and 2.5 Ga from Mo isotopes and Re-PGE signatures in shales. *Geochimica et Cosmochimica Acta, 71*(10), 2417-2435. doi:https://doi.org/10.1016/j.gca.2007.02.019

Williams, P. J., Barton, M. D., Johnson, D. A., Fontbote, L., De Haller, A., Mark, G., . . . Marschik, R. (2005). Iron Oxide Copper-Gold Deposits: Geology, Space-Time Distribution, and Possible Modes of Origin. In J. W. Hedenquist, J. F. H. Thompson, R. J. Goldfarb, & J. P. Richards (Eds.), *Economic Geology One Hundredth Anniversary Volume*: Society of Economic Geologists.

Wilmeth, D. T., Corsetti, F. A., Beukes, N. J., Awramik, S. M., Petryshyn, V., Spear, J. R., & Celestian, A. J. (2019). Neoarchean (2.7 Ga) lacustrine stromatolite deposits in the Hartbeesfontein Basin, Ventersdorp Supergroup, South Africa: Implications for oxygen oases. *Precambrian Research, 320*, 291-302. doi:https://doi.org/10.1016/j.precamres.2018.11.009

Wolery, T. J. (1992). *EQ3NR, a computer program for geochemical aqueous speciation-solubility calculations: theoretical manual, users guide, and related documentation (Version 7.0); Part 3*. Retrieved from CA (United States):

Wu, S., Zheng, Y., Wang, D., Chang, H., & Tan, M. (2017). Variation of copper isotopes in chalcopyrite from Dabu porphyry Cu-Mo deposit in Tibet and implications for mineral exploration. *Ore Geology Reviews, 90*, 14-24. doi:https://doi.org/10.1016/j.oregeorev.2017.10.001

Wyborn, L. A. I., Heinrich, C. A., & Jaques, A. L. (1994). Australian Proterozoic mineral systems: essential ingredients and mappable criteria. *Australian Institute of Mining and Metallurgy Publication Series*(94), 109-115.

Zavina-James, N. A. V., Zerkle, A. L., Steele, R. C. J., Warke, M. R., Izon, G., & Savage, P. S. (2021). A copper isotope investigation of methane cycling in Late Archaean sediments. *Precambrian Research, 362*, 106267. doi:https://doi.org/10.1016/j.precamres.2021.106267

Zhu, X. K., Guo, Y., Williams, R. J. P., O'Nions, R. K., Matthews, A., Belshaw, N. S., . . . Salvato, B. (2002). Mass fractionation processes of transition metal isotopes. *Earth and Planetary Science Letters, 200*(1-2), 47-62. doi:https://doi.org/10.1016/S0012-821X(02)00615-5

Zhu, X. K., O'Nions, R. K., Guo, Y., Belshaw, N. S., & Rickard, D. (2000). Determination of natural Cu-isotope variation by plasma-sourcem ass spectrometry: implications for use as geochemical tracers. *Chemical Geology, 163*(1-4), 139-149. doi:https://doi.org/10.1016/S0009-2541(99)00076-5

Zhu, Y., Fang, A., & Tan, J. (2011). Geochemistry of hydrothermal gold deposits: A review. *Geoscience Frontiers, 2*(3), 367-374.